Mobile Localisation of 5G and Beyond 5G Cellular Networks

Thesis submitted in accordance with the requirements of the University of Liverpool for the degree of Doctor in Philosophy

by

Boda Liu

31 July 2020

Declaration

The work in this thesis is based on research carried out at the University of Liverpool. No part of this thesis has been submitted elsewhere for any other degree or qualification and it is all my own work unless referenced to the contrary in the text.

Abstract

Mobile localisation is one of the main functions of the fifth generation (5G) and beyond 5G (B5G) cellular networks, enabling high quality location services (LCSs). In this thesis, a number of challenging problems on localisation are addressed for 5G and B5G networks under different use cases, including device-to-device (D2D) connectivity, unmanned aerial vehicle (UAV) mounted base station (BS), massive multiple-input multiple-output (MIMO) antenna, and intelligent surface (IS) array. The detailed contributions are shown as following items.

In the first contribution, I propose a cooperative localisation technique based on time-of-arrival (TOA), angle-of-arrival (AOA) and angle-of-departure (AOD) observed at BSs, and received-signal-strength (RSS) collected from collaborative mobile stations (MSs) in single-bounce multipath environment, named as CLTAAR, to mitigate non-line-of-sight (NLOS) error due to single-bounce scattering. This scheme is further improved by a proposed weight function of variance of measurements. Then, a grouping strategy is integrated with the proposed work to reduce the running time of estimation progress, named as eCLTAAR. The system performance is verified by simulations and Cramer-Rao Lower Bound (CRLB). It is shown that the proposed techniques outperform existing approaches in terms of localisation accuracy and running time.

In the second contribution, unmanned aerial vehicle (UAV)-base stations (BSs) assisted and received signal strength (RSS) based mobile station (MS) localisation is investigated. A practical air-to-ground path loss model is utilised, where the path loss exponent (PLE) varies with the elevation angle and altitude of UAV, and the accurate PLE estimate is often difficult to obtain. With unknown and unequal PLEs for different UAVs, the UAVs assisted localisation problem becomes nonlinear and non-convex, which cannot be solved by the existing methods. Two localisation approaches are proposed to solve the problem with known transmit power, unknown and unequal PLEs, and one approach with estimated

transmit power is proposed for the scenario with all the parameters unknown. Simulation results show a much higher accuracy achieved by the proposed schemes than the existing approaches with perfect knowledge of either one or all the parameters. In addition, an anti-intuitive finding verifies the analytical higher accuracy of localisation and ranging distance obtained with estimated parameters than that of the real parameters. Thus, it suggests to apply the estimated parameters rather than real parameters, even if the perfect knowledge is available. The effectiveness of proposed approaches are also verified by the Cramer-Rao lower bound (CRLB) derived.

In the last but not least contribution, we investigate an intelligent surface (IS) assisted massive MIMO based localisation. Large IS array (Ix) that in near-field regime is divided into multiple non-overlapping sub-arrays with approximated channel parameters allocated. Both approximated Fisher information matrix (aFIM) and exact FIM (eFIM) are derived. To improve performance of localisation, a localisation-aimed IS phase shifter (lo-ISpsf) is first proposed to minimise position error bound and orientation error bound, rather than maximise data rate as done by communication-aimed ISpsf (co-ISpsf) in the existing research. Simulation results show the much higher accuracy of proposed lo-ISpsf than that of existing co-ISpsf in different cases with various number of Ix elements and quantization bits. ISpsf of 1-bit quantizer is the most efficient in most cases. The numerical results also reflect the significant degradation on accuracy caused by absence of knowledge of IS position and orientation.

Acknowledgements

This thesis would not have been finished without loads of support and help from the following people. Therefore, I would like to take this opportunity to thank them all.
I would like to give my deepest gratitude to my supervisor Dr. Xu Zhu, for her guidance, support, and commitment. This work can not be finished without her invaluable comments and constant encouragement. I also appreciate concerns from Prof. Yi Huang for my research.
I would like to thank the University of Liverpool, as well as the Department of Electrical Engineering and Electronics, for providing outstanding training to research students.
I am grateful to Dr. Zhongxiang Wei in University College London and Dr. Yujie Liu in Xi'an Jiaotong-Liverpool University, who gave me lots of advices in my research work.
I would also like to thank Assistant Prof. Yufei Jiang in Harbin Institute of Technology, China, where I obtained lots of advices and guidance in my research work.
Finally, my gratitude is dedicated to my parents. I would had no chance to pursue my dreams in my life without their great support, patience and love. This thesis is dedicated to them.

Contents

List of Figures

List of Tables

Nomenclature

2G second generation

3G third generation

4G fourth generation

5G fifth generation

6G sixth generation

A2G air-to-ground

aAOA azimuth angle of arrival

aAOD azimuth angle of arrival

aEFIM approximated effective Fisher information matrix

aFIM approximated Fisher information matrix

AOA angle-of-arrival

AOD angle-of-departure

aOEB approximated orientation error bound

aPEB approximated position error bound

AS airframe shadowing

B5G beyond fifth generation

BS base station

CDF cumulative density function

CLTAAR Cooperative localisation of TOA, AOA, AOD and RSS

co-ISpsf communication-aimed ISpsf

CQI channel quality information

CRLB Cramer-Rao lower bound

D2D device-to-device

DRSS differential received signal strength

eAOA elevation angle of arrival

eAOD elevation angle of arrival

eCLTAAR enhanced CLTAAR

Edist effective ranging distance

EFIM effective Fisher information matrix

EPLE effective path loss exponent

EPt effective transmit power

FIM Fisher information matrix

G2G ground-to-ground

GPS Global Positioning System

GSAE Grid search ambiguity elimination

IoT Internet of Things

ISpsf intelligent surface phase shifter

IS intelligent surface

Ix intelligent surface array

LCS location service

lo-ISpsf localisation-aimed ISpsf

LOS line-of-sight

LS least-square

MIMO multiple-input-multiple-output

mm millimetre

MS mobile station

NLOS non-line-of-sight

OEB orientation error bound

PCAL-EPt-gsDRSS PCAL-gsDRSS enhanced by estimated EPt

PCAL-gsDRSS PCAL enhanced by DRSS assisted grid search

PCAL Piecewise convex approximation localisation

PDF probability density function

PEB position error bound

PLE path loss exponent

RAE relative approximation error

RB resolvable resource block

RSS received signal strength

Rx receiver array

SDP semi-definite programming

SISO single-input single-output

SNR signal-to-noise ratio

SOEB squared orientation error bound

SPEB squared position error bound

TDOA time-difference-of-arrival

TNN The Things Network

TOA time-of-arrival

TSE Taylor-series expansion

Tx transmitter array

UAV unmanned aerial vehicle

URA uniform rectangular array

wCLTAAR weighted CLTAAR

List of Symbols

The notations of frequently-used symbols are listed as follows.

M,N,C	number of MSs, BSs, and scatters
$PL_i, \widehat{PL}_i, \widetilde{PL}_i$	real, estimated and measured value of path loss at BS i
$PL_{m,k}$	path loss of signals from MS m to MS k
Pt, Pr_i	transmit power, RSS at BS i
$\mathbf{v}_m = [x_m, y_m]^{\mathrm{T}}$, $\mathbf{w}_i = [x_{\mathrm{BS}i}, y_{\mathrm{BS},i}]^{\mathrm{T}}$, $\mathbf{q}_c = [q_{x,c}, q_{y,c}, q_{z,c}]^{\mathrm{T}}$, $\mathbf{r}_{\mathrm{I}} = [x_{\mathrm{I}}, y_{\mathrm{I}}, z_{\mathrm{I}}]^{\mathrm{T}}$	coordinates of MS m, BS i, scatter c and IS
D_{mi}	direct distance between MS m and BS i
$r_{R,jc}$	distance between the c-th scatter c and MS m
$r_{T,ci}$	distance between the c-th scatter c and BS i
c_0	speed of light
f_c	carrier centre frequency
τ_{mci}	TOA of the single bounced path from MS m to BS i through scatter c
n_{mi}	observation noise of TOA
σ_τ	standard deviation of TOA
θ_{mc}	AOA from scatter c to MS m
$\epsilon_{\theta,mc}$	observation noise of AOA
ϑ_{ci}	AOD from BS i to scatter c
$\epsilon_{\theta,ci}$	observation noise of AOD

R_c	radius of scattering environment
λ	wavelength
$X_{S,m,k}$	shadowing of path loss between MS m and MS k
σ_{RSS}	standard deviation of shadowing of path loss
η	path loss exponent
A	RSS measured at reference distance
$h1, h2$	sets of group 1 and group 2
$\mathbf{F}_{\text{CLTAAR}}, \mathbf{F}_{BS-MS}, \mathbf{F}_{MS-MS}$	FIM of CLTAAR estimator, FIMs of BS-MS and MS-MS observations
$\mathbf{K}_{m,k}$	correlation matrix between MS m and MS k
d_i	distance between MS and BS i
θ_i	elevation angle at i-th UAV BS
h_i	altitude of i-th UAV BS
$d_{t,i}$	transition distance on EAPL model of i-th UAV BS
$d_{\text{lower},i}, d_{\text{upper},i}$	lower and upper bound of distance of interest
$A_{i,g_i}, B_{i,g_i}, C_{i,g_i}$	fitted parameters of sub-function of i-th UAV BS
$X_{\text{PL},i} = S_{\text{af},i} + X_{S,i}$	measurement error of path loss at i-th UAV BS, as sum of airframe bias and shadowing
$\alpha_{i,g_i} = [(\widetilde{PL}_i - \beta_{i,g_i})/A_{i,g_i}]^{1/B_{i,g_i}}$	i-th ranging distance
$\mathbf{v}_j$	j-th tentative estimate of MS location
$\overline{DRSS}_i, \widehat{DRSS}_i$	measured, sampled DRSS between UAV BS i and UAV BS N (the BS of lowest RSS)
$\widetilde{\widetilde{PL}}_i$	path loss obtained with measured RSS and estimated transmit power
$\mathbf{0}_M$, $\mathbf{1}_M$ $M \times 1$ vectors with all '0' elements and all '1' elements	
$\mathbf{I}_M$	$M \times M$ identity matrix
$\mathbf{Y}(f)$	received frequency-band signals
$\Lambda_{\text{S}}, \Lambda_{\text{R}}$	sets of cluster reflective paths and the IS-aided paths
$\mathbf{o}_{\text{BS}} = [\vartheta_{\text{BS}}, \varphi_{\text{BS}}]$, $\mathbf{o}_{\text{IS}} = [\nu_{\text{IS}}, \mu_{\text{IS}}]$, $\mathbf{o}_{\text{MS}} = [\theta_{\text{MS}}, \phi_{\text{MS}}]$	orientation of BS, IS and MS array
$\mathbf{R}(\mathbf{o})$	rotation matrix of orientation $\mathbf{o}$

$\mathbf{k}(\cdot,\cdot)$	unit directional vector
Δ_d	inter-element spacing
$\mathbf{p}_T, \mathbf{p}_\mathrm{R}, \mathbf{p}_\mathrm{I}$	element position at transmitter, receiver and IS array
$\mathbf{A}_\mathrm{R}, \mathbf{A}_\mathrm{T}, \mathbf{A}_\mathrm{bw}, \mathbf{A}_\mathrm{fw}$	sets of array response of receiver, transmitter, IS backward link and forward link
$\theta_l, \vartheta_l, \nu_{\mathrm{fw},l}, \nu_{\mathrm{bw},l}$	elevation angles of l-th path at MS, BS, IS forward link and backward link
$\phi_l, \varphi_l, \mu_{\mathrm{fw},l}, \mu_{\mathrm{bw},l}$	azimuth angles of l-th path at MS, BS, IS forward link and backward link
$\mathbf{h}_{\mathrm{I},1}, \mathbf{h}_{\mathrm{I},2}$	complex channel gain of forward link and backward link at IS
$\mathbf{T}_{\Lambda_\mathrm{R}}$	delay vector of IS-aided paths
$\mathbf{\Psi}_\mathrm{R}, \tilde{\mathbf{\Psi}}_\mathrm{R}$	continuous and discrete IS phase shifter
$\Delta\psi_l, \Delta\tilde{\psi}_l$	continuous and discrete phase shifts at the l-th IS element
b_I	number of bits of IS quantizer
A_eff	effective aperture of each Ix element
$a_\mathrm{eff}, G_\mathrm{eff}$	range, effective aperture of each Ix element
$\rho_\mathrm{fw}, \rho_\mathrm{bw}$	path attenuation of forward link and backward link
$\mathbf{H}_\mathrm{d}, \mathbf{H}_\mathrm{s}, \mathbf{H}_\mathrm{R}$	channel state information of direct path, cluster reflected path and IS-aided path
$\mathbf{F}_\mathrm{B}$	directional beamforming matrix
$N_\mathrm{T}, N_\mathrm{R}, N_\mathrm{IS}$	number of elements of Tx, Rx and Ix
P_T	transmit power
$\mathbf{n}_\mathrm{obs}, N_0$	observation noise and the PSD
$\mathbf{x}(f_\iota)$	transmit signals
$\mathbf{\Omega}, \boldsymbol{\omega}_1, \tilde{\boldsymbol{\psi}}, \boldsymbol{\omega}_2$	matrix of interested parameters, position-related parameters, location and orientation of MS and IS
$\mathcal{F}_{\boldsymbol{\omega}_1}, \mathcal{F}_{\boldsymbol{\omega}_2}, \mathcal{F}_\mathrm{MS}$	equivalent Fisher information matrix of $\boldsymbol{\omega}_1, \boldsymbol{\omega}_2$ and MS location information
$\nabla_{\boldsymbol{\omega}_2}(\boldsymbol{\omega}_1)$	Jacobian matrix of $\boldsymbol{\omega}_1$ over $\boldsymbol{\omega}_2$
$\mathcal{P}_\mathrm{MS,orin}, \mathcal{P}_\mathrm{MS,posi}, \mathcal{A}_\mathrm{MS,orin}, \mathcal{A}_\mathrm{MS,posi}$	exact SOEB and SPEB, approximated SOEB and SPEB

The operator $\tilde{(\cdot)}$ denotes the noisy measurements. $(\cdot)^{\mathrm{T}}$ and $(\cdot)^{\mathrm{H}}$ are the transpose operator and conjugate transpose operator, respectively. $diag\{\mathbf{z}\}$ diagonalises the vector $\mathbf{z}$. $\odot$ and $\bullet$ stands for Hadamard product and dot product. $\Re\{\cdot\}$, $\Im\{\cdot\}$, $|\cdot|$, $\|\cdot\|$, and $\angle\cdot$ respectively stand for real part, imaginary part, absolute, $l2$-norm, and phase angle operators. $\grave{\mathbf{a}}, \dot{\mathbf{a}}$ respectively represent the derivative of matrix $\mathbf{a}$ over the corresponding azimuth and elevation angle. $(\cdot)_{a:b,c:d}$ denote the block of the elements from the a-th row to the b-th row and from the c-th column to the d-th column. $\lfloor a \rfloor$ is the floor function that rounds the number a to the nearest integer smaller than a. For a set Λ, $|\Lambda|$ denotes its cardinality. The subscripts 'fw' and 'bw' represent the corresponding variables of the forward link and backward link.

Chapter 1

Introduction

1.1 Background and Motivation

Localisation techniques have attracted much attention of research and rapidly grown with the popularisation of personal electronic devices and commercial wireless networks over the past two decades. Location awareness is now an essential feature of many commonly used LCSs in both public, commercial and military wireless networks [1], such as emergency call and vehicle navigation, whose quality of service (QoS) is highly dependent on localisation accuracy. Thus, localisation techniques play a major impact on the performance of wireless networks [2].

The existing localisation techniques can be generally categorised as three types, network based, handset based and hybrid. The Global Positioning System (GPS) is a conventional handset based localisation system applied for localisation and navigation, but it has some limitations. For example, GPS in city canyons suffers from degrade performance when the satellite signals are usually blocked by buildings. Whereas a competitive technology, network based localisation has gained a lot of interest, since it can be widely deployed in any wireless networks with lower cost than GPS [1],[2]. Network based localisation systems localise targets through estimation with the measured properties of received signals, *e.g.*, time-of-arrival (TOA), angle-of-arrival (AOA), angle-of-departure (AOD) and received signal strength (RSS), with no additional cost. Moreover, network based localisation also improves with the evolution of cellular networks from the second generation (2G) to the fifth generation (5G).

Localisation in 5G networks is more accurate than that in the conventional networks,

since several disruptive technologies employed by 5G [3], *i.e.*, millimeter-wave (mmWave) communication, massive multiple-input-multiple-output (MIMO) antenna, and device-to-device (D2D) connectivity benefit the network based localisation with more accurate position-related parameters than those in the conventional networks from second generation (2G) to fourth generation (4G). 5G network based localisation is able to achieve sub-meter accuracy [4], which is even more accurate than GPS ($1 \sim 5$-meter accuracy). Location-awareness even becomes a key feature of 5G networks, where sufficiently accurate localisation results can be used to improve wireless network design and optimisation through many aspects, *e.g.*, signalling overhead and networking [5], and even provide users with multimedia applications of Gbps-order data rates and improved QoS required by 5G networks [6]. However, due to the high frequency and low wavelength, 5G signals are easily blocked by obstacles, resulting into high path loss (PL), non-line-of-sight (NLOS) propagation, and multipath effect in harsh environment. Wherein, NLOS and multipath effect might causes tremendous degradation on localisation based on TOA, AOA and AOD, if they are not mitigated or treated properly. Solution to the problems lies in deploying more relays, BSs and local networks, *e.g.*, D2D and machine-to-machine networks, in order to improve line-of-sight (LOS) probability and maintain the accuracy of measurements. 5G is the first generation that natively supports D2D communication [3]. Even if D2D has been included in 3G and 4G, it was just considered as an add-on to reduce the cost of local service provision. Thanks to D2D connectivity, mobile stations (MSs) in proximity are allowed to join the local network and collect the extra short-range relative measurements between the MSs, which are more reliable than the long-range measurements observed by base station (BS) in harsh environment. The advanced infrastructures of 5G are expected to afford both non-cooperative and cooperative localisation approaches.

On the other hand, unmanned aerial vehicle (UAV) supported communication is first standardised in 5G, where UAV mounted BSs is introduced as a flexible and temporary supplement to the terrestrial networks, and support the jammed or destroyed terrestrial BSs in disaster. Benefited from flexibility and wide field of vision of UAV BSs, UAV BS assisted localisation seems to be easier and more accurate than terrestrial localisation. However, UAV BS assisted localisation is challenging, since the practical UAV air-to-ground (A2G) channel models are different with the conventional ground-to-ground (G2G) channel models. For example, path loss exponents (PLEs) and variance of ground shadowing of A2G channel are not constants as those of G2G channel, but dependent on UAV altitude or elevation angle. UAV airframe shadowing (AS) is a special parameter of fixed-wing UAV,

and it is a function of time and fast fading. LOS probability of A2G channel is influenced by statistical parameter of buildings in the communication environment. These nuisance parameters must be estimated or considered in UAV BS assisted localisation, however, they were usually ignored by the previous research, which only applied the G2G channel models. That may cause significant impact on localisation performance. This gap in previous research motivates us to study UAV BSs assisted and RSS based localisation technique. A common sense is widely recognised by the existing work [7]-[8],[9],[10] that the higher accuracy of path loss parameters is, the better the localisation performs. However, we noticed that high accuracy could happen to the localisation with imperfect knowledge of path loss parameters. Based on this phenomenon, we study the effect of inaccurate path loss parameters on accuracy of ranging and localisation, and find the principle to explain it.

Massive MIMO is a promising technique for 5G, which exploits the potentially large capacity gains on the system with signals of small wavelength. It reduces the interference due to multipath components, and improves the resolvability of channels between BS and MS. With large amount of observations of signals, therefore, the massive MIMO system is able to extract sufficiently accurate position-related channel parameters from received signals through the existing algorithms, *e.g.*, maximum likelihood algorithm and orthogonal matching pursuit algorithm, resulting into much higher accuracy than single antenna based localisation. Thus, the measurements accuracy does not make the main impact on massive MIMO based localisation. The Cramer-Rao lower bounds (CRLBs) of massive MIMO based localisation accuracy in different scenarios are found inversely proportional to signal-to-noise ratio (SNR) at MS, and realised at sub-meter accuracy in [11] - [12]. As a result, the existing research mainly focused on beamforming optimisation for localisation, which influences SNR at MSs in each direction.

Another recent emerging technology of large array, intelligent surface (IS) is considered as a promising technology envisioned for beyond 5G (B5G) networks. ISs can be easily deployed on facades of a building, and ceiling and floor of indoor spaces. A passive IS consisting of large amount of meta-surfaces works as a reflective antenna array. With assistance of adjustable phase shifter on IS (ISpsf), which is used to adjust amplitudes and phases of signals, the propagation environment near an IS becomes controllable for the connected BSs. IS can also be applied to improve the performance of localisation through optimising ISpsf. The existing research on IS assisted localisation exactly applied the communication-aimed ISpsf, since it regards the IS factor as a scalar independent of

Fisher information matrix (FIM) of other channel parameters. However, the impact of IS incident and reflection angles on FIM was not considered. Moreover, for the IS of large array (*i.e.* $> 1e3$ elements) and extra-large array (*i.e.* $> 1e5$ elements), various parameters and FIMs appeal to different parts of the array, and far-field approximation in the existing work is impractical for array in near-field. To address these issues, each parameter of FIM must be considered in ISpsf design. FIM of near-field localisation is preferable than that of far-field, otherwise the far-field approximation error must be mitigated.

1.2 Thesis Structure

The rest of this thesis is organised as follows. The overview of mobile localisation and the applied algorithms and techniques are introduced in Chapter 2. In Chapter 3, cooperative localisation system is considered for MS in single bounced NLOS environment. In Chapter 4, UAV BS assisted and RSS based localisation system is considered, which addresses the problem with known and unknown path loss parameters. In Chapter 5, an IS assisted and massive MIMO based localisation system is considered. The impacts of IS size, far-field approximation error and number of ISpsf quantizer bits are investigated. The design of proposed localisation-aimed ISpsf is presented. Conclusions and future work are presented in the final chapter.

1.3 Contributions

Based on the perfect system (known system parameters, perfect channel estimation and interference mitigation, no synchronisation error, etc), the research conducted during this PhD study has produced the following main contributions:

1. A cooperative localisation technique with adaptive weights on hybrid measurements RSS, TOA, AOA, and AOD, named as CLTAAR, to mitigate NLOS errors caused by single-bounce scattering. To reduce the computation time of cooperative approach, an UE grouping strategy is utilised to decompose the original centralised cooperative localisation to two steps with little degradation on accuracy. Simulation results show that the proposed CLTAAR approach integrated with UE grouping scheme (eCLTAAR) outperforms the conventional cooperative localisation [2] in presence of single-bounce scattering.

2. The UAV BS assisted and RSS based localisation problem with unknown and unequal PLEs is solved by the proposed piecewise convex approximation aided localisation (PCAL) scheme. To the best of our knowledge, this is also the first work to consider UAV AS in the system model and investigate the impact of AS on UAV assisted and RSS based localisation. The ambiguous estimates of PCAL are dealt with by a proposed grid search assisted ambiguity elimination (GSAE) approach with known transmit power, and a proposed DRSS based grid search (gsDRSS) approach with unknown transmit power, which are more effective than the existing methods. The performance of PCAL-GSAE approaches the CRLB derived. Both analytical CRLB and simulation results prove that the proposed PCAL and PCAL-GSAE approaches with unknown and unequal PLEs achieves higher accuracy than the existing approaches with equal and perfectly known PLEs and approach with unknown and unequal PLEs. We also propose an anti-intuitive finding that, the estimated transmit power and PLEs of significant imperfection can achieve the higher accuracy of ranging and localisation than the real PLE and transmit power. Based on this finding, a new definition of effective PLE (EPLE) and effective transmit power (EPt) are proposed. An estimation algorithm of EPt is proposed to enhance PCAL-gsDRSS to PCAL-EPt-gsDRSS and approach the CRLB.The effect of equal and unequal EPLEs and EPt on localisation are analysed with both numerical results and analytical proof.

3. We investigate the performance of IS assisted and massive MIMO based localisation of single MS, through evaluating FIMs and CRLBs of all position-related channel parameters and location information with IS in both near-field and far-field. Based on the derived FIMs and CRLBs, an ISpsf optimisation algorithm is proposed to minimise position error bound (PEB) of MS. To the best of our knowledge, this work is exactly the first work on ISpsf design for localisation, which is different with the ISpsf designed in [13],[14]. The far field approximation error on localisation is also numerically assessed by various size of IS. Based on the numerical assessment, the approximation error of far-field localisation is mitigated by allocating non-overlapping sub-arrays with approximated FIM derived. The impacts of number of IS size, number of ISpsf quantizer bits and knowledge of IS location information on fundamental limits have been investigated with numerical results. Simulation results shows up to 100 times higher accuracy achieved by the proposed localisation-aimed ISpsf than the existing work.

1.4 Publication List

Journal Paper

1. B. Liu, X. Zhu, Y. Jiang, Z. Wei, and Y. Huang, "UAV and piecewise convex approximation assisted localization with unknown path loss exponents," *IEEE Trans. Veh. Tech.*, vol. 68, no. 12, pp. 12396-12400, Dec. 2019.

2. B. Liu, X. Zhu, Z. Wei, and Y. Huang, "Optimisation of Intelligent Surface Assisted and Massive MIMO Based System for Localisation," [to be submitted].

Conference Paper

B. Liu, X. Zhu, Y. Jiang, and Y. Huang, "Low complexity cooperative positioning in multipath environment," in *Proc. IEEE/CIC ICCC*, Beijing, China, Aug. 2018.

Chapter 2

Overview of Localisation Techniques

This chapter presents an overview of mobile localisation in cellular networks. The layout of mobile localisation is introduced in section 2.1. In section 2.2, the basic system model and most widely used measurements are described. In section 2.3, some fundamental algorithms and techniques applied for localisation in this thesis are provided.

2.1 Classification of Network Based Localisation

Mobile localisation has been standardised in cellular network protocols. The earliest official standardisation of mobile localisation was regulated by governmental institutions, the Federal Communications Commission (FCC) of the United States (U.S.), as E911 used for emergency services [15]-[16]. To dates, mobile localisation has been exploited for both public, private and commercial services, and network optimisation, and become the main feature of 5G networks. A fundamental layout of network based mobile localisation from 2G to 5G is displayed as Fig. 2.1, where the location server collects the observations from BSs, and estimates the location of MSs according to different level of accuracy acquired by the services.

This thesis only focuses on network based localisation approaches.

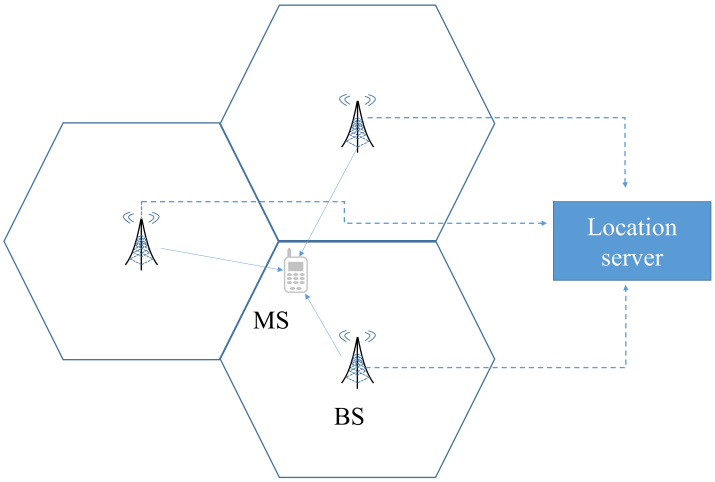

Figure 2.1: Layout of Mobile Localisation

2.2 Fundamental Network Based Localisation Techniques

The three fundamental mobile localisation techniques [15]-[16], as well as the hybrid technique, are displayed in Fig. 2.2, as :

- *Trilateration* : The position of MS is determined by the intersection points of ranging circles centred around the transmitter and in radius of distance measurements. This method is suitable for TOA and RSS based methods.

- *Triangulation* : The position of MS is determined by the intersection points of lines at the measured direction of signals. This method is suitable for AOA and AOD based methods.

- *Multilateration* : The position of MS is determined by the intersection of multiple hyperbolas obtained by the difference between two distance measurements. This method is suitable for TDOA and DRSS based methods.

- *Hybrid* : using multiple types of measurements can improve performance of localisation.

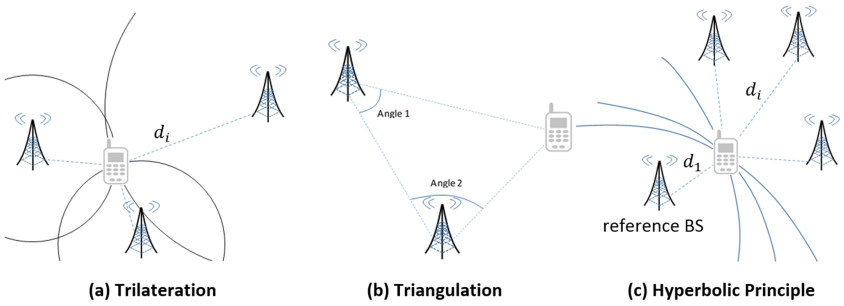

Figure 2.2: Fundamental mobile localisation techniques

2.3 Measurement Models and Localisation Algorithms

The most widely used measurements include ranging based measurements, *e.g.*, TOA and RSS, and angular based measurements, *e.g.*, AOA and AOD.

TOA : TOA is measured as the flight time of signals τ_i from the transmitter to the receiver, *i.e.*, $\tau_i = t_o - t_0$, where t_i is the arrival time from transmitter $\mathbf{w} = [x_i, y_i]^{\mathrm{T}}$ to receiver $\mathbf{v} = [x, y]^{\mathrm{T}}$, t_0 is the start time labelled in the signals. The measured propagation distance is calculated by multiplying the measured TOA with speed of light c, as following

$$\tilde{d}_i = c(\tau_i + n_\tau) \tag{2.1}$$

where n_τ is the measurement error of TOA observations. The real distance is expressed as

$$d_i = \|\mathbf{v} - \mathbf{w}_i\| \tag{2.2}$$

TOA based localisation techniques have been widely studied, due to its normally higher accuracy than other positioning techniques. A linear LS estimator was proposed for TOA based method under LOS environment [17]. TOA measurements of NLOS paths were identified by a normalised residual error test proposed in [18], and the location of target was determined by at least three LOS paths. Matched filter and energy detector based TOA estimators were studied in [19] with a threshold selection algorithm proposed.

AOA : AOA is derived by smart antenna array through estimating the direction of strongest signals from transmitter to receiver. The measured AOA of received signals at receiver can be expressed as

$$\tilde{\theta}_i = \tan^{-1}\left(\frac{y_i - y}{x_i - x}\right) + n_\theta \tag{2.3}$$

where $\tan^{-1}\left(\frac{y_i-y}{x_i-x}\right)$ is the real AOA. n_θ is the measurement error. The advantage of AOA based method is that only two AOA measurements of LOS paths suffice to localise one MS.

AOA based localisation techniques were limited in 2G$\sim$ 3G, due to the lack of smart antenna array, and finally standardised in 4G. AOA measurement, NLOS error has a major influence on the precision. The estimation error of AOA measure could vary from 0 to 360°. In [20], AOA measurements of NLOS paths were identified by comparing measurements with the Root Mean Square value. AOA based localisation was solved by LS estimator in [21]. CRLBs of AOA based method and hybrid TOA and AOA based method were evaluated for wideband signals in [22]. In [23], pre–coder indices of the MIMO were proved as strong angular information for AOA estimation.

RSS : RSS read at receiver can be used to estimate propagation distance through path loss model. RSS is obtained by calculating the integration of reference signals (RS), *i.e.*, position reference signal (PRS) and cell-specific reference signal (CRS) for 4G LTE system, during a certain sampling period. Denote the RSS as Pr, which is derived from path loss model as

$$Pr_i = Pt - 10\eta \log_1 0(d_i) + X_{S,i} \tag{2.4}$$

where η is PLE, $X_{S,i}$ is the shadowing. RSS based ranging distance is calculated as

$$\tilde{d}_i = 10^{\frac{Pt - Pr_i + X_{S,i}}{10\eta}} \tag{2.5}$$

RSS based methods can compromise with any networks without require any additional cost on hardware. The problem of RSS based localisation can be solved by the algorithms of TOA based localisation.

The system operational frequency also affects characteristics of radio propagation. For example, 5G path loss model, *e.g.*, close-in (CI) path loss model also contains a component of system operational frequency, which reflects the greater path loss value of signals at 5G

high band than that of low band, and consequently, the smaller cell radius than that of the existing 2G-4G. Moreover, the higher operational frequency also provides higher robustness against Doppler shift. However, the impact of system frequency f_c is not studied in Chapters 3 and 4, since it does not contain any location information. Based on the assumed perfect channel estimation and perfect knowledge of system, the measurement models of TOA, AOA, AOD and RSS employed by Chapter 3 are free of physical layer information, *e.g.*, f_c and signal bandwidth W, and only focus on geographical information. In contrast, f_c has significant influence on Chapter 5, due to the signal model. The impacts of f_c on TOA, AOA and AOD are intuitively reflected in the derivatives and FIMs calculated in (D.1)-(D.2), Appendix D.

2.4 Scattering for Multipath Effect

Scattering is a physical phenomena occurs when the radio wave is reflected by rough surface. A geometrical scattering model describes distribution of AOA and TOA of the received signals in multipath environment with a given PDF of scatters [24]. For simplicity, the term 'scattering' employed by this thesis refers to both reflection, diffraction, and scattering, and the term 'scatters' is referred to both reflectors, diffractors, and scatters in multipath propagation. The most common scattering model includes uniform circular scattering model [25], uniform ellipse scattering model [24], etc. An example of circular scattering model is displayed in Fig. 2.3, where the scatters are distributed on the circle around MS, and reflect signals to BS.

2.5 Massive MIMO Uniform Rectangular Array

In the massive MIMO communication system, the time-frequency resources are divided into multiple blocks, each of which simultaneously provides frequency-flat and static channel to serve multi-user. The normally defined massive MIMO contains at least 64 antennas, which is much greater than the conventional MIMO (2, 4 or 8 antennas). Each antenna has its own radio frequency (RF) and digital baseband chain. The number of RF chains determines the number of directional beams, which provide location information of the channel, *i.e.*, TOA, AOA and channel coefficients. The more RF chains applied, the narrower beams become, and the more accurate the estimated channel parameters are.

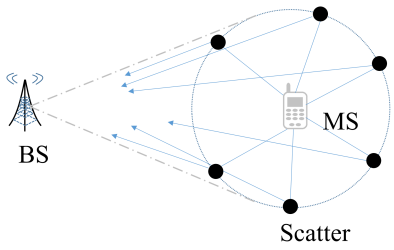

Figure 2.3: Circular scattering model

However, the number of RF chains is limited, due to finite total power and requirement of system complexity. Digital beamforming allows control of both amplitudes and phases of baseband signals.

For massive MIMO operating on TDD mode, the performance of system is not limited by the number of antennas. Moreover, due to reciprocity of propagation, channel estimation by uplink pilot sequence can be applied for the downlink channel. Thus, TDD mode is widely employed by massive MIMO systems.

In this thesis, uniform rectangular array (URA) (also named as uniform planar array) with identical elements spacing is applied for massive MIMO based localisation. An URA has N_{T} antenna elements uniformly distributed on the grids on a plane, as shown by Figure 2.4. For the massive MIMO array, the location of elements are the relative position of elements to the centre of array, and AOA and AOD are defined as the direction of signals with respect to the array orientation. Other commonly used models, like uniform linear array and uniform circular arrays are suitable for different telecommunication environment. The impact of different array shapes on FIM expressions obtained in this thesis is negligible, and the FIM expressions can be extended to other arrays.

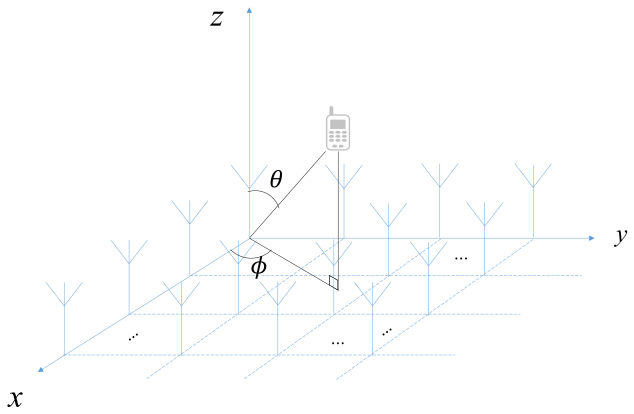

Figure 2.4: Layout of uniform rectangular array

2.6 Beamforming for Massive Array

Beamforming techniques employed by antenna arrays is used to transmit or receive signals on the desired direction. Beamforming is aimed at adjusting the amplitude and phase of signals, in order to enhance the signals on the desired direction by constructively interference while mitigate those on the other direction by destructive interference. The performance of localisation also depend on the applied beamforming schemes, due to different signal power on each directional beam. Some common beamforming schemes include directional beamforming [26], random beamforming [27], phased-array beamforming and timed array beamforming [28]. Note that, the beamforming technique employed by this thesis is only referred to analog beamforming (also named as RF chain beamforming), while digital beamforming and hybrid beamforming are out of the scopes of our research, since digital beamforming does not contain any location information.

2.7 Intelligent Surface Assisted Communication

IS is the promising technique envisioned for B5G and even future sixth generation (6G) networks. IS in this thesis is referred to reflective surface of electromagnetic materials, whose phase and amplitude responses at each individual element are electronically controlled with integrated electronics [29]. From the perspective of hardware, ISs have PIN

diodes embedded on connection parts to control each meta element switch on and off, and tune phase shift by adjusting the bias voltage on capacitors. Thus, the amplitudes and phase of reflected signals can be modified. Moreover, IS also works as steerable array. Based on the detected channel quality information (CQI) reported by BSs and MSs, the channel of CQI below the predefined threshold [30] is reinforced by IS, while for the channel of CQI above the threshold, of which MSs are directly served by the BSs through LOS paths. Therefore, IS can be utilised for many applications, such extending cell coverage to dead-zone, suppressing inter-user interference and improving security through focusing signals to desirable direction, etc.

IS design is always a challenging problem, which can be generally classified as two categorises, *i.e.*, electromagnetic based design and communication based design [31]. Electromagnetic based design of IS focuses on the functions of hardware, *e.g.*, reflection, transmission, polarization, etc. Communication based design of IS regards IS as a modification on phases and amplitudes of signals, and concentrate on the functions of IS and the impacts on the networks, *e.g.*, capacity of channel, cell coverage, energy efficiency, etc. For example, IS design of maximised data rate is formulated as optimisation problem of ISpsf with respect to maximised SNR, which is different with the IS assisted energy efficiency problem. Therefore, IS should be designed on a case-by-case basis.

The received signal power of IS-aided channel is up to 4 times than the LOS signal [29] in the classical two-ray model, where the incidence angle equal to reflection angle. The IS is also found more effective on increasing the signal-to-noise ratio (SNR) at MS than massive MIMO, since the received signal power increases with the number of reflector elements N_{IS} in the rate of $\mathcal{O}(N_{\mathrm{IS}}^2)$, which is higher than $\mathcal{O}(N_{\mathrm{IS}})$ achieved by massive MIMO arrays. The performance limits of near field large intelligent surface-assisted positioning was evaluated by CRLB in [13],[14],[32],[33],[34]. However, some recent work states that the benefits on SNR at the MS is upper bounded by the path loss from transmitter to the IS [35], and the polarisation mismatch between the transmitter and the near field IS varies with incident angle and plays a major impact on the received signal power [36].

2.8 Localisation Algorithms

There are hundreds of thousands of algorithms proposed in the existing work. Most of them were based on (multi)lateration, optimisation, maximum likelihood, Bayesian network, learning, database matching, etc. However, we focus on least-square and semi-

definite programming localisation algorithms. LS estimator is one of most common used (multi)lateration methods to derive the location of MS with closed form solution. It has low complexity, and is vulnerable to large measurement error. The LS estimator can be rewritten as optimisation of the higher accuracy through applying semi-definite relaxation.

2.8.1 Least-Square Based Method

Considering the localisation of one stationary MS assisted by N terrestrial BSs. Assume that the MS at the position $\mathbf{v} = [x, y]^{\mathrm{T}}$, is detected and located by N BSs, where coordinates of the i-th BS is $\mathbf{w}_i = [x_i, y_i]^{\mathrm{T}}, i = 1, 2, \ldots, N$. The real distance from MS to the i-th BS is denoted by $d_i = \|\mathbf{v} - \mathbf{w}_i\|$. The RSS based localisation problem solved by optimisation is formulated as following [2]

$$(P2.1) \qquad \min_{\mathbf{v}} \sum\nolimits_{i=1}^{N} (\widehat{PL}_i - PL_i)^2 \tag{2.6}$$

where the estimated path loss $\widehat{PL}_i$ and real path loss PL_i at the i-th BS are respectively expressed as $\widehat{PL}_i = 10\eta_i \log_{10} \tilde{d}_i$ and $PL_i = 10\eta_i \log_{10} d_i$, and $\tilde{d}_i$ is ranging distance.

The i-th measured path loss value is obtained by $\widetilde{PL}_i = Pt[dBm] - Pr_i[dBm]$, where Pt is the transmit power of MS, Pr_i is the RSS at the i-th BS. If the real PLE η_i is perfectly known, the ranging distance is calculated as $\tilde{d}_i = 10^{\widetilde{PL}_i/(10\eta_i)}$, otherwise, an estimated PLE $\hat{\eta}$ is applied for calculating the ranging distance as $\tilde{d}_i = 10^{\widetilde{PL}_i/(10\hat{\eta}_i)}$. $\widehat{PL}_i$ and PL_i in $(P2.1)$ are only dependent on ranging distance and PLE. $(P2.1)$ is converted to the general ranging based localisation problem $(P2.2)$, which is suitable for both RSS, DRSS, TOA and/or TDOA based localisation [2].

$$(P2.2) \qquad \min_{\hat{\mathbf{v}}} \sum_{i=1}^{N} (\hat{d}_i - d_i)^2 \tag{2.7}$$

where $\hat{d}_i = \|\hat{\mathbf{v}} - \mathbf{w}_i\|$ is the estimated distance between estimated location of MS and BS i, The solution to $(P2.2)$ is obviously $\hat{d}_i = d_i$. However, the real distance d_i is always unknown in practice, due to imperfect knowledge of position-related channel parameters. Thus, the solution to $(P2.2)$ lies in substituting ranging distance $\tilde{d}_i$ to d_i, whose accuracy is determined by both applied algorithm and accuracy of ranging distance $\tilde{d}_i$.

2.8.2 Semi-Definite Programming Based Method

A general form of semi-definite programming (SDP) problem is formulated as [37]

$$\text{minimise} \quad \mathbf{c}^{\mathrm{T}}\mathbf{x} \tag{2.8}$$

s.t.

$$\mathbf{F}(\mathbf{x}) \succcurlyeq \mathbf{0} \tag{2.9}$$

$$\mathbf{A}\mathbf{x} = \mathbf{B} \tag{2.10}$$

where $\mathbf{x}$ is the target variable, $\mathbf{c}$ is the set of known parameters. An SDP problem consists of a linear objective function and multiple equality and inequality constraints of both linear and convex functions. The linear matrix inequality (2.9) collects all inequality constraints, and (2.10) contains all equality constraints. An semi-definite cone can relax the inequality constraints. For example, semi-definite relaxation can be illustrated as

$$\begin{bmatrix} \mathbf{x}_1 & \mathbf{x}_2 \\ \mathbf{x}_2^{\mathrm{T}} & \mathbf{x}_3 \end{bmatrix} \succcurlyeq \mathbf{0} \Leftrightarrow \mathbf{x}_1\mathbf{x}_3 \succcurlyeq \mathbf{x}_2\mathbf{x}_2^{\mathrm{T}} \tag{2.11}$$

where $\mathbf{x}_1$ and $\mathbf{x}_3$ are symmetric matrices.

SDP is employed by our research, since the SDP relaxation can convert the quadratic functions of variables in localisation problem to linear, *e.g.*, (2.7).

Chapter 3

Low Complexity Cooperative Positioning in Multipath Environment

3.1 Introduction

Mobile localisation is an important yet challenging issue due to adverse propagation environment [2]. Widely used mobile localisation methods are based on parameters like TOA [38], AOA [20], AOD [39], and RSS [40],[41].

The main error of mobile localisation is the NLOS error caused by multipath and scattering environment, which significantly affects TOA, AOA, and AOD. The study on mitigating single-bounce NLOS error caused by scattering of different models can be found in [42]-[43]. But these methods are based on stationary environment, and their localisation accuracy is lower than that of the techniques in [44]-[45] which utilise successive measurements and study mobile tracking in scattering environment. Their results show that the accuracy can be improved by continuous iteration and utilising more measurements. Therefore, it is crucial to improve the original work by other methods which can supply more measurements, such as cooperative localisation.

The single-bounce scattering model is considered to be suitable for mm-wave transmission environment [46],[47]. Thus, it is worth studying localisation with single-bounce NLOS dominant scattering environment. The previous work on localisation with single-

bounce scattering was based on non-cooperative localisation. In the design of weight for each path in the problem formulation, they utilised equal weight [42],[43], or variance of estimated location [44],[48], or only the variance of TOA ranging [45] as weight to reduce the variation of estimation, but did not consider the effect of AOA and AOD on weight.

Cooperative localisation is an approach to localise the target with measurements collected from both known and unknown nodes in collaboration. Distributed cooperative localisation based on Bayesian estimation methods were investigated for wireless sensor networks (WSN) [49],[50] and wireless local area network (WLAN) [51]. Centralised cooperative localisation is more suitable for cellular networks thanks to the availability of Evolved Serving Mobile Location Center (E-SMLC) [52]. Most work on cooperative localisation [52],[53] did not consider NLOS errors due to scattering and requires higher computational complexity than non-cooperative localisation [54] in contrast to mobile users' demands for timely estimation of their location. However, most previous work on reducing running time of distributed cooperative localisation techniques like [49, 50] are limited by their own problem formulation and Bayesian estimation methods, and they cannot be employed by Centralised cooperative localisation which is solved by nonlinear programming.

In this chapter, a cooperative localisation technique is proposed, which employs not only RSS but also TOA, AOA, and AOD, to mitigate NLOS errors caused by single-bounce scattering. This work is different from the conventional work on cooperative localisation which usually ignore the NLOS error caused by scattering. To the best of our knowledge, this is the first work to consider cooperative localisation for mitigating the scattering effect on TOA, AOA, and AOD, named as CLTAAR. Also, it achieves higher accuracy than conventional cooperative localisation [2] in presence of single-bounce scattering. With prior knowledge on distribution of measurement error, an adaptive weight is proposed to improve CLTAAR to wCLTAAR of the higher robustness against measurement error. Second, an MS grouping strategy is utilised to decompose the original entire optimisation problem to multiple fractional optimisation problems, and save running time. The proposed MS grouping strategy does not make any change on estimation algorithm, so that it is compatible with others' estimation algorithms. CLTAAR enhanced by MS grouping scheme, named as eCLTAAR, is shown to achieve much less computational cost than CLTAAR and little reduction on accuracy. The CRLB is also derived for analytical assessment. Finally, a weight function of TOA, AOA, and AOD is also proposed to further mitigate NLOS errors of BS-MS detection in scattering environment, which has not been studied by the previous work [42]-[45].

The rest of this chapter is organised as follows. Section 3.2 illustrates the assumptions made and system model adopted by the work. CLTAAR and eCLTAAR technique with MS grouping strategy are proposed in Section 3.3, along with the CRLB. The simulation results and discussion are presented in Section 3.4. Finally, a summary is drawn in Section 3.5.

3.2 System Model and Problem Formulation

We assume a cluster of M collaborative MSs localised by B BSs through downlink observations collected from the $l = 1, \ldots, C$ single-bounce NLOS paths. Figure 3.1 displays an example of cooperative localisation with 1 BS and 2 collaborative MSs in single-bounce scattering environment, and the LOS direction is selected as the reference. Denote the position of m-th MS as $\mathbf{v}_m = [x_m, y_m]^{\mathrm{T}}, m = 1, \ldots, M$. The coordinate of i-th BS $\mathbf{w}_i = [x_{\mathrm{BS}i}, y_{\mathrm{BS}i}]^{\mathrm{T}}, i = 1, \ldots, B$ is perfectly known. Thus, the direct distance between the m-th MS and i-th BS is calculated as $D_{mi} = \|\mathbf{v}_m - \mathbf{w}_i\|$, and the distances from the c-th scatter to the MS and BS are respectively calculated as $r_{\mathrm{R},jc} = \|\mathbf{v}_j - \mathbf{q}_c\|$ and $r_{\mathrm{T},ci} = \|\mathbf{q}_c - \mathbf{w}_i\|$. Denote the real length of single-bounce path from MS m to BS i through scatter c as D_{mci}, then the estimate of TOA is expressed as [2, 38]

$$\tilde{\tau}_{mci} = (r_{\mathrm{R},jc} + r_{\mathrm{T},ci})/c_0 + n_{mi} \tag{3.1}$$

where $c_0 = 3e8$ m/s is the speed of light. $n_{mi} \sim \mathcal{N}(0, \sigma_\tau^2)$ is the zero-mean Gaussian distributed error. Thus, TOA derived ranging distance is $\tilde{r}_{mci} = \tilde{\tau}_{mci} 3e8$. The AOA θ_{ci} and AOD ϑ_{mc} of signals in the NLOS environment are modelled as [2],[20],[39]

$$\tilde{\theta}_{mc} = \theta_{mc} + \varepsilon_{\theta,mc} + \xi_{\theta,mc} \tag{3.2}$$

$$\tilde{\vartheta}_{ci} = \vartheta_{ci} + \varepsilon_{\vartheta,ci} + \xi_{\vartheta,ci} \tag{3.3}$$

where $\xi_{\theta,mc}$ and $\xi_{\vartheta,ci}$ are the extra angle deflected by a scatter in a single-bounce NLOS path for AOA and AOD, respectively. $\varepsilon_{\theta,mc} \sim \mathcal{N}(0, \sigma_\theta^2)$ and $\varepsilon_{\vartheta,ci} \sim \mathcal{N}(0, \sigma_\vartheta^2)$ are the measurement noise of AOA and AOD. With the fixed length between BS and MS, the position of a scatter determines the trace of a NLOS path. Thus, the coordinate of the scatter is calculated as $\mathbf{q}_c = \mathbf{w}_i + r_{\mathrm{T},ci}\mathbf{K}(\vartheta_{ci})$, and the position of MS is $\mathbf{v} = \mathbf{q}_c - r_{\mathrm{R},mc}\mathbf{K}(\theta_{mc})$, where $\mathbf{K}(\theta) = [\cos(\theta), \sin(\theta)]^{\mathrm{T}}$ is the unit direction function in 2D Cartesian coordinate system.

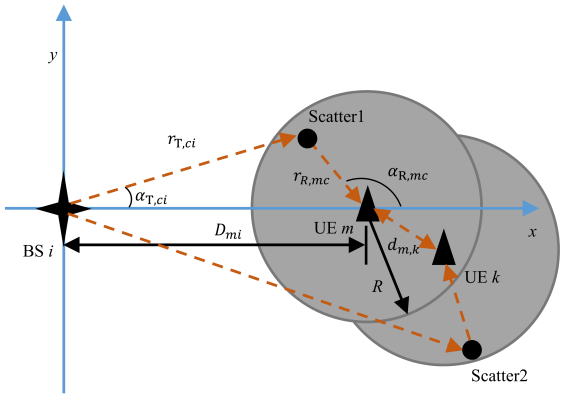

Figure 3.1: Cooperative localisation with the serving BS and MSs in single-bounce scattering scenario, where the distribution of scatters follows the uniform disk model.

Denote the angles of mci-th NLOS path apart from the BS-MS LOS direction as $\alpha_{\mathrm{T},mc}$ and $\alpha_{\mathrm{R},ci}$, *i.e.*, $\alpha_{\mathrm{T},ci} = \tilde{\vartheta}_{ci} - \vartheta_{ci}, \alpha_{\mathrm{R},mc} = \tilde{\theta}_{mc} - \theta_{mc}$, then the probability density function (pdf) of a uniform disk scattering model can be expressed as [25]

$$p(r_{\mathrm{R},mc}, \alpha_{\mathrm{R},mc}) = \begin{cases} \frac{r_{\mathrm{R},mc}}{\pi R_{\mathrm{c}}^2}, & 0 \leqslant r_{\mathrm{R},mc} \leqslant R_{\mathrm{c}}, -\pi \leqslant \alpha_{\mathrm{R},mc} \leqslant \pi \\ 0, & \text{otherwise} \end{cases} \tag{3.4}$$

where R_{c} is the radius of scattering environment. According to the cosine law, the total length of deflected path is expressed by

$$D_{mci} = r_{\mathrm{R},ci} + \sqrt{r_{\mathrm{R},ci}^2 + D_{mi}^2 + 2 r_{\mathrm{R},ci} D_{mi} \cos(\alpha_{\mathrm{R},mc})} \tag{3.5}$$

MS m localise the neighbouring MS k with the relative measurements RSS, and the RSS at MS m is modelled as close-in path loss model, *i.e.*, $Pr_m[\mathrm{dBm}] = Pt_k[\mathrm{dBm}] - (A + 10\eta \log_{10}(d_{m,k})) + X_{S,m,k}$ [2], where Pt is the transmit power, $A = 20 \log_{10}(4\pi f_c / c_0)$ is a known constant, f_c is the system frequency, η is path loss exponent, $X_{S,m,k} \sim \mathcal{N}(0, \sigma_{\mathrm{RSS}}^2)$ is shadowing, $d_{m,k} = \|\mathbf{v}_m - \mathbf{v}_k\|$ is the real distance between MS m and MS k. The pathloss measurement model is converted to the classical exponential-like ranging function $d_{m,k} = 10^{(Pt_k - Pr_m + X_{S,m,k} - A)/(10\eta)}$. Considering that shadowing $X_{S,m,k}$ is unknown in practice, the measured ranging distance is calculated as

$$\tilde{d}_{m,k} = 10^{\frac{\widehat{PL}_{m,k}}{10\eta}} \tag{3.6}$$

where $\widetilde{PL}_{m,k} = Pt_k - Pr_m + X_{S,m,k} - A$ is the pathloss observed at MS m. Note that, at least two NLOS paths are required to guarantee acceptable localisation results [42],[43],[55].

3.3 Cooperative Localisation for Mitigating NLOS Error Due to Single-Bounce Scattering Effect and the Mobile Station Grouping Scheme

First, we present CLTAAR technique to search the optimal location of collaborated MSs which achieve the minimum summation of residual error of BS-MS ranging and MS-MS ranging. Second, MS grouping strategy is proposed to reduce the complexity of cooperative approaches. Third, eCLTAAR is obtained from separating the unknown MSs in CLTAAR according to MS grouping method.

3.3.1 Cooperative Loclisation for Mitigating NLOS Error Due to Single-Bounce Scattering

Cooperative localisation is an approach to determine geographical location of the target with measurements collected from a number of nodes. The cooperative localisation is formalised as an optimisation problem with respect to multivariable objective function. The CLTAAR is formed by the BS-MS ranging and angle objective function $\mathrm{f}_{\mathrm{BS-MS}}$, and MS-MS ranging objective function $\mathrm{f}_{\mathrm{MS-MS}}$. The weight function w_{mci} denotes the weight of residual error for the c-th path between MS m and BS i, and it is derived as the variance of each term introduced by $\mathrm{f}_{\mathrm{BS-MS}}$

$$w_{mci} = \mathrm{var}(B_{mci}) + \mathrm{var}(\mathbf{A}_{mci})((\mathbf{v}_m - \mathbf{w}_i) \odot (\mathbf{v}_m - \mathbf{w}_i)) \tag{3.7}$$

where

$$\begin{aligned}
\mathrm{var}(B_{mci}) =& (c_0^2\sigma_\tau^2 + D_{mi}^2)(0.5 - 0.5e^{-2(\sigma_\theta^2+\sigma_\vartheta^2)}\cos(2\theta_{mci} - 2\vartheta_{mci})) - \\
& D_{mc}^2(e^{-0.5(\sigma_\theta^2+\sigma_\vartheta^2)}\sin(\theta_{mci} - \vartheta_{mci}))^2 \\
B_{mci} =& r_{mci}\sin(\tilde{\theta}_{mci} - \tilde{\vartheta}_{mci}) \\
\mathrm{var}(\mathbf{A}_{mci}) =& \begin{bmatrix} A1 & A2 \end{bmatrix} \\
\mathbf{A}_{mci} =& \begin{bmatrix} \sin(\tilde{\theta}_{mci}) + \sin(\tilde{\vartheta}_{mci})) & -(\cos(\tilde{\theta}_{mci}) + \cos(\tilde{\vartheta}_{mci})) \end{bmatrix} \\
A1 =& 1 - 0.5e^{-2\sigma_\theta^2}\cos(2\theta_{mci}) - (e^{-0.5\sigma_\theta^2}\sin(\theta_{mci}))^2 - 0.5e^{-2\sigma_\vartheta^2}\cos(2\vartheta_{mci}) -
\end{aligned}$$

$$
\begin{aligned}
& (e^{-0.5\sigma_{\vartheta}^2}\sin(\vartheta_{mci}))^2 \\
A2 =& 1 + 0.5e^{-2\sigma_{\theta}^2}\cos(2\theta_{mci}) - (e^{-0.5\sigma_{\theta}^2}\sin(\theta_{mci}))^2 + 0.5e^{-2\sigma_{\vartheta}^2}\cos(2\vartheta_{mci}) - \\
& (e^{-0.5\sigma_{\vartheta}^2}\sin(\vartheta_{mci}))^2
\end{aligned}
$$

CLTAAR is formulated as a least-square optimisation problem

$$(P3.1) : \hat{\mathbf{V}} = arg\min_{\mathbf{V}}\{\mathrm{f}_{\mathrm{BS-MS}}(\mathbf{V}) + \mathrm{f}_{\mathrm{MS-MS}}(\mathbf{V})\} \tag{3.8}$$

$$\mathrm{f}_{\mathrm{BS-MS}}(\mathbf{V}) = \sum_{m=1}^{M}\sum_{i=1}^{B}\sum_{c=1}^{C}\frac{1}{w_{mci}}(B_{mci} - \mathbf{A}_{mci}\mathbf{X}_{mi})^2 \tag{3.9}$$

$$\mathrm{f}_{\mathrm{MS-MS}}(\mathbf{V}) = \sum_{m=1}^{M}\sum_{k=1,k\neq j}^{M}\frac{1}{\sigma_{m,k}^2}(\tilde{d}_{j,k} - d_{j,k})^2 \tag{3.10}$$

where $\mathbf{V} = [\mathbf{v}_1, \ldots, \mathbf{v}_M]$, $\mathbf{X}_{mi} = \mathbf{v}_m - \mathbf{w}_i$. $\sigma_{m,k}^2$ is the variance of ranging distance derived from relative measurement between MS m and MS k. The nonlinear programming problem $(P3.1)$ can be solved by iterative numerical algorithms, *e.g.*, Quasi-Newton method and Nelder-Mead method.

3.3.2 Cooperative Localisation Enhanced by Mobile Station Grouping Scheme

MS grouping scheme reallocates the MSs to different groups in terms of σ_{RSS}. Thus, the original localisation problem is decomposed to multiple problems of smaller sets of unknown variables with running time reduced. In order to maintain a certain degree of accuracy, the MSs of the low measurement error are assigned to one group, and the MSs of the high error are assigned to the other group, so that the MSs of high measurement error can be isolated from those of low error. The degree of measurement error is indicated by the standard deviation of relative measurements from each MS. Then, MSs $m = 1, \ldots, M_1$ of the lower error are localised first, followed by those MSs $m = M_1 + 1, \ldots, M$ of the higher error. For example, a terminal group with two-grouping separation is shown in Figure 3.2, where MS $m = 1, 2, 3$ are in the group $h1$ to be first localised, while MS $m = 4$ is in the group $h2$ to be localised based on the results of group $h1$. Based on (3.9)-(3.10), the cost

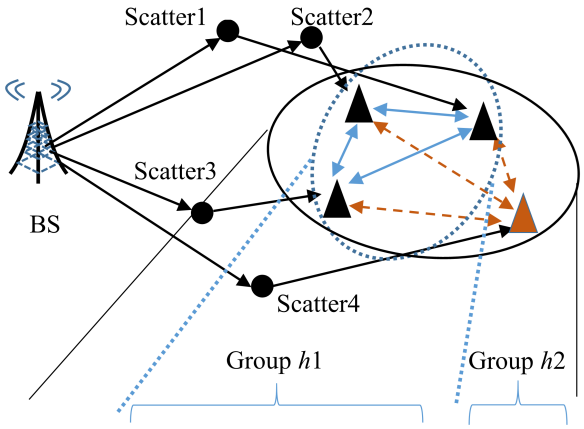

	MS1	**MS2**	**MS3**	**MS4**
MS1	NaN	$\tilde{d}_{1,2}$	$\tilde{d}_{1,3}$	$\tilde{d}_{1,4}$
MS2	$\tilde{d}_{2,1}$	NaN	$\tilde{d}_{2,3}$	$\tilde{d}_{2,4}$
MS3	$\tilde{d}_{3,1}$	$\tilde{d}_{3,2}$	NaN	$\tilde{d}_{3,4}$
MS4	$\tilde{d}_{4,1}$	$\tilde{d}_{4,2}$	$\tilde{d}_{4,3}$	NaN

Figure 3.2: Cooperative localisation enhanced by MS grouping, where 4 MSs are reallocated to 2 groups.

functions of localisation of the two groups of MSs are denoted by

$$\mathrm{f}_{\mathrm{BS-MS}h1}(\mathbf{V}_{h1}) = \sum_{m\in h1}\sum_{i=1}^{B}\sum_{c=1}^{C}\frac{1}{w_{mci}}(B_{mci}-\mathbf{A}_{mci}\mathbf{X}_{mi})^2$$

$$\mathrm{f}_{\mathrm{MS}h1-\mathrm{MS}h1}(\mathbf{V}_{h1}) = \sum_{m\in h1}\sum_{k\in h1,k\neq j}\frac{1}{\sigma^2_{m,k}}(\tilde{d}_{j,k}-d_{j,k})^2$$

$$\mathrm{f}_{\mathrm{BS-MS}h2}(\mathbf{V}_{h2}) = \sum_{m\in h2}\sum_{i=1}^{B}\sum_{c=1}^{C}\frac{1}{w_{mci}}(B_{mci}-\mathbf{A}_{mci}\mathbf{X}_{mi})^2$$

$$\mathrm{f}_{\mathrm{MS}h1-\mathrm{MS}h2}(\mathbf{V}_{h2}) = \sum_{m\in h1}\sum_{k\in h2,k\neq j}\frac{1}{\sigma^2_{m,k}}(\tilde{d}_{j,k}-d_{j,k})^2$$

$$\mathrm{f}_{\mathrm{MS}h2-\mathrm{MS}h1}(\mathbf{V}_{h2}) = \sum_{m\in h2}\sum_{k\in h1,k\neq j}\frac{1}{\sigma^2_{m,k}}(\tilde{d}_{j,k}-d_{j,k})^2$$

$$\mathrm{f}_{\mathrm{MS}h2-\mathrm{MS}h2}(\mathbf{V}_{h2}) = \sum_{m\in h2}\sum_{k\in h2,k\neq j}\frac{1}{\sigma^2_{m,k}}(\tilde{d}_{j,k}-d_{j,k})^2$$

Table 3.1: Computational Complexity of Estimation Solved by Quasi-Newton Method of ε - Optimality for the Worst Case (Q: number of groups, M_q: number of MS assigned to each group)

Analytical Complexity	
before MS grouping, *i.e.*, $(P3.1)$	after MS grouping, *i.e.*, $(P3.2)$
$\mathcal{O}((M^2+6M^2BC+4M^3)\varepsilon^{-2})$	$\mathbf{O}(\sum_{q=1}^{Q}(M_q^2+6BCM_q^2+4M_q^3)\varepsilon^{-2})$

Table 3.2: Normalised Computational Complexity of Estimation Solved by Quasi-Newton Method of ε - Optimality for the Worst Case ($\varepsilon=0.1, Q=2, M=4, M_1=3, M_2=1, B=1, C=4$)

Normalised Complexity	
before MS grouping, *i.e.*, $(P3.1)$	after MS grouping, *i.e.*, $(P3.2)$
2.65	1

Then, the problem $(P3.1)$ is divided to two parts

$$(P3.2): \hat{\mathbf{V}}_{h1} = arg\min_{\mathbf{V}_{h1}}\{\mathrm{f}_1(\mathbf{V}_{h1})\} \tag{3.11}$$

$$\mathrm{f}_1(\mathbf{V}_{h1}) = \mathrm{f}_{\mathrm{BS-MS}h1}(\mathbf{V}_{h1}) + \mathrm{f}_{\mathrm{MS}h1-\mathrm{MS}h1}(\mathbf{V}_{h1}) \tag{3.12}$$

$$\hat{\mathbf{V}}_{h2} = arg\min_{\mathbf{V}_{h2}}\{\mathrm{f}_2(\mathbf{V}_{h2})\} \tag{3.13}$$

$$\mathrm{f}_2(\mathbf{V}_{h2}) = \mathrm{f}_{\mathrm{BS-MS}h2}(\mathbf{V}_{h2}) + \mathrm{f}_{\mathrm{MS}h1-\mathrm{MS}h2}(\mathbf{V}_{h2}) + \mathrm{f}_{\mathrm{MS}h2-\mathrm{MS}h1}(\mathbf{V}_{h2}) + \mathrm{f}_{\mathrm{MS}h2-\mathrm{MS}h2}(\mathbf{V}_{h2}) \tag{3.14}$$

where $\hat{\mathbf{V}}_{h1}$ obtained from (3.11) is substituted to (3.13) to assist the estimation of $\mathbf{V}_{h2}$. The MS grouping scheme does not change the original method, and reduce computation time by divide the original optimisation problem into multiple optimisations with the less computation and unknown variables. Table I and II display comparison of analytical complexity of $(P3.1)$ and $(P3.2)$ solved by Quasi-Newton method of ε - optimality.

The complexity displayed in Tables I and II is evaluated in terms of the number of multiplications and square root. MS grouping method is expected to be effective with large terminal group which consists of many anchors and measurements.

Based on the above two parts, the eCLTAAR technique leverages the same objective function as CLTAAR technique, but reallocate the estimation sequence with MS grouping. The estimation of eCLTAAR technique can be summarised as Algorithm 1. For the real

Algorithm 1 eCLTAAR Algorithm

1: Reallocate the terminal group based on the obtained standard deviation of MS-MS relative measurement.
2: Estimate the coordinates of MS in group h1 $\hat{\mathbf{V}}_{h1}$ through (3.11)-(3.12).
3: Substitute $\hat{\mathbf{V}}_{h1}$ to (3.13)-(3.14), estimate the coordinates of the left MS in group h2 $\hat{\mathbf{V}}_{h2}$.

practice, the number of collaborated MS is expected to be not greater than six. Thus, a two-grouping separation is sufficient to apply for eCLTAAR in a cell.

3.3.3 Cramer-Rao Lower Bound on the Proposed Cooperative Localisation Methods

Cramer Rao Lower Bound (CRLB) expresses the minimum variance of an estimator. Now, we present the CRLB of the proposed CLTAAR and eCLTAAR location problem. Denote the mci-th variance of measurement error of TOA, AOA, AOD, and RSS as $Q_{r,mci} = \sigma_\tau^2, Q_{\theta,mci} = \epsilon_{\theta,mci}^2, Q_{\vartheta,mci} = \epsilon_{\vartheta,mci}^2, Q_{d,mi} = X_{S,m,k}^2$. Conditional pdf of TOA ranging distance at MS m is

$$p(\tilde{\mathbf{r}}_m|\mathbf{v}_m) = \prod_{i=1}^{B}\prod_{c=1}^{C} \frac{1}{\sqrt{2\pi Q_{r,mci}}} e^{-\frac{(\tilde{r}_{mci}-r_{mci})^2}{2Q_{r,mci}}} \tag{3.15}$$

The derivation of conditional pdf of the other measurements are omitted here, which follows the same idea as (3.15). Then, the joint conditional log-likelihood of TOA, AOA, AOD is

$$\Lambda_{\mathrm{BS-MS}}(\mathbf{v}_m) = \ln(p(\tilde{\mathbf{r}}_m|\mathbf{v}_m)p(\tilde{\boldsymbol{\theta}}_m|\mathbf{v}_m)p(\tilde{\boldsymbol{\vartheta}}_m|\mathbf{v}_m)) \tag{3.16}$$

The FIM of CLTAAR is calculated as

$$\mathbf{F}_{\mathrm{CLTAAR}} = \mathbf{F}_{\mathrm{BS-MS}} + \mathbf{F}_{\mathrm{MS-MS}} \tag{3.17}$$

where $\mathbf{F}_{\mathrm{BS-MS}}$ and $\mathbf{F}_{\mathrm{MS-MS}}$ represent the FIM of BS-MS observations and MS-MS observations, respectively. The FIM of MS m is calculated as that in [56]

$$\mathbf{F}_{\mathrm{BS-MS},m} = -\mathbb{E}\left[\left(\frac{\partial \Lambda_{\mathrm{BS-MS}}}{\partial \mathbf{v}_m}\right)^{\mathrm{T}}\left(\frac{\partial \Lambda_{\mathrm{BS-MS}}}{\partial \mathbf{v}_m}\right)\right] \tag{3.18}$$

FIM of eCLTAAR is similar as that of CLTAAR technique, but the FIM is separated into two groups. Therefore, the derivation of FIM and CRLB of eCLTAAR are separated in terms of different groups. FIM of the group $h1$ has the same format as that of MSs in group $h1$ in CLTAAR

$$\mathbf{F}_{h1} = \mathbf{F}_{\text{BS}-\text{MS}h1} + \mathbf{F}_{\text{MS}h1-\text{MS}h1} \tag{3.19}$$

FIM of MSs in group $h2$ is calculated as

$$\mathbf{F}_{h2} = \mathbf{F}_{\text{BS}-\text{MS},h2} + \mathbf{F}_{\text{MS}-\mathbf{MS},h2} \tag{3.20}$$

$$\mathbf{F}_{\text{BS}-\text{MS},h2} = \begin{bmatrix} \mathbf{F}_{\text{BS}-\text{MS},M_1+1} & \cdots & 0 \\ \vdots & \ddots & \vdots \\ 0 & \cdots & \mathbf{F}_{\text{BS}-\text{MS},M} \end{bmatrix} + \begin{bmatrix} \mathbf{F}_{\text{MS}-\text{MS},M_1+1} & \cdots & 0 \\ \vdots & \ddots & \vdots \\ 0 & \cdots & \mathbf{F}_{\text{MS}-\text{MS},M} \end{bmatrix} \tag{3.21}$$

$$\mathbf{F}_{\text{MS}-\text{MS},h2} = \begin{bmatrix} \mathbf{F}_{\text{MS}-\text{MS},M_1+1} & \mathbf{K}_{M_1+1,M_1+2} & \cdots & \mathbf{K}_{M_1+1,M} \\ \mathbf{K}_{M_1+2,M_1+1} & \mathbf{F}_{\text{MS}-\text{MS},M_1+2} & \cdots & \mathbf{K}_{M_1+2,M} \\ \vdots & \vdots & \ddots & \vdots \\ \mathbf{K}_{M,M_1+1} & \mathbf{K}_{M,M_1+2} & \cdots & \mathbf{F}_{\text{MS}-\text{MS},M} \end{bmatrix} \tag{3.22}$$

where $\mathbf{K}_{m,k}$ is correlation matrix between MS m and MS k. Finally, the CRLBs for CLTAAR and eCLTAAR are respectively calculated as inverse of their FIMs, where the CRLB of for MS m is obtained as the corresponding m-th block of matrix.

3.4 Simulation Results

In this section, the effect of the proposed CLTAAR and weight function, and eCLTAAR technique have been assessed by simulation. 1000 trials of 6-MS terminal group in radius of 50 m randomly are generated among classical 7 hexagon cells in radius of 1000 m, where only the serving BS is accessible for one trial. Signal frequency is 6 GHz. BS is 10 m high, and MS was 1.5 m high. 4 scatters are uniformly distributed near each MS in the circular area in radius of 200 m. And each NLOS path is measured once. Standard deviation of localisation measurements, i.e. TOA ranging, AOA, and AOD, are 60 m, 5°, and 5° respectively. MS-MS links are always LOS, and the standard deviation of shadowing of MS belonging to group $h1$ is random value between 4 dB, and that of MS in group $h2$ is 12 dB. The D2D path loss model in [57] is leveraged to generate relative measurements. The

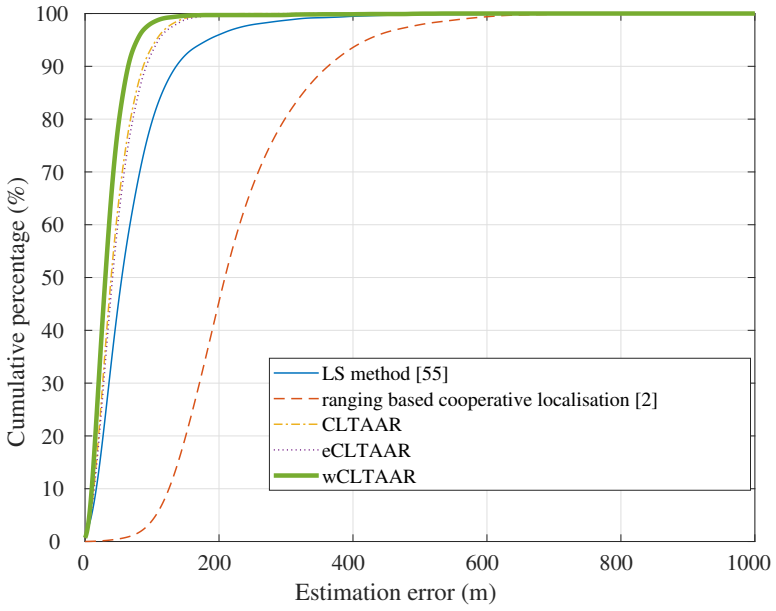

Figure 3.3: Accumulative percentage of estimation error of LS [55], ranging based cooperative localisation [2], CLTAAR, wCLTAAR and eCLTAAR.

setup data is same in all simulation unless specified otherwise. Least square (LS) estimation based on TOA, AOA, and AOD measured on single-bounce NLOS scattered path in [55] and conventional cooperative localisation based on BS-MS detected TOA and MS-MS detected RSS in [2], labelled as 'LS method' and 'ranging based cooperative localisation', are simulated to make comparisons with proposed work. The optimisation problems in the three cooperative approaches are solved by the Nelder-Mead method.

Figure 3.3 describes the higher localisation accuracy achieved by the proposed CLTAAR (no weight), weighted CLTAAR (wCLTAAR), and eCLTAAR techniques over the other two methods. The average localisation errors (ALEs) of the LS [55], ranging based cooperative localisation [2], CLTAAR, eCLTAAR, and wCLTAAR were about 86 m, 224 m, 51 m, 54 m, and 39 m. And STDs of them were about 86 m, 103 m, 32 m, 33 m, and 29 m. Whereas the ranging based cooperative localisation method [2] performed even worse than LS method [55], because it was not designed for localisation with one BS and scattering environment. But the proposed CLTAAR succeeds to integrate the ranging based cooperative localisation [2] with LS [55] and outperforms these two methods. Another proposed

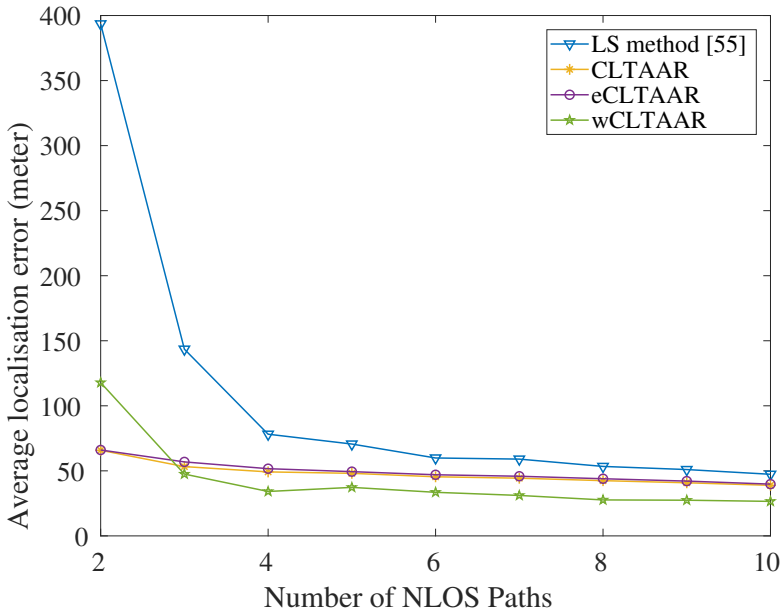

Figure 3.4: Average localisation error of LS [55], CLTAAR, wCLTAAR and eCLTAAR decreases with the number of NLOS measurements on each MS.

eCLTAAR technique is designed to reduce complexity of estimation, and its cumulative percentage error curve almost overlaps that of CLTAAR, which reflects the same degree of accuracy as CLTAAR. Due to weight function, estimation variation is reduced and an improvement of 12-meter average error have been saved by wCLTAAR than CLTAAR.

Figure 3.4 shows that the ALEs of LS [55], CLTAAR, eCLTAAR, and wCLTAAR methods decrease with the number of NLOS paths. eCLTAAR achieves the similar performance as CLTAAR, reflecting the negligible degradation on accuracy casued by MS grouping scheme. ALE of existing LS method [25] is much higher than our proposed methods at the beginning, and decreases with the number of measurements increasing, until approaching those of CLTAAR and eCLTAAR at the end. The proposed wCLTAAR method achieves about half ALE than the other methods. However, it does not work well at the beginning of the trace, since lack of measurements disables the effectiveness of proposed weight function.

The running time is greatly saved by eCLTAAR technique, compared to CLTAAR. The average time spent on localising each MS was about 0.131078 s by CLTAAR technique,

while it were 0.034214 s and 0.997767 s by eCLTAAR and wCLTAAR, indicating a reduction of almost 74% running time. Whereas wCLTAAR consumed extra 5 times running time, due to the additional variables brought by the weight function.

3.5 Summary

In this chapter, we have proposed CLTAAR, wCLTAAR and eCLTAAR approaches to localise collaborative MSs in single-bounce scattering environment, and the CRLBs for CLTAAR and eCLTAAR have been derived. The proposed eCLTAAR technique achieves nearly the same accuracy as and much less computational cost than CLTAAR through applying MS grouping scheme. According to simulation results, about 74% running time was saved by eCLTAAR. The proposed wCLTAAR approach with weight function based on the knowledge of distribution of TOA, AOA, and AOD measurements achieves about twice accuracy than CLTAAR.

Chapter 4

Unmanned Aircraft Vehicle Supported And Received Signal Strength Based Localisation

4.1 Introduction

Unmanned aerial vehicle (UAV) mounted base station (BS) is regarded as a promising complementary solution for 5G in emergency cases like network damage and congestion [58]. UAV-BS provides better LCSs than ground BS due to higher probability of line of sight [59].

Received signal strength (RSS) based localisation of mobile station (MS) [60] has been widely used due to its low cost and low complexity. The terrestrial localisation approaches in [7],[8],[61],[62],[63],[64],[65] utilised RSS based exponential-like ranging function, is obtained by calculating the logarithm of RSS, to estimate mobile station (MS) location. In [8], both RSS and differential RSS based localisation methods were proposed, with anchor coordinates uncertainties and imperfect knowledge of PLE. A multilateration method, referred to as bias-compensated weighted least-square (bcWLS), was proposed in [63], where the perturbations in both RSS measurement error and anchor uncertainties are mitigated. In [64], geometric parameters were proposed for anchor deployment in localisation. A particle filter based on data fusion was proposed in [65]. Multi-dimensional scaling techniques were proposed in [66] to build the connectivity map of deployed sensors.

The ranging function in RSS based localisation is highly dependent on path loss model. In [61],[66], a two-dimensional path loss model was utilised for terrestrial localisation. In [67], [68], a three-dimensional terrestrial path loss model was utilised for UAV assisted and RSS based localisation. However, the UAV air-to-ground path loss model has been reported to be highly dependent on the elevation angle of the path and UAV's altitude [69],[70],[71][72],[73], which was not considered by most existing work. In [73], a localisation approach for elevation angle dependent path loss (EAPL) model was proposed. However, perfectly known and equal PLEs were assumed for all UAVs, which is impractical. With unknown and unequal PLEs, the RSS based localisation problem becomes nonlinear and non-convex, which cannot be solved by the existing approaches.

The accuracy of RSS based localisation with unknown path loss parameters is directly influenced by the estimated PLEs and transmit power [7]-[10],[61]-[63],[74]. The importance of PLEs has been found by the existing work [8],[65],[75], which claimed that the robustness of ranging function against shadowing increases with the values of PLEs. Localisation of MS with unknown transmit power was investigated in [61]. Noncooperative and cooperative localisation approaches with unknown transmit power and unknown path loss exponent (PLE) were studied in [62]. In [7], least-square absolute error of ranging was minimised for localisation. In [10], the Levenberg-Marquardt algorithm (L-M) was proposed to solve the nonlinear problem with unknown and unequal PLEs, whose accuracy is largely subject to measurement errors, due to the potential inappropriate damping factor employed by L-M and unreliable initialisation of PLEs. The above existing approaches are mainly developed with respect to three objectives: 1. to optimise PLEs and transmit power to minimise the differences between path loss measures and path loss estimates, *e.g.*, [61]; 2. to calculate parameters as the ratio between the path loss measures and logarithm of distance estimates, *e.g.*, [62]; 3. to optimise parameters to minimise the residual error of the objective function, *e.g.*, [63]. All of these TSE approximated ranging distance based schemes are severely deteriorated by the imperfect knowledge of path loss model and significant measurement error in harsh environment. The authors of [9],[61],[62], [76] focused on localisation algorithms and finding the optimal coordinates of MS, where the proposed algorithms are aimed at estimating accurate PLEs and transmit power, since they insisted on that localisation accuracy increases with accuracy of estimated PLE and transmit power [77]. PLEs and transmit power are exclusively regarded as crucial environmental parameters of ranging function. However, we find that some proper values of estimated PLEs and transmit power could offer higher accuracy of ranging distance and localisation than

the real PLE and transmit power, which is contrary to the opinion of existing research. Therefore, we are also motivated to investigate the effect of these proper values of PLE and transmit power.

Moreover, the effect of airframe shadowing (AS) due to fixed-wings UAV [59] could cause signal attenuation of up to 35 dB [72]. Therefore, it is necessary to consider the effect of AS on localisation when fixed-wings UAVs are employed, which is absent in existing work, *e.g.*, [78].

In this chapter, we propose a fixed-wings UAV-BSs aided and RSS based localisation technique with unknown and unequal PLEs. Our work is different with the previous work in the following aspects.

1. The nonlinear and non-convex RSS based localisation problem with unknown and unequal PLEs is solved by a piecewise convex approximation aided localisation (PCAL) scheme, with two-step approximations: (a) convert the problem to a nonlinear convex problem through piecewise convex approximation and curve fitting; (b) convert the resulting nonlinear convex problem to a linear convex problem through Taylor's series expansion (TSE) approximation. Unlike the existing methods [7],[8],[61]-[63], PCAL does not require the PLEs associated with different UAVs to be perfectly known and equal to each other, and therefore it is more practical. In this work, the A2G path loss model with unknown and unequal PLEs of different UAV BSs are considered as nuisance parameters and estimated along with the locations of the source nodes.

2. Thanks to its robustness against shadowing, especially AS, the proposed PCAL approach with unknown and unequal PLEs achieves higher accuracy than the approaches [7],[8],[63] with equal and perfectly known PLEs, as well as the approach in [10] with unknown and unequal PLEs. This is because the ranging function via piecewise convex approximation and TSE has much lower variance than those in [7],[8],[10],[63]. To the best of our knowledge, this is also the first work to investigate the impact of AS on UAV assisted and RSS based localisation. The Cramer-Rao lower bound (CRLB) on localisation error is derived to verify the effectiveness of PCAL.

3. With N UAV-BSs to locate one MS, PCAL produces 2^N objective functions and tentative estimates. A grid search assisted ambiguity elimination (GSAE) approach and a differential RSS based grid search (gsDRSS) approach are proposed to obtain

the final estimate of MS location by taking an average of the tentative estimates selected via grid search. GSAE is more effective than the piecewise-linear minimisation (PLM) method [37], because the uncertainty due to shadowing is mitigated by the averaging progress. gsDRSS eliminates the ambiguity through searching the grid of minimum estimation error of DRSS values, at the cost of lower complexity than GSAE. Additionally, gsDRSS also can be used to estimate transmit power and PLEs. The performance of PCAL-GSAE approaches the CRLB derived. PCAL-gsDRSS with unknown transmit power achieves higher accuracy than PCAL with perfectly known transmit power.

4. Through investigating PCAL-gsDRSS scheme and the existing RSS based approaches with unknown PLEs and unknown transmit power, an anti-intuitive finding is drawn by this work that, the real transmit power and PLEs cannot provide accurate localisation or ranging distance, however, some particular values, named as effective transmit power (EPt) and effective PLE (EPLE), can provide 0 localisation and ranging error. Moreover, analysis has proved that a range of values near EPt and EPLE, named as effective transmit power range (EPt-range) and effective path loss exponent range (EPLE-range), have higher accuracy of localisation and ranging than the real parameters. An SDP based algorithm is proposed to estimate EPt, and derive the PCAL-EPt-gsDRSS scheme, which is more accurate than PCAL-GSAE and PCAL-gsDRSS. The effect of EPLE on localisation is investigated.

The rest of this chapter is organised as follows. The system model is presented in Section 4.2. The problem formulation of UAV BS assisted and RSS based localisation is formulated, and solved by proposed algorithms with considering both known and unknown transmit power in Section 4.3. The effects of transmit power and PLE on RSS based localisation and ranging distance are analysed in section 4.4, based on which an enhanced algorithm is proposed. Section 4.5 demonstrates the simulation results, and Section 4.6 gives the summary.

4.2 System Model and Problem Formulation

We consider the localisation of an MS assisted by N UAV-BSs. Assume that the MS with the coordinate vector $\mathbf{v} = [x, y, z]^T$ is detected and located by N UAV-BSs at a time instant (Fig. 4.1). Each UAV-BS supported cell is of horizontal radius R, and the accurate

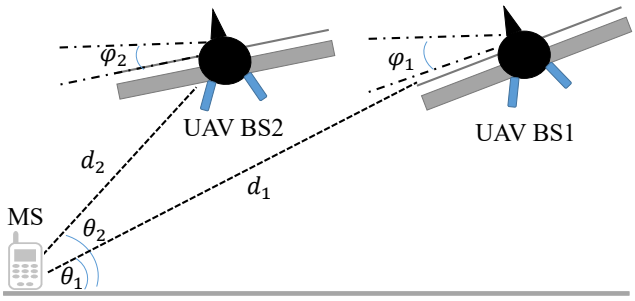

Figure 4.1: Ground MS is located by multiple fixed-wing UAV-BSs

coordinates of the i-th UAV-BS is $\mathbf{w}_i = [x_i, y_i, z_i]^T$, $i = 1, 2, \ldots, N$. The elevation angle of the i-th UAV-BS is θ_i, and the UAV roll angle is φ_i. φ_i and UAV's altitude h_i are available at the UAV control system and barometer/GPS. The localisation problem is

$$(P4.1) \qquad \min_{\mathbf{v}} \sum_{i=1}^{N} (\widehat{PL}_i - \widetilde{PL}_i)^2 \tag{4.1}$$

where $\widehat{PL}_i$ and $\widetilde{PL}_i$ are the estimated and measured path loss at the i-th UAV-BS, respectively.

Considering the effect of AS [72] on path loss, the sum of log-normal random term of AS and the elevation angle dependent terrestrial shadowing (TS) [73] between MS and the i-th UAV-BS is denoted by $X_{S,i}$, with $X_{S,i} \sim \mathcal{N}(0, \sigma^2_{RSS,i})$, and $\sigma^2_{RSS,i} = \sigma^2_{TS,i} + \sigma^2_{AS,i}$, where $\sigma_{TS,i}$ and $\sigma_{AS,i}$ are standard deviation of TS and AS, respectively. With fading smoothed out, the combined path loss and shadowing is expressed as

$$PL_i = Pt\,[\text{dBm}] - Pr_i\,[\text{dBm}] + X_{PL,i} \tag{4.2}$$

where $X_{PL,i} = S_{\text{af},i} + X_{S,i}$ denotes the path loss measurement error, and $S_{\text{af},i}$ is a constant predetermined by the roll angle φ_i. Obviously, $\widetilde{PL}_i = Pt\,[\text{dBm}] - Pr_i\,[\text{dBm}]$, where Pt is the transmit power, and Pr_i is the receive signal power at the i-th UAV.

The EAPL of the i-th UAV is calculated as [73]

$$\widehat{PL}_i = 10\eta_i \log_{10}(d_i) \tag{4.3}$$

$$\eta_i = \frac{a_1}{1 + a_0 e^{-b_0 \theta_i}} + b_1 \tag{4.4}$$

where a_0, a_1, b_0, b_1 are the environmental related parameters, and $\theta_i = \arcsin(h_i/d_i)$ is the elevation angle of the i-th UAV, with h_i being altitude of the i-th UAV, and $d_i = \|\mathbf{v}-\mathbf{w}_i\|$ is defined as the distance from the i-th UAV-BS to MS. Assuming that the perfect knowledge of UAV's altitude h_i is perfectly known, the EAPL in (3) is a function of single variable d_i.

4.3 UAV Assisted and Piecewise Convex Approximation Aided Localisation

It is obvious that $(P4.1)$ is a nonlinear and non-convex optimisation problem. In Subsection 4.3.1, we convert $(P4.1)$ into a convex problem via piecewise convex approximation and curve fitting, and then into a linear problem via TSE. The approximation processes yield 2^N tentative estimates. The estimation ambiguity is eliminated by the GSAE approach in Subsection 4.3.2. Localisation with unknown transmit power is considered in Subsection 4.3.3. The CRLB of PCAL is derived in Subsection 4.3.4.

4.3.1 Piecewise Convex Approximation Aided Localisation

1) Transformation to a Convex Problem via Piecewise Convex Approximation and Curve Fitting: As EAPL is close to a sigmoid curve [73], it can be partitioned into two sub-functions within the propagation distance of interest through piecewise convex approximation [79]. The transition point on EAPL of the i-th UAV is at distance $d_i = d_{t,i}$, which is selected as either a global maxima of the first derivative of EAPL (suitable for model in [73]) or a global minima of the EAPL function (suitable for model in [71]). Assume that the EAPL of the i-th UAV is partitioned into a piecewise convex function of two sub-functions in the intervals of $[d_{lower,i}, d_{t,i}]$ and $[d_{t,i}, d_{upper,i}]$, respectively, where $d_{lower,i}$ and $d_{upper,i}$ are the lower and upper bounds of the propagation distance of interest. Assisted by curve fitting, all the sub-functions are approximated to power functions as

$$\widehat{PL}_{i,g_i} \approx A_{i,g_i} d_i^{B_{i,g_i}} + C_{i,g_i} \tag{4.5}$$

where A_{i,g_i}, B_{i,g_i}, and C_{i,g_i} are the fitted parameters of each sub-function, and $g_i = 0$ or 1 indicates the first or second sub-function, respectively. The approximated path loss (4.5)

can be regarded as a two-slope model. Through simple mathematical manipulations on (4.5), an explicit power-like ranging function is derived as

$$d_i = (1 - g_i)d_{i,0} + g_i d_{i,1} \tag{4.6}$$

where $d_{i,g_i} = ((\widehat{PL}_{i,g_i} - C_{i,g_i})/A_{i,g_i})^{1/B_{i,g_i}}$. Round $\widetilde{PL_i}$ to the interval $[PL(d_{lower,i}), PL(d_{upper,i})]$, in case of complex distance estimation caused by significant shadowing. If one MS is detected by N UAV-BSs, there are total 2^N combinations of (4.5), and 2^N tentative estimates of MS localisation, $\mathbf{v}_j$, $j = 1,2, \ldots, 2^N$. Substituting (4.5) into (4.1) yields $(P4.2)$ for one of the 2^N estimates as

$$(P4.2) \quad \min_{\mathbf{v}_j, d_i} \sum\nolimits_{i=1}^{N} (A_{i,g_i} d_i^{B_{i,g_i}} + \beta_{i,g_i} - \widetilde{PL}_i)^2 \tag{4.7}$$

where $\beta_{i,g_i} = S_{\mathrm{af},i} + C_{i,g_i}$.

2) Transformation to a Linear Problem via Taylor's Series Expansion: The above nonlinear convex problem can be solved by maximum likelihood (ML) estimator. However, it usually requires an accurate initial guess to achieve the global optimal point rather than the local optimal point. To overcome the shortcoming of ML estimator, (4.7) can be rewritten as a linear convex optimisation problem. If $S_{\mathrm{af},i}$ is known, the distance estimation of either interval in (4.6) can be further approximated to linear ranging function through the first-order TSE

$$d_{i,g_i} = \left| \frac{\widetilde{PL}_i - \beta_{i,g_i} + X_{S,i}}{A_{i,g_i}} \right|^{\frac{1}{B_{i,g_i}}} \approx \alpha_{i,g_i} + n_{i,g_i} \tag{4.8}$$

where the absolute operator is utilised to guarantee real value of d_{i,g_i}.

Taking the square of both left-hand and right-hand sides of (4.8) yields $d_{i,g_i}^2 - 2\alpha_{i,g_i} d_{i,g_i} + \alpha_{i,g_i}^2 = n_{i,g_i}^2$, where $\alpha_{i,g_i} = |(\widetilde{PL_i} - \beta_{i,g_i})/A_{i,g_i}|^{1/B_{i,g_i}}$, and $n_{i,g_i}^2 = X_{S,i}^2/(A_{i,g_i}^2 B_{i,g_i}^2)|(\widetilde{PL_i} - \beta_{i,g_i})/A_{i,g_i}|^{2/B_{i,g_i}-2}$ is the mean square error (MSE) of ranging, and variance of n_i is $\sigma_{i,g_i}^2 = \sigma_{RSS,i}^2 |(\widetilde{PL_i} - \beta_{i,g_i})/A_{i,g_i}|^{2/B_{i,g_i}-2}/(A_{i,g_i} B_{i,g_i})^2$. The MSE is smaller than those in [7],[8],[10],[63] due to the two-step approximations. For the scenario with MS in the cell of radius $R = 2000$ m, $h_i = 1000$ m, and environmental data for urban area is $a_0 = 45$, $a_1 = -1.5$, $b_0 = 10$, $b_1 = 3.5$, the minimum standard deviation in (4.8) $\sigma_{i,g_i} \approx 30\,\sigma_{RSS,i}$, is smaller than that in [7],[8],[10],[63] (about $115\,\sigma_{RSS,i}$). If g_i is known, $(P4.2)$ is further

converted to a semi-definite programming (SDP) problem:

$$(P4.3) \qquad \min_{\mathbf{v},d_i,D_i,\mathbf{Z}} \sum_{i=1}^{N} p_{i,g_i}(D_i - 2\alpha_{i,g_i}d_{i,g_i}) \tag{4.9}$$

s.t.

$$D_i = \begin{bmatrix} \mathbf{w}_i \\ -1 \end{bmatrix}^T \begin{bmatrix} \mathbf{I}_3 & \mathbf{v} \\ \mathbf{v}^{\mathrm{T}} & \mathrm{Z} \end{bmatrix} \begin{bmatrix} \mathbf{w}_i \\ -1 \end{bmatrix} \tag{4.10}$$

$$\begin{bmatrix} D_i & d_{i,g_i} \\ d_{i,g_i} & 1 \end{bmatrix} \succcurlyeq \mathbf{0}, \tag{4.11}$$

$$d_{lower,i} \leqslant d_{i,g_i} \leqslant d_{t,i} \text{ or } d_{t,i} \leqslant d_{i,g_i} \leqslant d_{upper,i} \tag{4.12}$$

$$\begin{bmatrix} \mathbf{I}_3 & \mathbf{v} \\ \mathbf{v}^T & \mathrm{Z} \end{bmatrix} \succcurlyeq \mathbf{0} \tag{4.13}$$

where $p_{i,g_i} = 1/\sigma^2_{i,g_i}$ is the weight of objective function, and $\mathbf{I}_3$ is 3-by-3 identity matrix, and $\mathrm{Z} \succcurlyeq \mathbf{v}^T\mathbf{v}$ is the auxiliary variable. $(P4.3)$ can be solved by interior-point method.

4.3.2 Elimination of Estimation Ambiguity

The proposed PCAL approach benefits from the low MSE of ranging. However, when the interval of ranging distance g_i is unknown, estimation ambiguity introduced by piecewise functions brings extra estimation error. It is eliminated by the GSAE approach: first finding a reference point $\mathbf{v}_{GS}$ through solving (4.7) by grid search, and then taking an average of the coordinates of the $M = 2^N - N$ tentative estimates $\mathbf{v}_j$ closest to $\mathbf{v}_{GS}$, which forms the set Λ.

$$\bar{\mathbf{v}} = \frac{1}{M}\sum_{j\in\Lambda} \mathbf{v}_j \tag{4.14}$$

The overall algorithm of PCAL alongside GSAE is summarised in Algorithm 2.

The proposed scheme can be extended to a multi-MS scenario. The number of simultaneously located MSs is limited by the number of resolvable resource blocks (RBs) within a cell at each transmission time interval, and the number of MSs requesting the same quality of LCS [80]. For example, within a cell where a total bandwidth of 10 MHz (50 RBs) [80]

Algorithm 2 PCAL-GSAE Algorithm

1: Find the transition point of EAPL of each UAV, $d_{t,i}$, $i = 1, 2, \ldots, N$, in a certain range of $[d_{lower,i}, d_{upper,i}]$.
2: Obtain the $2N$ fitted functions (4.5) through piecewise convex approximation and curve fitting.
3: Calculate the $2N$ ranging functions through (4.8). Substitute them into (4.9)∼(4.13) and obtain 2^N tentative estimates of the MS location, $\mathbf{v}_j$, $j = 1, 2, \ldots, 2^N$.
4: Obtain the solution $\mathbf{v}_{GS}$ to (4.7) through grid search.
5: Select the $M = 2^N - N$ tentative estimates closest to the location of point $\mathbf{v}_{GS}$, and calculate the average of their coordinates as in (4.14).

is uniformly allocated to 50 MSs, the number of MSs to be located simultaneously is less than or equal to 50, due to different LCS qualities requested.

4.3.3 Localisation with Unknown Transmit Power

The transmit power Pt of MS is another key parameter of path loss model. It might be unknown or inaccurate in practical networks. In the existing research [2],[7], [61],[62],[66], the ranging functions can be approximated to a linear function of Pt through TSE, so that Pt and $\hat{\mathbf{v}}$ are jointly estimated by the formulated convex optimisation problem. However, they are not applicable for our proposed PCAL method, due to non-linearity of our power-like ranging function (4.8). To enable PCAL localise MS with unknown transmit power, a DRSS assisted grid search (gsDRSS) method is proposed to estimate the transmit power of MS. Assume the N-th UAV BS observed the lowest RSS, the measured DRSS at i-th UAV BS is $\overline{DRSS}_i = Pr_i - Pr_N - Xs_i + Xs_N - S_{\mathrm{af},i} + S_{\mathrm{af},N}$. Generate sampling grids $\mathbf{g}_n = [x_{\mathrm{grid},n}, y_{\mathrm{grid},n}, z_{\mathrm{grid},n}]^{\mathrm{T}}, n = 1, \ldots, N_{\mathrm{ini}}$ on the coverage of N UAV BSs with grid spacing W_{gs}, the distance from the n-th grid to i-th UAV BS is calculated as $d_{n,i} = \|\mathbf{g}_n - \mathbf{w}_i\|$, and the sampled DRSS is calculated as $\widehat{DRSS}_{n,i} = 10\eta_{n,i} log_{10}(d_{n,i}) - 10\eta_{n,N} log_{10}(d_{n,N})$, where $d_{n,N}$ is the corresponding propagation distance from n-th grid to i-th UAV BS. The location of MS is roughly estimated at the grid achieving the minimum sum error between sampled DRSS and measured DRSS

$$\min_{\hat{\mathbf{g}} \in \mathbf{g}_n} \sum_{i=1}^{N-1} |\widehat{DRSS}_{n,i} - \overline{DRSS}_{n,i}| \tag{4.15}$$

Algorithm 3 PCAL-gsDRSS Algorithm

1: Generate N_{ini} grids on the coverage of N UAV BSs with spacing $W_{\text{gs}} = 0.01R$. Calculate $\widehat{DRSS}_{n,i}$ at each grid $\mathbf{g}_n, i = 1, \ldots, N-1$.
2: Substitute $\overline{DRSS}_i$ and $\widehat{DRSS}_{n,i}$ to (4.15) and obtain the optimal solution $\hat{\mathbf{g}}$ through grid searching method.
3: Substitute $\hat{\mathbf{g}}$ into (4.3)-(4.6) to calculate estimated transmit power $\widehat{Pt}$, estimated path loss values $\widetilde{\widehat{PL}}_i$, and select the fitted parameters $\tilde{A}_{i,g_i}, \tilde{B}_{i,g_i}, \tilde{C}_{i,g_i}$.
4: Substitute $\widetilde{\widehat{PL}}_i$ and $\tilde{A}_i, \tilde{B}_i, \tilde{C}_i$ to PCAL and determine the final localisation of $\mathbf{v}$.

Based on the rough estimate on MS location $\hat{\mathbf{g}}$, the estimated distance $\acute{d}_i = \|\hat{\mathbf{g}} - \mathbf{w}_i\|$ is substituted to (4.3)-(4.6) to obtain the sampled path loss $\widetilde{PL}_i$, and select the sub-function with fitted parameters $\tilde{A}_{i,g_i}, \tilde{B}_{i,g_i}, \tilde{C}_{i,g_i}$. Then the estimated transmit power is calculated as

$$\widehat{Pt} = \frac{1}{N} \sum_{i=1}^{N} (\widetilde{PL}_i + Pr_i) \tag{4.16}$$

The estimation ambiguity is eliminated through comparing the estimated path loss measurement $\widetilde{\widehat{PL}}_i = \widehat{Pt} - Pr_i$ with the value at transition point $PL(d_{t,i})$. The entire algorithm of PCAL-gsDRSS with unknown Pt is shown in Algorithm 3.

4.3.4 CRLB of Localisation Error of PCAL Algorithm

The CRLB on localisation error is derived to evaluate the effectiveness of the proposed PCAL approach. In case of small curve fitting errors, the CRLB of localisation, σ^2_{CRLB}, is approximately an unbiased CRLB. The probability density function (PDF) of (4.5) distorted by shadowing is given by

$$f_{PL_i|d_i} = \frac{1}{\sqrt{2\pi}\sigma_{RSS}} e^{-\frac{(PL_i - (A_i d_i^{B_i} + \beta_i))^2}{2\sigma^2_{RSS,i}}} \tag{4.17}$$

The Fisher information matrix (FIM) of location estimate is computed as the expectation of log-likelihood conditioned on $\mathbf{v}$, *i.e.*, $\mathbf{F} = \mathbb{E}\left[\left(\frac{\partial \mathbf{G}}{\partial \mathbf{v}}\right)\left(\frac{\partial \mathbf{G}}{\partial \mathbf{v}}\right)^{\mathrm{T}}\right]$, where $\mathbf{G} = [\ln(f_{PL_1|d_1}), \ldots, \ln(f_{PL_N|d_N})]$. Thus, it can be derived that

$$\mathbf{F} = \sum_{i=1}^{N} \frac{1}{\sigma^2_{RSS,\,i}} (A_i B_i)^2 d_i^{2B_i - 4} (\mathbf{v} - \mathbf{w}_i)(\mathbf{v} - \mathbf{w}_i)^T \tag{4.18}$$

Table 4.1: Computational Complexity Analysis. N: Number of UAV-BSs, V: Dimension of MS Coordinates.

Algorithm	Computational Complexity
PCAL-GSAE	$\mathcal{O}(N^{4.5})$
PCAL-EPt-gsDRSS	$\mathcal{O}(N^{3.5}) + \mathcal{O}(N^{4.5})$
LSRE [7]	$\mathcal{O}(N^{4.5})$
RSDPE [8]	$\mathcal{O}(N^{3.5})$
LSRE-SDP [9]	$\mathcal{O}(N^{3.5})$
LSO-PLEc [10]	$\mathcal{O}((V+2)^3)$

Denoting $\mathbf{J} = \mathbf{F}^{-1}$ as the inverse of $\mathbf{F}$, and the CRLB is computed as the trace of $\mathbf{J}$, *i.e.*, $\sigma^2_{CRLB\text{-}PCAL} \geqslant tr[\mathbf{J}]$.

Apparently, the unbiased CRLB is dependent on both fitted parameters and propagation distance. Note that, FIM and CRLB are independent of $S_{\text{af},i}$ and β_i.

Define the ratio of the CRLB of distance estimation of the approaches in [7],[8],[10],[63] to that of PCAL as $\varepsilon = \sigma^2_{CRLB\text{-}log,distance}/\sigma^2_{CRLB\text{-}PCAL,distance} = (A_i^2 B_i^2 d_i^{2B_i} \ln^2 10)/(100\eta_i^2)$, where the CRLBs of [7],[8],[10],[63] are the same since they both apply the same path loss model. When UAV is at $h_i = 500$ m high, $\varepsilon \geqslant 38.46$ is achieved at any position within a cell, implying higher localisation accuracy of PCAL compared to [7],[8],[10],[63].

4.3.5 Complexity Analysis

Table I presents the complexity analysis following the analysis approach in [81]. The complexities of LSRE [7], RSDPE [8], LSRE-SDP [9] and LSO-PLEc [10] are also presented for comparison. The order of complexity of PCAL-GSAE is the same as that of LSRE [7]. PCAL-GSAE requires higher complexity than RSDPE [8] and LSE-PLEc [10], but achieves a significant performance gain over all of them, as shown in Section 4.5. The complexity of GSAE is negligible compared to that of PCAL. The complexity of PCAL-GSAE is the same as that of PCAL without ambiguity, since the 2^N tentative estimates are independent of each other.

4.4 Effective Transmit Power and Effective Pathloss Exponents

In this section, we propose EPt and EPLE to reveal the effect of Pt and η_i on ranging accuracy. An anti-intuitive finding is drawn as the accuracy of ranging and localisation is not related to the accuracy of estimated transmit power $\widehat{Pt}$ and estimated pathloss exponent $\hat{\eta}_i$.

4.4.1 Effective Transmit Power

In this subsection, we propose an anti-intuitive finding that proper values of $\overline{Pt}_i$ and $\tilde{\eta}_i$, named as "EPt" and "EPLE", can compensate measurement error on path loss, *e.g.*, $X_{\mathrm{PL},i}$, and induce the higher accuracy of ranging distances and localisation than the real values. On the contrary, a common sense on localisation techniques has recognised the beneficial effects of accurate estimation of PLEs and transmit power on localisation [77]. However, according to our investigation on the proposed approaches and existing work, it is unnecessary to maintain high accuracy of estimation of PLEs and transmit power. For example, Fig. 4.2 shows the scenario where the highest accuracy of localisation is not achieved at real transmit power $Pt = 23$ dBm, but another value $\widehat{Pt} = 0$ dBm. Therefore, it is straightforward to infer that the real transmit power Pt works as a trivial parameter in localisation.

EPt is defined as the proper value of transmit power with perfect compensation on error of $X_{\mathrm{PL},i}$, such that it induces ranging distance and localisation of 0 error. For both exponential-like and power-like ranging functions, the basic localisation problem $(P2.2)$ is recalled, and the localisation problem with unknown EPt $\overline{Pt}_i$ can be rewritten as following

$$(P4.4) \qquad \min_{\overline{Pt}_i} \sum_{i=1}^{N} (\hat{d}_i - d_i)^2 = 0 \tag{4.19}$$

where the estimated distance $\hat{d}_i$ is obtained from distance estimation function as $\hat{d}_{\exp}(\widehat{Pt}_i) = 10^{(\widehat{Pt}_i - Pr_i + X_{\mathrm{PL},i})/(10\eta_i)}$ for the classical exponential-like ranging function, and $\hat{d}_{\mathrm{po}}(\widehat{Pt}_i) = |(\widehat{Pt}_i - Pr_i - \beta_{i,g_i} + X_{\mathrm{PL},i})/(A_{i,g_i})|^{1/B_{i,g_i}}$ for our proposed power-like ranging function. Assuming perfect knowledge of path loss model, the solution to $(P4.4)$, $\widehat{Pt}_i = \overline{Pt}_i$ is ob-

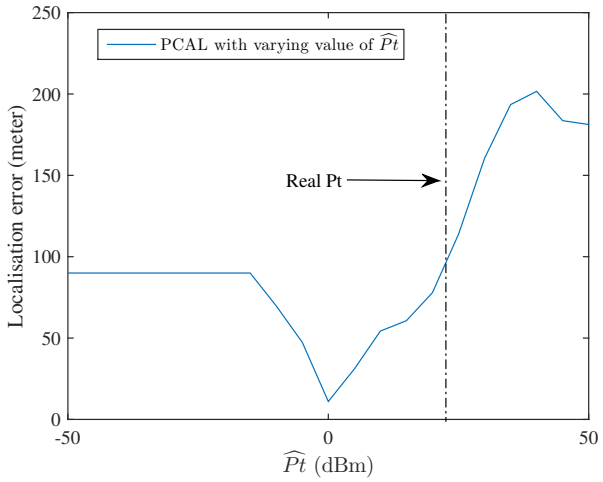

Figure 4.2: Localisation error of MS fluctuates with substituted transmit power, $\widehat{Pt} = -50, -45, \ldots, 50$ dBm, when real transmit power $Pt = 23$ dBm.

tained by $\hat{d}_i = d_i$, resulting into EPt for (3.6), $\overline{Pt}_{\text{exp},i}$, and EPt for (4.6), $\overline{Pt}_{\text{po},i}$, as :

$$\overline{Pt}_{\text{exp},i} = Pt - X_{PL,i} \tag{4.20}$$

and

$$\overline{Pt}_{\text{po},i} = Pt - X_{PL,i} \text{ or } -Pt + 2Pr_i - X_{\text{PL},i} + 2\beta_{i,g_i} \tag{4.21}$$

(4.20)-(4.21) describe EPt as sum of Pt and an offset, which value is opposite to measurement error, *i.e.*, $-X_{PL,i}$. The second value of $\overline{Pt}_{\text{po},i}$ is due to the absolute operator of $\hat{d}_{\text{po}}$.

A range of values near EPt, which is defined as "effective transmit power range" (EPt-range), also performs better than real Pt. The resulting interval of ranging distance $\hat{d}_i$ near real distance d_i is defined as "effective distance range" (Edist-range), where $\widehat{Pt}_i$ in EPt-range performs better than real Pt, *i.e.*, $|\hat{d}_i - d_i| < |\tilde{d}_i - d_i|$, and $\tilde{d}_i = |(\widetilde{PL}_i - \beta_{i,g_i})/A_{i,g_i}|^{1/B_{i,g_i}}$ or $10^{\widetilde{PL}_i/(10\eta_i)}$ is the ranging distance of real Pt. After simple mathematical manipulations, it is rewritten as

$$\tilde{d}_i < \hat{d}_i < 2d_i - \tilde{d}_i, \text{ or } , \max\{0, 2d_i - \tilde{d}_i\} < \hat{d}_i < \tilde{d}_i \tag{4.22}$$

EPt-range is bounded by real Pt and another different value, named as 'critical transmit power' (cr-Pt), of which the ranging error is equal to that of the real Pt.

Lemma 1: Ranging distances in EPt-range achieve higher accuracy than that of real Pt. The cr-Pt defined for (3.6) is calculated as $\breve{Pt}_{\text{exp},i} = Pr_i - X_{\text{PL},i} + 10\eta_i \log_{10}(2d_i - \tilde{d}_i)$, and the cr-Pt defined for (4.6) is calculated as $\breve{Pt}_{\text{po},1,i} = t1 + t2$, $\breve{Pt}_{\text{po},2,i} = t1 - t2$, $\breve{Pt}_{\text{po},3,i} = t1 + t3$, $\breve{Pt}_{\text{po},4,i} = t1 - t3$, where the parameters $t1, t2, t3$ are displayed in Appendix A. Substituting (3.6) and (4.6) to (4.22), the EPt-range for exponential-like ranging function (3.6) is simply derived as

$$\widehat{Pt}_i \in \begin{cases} (-\infty, Pt), & \text{Event A} \\ (\breve{Pt}_{\text{exp},i}, Pt), & \text{Event B} \\ (Pt, \breve{Pt}_{\text{exp},i}), & \text{Event C} \end{cases} \tag{4.23}$$

where the Event A $\sim$ Event C are defined in Appendix A. The EPt-range for power-like ranging function (4.6) is

$$\widehat{Pt}_i \in \begin{cases} (-\infty, \breve{Pt}_{\text{po},4,i}) \cup (\breve{Pt}_{\text{po},3,i}, +\infty), & \text{Event D} \\ (\breve{Pt}_{\text{po},3,i}, \breve{Pt}_{\text{po},1,i}) \cup (\breve{Pt}_{\text{po},2,i}, \breve{Pt}_{\text{po},4,i}), & \text{Event E or Event G} \\ (\breve{Pt}_{\text{po},1,i}, \breve{Pt}_{\text{po},3,i}) \cup (\breve{Pt}_{\text{po},4,i}, \breve{Pt}_{\text{po},2,i}), & \text{Event F or Event I} \\ (\breve{Pt}_{\text{po},4,i}, \breve{Pt}_{\text{po},3,i}) & \text{Event H} \end{cases} \tag{4.24}$$

where the Event D $\sim$ Event I are defined in Appendix A.

Lemma 1 is illustrated in Figs. 4.3 and 4.4. Event A refers to significant measurement error $X_{\text{PL},i}$ that produces ranging distance twice than real distance. Events B and C claims that whether EPt-range and cr-EPt greater or smaller than real Pt is consistent with the $X_{\text{PL},i}$. Events D, E and F reflect much lower ranging error and wider interval than Events A, B and C, indicating the higher accuracy of power-like ranging function (4.6) over exponential-like ranging function (3.6). Following the definition of EPLE and EPLE-range, it is easy to expand to general communication environment with more types of measurement error, *e.g.*, thermal noise, fast fading, multipath effect, etc.

Due to poor knowledge of $X_{PL,i}$ and d_i, it is difficult to calculate EPt and EPt-range in practice. However, estimated EPt can be obtained with assumed identical accuracy improvement of ranging distance. Assuming that each $\overline{Pt}_{\text{po},i}$ makes identical effect on ranging distances, *i.e.*, $\hat{d}_{\text{po},i} = \tilde{d}_i P_{\text{cb}}$, where $P_{\text{cb}} > 0$ is the resulting calibration on ranging distances, $\Delta Pt_{\text{df},i} = \overline{Pt}_{\text{po},i} - Pt$ is the difference between the i-th EPt and real Pt. When $P_{\text{cb}} > 0$, the ratio of estimated distance over ranging distance $\hat{d}_{\text{po},i}/d_i = P_{\text{cb}}(1 + X_{\text{PL},i}/(PL_i - \beta_{i,g_i}))^{1/B(i,g_i)}$ is a convex function with respect to $X_{\text{PL},i}$, with variance $\sigma_{\text{cb},i} =$

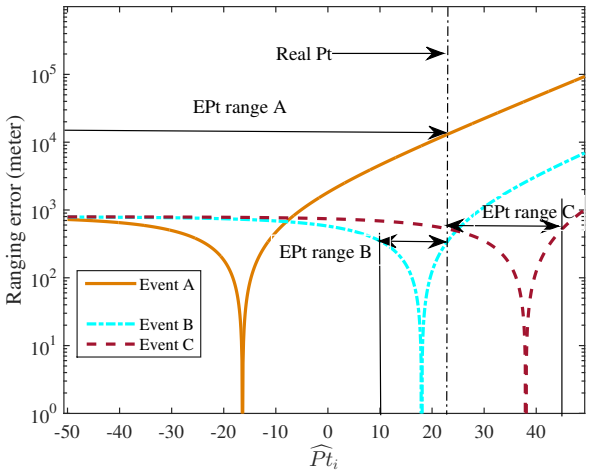

Figure 4.3: Ranging error of the i-th BS derived from values in the EPt-range (4.23) is lower than that from the real $Pt = 23$ dBm, when real distance $d_i = 790$ m, real path loss value is $PL_i = 92$ dB, measurement error is $X_{\mathrm{PL},i} = 40, 5, -15$ dB, corresponding to Events A, B and C, respectively.

$\sigma_{i,g_i}/(\widetilde{PL}_i - \beta_{i,g_i}))^{2/B_{i,g_i}}$. Thus, the squared ranging distance with calibration is rewritten as $D_{\mathrm{cb},i} = Q_{\mathrm{cb}}^2 d_i^2$. The optimum is achieved at $D_{\mathrm{cb},i}/\tilde{d}_i^2 = 1$. Moreover, $(D_{\mathrm{cb},i}/\tilde{d}_i^2)^{-1}$ should be considered, since negative value of B_{i,g_i} could result into $D_{\mathrm{cb},i}/\tilde{d}_i^2 < 1$. Therefore, the estimation problem of EPt is formulated as $\min_{Q_{\mathrm{cb}}} \sum_{i=1}^{N} D_{\mathrm{cb},i}/\tilde{d}_i^2 + (D_{\mathrm{cb},i}/\tilde{d}_i^2)^{-1}$, which can be converted to an SDP problem

$$(P4.5) \qquad \min_{Q_{\mathrm{cb}}, D_{\mathrm{cb},i}, \mathbf{v}_{\mathrm{cb}}} \sum_{i=1}^{N} F_{\mathrm{ratio},i} \tag{4.25}$$

$$s.t.$$

$$F_{\mathrm{ratio},i} \geqslant \frac{D_{\mathrm{cb},i}}{\hat{p}_{i,g_i}^2} \tag{4.26}$$

$$\begin{bmatrix} \hat{p}_{i,g_i}^2 D_{\mathrm{cb},i} & \tilde{d}_i \\ \tilde{d}_i & F_{\mathrm{ratio},i} \end{bmatrix} \geqslant 0 \tag{4.27}$$

$$\begin{bmatrix} \mathbf{I}_2 & \mathbf{v}_{\mathrm{cb}} - \mathbf{w}_i Q_{\mathrm{cb}} \\ (\mathbf{v}_{\mathrm{cb}} - \mathbf{w}_i Q_{\mathrm{cb}})^{\mathrm{T}} & D_{\mathrm{cb},i}^2 \end{bmatrix} \geqslant 0 \tag{4.28}$$

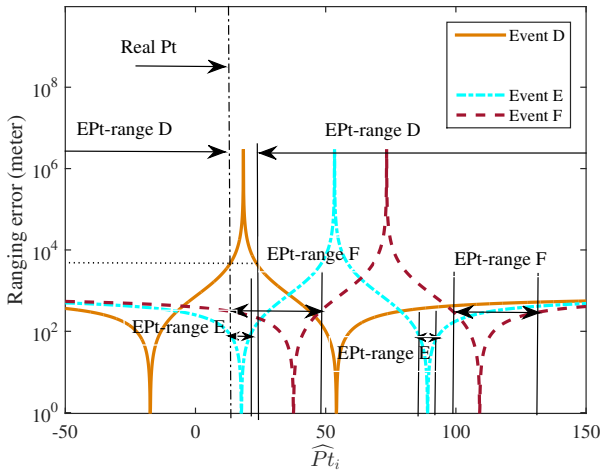

Figure 4.4: Ranging error of the i-th BS derived from values in the EPt-range (4.24) is lower than that from the real $Pt = 23$ dBm, when real distance $d_i = 790$ m, real path loss value is $PL_i = 92$ dB, fitted parameters are $A_{i,g_i} = -2.6527e+04, B_{i,g_i} = -0.9959, \beta_{i,g_i} = 141.8248$, measurement error is $X_{\mathrm{PL},i} = 40, 5, -15$ dB, corresponding to Events D, E and F, respectively.

where $\tilde{p}_{i,g_i} = 1/\sigma_{\mathrm{cb},i}$ is the weight of objective function. With $\tilde{\eta}_i$ obtained in gsDRSS and the calculated $P_{\mathrm{cb}} = 1/Q_{\mathrm{cb}}$, the estimated EPt is calculated as

$$\widehat{\widetilde{Pt}}_i = Pt + \Delta Pt_{\mathrm{df},i} \tag{4.29}$$

where $\Delta Pt_{\mathrm{df},i} = \beta_{i,g_i} + \widetilde{PL}_i - P_{\mathrm{cb}}^{B_{i,g_i}} |(\widetilde{PL}_i - \beta_{i,g_i})|$. Thus, the path loss measure is refined $\widehat{\widetilde{PL}}_i = \widehat{\widetilde{Pt}}_i - Pr_i$. The entire progress of PCAL-EPt-gsDRSS with unknown Pt is shown in Algorithm 4.

Algorithm 4 PCAL-EPt-gsDRSS Algorithm

1: Obtain estimated path loss measurement $\widehat{\widetilde{PL}}_i$ and $\tilde{A}_i, \tilde{B}_i, \tilde{C}_i$ through steps 1 $\sim$ 3 of PCAL-gsDRSS scheme, and substitute them to (4.8) to derive $\tilde{d}_i$.
2: Obtain Q_{cb} through solving $(P4.5)$ with $\tilde{d}_i$ and $\tilde{A}_i, \tilde{B}_i, \tilde{C}_i$.
3: Substitute Q_{cb} and $\tilde{\eta}_i$ into (4.29) to obtain the estimated EPt $\widehat{\widetilde{Pt}}_i$, and refine path loss measurements as $\widehat{\widetilde{PL}}_i$.
4: Substitute $\widehat{\widetilde{PL}}_i$ and $\tilde{A}_i, \tilde{B}_i, \tilde{C}_i$ to PCAL scheme.

4.4.2 Effective PLE

EPLE and EPLE-range are defined in the similar way as that of EPt and EPt-range, *i.e.*, EPLE is the PLE that perfectly compensates the ranging error caused by $X_{\mathrm{PL},i}$, and EPLE-range is referred to the values near EPLE and of lower ranging error than real PLE. To derive EPLE and EPLE-range, the terrestrial network based localisation with conventional exponential-like ranging function is used to assess the effect of PLE on accuracy of localisation and ranging distance, but the power-like ranging function is not employed by this section, since it is free of PLE. Recall ($P2.1$) again, the ranging based localisation problem is rewritten as optimisation of PLE, as shown by ($P4.6$).

$$(P4.6) \qquad \min_{\hat{\eta}} \sum_{i=1}^{N} (d_i - \hat{d}_i)^2 = 0 \tag{4.30}$$

s.t.

$$\hat{d}_i = 10^{\frac{\widetilde{PL}_i}{10\hat{\eta}_i}} \tag{4.31}$$

The solution to ($P4.6$) is as well $\hat{d}_i = d_i$. Assuming known real distance d_i, EPLE of the i-th BS, $\bar{\eta}_i$ is simply calculated as (4.32).

$$\bar{\eta}_i = \frac{\widetilde{PL}_i \eta_i}{PL_i} \tag{4.32}$$

A range of PLE values $\hat{\eta}_i$ near the i-th EPLE and showing higher accuracy than real PLE is defined as EPLE-range, and the corresponding interval of distances is also defined as Edist-range, *i.e.*, $\hat{d}_i = 10^{\widetilde{PL}_i/(10\eta_i)} \in (\max\{0, d_i - \tilde{d}_i\}, \tilde{d}_i)$. EPLE-range is bounded by both real PLE and another different PLE value $\check{\eta}_i$, named as 'critical PLE' (cr-PLE), of which the ranging error is equal to that of real PLE.

Lemma 2: Ranging distance corresponding to any value in the EPLE range achieves lower error than that with real PLE. Define the cr-PLE as $\check{\eta}_i = \frac{(PL_i + X_{S,i})\eta_i}{PL_i + 10\eta_i \log_{10}\left(2 - 10^{\frac{X_{S,i}}{10\eta_i}}\right)}$, and the EPLE range is

$$\hat{\eta}_i \in \begin{cases} (\eta_i, \check{\eta}_i)\,, & \text{Event J} \\ (\check{\eta}_i, \eta_i)\,, & \text{Event K} \\ (\eta_i, +\infty)\,, & \text{Event L} \end{cases} \tag{4.33}$$

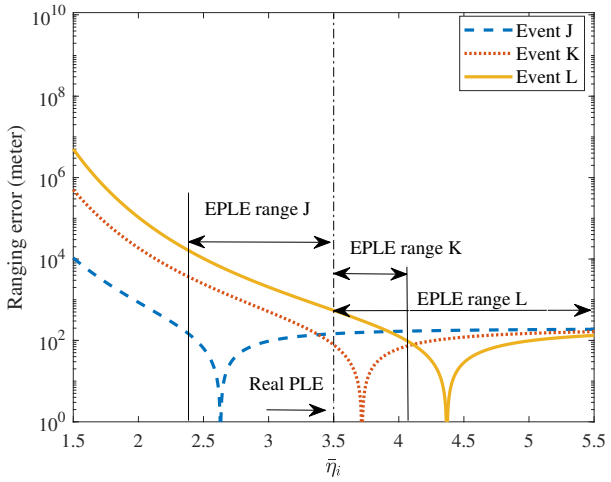

Figure 4.5: Ranging error of the i-th BS derived from values in the EPLE range is lower than that from the real PLE $\eta_i = 3.5$, when real distance $d_i = 200$ m, real path loss measure is $PL_i = 81$ dB, shadowing is $X_{S,i} = -20, 5, 20$ dB, corresponding to Events J, K and L.

where $\epsilon_i = \frac{X_{S,i}}{10\log_{10} 2}$. Events J, K and L are defined in Appendix B.

Proof: See Appendix B.

Lemma 2 is illustrated by Fig. 4.5. Events J and K claim that whether EPLE range and cr-PLE greater or smaller than real PLE is dependent on $X_{S,i}$. Event L indicates significant $X_{S,i}$ that produces ranging distance twice than real distance d_i. The length of EPLE range of Events J and K is proportional to $|X_{S,i}|$ with moderate measurement error $X_{S,i}$. EPLE range becomes infinitely long with sufficiently large value of $X_{S,i}$. EPLEs and EPLE-ranges of N BSs are difficult to obtain, due to unknown real path loss PL_i and unknown real distance d_i in practice.

4.4.3 Analysis on the Effect of Effective Transmit Power and Effective Pathloss Exponents on Localisation

EPt and EPLE both improve the localisation performance through modifying ranging function with Edist. Assume perfectly known EPt-ranges and EPLE-ranges, and denote $\hat{d}_{\mathrm{e},i}$ as both distances obtained with equal EPt (eEPt) Pt_{e} and equal EPLE (eEPLE) η_{e},

the existing LS estimator based localisation is expressed as

$$(P4.7) \qquad \min_{\hat{d}_{\mathrm{e},i},\mathbf{v}_\mathrm{e}} \|\mathbf{A}\mathbf{v}_\mathrm{e} - \mathbf{B}_\mathrm{c}\|^2 \tag{4.34}$$

s.t.

$$\mathbf{B}_\mathrm{c} = [\mathbf{b}_{\mathrm{e},1}, \ldots, \mathbf{b}_{\mathrm{e},N}]^\mathrm{T} - \mathbf{S} \tag{4.35}$$

where $\mathbf{B}_\mathrm{c}$ is the ranging matrix, and $\mathbf{b}_{\mathrm{e},i} = \hat{d}^2_{\mathrm{e},i}$ is the squared ranging distance of eEPLE or eEPt. $\mathbf{A} = [-2\mathbf{W}^\mathrm{T}_\mathrm{di}\ \mathbf{1}_\mathrm{N}]$, $\mathbf{W}_\mathrm{di} = [\mathbf{w}_1 - \mathbf{w}_2, \ldots, \mathbf{w}_1 - \mathbf{w}_N]$. $\mathbf{L} = [\mathbf{I}_V, \mathbf{0}_V]$, V is the dimension of MS coordinates. $\mathbf{S} = [\|\mathbf{w}_1\|^2, \ldots, \|\mathbf{w}_N\|^2]^\mathrm{T}$.

Proposition 1 The estimated location of MS $\hat{\mathbf{v}}_\mathrm{e}$ converges from infinite far position to the converged point $\mathbf{v}_0 = \mathbf{\Phi}(\mathbf{1}_N - \mathbf{S}))$, when η_e increases from $\eta_\mathrm{e} = 0$ to $\eta_\mathrm{e} = +\infty$, or Pt_e decreases from $Pt_\mathrm{e} = +\infty$ to 0. There is no closed form solution to $(P4.7)$, since it is nonlinear and non-convex problem.

Proof : The localisation result $\hat{\eta}_\mathrm{e}$ obtained by $(P4.7)$ $\hat{\mathbf{v}}_\mathrm{e}$ is consistent on $\eta_\mathrm{e} \in (0^+, +\infty)$ and $Pt_\mathrm{e} \in (-\infty, +\infty)$. It is straightforward to calculate that, when $\eta_\mathrm{e} \to 0^+$ or $Pt_\mathrm{e} \to +\infty$, the ranging distance approaches infinite $\hat{d}^2_{\mathrm{e},i} = +\infty$. Therefore, MS is localised at infinite far point $\hat{\mathbf{v}}_\mathrm{e} = [\pm\infty, \pm\infty]^\mathrm{T}$; and when $\eta_\mathrm{e} \to +\infty$ or $Pt_\mathrm{e} \to -\infty$, $\hat{d}^2_{\mathrm{e},i} \approx 1$, MS is localised at $\hat{\mathbf{v}}_\mathrm{e} = \mathbf{\Phi}(\mathbf{1}_N - \mathbf{S})$. Thus, Proposition 1 is proved.

Define the line formed by all the estimates $\hat{\mathbf{v}}_\mathrm{e}$ with $\hat{\eta}_\mathrm{e}$ varying between $(0^+, +\infty)$ as 'estimation-line', there must be at least one point on the estimation-line closest to MS on the 2D/3D plane, indicating at least one local minimum of localisation error function. Fig. 4.6 displays an example of estimation-lines obtained by grid searched eEPLE $\hat{\eta}_\mathrm{e} \in [2\ 6]$ and eEPt $\widehat{Pt}_\mathrm{e} \in [-50, 50]$ dBm, and $N = 4$ BSs deployed in square region, when the real PLE is $\eta_i = 3$, and real $Pt = 23$ dBm. The convergence directions of both estimation-lines are toward the centre of BSs with $\hat{\eta}_\mathrm{e} \to +\infty$, by passing the point of minimum localisation error at $\hat{\eta}_\mathrm{e} \approx 2.66$ and $\widehat{Pt}_\mathrm{e} = 34$ dBm, respectively. Figs. 4.7 and 4.8 display the ranging error $|\hat{d}_{\mathrm{e},i} - d_i|$ of the varying eEPLE and varying eEPt. If the real location of MS is on the same side as the estimation-lines, *e.g.*, when $\mathbf{v} = [400, -400]^\mathrm{T}$, the minimum error will be achieved at the converged point $[0, 0]^\mathrm{T}$. The values of PLE $\hat{\eta}_{\mathrm{e},i} > \eta_\mathrm{e}$ achieves less ranging error than those PLE $\hat{\eta}_{\mathrm{e},i} < \eta_\mathrm{e}$. Thus, it is suggested to use the larger PLE values and smaller Pt values for initialisation of RSS based localisation with unknown PLEs and/or unknown Pt, which is consistent with the findings in [77].

Different with eEPLE that is shared by N BSs, unequal EPLE (unEPLE) η_g and

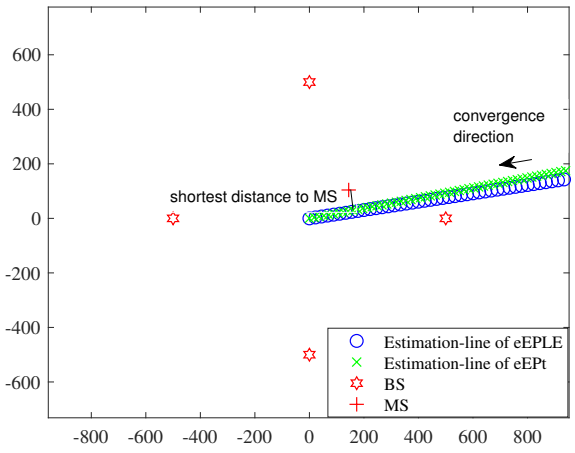

Figure 4.6: Estimation-line of LS estimator with varying eEPLE $\hat{\eta}_{\mathrm{e}} \in [1.50, 5.50]$ and varying eEPt $Pt_{\mathrm{e}} \in [-50, 50]$ dBm.

unequal EPt (unEPt) are referred to as an individual eEPLE and eEPt shared by several of N BSs. Suppose N BSs are assigned to R_{BS} groups, and the r-th group contains one unEPLE $\eta_{\mathrm{g},r}$ and one unEPt $Pt_{\mathrm{g},r}$, $n_r \geqslant 2$ BSs, and coordinates of the K_r BSs in this group is $\mathbf{w}_{\mathrm{g},r,k}, k = 1, \ldots, K_r$. Let $d_{\mathrm{g},r,k}$ denote the Edist of BS k in the r-th group obtained with unEPLE or unEPt, *i.e.*, $d_{\mathrm{g},r,k} = 10^{\widetilde{PL}_{\mathrm{g},r,k}/(10\eta_{\mathrm{g},r})}$ or $10^{\widehat{PL}_{\mathrm{g},r,k}/(10\eta_r)}$, where $\widehat{PL}_{\mathrm{g},r,k} = Pt_{\mathrm{g},r} - Pr_{r,k} + X_{S,r,k}$. For the default sequence of BSs, the vector of path loss measures and information matrix are same as those of $(P4.6)$, which is converted to $(P4.8)$.

$$(P4.8) \qquad \min_{\hat{\boldsymbol{d}}_{\mathrm{g}}, \hat{\mathbf{v}}_{\mathrm{g}}} \sum_{i=1}^{N} \|\mathbf{A}\hat{\mathbf{v}}_{\mathrm{g}} - \mathbf{B}_{\mathrm{g}}\|^2 \tag{4.36}$$

s.t.

$$\mathbf{B}_{\mathrm{g}} = [\mathbf{b}_1, \ldots, \mathbf{b}_R]^{\mathrm{T}} - \mathbf{S} \tag{4.37}$$

$$\mathbf{b}_r = [d^2_{\mathrm{g},r,1}, \ldots, d^2_{\mathrm{g},r,K_r}] \tag{4.38}$$

where $\mathbf{B}_{\mathrm{g}}$ is ranging matrix of unEPLEs or unEPt, $\mathbf{b}_r$ is the submatrix of the r-th group. There is no closed form solution to $(P4.8)$, since it is nonlinear and non-convex problem.

The estimates $\hat{\mathbf{v}}_{\mathrm{g}}$ obtained with continuous search on $\hat{\eta}_{\mathrm{g},r} \in [1.5, 5.5]$ and $\widehat{Pt}_{\mathrm{g},r} \in$

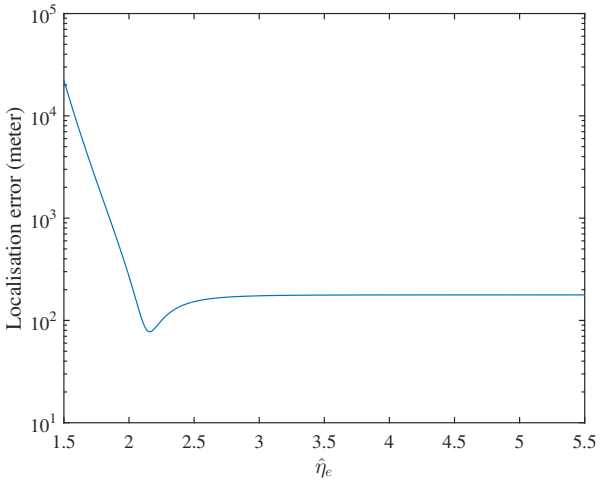

Figure 4.7: Localisation error of LS estimator with varying eEPLE $\hat{\eta}_{\mathrm{e}} \in [1.5, 5.5]$, when the real PLE is $\eta = 3$.

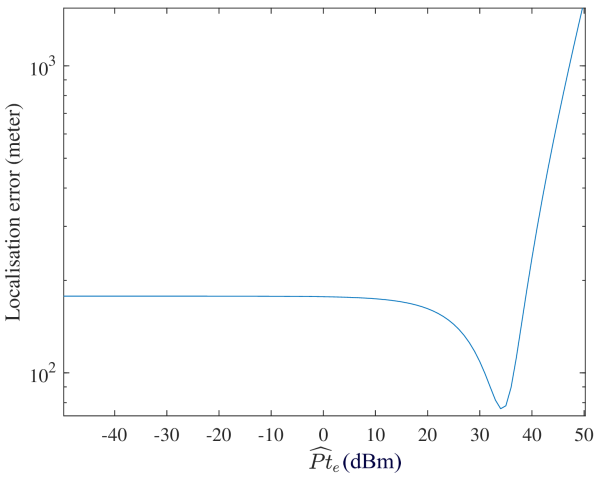

Figure 4.8: Localisation error of LS estimator with varying eEPt $Pt_{\mathrm{e}} \in [-50, 50]$ dBm, when the real transmit power is $Pt = 23$ dBm.

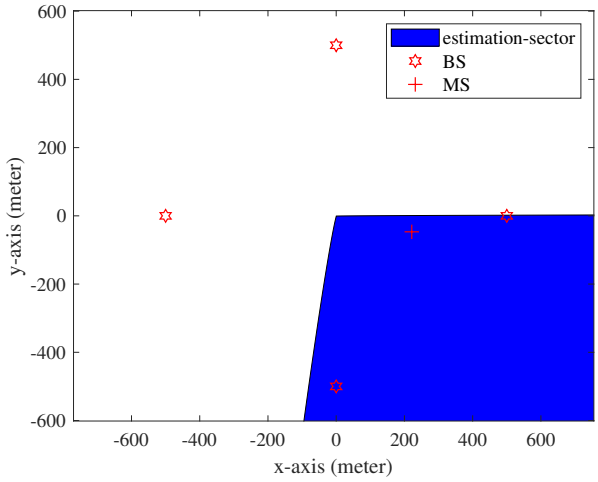

Figure 4.9: Estimation sector obtained by $N = 4$ BSs of two groups with $\hat{\eta}_{\mathrm{g},r} \in [1.5, 5.5]$ or $\widehat{Pt}_{\mathrm{g},r} \in [-50, 50]$ dBm.

$[-50, 50]$ dBm are also continuous on the map. Define the region filled by the continuous estimates as 'estimation-sector', the range of each estimation-sector can be expanded to infinite farther when unEPLEs approaches 0 or unEPt approaches $+\infty$. Thus, MS is probably covered by the estimation-sector derived. For the sake of convenience, the two edges of each estimation-sector are approximated to straight lines from the converged point $\mathbf{v}_0$ to infinitely far position. Therefore, the coverage of estimation-sector is only determined by its central angle θ_{C}, which is bounded by the two edges, *i.e.*, the two outermost estimation-lines. The r-th estimation boundary is actually the estimation-line obtained by $\hat{\eta}_{g,r} \in [\eta_{\mathrm{low}}, \eta_{\mathrm{up}}]$ and the unEPLEs of other groups fixed at $\eta_{\mathrm{g},r} \to +\infty$, or $\widehat{Pt}_{g,r} \in [Pt_{\mathrm{low}}, Pt_{\mathrm{up}}]$ and the unEPt of other groups fixed at $\widehat{Pt}_{g,r} \to -\infty$, where the parameters labelled by subscripts 'low' and 'up' corresponds to the lower and upper bound.

Fig. 4.9 presents the case that the real location of MS is covered by the estimation-sector of unEPLEs and unEPt obtained by $(P4.8)$, when $N = 4$ BSs are allocated to $R_{\mathrm{BS}} = 2$ groups, real PLEs are respectively 3.39, 3.40, 3.28, 2.06, and real $Pt = 23$ dBm. The estimation-sector of unEPLEs and unEPt are completely overlapped with each other. With proper values of unEPLEs or unEPt, $(P4.8)$ could achieve 0 localisation error. Fig. 4.10 presents the localisation error varies with different unEPLEs, when 2nd unEPLE $\hat{\eta}_{\mathrm{g},2}$ is fixed at constants. The minimum error is realised at $\hat{\eta}_{\mathrm{g},1} = 3.74, \hat{\eta}_{\mathrm{g},2} = 3.32$. Fig. 4.11 presents that localisation error varies with different unEPt, when 2nd unEPLE $\widehat{Pt}_{\mathrm{g},2}$ is

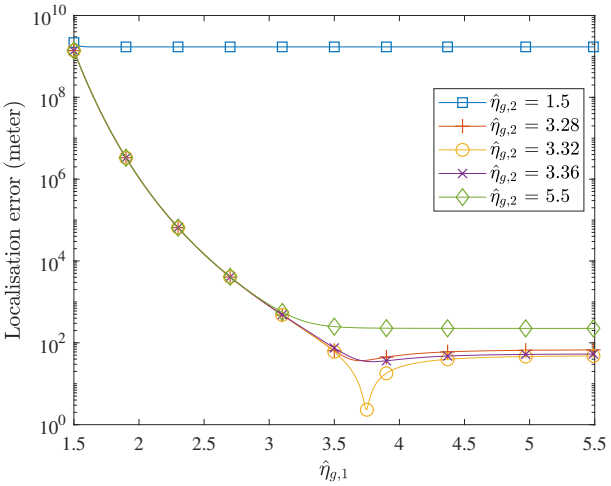

Figure 4.10: Localisation error achieved by unEPLEs with $N = 4$ BSs of two groups, the 1st unEPLE is sampled with interval $\Delta\eta = 0.01$, the 2nd unEPLE fixed at $\hat{\eta}_2 = 1.50, 3.28, 3.32, 3.36, 5.5$.

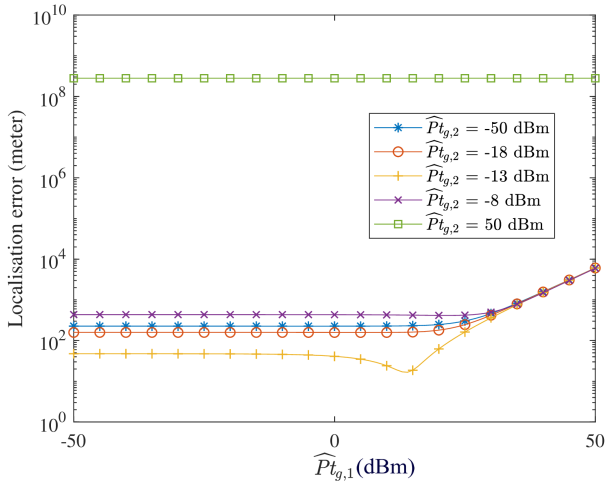

Figure 4.11: Localisation error achieved by unEPt with $N = 4$ BSs of two groups, the 1st unEPt is sampled with interval $\Delta Pt = 1$ dBm, the 2nd unEPt fixed at $\widehat{Pt}_{\mathrm{g},2} = -50, -18, -13, -8, 50$ dBm.

fixed at constants. The minimum error is realised at $\widehat{Pt}_{\mathrm{g},1} = 14$ dBm, $\widehat{Pt}_{\mathrm{g},2} = -13$ dBm. For both unEPLEs and unEPt, the localisation error is reduced dramatically near the optimal values. Thus, it is difficult to obtain the optimal unEPLEs and unEPt.

Lemma 3 Denote the localisation accuracy achieved by unEPLEs and eEPLE as $\|\mathbf{E}_{\mathrm{g}}\|$ and $\|\mathbf{E}_{\mathrm{e}}\|$, respectively. LS optimisation with unEPLE is usually more accurate than that of eEPLE, *i.e.*,

$$\|\mathbf{E}_{\mathrm{g}}\| \leqslant \|\mathbf{E}_{\mathrm{e}}\| \tag{4.39}$$

Proof: See Appendix C.

Following the same progress as Appendix C, it is easy to draw the corresponding property of unEPt and eEPt.

4.5 Simulation Results

The performance of the proposed PCAL-GSAE scheme is evaluated by Monte-Carlo simulation with $N = 4$ UAV-BSs supported hexagon cells and system frequency of 2GHz. The AS standard deviation is set to $\sigma_{AS,i} = 4.4$ dB [72] in Figs. 4.14 $\sim$ 4.17. Assume perfect knowledge of the EAPL parameters a_0, a_1, b_0 and b_1 given in Section 4.3.

Fig. 4.12 depicts the approximated path loss in (4.5), compared with the original EAPL [73], when all UAVs' altitude is $h_i = 500$ m (i=1,...,4) and the cell radius is $R = 1000$ m. The approximated path loss by piecewise convex approximation and curve fitting are expressed as

$$\widehat{PL_i} \approx \begin{cases} 5.772\text{e-}9\, d_i^{3.15} + 52.31 & d_{lower,i} \leqslant d_i \leqslant d_t \\ -6.772\text{e}4\, d_i^{-0.9792} + 144.6 & d_t < d_i \leqslant d_{upper,i} \end{cases}$$

where $d_{lower,i} = h_i$, and $d_{upper,i} = 2R$, and $d_{t,i} = 1098$ m. The approximation results without the PLE knowledge match the EAPL model perfectly within $d \in [d_{lower,i}, d_{upper,i}]$.

Fig. 4.13 shows the cumulative density function (CDF) of PCAL-GSAE, with the same simulation setup as Fig. 4.12, in comparison to those of the approaches in [7],[8],[10],[63] with perfectly known and equal PLEs and the LSO-PLEc approach in [10]. PCAL-GSAE significantly outperforms the other approaches when the estimation error is larger than 50 m, due to its higher robustness against TS, while an error of less than 50 m indicates an occasional case where ambiguity error plays a dominant role. Fig. 4.14 shows that with AS, the proposed PCAL-GSAE scheme maintains a performance comparable to the case without AS, while the other approaches suffer significant performance degradation

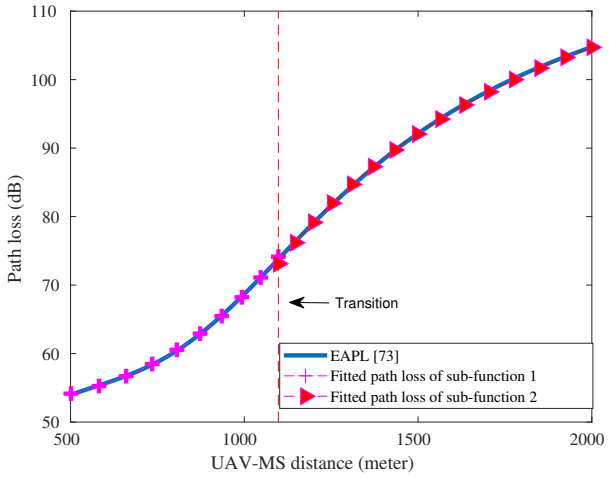

Figure 4.12: Curve fitted path loss model in comparison to EAPL [69] with UAV altitudes $h_i = 500$ m (i=1,...,4) and cell radius $R = 1000$ m.

compared to Fig. 4.13.

Fig. 4.15 shows the average localisation error versus cell radius, which varies from 500 m to 1000 m, with UAV altitude $h_i = 200$ m (i=1,...,4). When combined with PCAL, the proposed GSAE approach is more effective to eliminate ambiguity than the PLM approach in [37]. The performance of PCAL-GSAE is close to the CRLB derived. Also, PCAL-GSAE achieves higher accuracy than PCAL without ambiguity, because averaging over the selected tentative estimates is effective in mitigating errors caused by shadowing. And the localisation error caused by the ambiguity is much smaller than that of shadowing. PCAL with real PLE values demonstrates a much worse performance than PCAL with unknown PLEs, since the approximations in (4.5) and (4.6) and GSAE are disabled under perfect knowledge of PLEs, which makes the algorithm more vulnerable to shadowing.

Fig. 4.16 illustrates the average estimation error of transmit power derived by proposed PCAL-gsDRSS, PCAL-EPt-gsDRSS and existing LSRE-SDP [9] versus cell radius, when the simulation setup data is same as Fig. 4.15. The three approaches have a deceasing estimation error as the cell radius increase, where the error of PCAL-gsDRSS and PCAL-EPt-gsDRSS is much higher than that of LSRE-SDP, in contrast to their performance shown in Fig. 4.17. This result indicates the localisation accuracy is not related to the accuracy of estimated transmit power. Comparing Fig. 4.17 with Fig. 4.15, it is obvious that the accuracy of PCAL-gsDRSS, PCAL-EPt-gsDRSS and LSRE-SDP [9] is higher

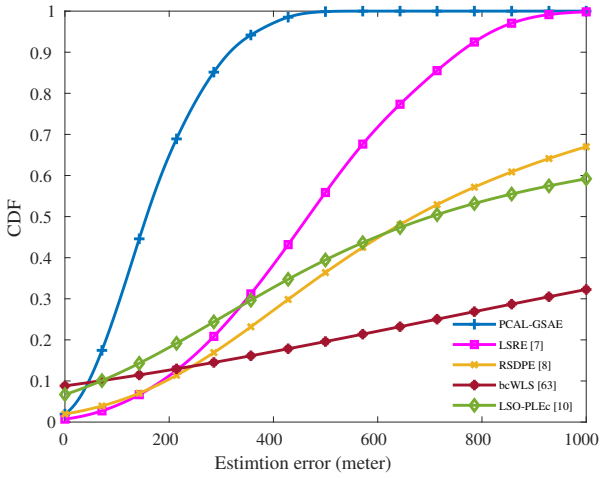

Figure 4.13: CDFs of estimation error of PCAL-GASE, LSRE [7], RSDPE [8], bcWLS [63] and LSO-PLEc [10] with $N = 4$ UAV-BSs and TS only.

than that of PCAL and LSRE [7] with known transmit power. The results validate the statement made in section 4.4, as the real Pt is not beneficial for localisation. However, the estimated Pt and EPt improve accuracy of localisation through mitigating impact of $X_{S,i}$ on ranging distances. Therefore, it is suggested to use estimated Pt rather than real value in localisation, even if the real Pt was perfectly known.

The suggestion made by our work is opposite to the existing research, which reason is attributed to the difference of localisation scenario. More specifically, for our work, only a few measurements are accessible for localisation, and the uncertainties on RSS, *i.e.*, Gaussian distributed error $X_{S,i}$, play the major impact on localisation than those on η_i and Pt,. Thus, the estimated η_i and Pt are preferable to real values, in order to alleviate the impact of $X_{S,i}$. However, for localisation scenarios in [61],[62],[66], [77], the uncertainties on RSS are efficiently mitigated by sufficiently large amount of RSS measurements, while the uncertainties of η_i and Pt are remained as the major resource of localisation error. Therefore, it is summarised that, the number of available measurements determines whether using real parameters or estimated parameters.

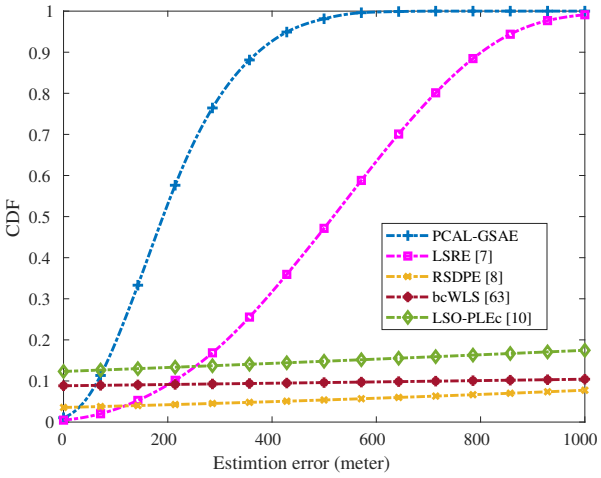

Figure 4.14: CDFs of estimation error of PCAL-GASE, LSRE [7], RSDPE [8], bcWLS [63] and LSO-PLEc [10] with $N = 4$ UAV-BSs, TS and AS of standard deviation $\sigma_{AS} = 4.4$ dB.

4.6 Summary

We have proposed a PCAL scheme for multiple UAV-BSs assisted and RSS based MS localisation without requiring PLEs to be equal and perfectly known. The two-step approximations by piecewise convex approximation and curve fitting yield a convex localisation problem that matches the EAPL model [73] very well. The localisation problem is then converted to linear via TSE which can be solved by SDP with comparable complexity to that of [7]. The proposed PCAL approach with unknown and unequal PLEs significantly outperforms the approaches in [7],[8],[10],[63] with perfectly known and equal PLEs, and [10] with unknown and unequal PLEs. It also demonstrates higher robustness against shadowing especially AS in the scenario of UAV. The proposed GSAE method can eliminate ambiguity more effectively than the PLM method in [37]. For localisation with unknown transmit power, the proposed PCAL-gsDRSS scheme achieves twice accuracy than that of the approach in [9]. With assumed known EPt and EPLE, localisation and ranging distance are proved more accurate than that using real PLE and *Pt*. Based on estimated EPt, the proposed PCAL-EPt-gsDRSS can reduce at least 20 meter localisation error than that of PCAL-gsDRSS. The effect of EPLE is verified by analysis.

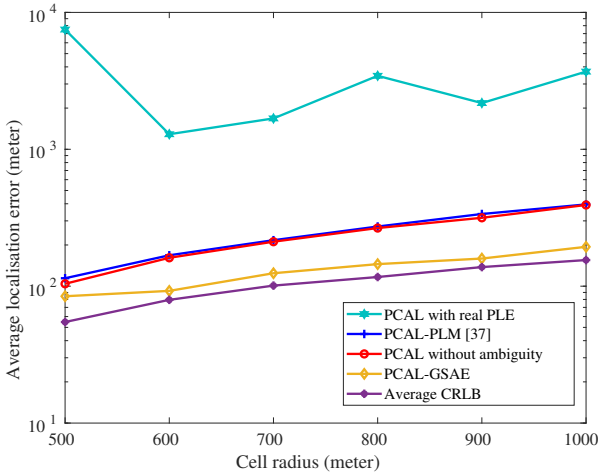

Figure 4.15: Average localisation error of PCAL with real PLEs, PCAL-PLM [37], PCAL without ambiguity, PCAL-GSAE, and average CRLB with $N = 4$ UAV-BSs, UAV altitudes $h_i = 200$ m (i=1,...,4), and AS of standard deviation $\sigma_{AS} = 4.4$ dB.

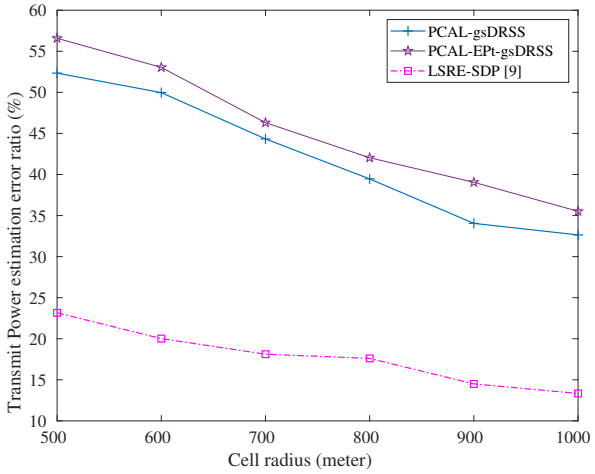

Figure 4.16: Average transmit power estimation error ratio of PCAL-gsDRSS, PCAL-EPt-gsDRSS, LSRE-SDP [9], when the real Pt=23 dBm is unknown, and AS of standard deviation $\sigma_{AS} = 4.4$ dB.

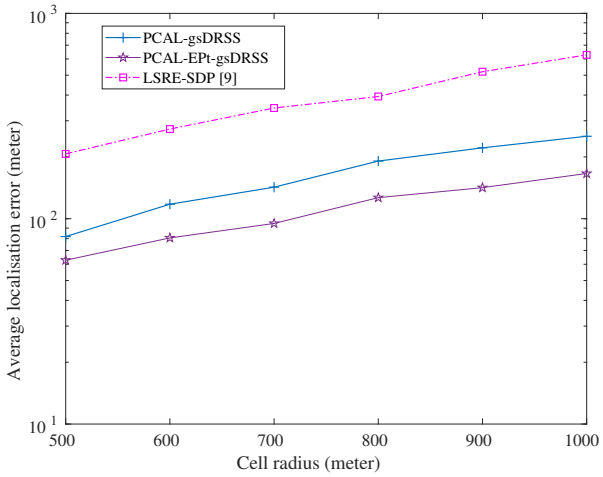

Figure 4.17: Average localisation error of PCAL-gsDRSS, PCAL-EPt-gsDRSS, LSRE-SDP [9], when the real Pt=23 dBm is unknown, and AS of standard deviation $\sigma_{AS} = 4.4$ dB.

Chapter 5

Intelligent Surface Assisted And Massive MIMO Based Localisation

5.1 Introduction

The B5G or 6G networks will be intelligent systems and provide users with the wider bandwidths, higher data rate (1 Tb/s) and higher accuracy localisation [82]. These requirements are fufilled by massive arrays and IS based new architecture [83].

Massive MIMO based localisation will continue to develop towards the higher accuracy empowered by the larger transmitter and receiver arrays. The existing research mainly focuses on analysing the performance limits. In [84], PEB and OEB of both uplink and downlink localisation was proved inversely proportional to the number of antenna elements. The asymptotic orthogonality of massive MIMO was proved with sufficiently large array and signal bandwidth. In [85],[86], the FIM of NLOS components was presented as significant location information for localisation [85], and [86] also stated that reasonable performance of positioning gained by NLOS components of moving target [86]. In [87], fundamental bounds on position and orientation of targets in mm-wave communication system were derived. A refinement algorithm was proposed to resolve position-related channel parameters of both LOS and NLOS paths. Single anchor based indoor localisation was studied in [12]. The performance of different array configurations with signals synchronisation error and beamforming quantization error was numerically evaluated by FIM and CRLB.

A lot of recent research focused on exploiting randomness of propagation environment

and improving QoS of communication, including two notable techniques, IS and spatial modulation (SM) technique. Recent research on IS based IM [88] proposed to adjust the IS phases according to the indices of selected receive antenna with the maximised instantaneous received SNR. The received signal quality in fading channels is improved. The existing work on IS assisted localisation concentrates on the performance of near-field and far-field localisation. For given propagation distances, a large IS could be in near-field regime while transmitters and receivers are in far-field regime. IS assisted far-field localisation was studied in [13],[14]. In [14], the adaptive beamforming and ISpsf design algorithms were proposed to optimise the performance of far-field IS assisted communication and positioning. In [13], PEB and OEB of IS assisted massive MIMO system were found decrease with the size of IS. However, according to the signal models of IS proposed in [89],[35],[36], the channel parameters of IS vary with the position of IS elements, thus the far-field regime could bring non-negligible approximation error on near-field localisation. In [90], near-field and far-field was distinguished by *Fraunhofer distance*, based on which the entire array was divided into multiple sub-arrays of approximated parameters. The results show that the performance of sub-arrays is getting close to that of standard entire array with increasing propagation distance, in contrast with [32], [33],[34]. To clear up confusion, it is necessary to investigate the impact of far-field approximation on the performance of localisation.

The existing work on ISpsf design in IS assisted localisation [13], [14],[32] propose to optimise ISpsf with respect to maximising data rate, rather than maximising localisation accuracy. The reason might be attributed to that, in the aforementioned work, the terms containing IS parameters are merged to a scalar before calculating FIM. However, for a large steerable IS assisted system, CRLBs of channel parameters and MS location information vary with the position of IS elements and the directions of impinging signals [13], [36]. Thus, this gap on IS assisted localisation motivates us to study the optimal localisation-aimed ISpsf.

In this chapter, we study the performance of localisation of an IS assisted massive MIMO system with single BS and single MS, where BS and MS are in LOS links towards the IS, and BS beamforming is pointing at the IS. Our work is different from the existing works [13], [14],[32] in the following aspects.

1. We derive the expressions of exact FIMs (eFIMs), approximated FIMs (aFIMs) and CRLBs of channel parameters and MS location information. eFIM of both channel

parameters and the controllable phases of IS is proved non-invertible and meaningless for localisation. Based on the derived FIMs and CRLBs, localisation assisted by both ISs with known and unknown position is investigated. Numerical results reveal that PEB and OEB of MS are generally increasing with the number of employed IS elements, while that of unknown IS fluctuates severely, even if the number of IS elements stays in near-field zone.

2. Based on the derived FIM and CRLB, a localisation-aimed ISpsf is proposed to maximise the performance of localisation, and the ISpsf that maximises the estimation accuracy of each parameter is also investigated. To the best of our knowledge, this is the first work studying the impact of IS parameters on the ISpsf design and the performance of localisation. Our simulation results shows considerable improvement on the performance of localisation brought by localisation-aimed ISpsf than that using the communication-used ISpsf. With the derived localisation-aimed ISpsf, performance of localisation is investigated with 1, 4, 8-bit quantizers. The results show that the expensive quantizer is only valuable for large IS array with awareness of both position and orientation.

The rest of this chapter is organised as follows. The system model, channel model and signal model are presented in section 5.2. The power consumption model is introduced in Section 5.2. FIMs and CRLBs of channel parameters and MS location information are derived in section 5.3. The problem formulation of ISpsf design is described in section 5.4, with localisation-aimed ISpsf derived. Section 5.5 demonstrates the simulation results, and Section 5.6 gives the summary.

5.2 System Model

We consider the IS-based massive MIMO narrowband downlink communication FDD system operating at frequency f_c. Signal bandwidth W is separated into U frequency bins, where the frequency of the ι-th subcarrier is f_ι. BS is selected as the reference of the 3D Cartesian coordinate system, *i.e.*, the coordinate and orientation angle of BS is $\mathbf{w} = [0, 0, z_{\text{BS}}]^{\text{T}}$ and $\mathbf{o}_{\text{BS}} = [\vartheta_{\text{BS}}, \varphi_{\text{BS}}]^{\text{T}} = [0, 0]^{\text{T}}$. The MS with coordinate $\mathbf{v} = [x_{\text{MS}}, y_{\text{MS}}, z_{\text{MS}}]^{\text{T}}$ and orientation of antenna array $\mathbf{o}_{\text{MS}} = [\theta_{\text{MS}}, \phi_{\text{MS}}]^{\text{T}}$, is detected and localised by the BS. The observed location information at BS is collected from one direct path

between BS and MS, C single bounced NLOS paths via C clusters, and N_{IS} paths via an IS. Both BS, MS and IS are respectively equipped with URA of $N_{\mathrm{T}}, N_{\mathrm{R}}$ and N_{IS} elements distributed on rectangular grids with constant element spacing $\Delta_d = 0.5\lambda$, where λ is wavelength. The C clusters are located at unknown position $\mathbf{q}_c = [q_{x,c}, q_{y,c}, q_{z,c}], c = 1, \ldots, C$, and the IS with orientation $\mathbf{o}_{\mathrm{IS}} = [\nu_{\mathrm{IS}}, \mu_{\mathrm{IS}}]^{\mathrm{T}}$ is located at $\mathbf{r}_{\mathrm{I}} = [x_{\mathrm{I}}, y_{\mathrm{I}}, z_{\mathrm{I}}]$. The IS can be regarded as a reconfigurable planar array of N_{IS} passive reflector elements, which adjusts the reflected path to optimise the channel response by inducing various phase shifts and amplitude attenuation to each path. In the scenario as shown by Fig. 5.1, the BS transmits signals to the MS through $L = 1 + C + N_{\mathrm{IS}}$ paths, including 1 direct path, $C \geqslant 0$ reflected paths via the clusters, and $N_{\mathrm{IS}} \geqslant 0$ reflected paths via the IS. Assume that BS and MS are in far-field scenario, IS is in near-field with various parameters at each reflector element. The first arrival path from BS to MS is considered as the direct path, parameters and matrices of which are labelled by subscript '1'. Whereas the sets of cluster reflective paths and the IS-aided paths are denoted by Λ_{s} and Λ_{R}, where $|\Lambda_{\mathrm{s}}| = C$, $|\Lambda_{\mathrm{R}}| = N_{\mathrm{IS}}$. The IS can be regarded as a reflective antenna array in the system, which works as the receiver in BS-IS direct link and the transmitter in the IS-MS direct link, known as "forward link" (fw) and "backward link" (bw) [31].

5.2.1 Array Model

In a downlink system, BS is the transmitter and MS is the receiver. The unit-norm antenna steering vectors [40] of receiver antenna (Rx) and transmitter antenna (Tx) of the l-th path are respectively expressed as

$$\mathbf{a}_{\mathrm{R},l}(\theta_l, \phi_l, \theta_{\mathrm{MS}}, \phi_{\mathrm{MS}}) \equiv \frac{1}{\sqrt{N_{\mathrm{R}}}} e^{-j2\pi \boldsymbol{\chi}_{\mathrm{R}} \mathbf{k}(\theta_l, \phi_l)} \in \mathbb{C}^{N_{\mathrm{R}} \times 1}, \tag{5.1a}$$

$$\theta_l \equiv \arccos\left(\frac{v_{\mathrm{R},z,l}}{\|\mathbf{v}_{\mathrm{R},l}\|}\right), \tag{5.1b}$$

$$\phi_l \equiv \arctan\left(\frac{v_{\mathrm{R},y,l}}{v_{\mathrm{R},x,l}}\right), \tag{5.1c}$$

$$\mathbf{v}_{\mathrm{R},l} = [v_{\mathrm{R},x,l}, v_{\mathrm{R},y,l}, v_{\mathrm{R},z,l}]^{\mathrm{T}} = \mathbf{R}(\mathbf{o}_{\mathrm{MS}})^{-1}(\mathbf{v}_l - \mathbf{v}) \tag{5.1d}$$

and

$$\mathbf{a}_{\mathrm{T},l}(\vartheta_l, \varphi_l, \theta_{\mathrm{BS}}, \phi_{\mathrm{BS}}) \equiv \frac{1}{\sqrt{N_{\mathrm{T}}}} e^{-j2\pi \boldsymbol{\chi}_{\mathrm{T}} \mathbf{k}(\vartheta_l, \varphi_l)} \in \mathbb{C}^{N_{\mathrm{T}} \times 1}, \tag{5.2a}$$

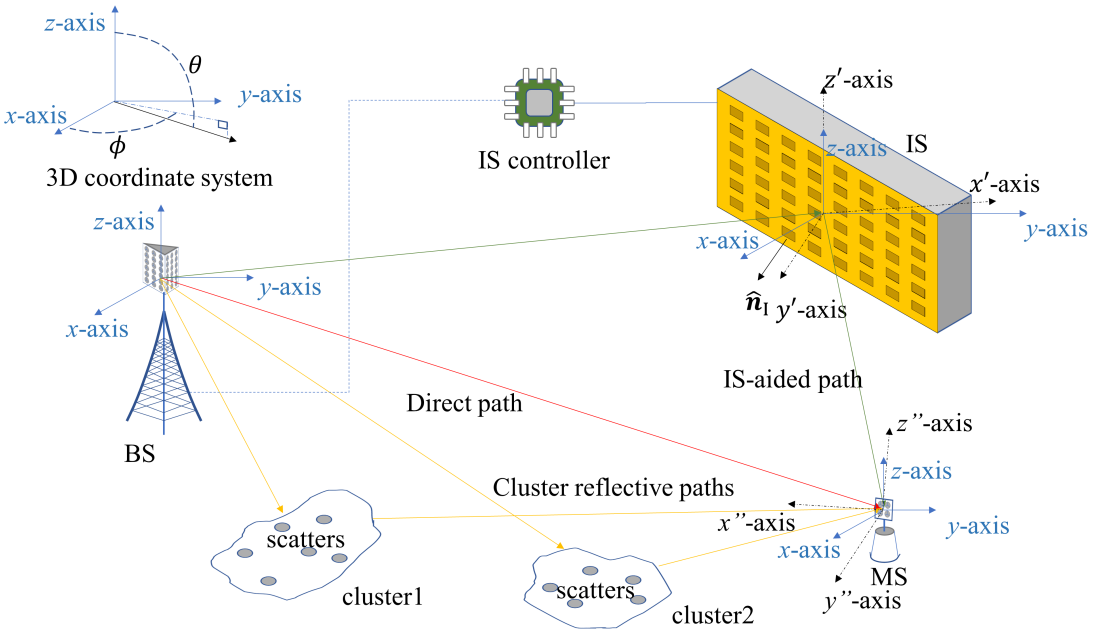

Figure 5.1: IS-assisted massive MIMO system

$$\vartheta_l \equiv \arccos\left(\frac{w_{\mathrm{T},z,l}}{\|\mathbf{w}_{\mathrm{T},l}\|}\right), \tag{5.2b}$$

$$\varphi_l \equiv \arctan\left(\frac{w_{\mathrm{T},y,l}}{w_{\mathrm{T},x,l}}\right), \tag{5.2c}$$

$$\mathbf{w}_{\mathrm{T},l} = [w_{\mathrm{T},x,l}, w_{\mathrm{T},y,l}, w_{\mathrm{T},z,l}]^{\mathrm{T}} = \mathbf{R}(\mathbf{o}_{\mathrm{BS}})^{-1}(\mathbf{v}_l - \mathbf{w}) \tag{5.2d}$$

where $\boldsymbol{\chi}_{\mathrm{R}} = (\mathbf{R}(\mathbf{o}_{\mathrm{MS}})\mathbf{p}_{\mathrm{R}})^{\mathrm{T}} \in \mathbb{C}^{N_{\mathrm{R}}\times 3}$ and $\boldsymbol{\chi}_{\mathrm{T}} = (\mathbf{R}(\mathbf{o}_{\mathrm{BS}})\mathbf{p}_{\mathrm{T}})^{\mathrm{T}} = \mathbf{p}_{\mathrm{T}}^{\mathrm{T}} \in \mathbb{C}^{N_{\mathrm{T}}\times 3}$ are respectively the coordinates of Rx elements and Tx elements. $\mathbf{v}_{\mathrm{R},l}$ and $\mathbf{w}_{\mathrm{T},l}$ are the coordinates of either the BS, scatter, reflector element or MS. $\mathbf{R}(\mathbf{o}_{\mathrm{MS}})$ is the rotation matrix. $\mathbf{p}_{\mathrm{R}} \in \mathbb{C}^{3\times N_{\mathrm{R}}}$ and $\mathbf{p}_{\mathrm{T}} \in \mathbb{C}^{3\times N_{\mathrm{T}}}$ are the matrices of relative coordinates of each antenna element from the corresponding array centre. d_{R} and d_{T} are the element intervals of Rx and Tx. θ_l, ϕ_l, ϑ_l and φ_l respectively represent the elevation angle and azimuth angle of the l-th path at the MS, and those at the BS, which are named as elevation angle of arrival (eAOA), azimuth angle of arrival (aAOA), elevation angle of departure (eAOD) and azimuth angle of departure (aAOD) in the downlink communication system. $\mathbf{k}(\theta_l, \phi_l)$ is the unit direction vector, which is a function of (θ_l, ϕ_l), and it is calculated as $\mathbf{k}(\theta, \phi) = [\cos\phi\sin\theta, \sin\phi\sin\theta, \cos\theta]^{\mathrm{T}}$. Define $\mathbf{A}_{\mathrm{R}} = [\mathbf{a}_{\mathrm{R},1}, \ldots, \mathbf{a}_{\mathrm{R},L}]$ and $\mathbf{A}_{\mathrm{T}} = [\mathbf{a}_{\mathrm{T},1}, \ldots, \mathbf{a}_{\mathrm{T},L}]$ as the sets of receiver and trans-

mitter steering vectors of all paths. μ_l and ν_l denote the azimuth angle and elevation angle of signal observed at the IS.

For the l-th path reflected by the IS, the antenna steering vector of IS reflector (Ix) toward the direction (ν_l, μ_l) is defined as $\mathbf{a}_{\mathrm{I}}(\nu_l, \mu_l) \equiv \frac{1}{\sqrt{N_{\mathrm{IS}}}} e^{-j\boldsymbol{\chi}_{\mathbf{I}}\mathbf{k}(\nu_l,\mu_l)}$, where $\boldsymbol{\chi}_{\mathrm{I}} \in \mathbb{C}^{N_{\mathrm{IS}}\times 3}$ denotes the Ix element coordinates. Considering nonidentical incident angle and reflective angle of the N_{IS} Ix elements, the generic elements of array response of the p-th forward path and the p-th backward path are respectively expressed as

$$a_{\mathrm{fw},p} \equiv \frac{1}{\sqrt{N_{\mathrm{IS}}}} e^{-j2\pi\boldsymbol{\chi}_{\mathrm{I},\boldsymbol{p}}\mathbf{k}(\mu_{\mathrm{fw},p},\nu_{\mathrm{fw},p})} \in \mathbb{C}^{N_{\mathrm{IS}}\times 1} \tag{5.3a}$$

$$\mu_{\mathrm{fw},p} = \tan^{-1}\left(\frac{y_{p,\mathrm{BS}}}{x_{p,\mathrm{BS}}}\right) \tag{5.3b}$$

$$\nu_{\mathrm{fw},p} = \cos^{-1}\left(\frac{z_{p,\mathrm{BS}}}{\|\mathbf{r}_{p,\mathrm{BS}}\|}\right) \tag{5.3c}$$

$$\mathbf{r}_{p,\mathrm{BS}} \equiv [x_{p,\mathrm{BS}}, y_{p,\mathrm{BS}}, z_{p,\mathrm{BS}}]^{\mathrm{T}} \tag{5.3d}$$

and

$$a_{\mathrm{bw},p} \equiv \frac{1}{\sqrt{N_{\mathrm{IS}}}} e^{-j2\pi\boldsymbol{\chi}_{\mathrm{I},\boldsymbol{p}}\mathbf{k}(\mu_{\mathrm{bw},p},\nu_{\mathrm{bw},p})} \in \mathbb{C}^{N_{\mathrm{IS}}\times 1} \tag{5.4a}$$

$$\mu_{\mathrm{bw},p} = \tan^{-1}\left(\frac{y_{p,\mathrm{MS}}}{x_{p,\mathrm{MS}}}\right) \tag{5.4b}$$

$$\nu_{\mathrm{bw},p} = \cos^{-1}\left(\frac{z_{p,\mathrm{MS}}}{\|\mathbf{r}_{p,\mathrm{MS}}\|}\right) \tag{5.4c}$$

$$\mathbf{r}_{p,\mathrm{MS}} \equiv [x_{p,\mathrm{MS}}, y_{p,\mathrm{MS}}, z_{p,\mathrm{MS}}]^{\mathrm{T}} \tag{5.4d}$$

where the subscript $p = \{1, \ldots, N_{\mathrm{IS}}\}$ is a special index of Ix elements. The coordinates of rotated Ix elements are collected in the set $\boldsymbol{\chi}_{\mathrm{I}} = (\mathbf{R}(\mathbf{o}_{\mathrm{IS}})\mathbf{p}_{\mathrm{I}})^{\mathrm{T}} \in \mathbb{C}^{N_{\mathrm{IS}}\times 3}$, where the p-th row vector is expressed as $\boldsymbol{\chi}_{\mathrm{I},p}$, and $\mathbf{p}_{\mathrm{I}} \in \mathbb{C}^{3\times N_{\mathrm{R}}}$ is the matrix of the relative position of Ix element from the IS centre. Thus, the coordinates of the p-th Ix element observed at the BS is $\boldsymbol{\chi}_{\mathrm{BS},p} = \mathbf{r}_{\mathrm{I}} + \boldsymbol{\chi}^{\mathrm{P}}_{\mathrm{I},p}$. $\mu_{\mathrm{fw},p}$ and $\nu_{\mathrm{fw},p}$ denote the observed azimuth angle and elevation angle of the incident wave at the p-th Ix element, and $\mu_{\mathrm{bw},p}$ and $\nu_{\mathrm{bw},p}$ are those of the reflective wave. $\mathbf{r}_{p,\mathrm{BS}}$ and $\mathbf{r}_{p,\mathrm{MS}}$ respectively represent the relative coordinates of the BS and MS from the p-th Ix element observed at the IS. The distance from BS and MS to the p-th Ix element are calculated as $r_{\mathrm{fw},p} = \|\mathbf{r}_{\mathrm{I}} + \boldsymbol{\chi}_{\mathrm{I},p} - \mathbf{w}\|$ and $r_{\mathrm{bw},p} = \|\mathbf{v} - (\mathbf{r}_{\mathrm{I}} + \boldsymbol{\chi}^{\mathrm{T}}_{\mathrm{I},p})\|$. Therefore, the BS coordinates observed at IS can be calculated as $\mathbf{r}_{p,\mathrm{BS}} = \mathbf{R}(\mathbf{o}_{\mathrm{IS}})^{-1}(\mathbf{w} - (\mathbf{r}_{\mathrm{I}} + \boldsymbol{\chi}^{\mathrm{T}}_{\mathrm{I},p}))$ or

$\mathbf{r}_{p,\mathrm{BS}} = r_{\mathrm{fw},p}\mathbf{k}(\nu_{\mathrm{fw},p}, \mu_{\mathrm{fw},p})$, and the observed coordinates of MS are calculated as $\mathbf{r}_{p,\mathrm{MS}} = \mathbf{R}(\mathbf{o}_{\mathrm{IS}})^{-1}(\mathbf{v} - (\mathbf{r}_{\mathrm{I}} + \boldsymbol{\chi}_{\mathrm{I},p}^{\mathrm{T}}))$ or $\mathbf{r}_{p,\mathrm{MS}} = r_{\mathrm{bw},p}\mathbf{k}(\nu_{\mathrm{bw},p}, \mu_{\mathrm{bw},p})$.

The equations (5.1)∼(5.4) interpret the relation between channel parameters and location information. For the downlink system, the observed location of MS can be expressed as

$$\mathbf{v} = \begin{cases} r_{1,c}\mathbf{k}(\vartheta_l, \varphi_l) - \mathbf{R}(\mathbf{o}_{\mathrm{MS}})(r_{2,c}\mathbf{k}(\theta_l, \phi_l)), & l \in \Lambda_{\mathrm{s}} \\ \mathbf{r}_{\mathrm{I}} + \boldsymbol{\chi}_{\mathrm{I},p}^{\mathrm{T}} + \mathbf{R}(\mathbf{o}_{\mathrm{IS}})(r_{\mathrm{bw},p}\mathbf{k}(\nu_{\mathrm{bw},p}, \mu_{\mathrm{bw},p})), & l \in \Lambda_{\mathrm{R}} \end{cases} \tag{5.5}$$

where $r_{1,c}$ and $r_{2,c}$ are the distance from BS and MS to the c-th cluster. Note that, for the uplink system and $l \in \Lambda_{\mathrm{R}}$, the position of MS is $\mathbf{v} = \mathbf{r}_{\mathrm{I}} + \boldsymbol{\chi}_{\mathrm{I},p}^{\mathrm{T}} + \mathbf{R}(\mathbf{o}_{\mathrm{IS}})(r_{\mathrm{fw},p}\mathbf{k}(\nu_{\mathrm{fw},p}, \mu_{\mathrm{fw},p}))$.

5.2.2 Channel Model

Define $\mathbf{A}_{\mathrm{R}} = [\mathbf{a}_{\mathrm{R},1}, \ldots, \mathbf{a}_{\mathrm{R},L}]$ and $\mathbf{A}_{\mathrm{T}} = [\mathbf{a}_{\mathrm{T},1}, \ldots, \mathbf{a}_{\mathrm{T},L}]$ as the sets of receiver and transmitter steering vectors of all paths, and $\boldsymbol{\beta} = [\beta_1, \ldots, \beta_L]$ is the complex channel gain vector, where $\beta_l = \rho_l e^{j\zeta_l}$, ρ_l and $\zeta_l \in [0,\ 2\pi]$ are respectively the signal power and arbitrary path phase of the l-th path, and $\boldsymbol{\alpha}_\tau = [\alpha_1, \ldots, \alpha_L]$ is the delay vector, then the direct channel and cluster reflective channels can be expressed as given by:

$$\mathbf{H}_{\mathrm{d}} \equiv \beta_1\alpha_1\mathbf{a}_{\mathrm{R}}\mathbf{a}_{\mathrm{T}}^{\mathrm{H}} \in \mathbb{C}^{N_{\mathrm{R}} \times N_{\mathrm{T}}} \tag{5.6}$$

and

$$\mathbf{H}_{\mathrm{s}} \equiv \mathbf{A}_{\mathrm{R},\Lambda_{\mathrm{s}}}\mathbf{b}_{\beta,\mathrm{s}}\mathbf{T}_{\mathrm{s}}\mathbf{A}_{\mathrm{T},\Lambda_{\mathrm{s}}} = \sum_{l \in \Lambda_{\mathrm{s}}} \beta_l\alpha_l\mathbf{a}_{\mathrm{R},l}\mathbf{a}_{\mathrm{T},l}^{\mathrm{H}} \in \mathbb{C}^{N_{\mathrm{R}} \times N_{\mathrm{T}}} \tag{5.7}$$

where $\mathbf{A}_{\mathrm{R},\Lambda_{\mathrm{s}}} \subset \mathbf{A}_{\mathrm{R}}$ and $\mathbf{A}_{\mathrm{T},\Lambda_{\mathrm{s}}} \subset \mathbf{A}_{\mathrm{T}}$ are the collections of antenna steering vectors of cluster reflective paths. $\mathbf{b}_{\beta,\mathrm{s}} = diag\{\boldsymbol{\beta}_{\Lambda_{\mathrm{s}}}\}$, $\mathbf{T}_{\mathrm{s}} = diag\{\boldsymbol{\alpha}_{\Lambda_{\mathrm{s}}}\}$, wherein $\boldsymbol{\beta}_{\Lambda_{\mathrm{s}}} \subset \boldsymbol{\beta}$, $\boldsymbol{\alpha}_{\Lambda_{\mathrm{R}}} \subset \boldsymbol{\alpha}_\tau$, the elements of the cluster reflective path $l \in \Lambda_{\mathrm{s}}$ are $\beta_l \in \boldsymbol{\beta}_{\Lambda_{\mathrm{s}}}$, $\alpha_l \in \boldsymbol{\alpha}_{\Lambda_{\mathrm{s}}}$, and $|\beta_l| = 1$, $\alpha_l = e^{-j2\pi f\tau_l}$, τ_l is the l-th time delay, f is the frequency.

Define $\mathbf{A}_{\mathrm{fw}} = [a_{\mathrm{fw},1}, \ldots, a_{\mathrm{fw},N_{\mathrm{IS}}}]^{\mathrm{T}}$ and $\mathbf{A}_{\mathrm{bw}} = [a_{\mathrm{bw},1}, \ldots, a_{\mathrm{bw},N_{\mathrm{IS}}}]^{\mathrm{T}}$ as the IS steering vectors applied for forward link and backward link, the reflective channel via the IS of

perfect efficiency can be obtained as:

$$\mathbf{H}_{\mathrm{R}} \equiv \mathbf{H}_{\mathrm{I},2}\mathbf{T}_{\Lambda_{\mathrm{R}}}\mathbf{\Psi}_{\mathrm{I}}\mathbf{H}_{\mathrm{I},1} \in \mathcal{C}^{N_{\mathrm{R}}\times N_{\mathrm{T}}} \tag{5.8a}$$

$$\mathbf{H}_{\mathrm{I},1} \equiv \mathbf{A}_{\mathrm{fw}}\mathbf{h}_{\mathrm{I},1}\mathbf{A}^{\mathrm{H}}_{\mathrm{T},\Lambda_{\mathrm{R}}} \in \mathcal{C}^{N_{\mathrm{IS}}\times N_{\mathrm{T}}} \tag{5.8b}$$

$$\mathbf{H}_{\mathrm{I},2} \equiv \mathbf{A}_{\mathrm{R},\Lambda_{\mathrm{R}}}\mathbf{h}_{\mathrm{I},2}\mathbf{A}^{\mathrm{H}}_{\mathrm{bw}} \in \mathcal{C}^{N_{\mathrm{R}}\times N_{\mathrm{IS}}} \tag{5.8c}$$

where $\mathbf{A}_{\mathrm{R},\Lambda_{\mathrm{R}}} \subset \mathbf{A}_{\mathrm{R}}$ and $\mathbf{A}_{\mathrm{T},\Lambda_{\mathrm{R}}} \subset \mathbf{A}_{\mathrm{T}}$ are the sets of Rx and Tx steering vectors of IS-aided paths. $\mathbf{H}_{\mathrm{I},1}$ and $\mathbf{H}_{\mathrm{I},2}$ denote the channel vectors of forward link and backward link, where $\mathbf{h}_{\mathrm{I},1} = diag\{[h_{\mathrm{fw},1},\ldots,h_{\mathrm{fw},N_{\mathrm{IS}}}]\}$ and $\mathbf{h}_{\mathrm{I},2} = diag\{[h_{\mathrm{bw},1},\ldots,h_{\mathrm{bw},N_{\mathrm{IS}}}]\}$ are the matrices of complex channel gain. $\mathbf{T}_{\Lambda_{\mathrm{R}}} = diag\{\boldsymbol{\alpha}_{\Lambda_{\mathrm{R}}}\}$ is the delay vector of IS-aided paths. $\mathbf{\Psi}_{\mathrm{I}} = diag\{\Gamma_{\mathrm{R}}\}diag\{\mathbf{\Psi}_{\mathrm{R}}\}$, and $\Gamma_{\mathrm{R}} = [\epsilon_{\mathrm{eff},1},\ldots,\epsilon_{\mathrm{eff},N_{\mathrm{IS}}}]$ and $\mathbf{\Psi}_{\mathrm{R}} = [e^{j\psi_1},\ldots,e^{j\psi_{N_{\mathrm{IS}}}}]$ are the vectors of signal amplitude control and phase shifts, and $\epsilon_{\mathrm{eff},p} \in [0,1]$ is the energy efficiency controlled by the p-th passive Ix element, ψ_p is the adjustable phase. To maximise the reflected signals, $\Gamma_{\mathrm{R}} = \mathbf{1}^{\mathrm{T}}_{N_{\mathrm{IS}}}$ is applied for the sequel of this paper, thus, $\mathbf{\Psi}_{\mathrm{I}} = diag\{\mathbf{\Psi}_{\mathrm{R}}\}$. The practical IS with b_{I}-bit quantizers cannot produce continuous phase shift between $[0,2\pi]$. Thus, a random quantization error $\Delta\psi_p \in [-\frac{2\pi}{2^{b_{\mathrm{I}}+1}}, \frac{2\pi}{2^{b_{\mathrm{I}}+1}}]$ should be considered for the IS-aided paths, and the matrix of discrete phase shift is expressed as $\tilde{\mathbf{\Psi}}_{\mathrm{I}} = diag\{\tilde{\mathbf{\Psi}}_{\mathrm{R}}\}$, $\tilde{\mathbf{\Psi}}_{\mathrm{R}} = [e^{\tilde{\psi}_1},\ldots,e^{\tilde{\psi}_{N_{\mathrm{IS}}}}]$, where $\tilde{\psi}_l = \psi_l + \Delta\psi_l$.

The path loss model of the IS-aided channel in single-input single-output (SISO) system proposed in [89] is utilised to derive channel coefficients of the IS-based massive MIMO system. Assume identical effective aperture of each Ix element, *i.e.*, $A_{\mathrm{eff}} = a_{\mathrm{eff}}G_{\mathrm{eff}}$, where $a_{\mathrm{eff}} = \lambda^2/(4\pi)$, and $G_{\mathrm{eff}}(\psi_{\mathrm{ib}}) = \gamma_{\mathrm{cp}}\cos^{2q_0}(\psi_{\mathrm{ib}})$ is the element radiation pattern, $\gamma_{\mathrm{cp}} = 4q_0+2$ is the coefficient satisfying conservation of power, ψ_{ib} denotes the broadside angle, q_0 is the element gain. Assume that the polarization between Tx, IS and Rx is perfectly matched, and the effective aperture is $a_{\mathrm{eff}} = \lambda^2/4$, the path loss of IS-aided channel is given as [89]:

$$L_{\mathrm{IS}} = \left(\left|\sum_{p=1}^{N_{\mathrm{IS}}} e^{j\psi_p}\rho_{\mathrm{I},p}\alpha_p\right|^2 \epsilon_{\mathrm{eff},p}\right)^{-1} \tag{5.9}$$

$$\rho_{\mathrm{I},p} = \underbrace{\sqrt{\frac{a_{\mathrm{eff}}(+\hat{\mathbf{r}}_{\mathrm{fw},p}\bullet\hat{\mathbf{n}}_{\mathrm{I}})^{2q_0}}{4\pi r^2_{\mathrm{fw},p}}}}_{\equiv\ \rho_{\mathrm{fw},p}} \underbrace{\sqrt{\frac{a_{\mathrm{eff}}(+\hat{\mathbf{r}}_{\mathrm{bw},p}\bullet\hat{\mathbf{n}}_{\mathrm{I}})^{2q_0}}{4\pi r^2_{\mathrm{bw},p}}}}_{\equiv\ \rho_{\mathrm{bw},p}} \tag{5.10}$$

$$\alpha_p = \underbrace{e^{-j2\pi f \tau_{\mathrm{fw},p}}}_{\equiv \alpha_{\mathrm{fw},p}} \underbrace{e^{-j2\pi f \tau_{\mathrm{bw},p}}}_{\equiv \alpha_{\mathrm{bw},p}} \tag{5.11}$$

where α_p and $\rho_{\mathrm{I},p}$ denote the time shift factor and power attenuation of the p-th path induced by signal propagation, where the time delay is calculated as $\tau_p = \tau_{\mathrm{fw},p} + \tau_{\mathrm{bw},p}$, $\tau_{\mathrm{fw},p} = r_{\mathrm{fw},p}/c$, $\tau_{\mathrm{bw},p} = r_{\mathrm{bw},p}/c$, and c is the speed of light. When the radiation pattern is $G_{\mathrm{eff}}(\psi_{cp} = 0) = \pi$, it is obtained that the gain of each Ix element is $q_0 \approx 0.285$. The term $\cos(\psi_{\mathrm{ib}})$ of the incident wave and reflected wave are respectively replaced by the dot products $(-\hat{\mathbf{r}}_{\mathrm{fw},p} \bullet \hat{\mathbf{n}}_{\mathrm{I}})$ and $(+\hat{\mathbf{r}}_{\mathrm{bw},p} \bullet \hat{\mathbf{n}}_{\mathrm{I}})$. The unit vectors $\hat{\mathbf{r}}_{\mathrm{fw},p} \equiv -(\mathbf{r}_{\mathrm{I}} + \boldsymbol{\chi}_{\mathrm{I},p}^{\mathrm{T}} - \mathbf{w})/r_{\mathrm{fw},p}$ and $\hat{\mathbf{r}}_{\mathrm{bw},p} \equiv -(\mathbf{r}_{\mathrm{I}} + \boldsymbol{\chi}_{\mathrm{I},p}^{\mathrm{T}} - \mathbf{v})/r_{\mathrm{bw},p}$ respectively indicate the direction of the incident wave and reflected wave on the p-th Ix element. According to (5.3d) and (5.4d), these functions satisfy that $\hat{\mathbf{r}}_{\mathrm{fw},p} = \mathbf{R}(\mathbf{o}_{\mathrm{IS}})\mathbf{k}(\nu_{\mathrm{fw},p}, \mu_{\mathrm{fw},p})$ and $\hat{\mathbf{r}}_{\mathrm{bw},p} = \mathbf{R}(\mathbf{o}_{\mathrm{IS}})\mathbf{k}(\nu_{\mathrm{bw},p}, \mu_{\mathrm{bw},p})$. The outward-facing perpendicular direction of the IS is expressed as $\hat{\mathbf{n}}_{\mathrm{I}} = [n_x, n_y, n_z]^{\mathrm{T}} = \mathbf{R}(\mathbf{o}_{\mathrm{IS}})[0, 1, 0]^{\mathrm{T}}$. And the dot product is calculated as $+\hat{\mathbf{r}}_{\mathrm{bw},p} \bullet \hat{\mathbf{n}}_{\mathrm{I}} = \hat{\mathbf{r}}_{\mathrm{bw},p}^{\mathrm{T}} \hat{\mathbf{n}}_{\mathrm{I}} = \sin(\mu_{\mathrm{bw},p}) \sin(\nu_{\mathrm{bw},p})$ and $+\hat{\mathbf{r}}_{\mathrm{fw},p} \bullet \hat{\mathbf{n}}_{\mathrm{I}} = \hat{\mathbf{r}}_{\mathrm{fw},p}^{\mathrm{T}} \hat{\mathbf{n}}_{\mathrm{I}} = \sin(\mu_{\mathrm{fw},p}) \sin(\nu_{\mathrm{fw},p})$, where the rotation matrix $\mathbf{R}(\mathbf{o}_{\mathrm{IS}})$ is mitigated. Thus, the path attenuation of the forward link and backward link are rewritten as $\rho_{\mathrm{fw},p} = \sqrt{\frac{a_{\mathrm{eff}}(\sin(\mu_{\mathrm{fw},p}) \sin(\nu_{\mathrm{fw},p}))^{2q_0}}{4\pi^2 r_{\mathrm{fw},p}^2}}$, $\rho_{\mathrm{bw},p} = \sqrt{\frac{a_{\mathrm{eff}}(\sin(\mu_{\mathrm{bw},p}) \sin(\nu_{\mathrm{bw},p}))^{2q_0}}{4\pi^2 r_{\mathrm{bw},p}^2}}$.

Path loss at IS L_{IS} in (5.9) can be decomposed into three components: controllable phase shift $e^{j\psi_p}$, power attenuation $\rho_{\mathrm{I},p}$, time shift factor α_p. Substitute (5.9)-(5.11) to (5.8), and replace the subscript 'p' with 'l', then the l-th complex channel coefficient can be obtained as $h_l = \beta_l \alpha_l, \rho_{\mathrm{I},l} = \rho_{\mathrm{fw},l} \rho_{\mathrm{bw},l}$, which is decomposed into the channel impulse response of the forward link and the backward link, *i.e.*, $|h_{\mathrm{fw},l}|^2 = a_{\mathrm{eff}} \rho_{\mathrm{fw},l}^2$ and $|h_{\mathrm{bw},l}|^2 = a_{\mathrm{eff}} \rho_{\mathrm{bw},l}^2$. Following the same way, the time shift factor of the IS-aided path can be obtained as $\boldsymbol{\alpha}_{\Lambda_{\mathrm{R}}} = [\alpha_1, \ldots, \alpha_{N_{\mathrm{IS}}}], \alpha_p = \alpha_{\mathrm{fw},p} \alpha_{\mathrm{bw},p}$. The IS-aided channel can be obtained as follows:

$$\mathbf{H}_{\mathrm{R}} = \mathbf{T}_\tau \mathbf{b}_\beta \mathbf{P}_{\mathrm{I}} \mathbf{V}_{\mathrm{I}} \tag{5.12a}$$

$$\mathbf{T}_\tau = diag\{\alpha_1, \ldots, \alpha_L\} \tag{5.12b}$$

$$\mathbf{b}_\beta = diag\{\mathbf{b}_{\beta,\mathrm{R}} \odot \mathbf{b}_{\beta,\mathrm{T}}\}, \mathbf{b}_{\beta,\mathrm{R}} = [\boldsymbol{\beta}_{1:1+C}, \tilde{\boldsymbol{\rho}}_{\mathrm{bw}}], \mathbf{b}_{\beta,\mathrm{T}} = [\mathbf{1}_{1+C}^{\mathrm{T}}, \boldsymbol{\rho}_{\mathrm{fw}}] \tag{5.12c}$$

$$\mathbf{P}_{\mathrm{I}} = diag\{\mathbf{1}_{1+C}^{\mathrm{T}}, e^{j\psi_1}, \ldots, e^{j\psi_{N_{\mathrm{IS}}}}\} \tag{5.12d}$$

$$\mathbf{V}_{\mathrm{I}} = diag\{\mathbf{A}_{\mathrm{I}}\}, \mathbf{A}_{\mathrm{I}} = [\mathbf{1}_{1+C}^{\mathrm{T}}, a_{\mathrm{bw},1}^{\mathrm{H}} a_{\mathrm{fw},1}, \ldots, a_{\mathrm{bw},N_{\mathrm{IS}}}^{\mathrm{H}} a_{\mathrm{fw},N_{\mathrm{IS}}}\}] \tag{5.12e}$$

where $\mathbf{b}_\beta = diag\{\boldsymbol{\beta}\}$ is the diagonal matrices of complex channel gain of all paths, and $\boldsymbol{\beta} = [\beta_1, \ldots, \beta_L]$. The matrix of complex channel gain is expressed as the product of

two intermediate matrices $\mathbf{b}_\beta = \mathbf{b}_{\beta,\mathrm{R}}\mathbf{b}_{\beta,\mathrm{T}}$, in order to distinguish the contribution of the forward link and the backward link on $\mathbf{b}_\beta$, and $\tilde{\boldsymbol{\rho}}_{\mathrm{bw}} = [\rho_{\mathrm{bw},1}e^{j\zeta_{2+C}}, \ldots, \rho_{\mathrm{bw},N_{\mathrm{IS}}}e^{j\zeta_L}]$, $\boldsymbol{\rho}_{\mathrm{fw}} = [\rho_{\mathrm{fw},1}, \ldots, \rho_{\mathrm{fw},N_{\mathrm{IS}}}]$.

When the IS is sufficiently far from the transmitter, the N_{IS} paths of forward link are approximately parallel. Then it is reasonable to apply the approximation of path attenuation and incident angles $\rho_{\mathrm{fw},p} \approx \rho_{\mathrm{fw},0}, \mu_{\mathrm{fw},p} \approx \mu_{\mathrm{fw},0}, \nu_{\mathrm{fw},p} \approx \nu_{\mathrm{fw},0}$. Similarly, when the receiver is sufficiently far from the IS, the paths of backward link are approximately parallel, resulting into approximation on path attenuation and reflection angles $\rho_{\mathrm{bw},p} \approx \rho_{\mathrm{bw},0}, \alpha_{\mathrm{bw},p} \approx \alpha_{\mathrm{bw},0}$, reflective angles $\mu_{\mathrm{bw},p} \approx \mu_{\mathrm{bw},0}, \nu_{\mathrm{bw},p} \approx \nu_{\mathrm{bw},0}$. Therefore, IS array responses respectively approximate to $a_{\mathrm{fw},p} \approx a_{\mathrm{fw},0}, a_{\mathrm{bw},p} \approx a_{\mathrm{bw},0}$. Then the approximated channel vector of (5.10) is obtained as

$$\mathbf{H}_{\mathrm{R,far}} \approx \left(\rho_{\mathrm{fw},0}\rho_{\mathrm{bw},0}\sum_{p\in N_{\mathrm{IS}}}\alpha_p e^{j\tilde{\psi}_p}\right)\mathbf{a}_{\mathrm{R},0}\mathbf{a}_{\mathrm{bw},0}^{\mathrm{H}}\mathbf{a}_{\mathrm{fw},0}\mathbf{a}_{\mathrm{T},0}^{\mathrm{H}} \tag{5.13}$$

where $\mathbf{a}_{\mathrm{R},0}$ and $\mathbf{a}_{\mathrm{T},0}$ are the array response with approximated AOA and AOD of IS aided paths.

5.2.3 Signal Model

Therefore, when the transmitter emits a signal $\mathbf{x}(t) \in \mathcal{C}^{N_B\times 1}$ through N_B beams, the perfectly synchronised narrowband received signal during observation time T_o is expressed as

$$\mathbf{Y}(t) \equiv \sum_{l=1}^{L}\underbrace{\sqrt{N_{\mathrm{R}}N_{\mathrm{T}}P_{\mathrm{T}}}\left(\mathbf{H}_{\mathrm{d}} + \mathbf{H}_{\mathrm{s}} + \mathbf{H}_{\mathrm{R}}\right)\mathbf{F}_{\mathrm{B}}\mathbf{x}(t-\tau_l)}_{\equiv\ \mathbf{Y}(t)} + \mathbf{n}_{\mathrm{obs}} \in \mathbb{C}^{N_{\mathrm{R}}\times 1}, 0 \leqslant t \leqslant T_o \tag{5.14}$$

where $\mathbf{F}_{\mathrm{B}} \equiv \sqrt{P_{\mathrm{T}}}[\mathbf{f}_{\mathrm{B},1}, \ldots, \mathbf{f}_{\mathrm{B},N_{\mathrm{B}}}] \in \mathbb{C}^{N_{\mathrm{T}}\times N_B}$ is the directional beamforming matrix, and $\mathbf{f}_{\mathrm{B},b} = \mathbf{a}_{\mathrm{T},b}(\vartheta_b, \varphi_b)$, P_{T} is the transmit power. $\mathbf{n}_{\mathrm{obs}}$ is the additive white Gaussian noise with PSD N_0. Note that, the beamforming matrix is normalised $trace\{\mathbf{F}_{\mathrm{B}}^{\mathrm{H}}\mathbf{F}_{\mathrm{B}}\} = 1$, and the direction of beams (ϑ_b, φ_b) is uniformly distributed in the range of $[\vartheta_l - \pi,\ \vartheta_l + \pi]$ and $[\varphi_l - \pi/2, \varphi_l + \pi/2]$. Thus, the received signal follows the biased complex Gaussian distribution, *i.e.*, $\mathbf{Y}(t) \sim \mathcal{CN}(\mathbf{Y}(t), \mathbf{n}_{\mathrm{obs}})$.

If the sets of index of cluster reflective paths and IS-aided paths are $\Lambda_{\mathrm{s}} = [2, \ldots, 1+C]$, $\Lambda_{\mathrm{R}} = [2+C, \ldots, L]$, thus the paths labelled by subscripts $c = 1, \ldots, C$ and $p = 1, \ldots, N_{\mathrm{IS}}$

respectively corresponds to the subscripts $l = 2, \ldots, 1 + C$ and $l = 2 + C, \ldots, L$. When IS is in the far-field, the approximated channel of IS (5.13) is substituted into (5.14), and the received signal is rewritten as

$$\begin{aligned}\mathbf{Y}(t) =& \sqrt{N_{\mathrm{R}} N_{\mathrm{T}} P_{\mathrm{T}}} \beta_1 \alpha_1 \mathbf{a}_{\mathrm{R}} \mathbf{a}_{\mathrm{T}}^{\mathrm{H}} \mathbf{F}_{\mathrm{B}} \mathbf{x}(t - \tau_1) + \sum_{l=2}^{1+C} \beta_l \alpha_l \mathbf{a}_{\mathrm{R},l} \mathbf{a}_{\mathrm{T},l}^{\mathrm{H}} \mathbf{F}_{\mathrm{B}} \mathbf{x}(t - \tau_l) \\ &+ \left(\rho_{\mathrm{fw},0} \rho_{\mathrm{bw},0} \sum_{l=2+C}^{L} \alpha_l e^{j\tilde{\psi}_l} \right) \mathbf{a}_{\mathrm{R},0} \mathbf{a}_{\mathrm{bw},0}^{\mathrm{H}} \mathbf{a}_{\mathrm{fw},0} \mathbf{a}_{\mathrm{T},0}^{\mathrm{H}} \mathbf{F}_{\mathrm{B}} \mathbf{x}(t - \tau_l) + \mathbf{n}_{\mathrm{obs}}\end{aligned} \tag{5.15}$$

5.3 CRLB of Channel Parameters and Localisation Error

In this section, we first present FIM of all channel parameters for the near-field IS, and far-field MS and BS. Then, EFIM of position-related channel parameters is obtained and used to eliminate the impact of phase shifts. Based on the EFIM, CRLB of MS location parameters is obtained with unknown location of IS and clusters. The impact of N_{T} and N_{R} on EFIM and CRLB are also analysed in this section.

5.3.1 Fisher Information Matrix of Channel Parameters

Define the set of interested parameters as $\boldsymbol{\Omega} \equiv [\boldsymbol{\omega}_1, \tilde{\boldsymbol{\psi}}] \in \mathbb{C}^{1 \times N_1}, N_1 = 7L + 5N_{\mathrm{IS}}$, where the position-related channel parameters are defined as $\boldsymbol{\omega}_1 \equiv [\boldsymbol{\theta}, \boldsymbol{\phi}, \boldsymbol{\nu}_{\mathrm{bw}}, \boldsymbol{\mu}_{\mathrm{bw}}, \boldsymbol{\nu}_{\mathrm{fw}}, \boldsymbol{\mu}_{\mathrm{fw}}, \boldsymbol{\vartheta}, \boldsymbol{\varphi}, \boldsymbol{\beta}_{\Re}, \boldsymbol{\beta}_{\Im}, \boldsymbol{\tau}]^{\mathrm{T}} \in \mathbb{C}^{N_2 \times 1}, N_2 = 7L + 4N_{\mathrm{IS}}$, and parameters of each path are respectively defined as $\boldsymbol{\theta} \equiv [\theta_1, \ldots, \theta_L]$, $\boldsymbol{\phi} \equiv [\phi_1, \ldots, \phi_L]$, $\boldsymbol{\nu}_2 \equiv [\nu_{\mathrm{bw},1}, \ldots, \nu_{\mathrm{bw},N_{\mathrm{IS}}}]$, $\boldsymbol{\mu}_2 \equiv [\mu_{\mathrm{bw},1}, \ldots, \mu_{\mathrm{bw},N_{\mathrm{IS}}}]$, $\boldsymbol{\nu}_1 \equiv [\nu_{\mathrm{fw},1}, \ldots, \nu_{\mathrm{fw},N_{\mathrm{IS}}}]$, $\boldsymbol{\mu}_1 \equiv [\mu_{\mathrm{fw},1}, \ldots, \mu_{\mathrm{fw},N_{\mathrm{IS}}}]$, $\boldsymbol{\vartheta} \equiv [\vartheta_1, \ldots, \vartheta_L]$, $\boldsymbol{\varphi} \equiv [\varphi_1, \ldots, \varphi_L]$, $\boldsymbol{\tau} \equiv [\tau_1, \ldots, \tau_L]$, $\boldsymbol{\beta}_{\Re} = \Re\{[\beta_1, \ldots, \beta_L]\}$, $\boldsymbol{\beta}_{\Im} = \Im\{[\beta_1, \ldots, \beta_L]\}$, $\tilde{\boldsymbol{\psi}} \equiv [\tilde{\psi}_1, \ldots, \tilde{\psi}_{N_{\mathrm{IS}}}]$. The FIM of the received signal $\mathbf{Y}$ over the vector of interested parameters $\boldsymbol{\Omega}$ is generally calculated as

$$\mathbf{J}_{\boldsymbol{\Omega}} = -\mathbb{E}\left\{ \frac{\partial^2 \ln f(\mathbf{Y}|\boldsymbol{\Omega})}{\partial \boldsymbol{\Omega} \partial \boldsymbol{\Omega}^{\mathrm{T}}} \right\} \tag{5.16}$$

and the log-likelihood of $\mathbf{Y}(t)$ conditioned at $\boldsymbol{\Omega}$ is calculated as

$$\ln f(\mathbf{Y}(t)|\boldsymbol{\Omega}) \propto 2\Re\{\mathbf{Y}(t)^{\mathrm{H}} \mathbf{Y}(t)\} - \mathbf{Y}(t)^{\mathrm{H}} \mathbf{Y}(t) \tag{5.17}$$

And the 1st derivative of received signal $\mathbf{Y}(t)$ (5.14) over $\boldsymbol{\Omega}$ is expressed as $\mathbf{Y}_{\boldsymbol{\Omega}} = [\mathbf{Y}_{\boldsymbol{\theta}}, \mathbf{Y}_{\boldsymbol{\phi}}, \mathbf{Y}_{\boldsymbol{\nu}_2}, \mathbf{Y}_{\boldsymbol{\mu}_2}, \mathbf{Y}_{\boldsymbol{\nu}_1}, \mathbf{Y}_{\boldsymbol{\mu}_1}, \mathbf{Y}_{\boldsymbol{\vartheta}}, \mathbf{Y}_{\boldsymbol{\varphi}}, \mathbf{Y}_{\boldsymbol{\beta}_{\Re}}, \mathbf{Y}_{\boldsymbol{\beta}_{\Im}}, \mathbf{Y}_{\boldsymbol{\tau}}, \mathbf{Y}_{\tilde{\boldsymbol{\psi}}}]$, wherein the derivative of signal over Rx AOA $\mathbf{Y}_{\boldsymbol{\theta}} = [\mathbf{y}_{\theta_1}, \ldots, \mathbf{y}_{\theta_L}]$ is calculated as

$$\mathbf{y}_{\theta_l} = \begin{cases} \alpha_l \beta_l \dot{\mathbf{a}}_{\mathrm{R},l} \mathbf{a}_{\mathrm{T},l}^{\mathrm{H}} \mathbf{F}_{\mathrm{B}} \mathbf{x}, & l \in \Lambda_{\mathrm{s}} \text{ or } l = 1 \\ \alpha_l \beta_l e^{j\psi_l} a_{\mathrm{bw},l}^{\mathrm{H}} a_{\mathrm{fw},l} \dot{\mathbf{a}}_{\mathrm{R},l} \mathbf{a}_{\mathrm{T},l}^{\mathrm{H}} \mathbf{F}_{\mathrm{B}} \mathbf{x}, & l \in \Lambda_{\mathrm{R}} \end{cases} \tag{5.18}$$

All the other derivative functions are calculated as (D.1) in Appendix D. Substitute (5.14) to (5.16), the eFIM with IS in near-field is calculated as (5.19) in the next page, where the element of FIM at the u-th row and v-th column is calculated as $\mathbf{J}_{u,v} = \frac{1}{N_0} \int_0^{T_o} \Re \left\{ \left(\frac{\partial \mathbf{Y}(t)}{\partial \boldsymbol{\Omega}_u} \right)^{\mathrm{H}} \frac{\partial \mathbf{Y}(t)}{\partial \boldsymbol{\Omega}_v} \right\} \mathrm{d}t$.

For the IS in far-field, channel parameters at Ix elements are approximated to those at the IS centre, the approximated derivative functions are obtained by substituting the the far-field signal model (5.15) to (5.16), as $\mathbf{Y}_{\mathrm{ap},\boldsymbol{\Omega}} = [\mathbf{Y}_{\mathrm{ap},\boldsymbol{\theta}}, \mathbf{Y}_{\mathrm{ap},\boldsymbol{\phi}}, \mathbf{Y}_{\mathrm{ap},\boldsymbol{\nu}_2}, \mathbf{Y}_{\mathrm{ap},\boldsymbol{\mu}_2}, \mathbf{Y}_{\mathrm{ap},\boldsymbol{\nu}_1}, \mathbf{Y}_{\mathrm{ap},\boldsymbol{\mu}_1}, \mathbf{Y}_{\mathrm{ap},\boldsymbol{\vartheta}}, \mathbf{Y}_{\mathrm{ap},\boldsymbol{\varphi}}, \mathbf{Y}_{\mathrm{ap},\boldsymbol{\beta}_{\Re}}, \mathbf{Y}_{\mathrm{ap},\boldsymbol{\beta}_{\Im}}, \mathbf{Y}_{\mathrm{ap},\boldsymbol{\tau}}, \mathbf{Y}_{\mathrm{ap},\tilde{\boldsymbol{\psi}}}]$. For the sake of simplicity, the expression of $\mathbf{Y}_{\mathrm{ap},\boldsymbol{\Omega}}$ is omitted.

Assume L uncorrelated paths, the FIM (5.19) can be rewritten as a block diagonal

$$\mathbf{J}_{\boldsymbol{\Omega}} = \gamma_1 \begin{bmatrix}
\mathbf{J}_{\boldsymbol{\theta}\boldsymbol{\theta}} & \mathbf{J}_{\boldsymbol{\theta}\boldsymbol{\phi}} & \mathbf{J}_{\boldsymbol{\theta}\boldsymbol{\nu}_2} & \mathbf{J}_{\boldsymbol{\theta}\boldsymbol{\mu}_2} & \mathbf{J}_{\boldsymbol{\theta}\boldsymbol{\nu}_1} & \mathbf{J}_{\boldsymbol{\theta}\boldsymbol{\mu}_1} & \mathbf{J}_{\boldsymbol{\theta}\boldsymbol{\vartheta}} & \mathbf{J}_{\boldsymbol{\theta}\boldsymbol{\varphi}} & \mathbf{J}_{\boldsymbol{\theta}\boldsymbol{\beta}_{\Re}} & \mathbf{J}_{\boldsymbol{\theta}\boldsymbol{\beta}_{\Im}} & \mathbf{J}_{\boldsymbol{\theta}\boldsymbol{\tau}} & \mathbf{J}_{\boldsymbol{\theta}\tilde{\boldsymbol{\psi}}} \\
\mathbf{J}_{\boldsymbol{\phi}\boldsymbol{\theta}} & \mathbf{J}_{\boldsymbol{\phi}\boldsymbol{\phi}} & \mathbf{J}_{\boldsymbol{\phi}\boldsymbol{\nu}_2} & \mathbf{J}_{\boldsymbol{\phi}\boldsymbol{\mu}_2} & \mathbf{J}_{\boldsymbol{\phi}\boldsymbol{\nu}_1} & \mathbf{J}_{\boldsymbol{\phi}\boldsymbol{\mu}_1} & \mathbf{J}_{\boldsymbol{\phi}\boldsymbol{\vartheta}} & \mathbf{J}_{\boldsymbol{\phi}\boldsymbol{\varphi}} & \mathbf{J}_{\boldsymbol{\phi}\boldsymbol{\beta}_{\Re}} & \mathbf{J}_{\boldsymbol{\phi}\boldsymbol{\beta}_{\Im}} & \mathbf{J}_{\boldsymbol{\phi}\boldsymbol{\tau}} & \mathbf{J}_{\boldsymbol{\phi}\tilde{\boldsymbol{\psi}}} \\
\mathbf{J}_{\boldsymbol{\nu}_2\boldsymbol{\theta}} & \mathbf{J}_{\boldsymbol{\nu}_2\boldsymbol{\phi}} & \mathbf{J}_{\boldsymbol{\nu}_2\boldsymbol{\nu}_2} & \mathbf{J}_{\boldsymbol{\nu}_2\boldsymbol{\mu}_2} & \mathbf{J}_{\boldsymbol{\nu}_2\boldsymbol{\nu}_1} & \mathbf{J}_{\boldsymbol{\nu}_2\boldsymbol{\mu}_1} & \mathbf{J}_{\boldsymbol{\nu}_2\boldsymbol{\vartheta}} & \mathbf{J}_{\boldsymbol{\nu}_2\boldsymbol{\varphi}} & \mathbf{J}_{\boldsymbol{\nu}_2\boldsymbol{\beta}_{\Re}} & \mathbf{J}_{\boldsymbol{\nu}_2\boldsymbol{\beta}_{\Im}} & \mathbf{J}_{\boldsymbol{\nu}_2\boldsymbol{\tau}} & \mathbf{J}_{\boldsymbol{\nu}_2\tilde{\boldsymbol{\psi}}} \\
\mathbf{J}_{\boldsymbol{\mu}_2\boldsymbol{\theta}} & \mathbf{J}_{\boldsymbol{\mu}_2\boldsymbol{\phi}} & \mathbf{J}_{\boldsymbol{\mu}_2\boldsymbol{\nu}_2} & \mathbf{J}_{\boldsymbol{\mu}_2\boldsymbol{\mu}_2} & \mathbf{J}_{\boldsymbol{\mu}_2\boldsymbol{\nu}_1} & \mathbf{J}_{\boldsymbol{\mu}_2\boldsymbol{\mu}_1} & \mathbf{J}_{\boldsymbol{\mu}_2\boldsymbol{\vartheta}} & \mathbf{J}_{\boldsymbol{\mu}_2\boldsymbol{\varphi}} & \mathbf{J}_{\boldsymbol{\mu}_2\boldsymbol{\beta}_{\Re}} & \mathbf{J}_{\boldsymbol{\mu}_2\boldsymbol{\beta}_{\Im}} & \mathbf{J}_{\boldsymbol{\mu}_2\boldsymbol{\tau}} & \mathbf{J}_{\boldsymbol{\mu}_2\tilde{\boldsymbol{\psi}}} \\
\mathbf{J}_{\boldsymbol{\nu}_1\boldsymbol{\theta}} & \mathbf{J}_{\boldsymbol{\nu}_1\boldsymbol{\phi}} & \mathbf{J}_{\boldsymbol{\nu}_1\boldsymbol{\nu}_2} & \mathbf{J}_{\boldsymbol{\nu}_1\boldsymbol{\mu}_2} & \mathbf{J}_{\boldsymbol{\nu}_1\boldsymbol{\nu}_1} & \mathbf{J}_{\boldsymbol{\nu}_1\boldsymbol{\mu}_1} & \mathbf{J}_{\boldsymbol{\nu}_1\boldsymbol{\vartheta}} & \mathbf{J}_{\boldsymbol{\nu}_1\boldsymbol{\varphi}} & \mathbf{J}_{\boldsymbol{\nu}_1\boldsymbol{\beta}_{\Re}} & \mathbf{J}_{\boldsymbol{\nu}_1\boldsymbol{\beta}_{\Im}} & \mathbf{J}_{\boldsymbol{\nu}_1\boldsymbol{\tau}} & \mathbf{J}_{\boldsymbol{\nu}_1\tilde{\boldsymbol{\psi}}} \\
\mathbf{J}_{\boldsymbol{\mu}_1\boldsymbol{\theta}} & \mathbf{J}_{\boldsymbol{\mu}_1\boldsymbol{\phi}} & \mathbf{J}_{\boldsymbol{\mu}_1\boldsymbol{\nu}_2} & \mathbf{J}_{\boldsymbol{\mu}_1\boldsymbol{\mu}_2} & \mathbf{J}_{\boldsymbol{\mu}_1\boldsymbol{\nu}_1} & \mathbf{J}_{\boldsymbol{\mu}_1\boldsymbol{\mu}_1} & \mathbf{J}_{\boldsymbol{\mu}_1\boldsymbol{\vartheta}} & \mathbf{J}_{\boldsymbol{\mu}_1\boldsymbol{\varphi}} & \mathbf{J}_{\boldsymbol{\mu}_1\boldsymbol{\beta}_{\Re}} & \mathbf{J}_{\boldsymbol{\mu}_1\boldsymbol{\beta}_{\Im}} & \mathbf{J}_{\boldsymbol{\mu}_1\boldsymbol{\tau}} & \mathbf{J}_{\boldsymbol{\mu}_1\tilde{\boldsymbol{\psi}}} \\
\mathbf{J}_{\boldsymbol{\vartheta}\boldsymbol{\theta}} & \mathbf{J}_{\boldsymbol{\vartheta}\boldsymbol{\phi}} & \mathbf{J}_{\boldsymbol{\vartheta}\boldsymbol{\nu}_2} & \mathbf{J}_{\boldsymbol{\vartheta}\boldsymbol{\mu}_2} & \mathbf{J}_{\boldsymbol{\vartheta}\boldsymbol{\nu}_1} & \mathbf{J}_{\boldsymbol{\vartheta}\boldsymbol{\mu}_1} & \mathbf{J}_{\boldsymbol{\vartheta}\boldsymbol{\vartheta}} & \mathbf{J}_{\boldsymbol{\vartheta}\boldsymbol{\varphi}} & \mathbf{J}_{\boldsymbol{\vartheta}\boldsymbol{\beta}_{\Re}} & \mathbf{J}_{\boldsymbol{\vartheta}\boldsymbol{\beta}_{\Im}} & \mathbf{J}_{\boldsymbol{\vartheta}\boldsymbol{\tau}} & \mathbf{J}_{\boldsymbol{\vartheta}\tilde{\boldsymbol{\psi}}} \\
\mathbf{J}_{\boldsymbol{\varphi}\boldsymbol{\theta}} & \mathbf{J}_{\boldsymbol{\varphi}\boldsymbol{\phi}} & \mathbf{J}_{\boldsymbol{\varphi}\boldsymbol{\nu}_2} & \mathbf{J}_{\boldsymbol{\varphi}\boldsymbol{\mu}_2} & \mathbf{J}_{\boldsymbol{\varphi}\boldsymbol{\nu}_1} & \mathbf{J}_{\boldsymbol{\varphi}\boldsymbol{\mu}_1} & \mathbf{J}_{\boldsymbol{\varphi}\boldsymbol{\vartheta}} & \mathbf{J}_{\boldsymbol{\varphi}\boldsymbol{\varphi}} & \mathbf{J}_{\boldsymbol{\varphi}\boldsymbol{\beta}_{\Re}} & \mathbf{J}_{\boldsymbol{\varphi}\boldsymbol{\beta}_{\Im}} & \mathbf{J}_{\boldsymbol{\varphi}\boldsymbol{\tau}} & \mathbf{J}_{\boldsymbol{\varphi}\tilde{\boldsymbol{\psi}}} \\
\mathbf{J}_{\boldsymbol{\beta}_{\Re}\boldsymbol{\theta}} & \mathbf{J}_{\boldsymbol{\beta}_{\Re}\boldsymbol{\phi}} & \mathbf{J}_{\boldsymbol{\beta}_{\Re}\boldsymbol{\nu}_2} & \mathbf{J}_{\boldsymbol{\beta}_{\Re}\boldsymbol{\mu}_2} & \mathbf{J}_{\boldsymbol{\beta}_{\Re}\boldsymbol{\nu}_1} & \mathbf{J}_{\boldsymbol{\beta}_{\Re}\boldsymbol{\mu}_1} & \mathbf{J}_{\boldsymbol{\beta}_{\Re}\boldsymbol{\vartheta}} & \mathbf{J}_{\boldsymbol{\beta}_{\Re}\boldsymbol{\varphi}} & \mathbf{J}_{\boldsymbol{\beta}_{\Re}\boldsymbol{\beta}_{\Re}} & \mathbf{J}_{\boldsymbol{\beta}_{\Re}\boldsymbol{\beta}_{\Im}} & \mathbf{J}_{\boldsymbol{\beta}_{\Re}\boldsymbol{\tau}} & \mathbf{J}_{\boldsymbol{\beta}_{\Re}\tilde{\boldsymbol{\psi}}} \\
\mathbf{J}_{\boldsymbol{\beta}_{\Im}\boldsymbol{\theta}} & \mathbf{J}_{\boldsymbol{\beta}_{\Im}\boldsymbol{\phi}} & \mathbf{J}_{\boldsymbol{\beta}_{\Im}\boldsymbol{\nu}_2} & \mathbf{J}_{\boldsymbol{\beta}_{\Im}\boldsymbol{\mu}_2} & \mathbf{J}_{\boldsymbol{\beta}_{\Im}\boldsymbol{\nu}_1} & \mathbf{J}_{\boldsymbol{\beta}_{\Im}\boldsymbol{\mu}_1} & \mathbf{J}_{\boldsymbol{\beta}_{\Im}\boldsymbol{\vartheta}} & \mathbf{J}_{\boldsymbol{\beta}_{\Im}\boldsymbol{\varphi}} & \mathbf{J}_{\boldsymbol{\beta}_{\Im}\boldsymbol{\beta}_{\Re}} & \mathbf{J}_{\boldsymbol{\beta}_{\Im}\boldsymbol{\beta}_{\Im}} & \mathbf{J}_{\boldsymbol{\beta}_{\Im}\boldsymbol{\tau}} & \mathbf{J}_{\boldsymbol{\beta}_{\Im}\tilde{\boldsymbol{\psi}}} \\
\mathbf{J}_{\boldsymbol{\tau}\boldsymbol{\theta}} & \mathbf{J}_{\boldsymbol{\tau}\boldsymbol{\phi}} & \mathbf{J}_{\boldsymbol{\tau}\boldsymbol{\nu}_2} & \mathbf{J}_{\boldsymbol{\tau}\boldsymbol{\mu}_2} & \mathbf{J}_{\boldsymbol{\tau}\boldsymbol{\nu}_1} & \mathbf{J}_{\boldsymbol{\tau}\boldsymbol{\mu}_1} & \mathbf{J}_{\boldsymbol{\tau}\boldsymbol{\vartheta}} & \mathbf{J}_{\boldsymbol{\tau}\boldsymbol{\varphi}} & \mathbf{J}_{\boldsymbol{\tau}\boldsymbol{\beta}_{\Re}} & \mathbf{J}_{\boldsymbol{\tau}\boldsymbol{\beta}_{\Im}} & \mathbf{J}_{\boldsymbol{\tau}\boldsymbol{\tau}} & \mathbf{J}_{\boldsymbol{\tau}\tilde{\boldsymbol{\psi}}} \\
\mathbf{J}_{\tilde{\boldsymbol{\psi}}\boldsymbol{\theta}} & \mathbf{J}_{\tilde{\boldsymbol{\psi}}\boldsymbol{\phi}} & \mathbf{J}_{\tilde{\boldsymbol{\psi}}\boldsymbol{\nu}_2} & \mathbf{J}_{\tilde{\boldsymbol{\psi}}\boldsymbol{\mu}_2} & \mathbf{J}_{\tilde{\boldsymbol{\psi}}\boldsymbol{\nu}_1} & \mathbf{J}_{\tilde{\boldsymbol{\psi}}\boldsymbol{\mu}_1} & \mathbf{J}_{\tilde{\boldsymbol{\psi}}\boldsymbol{\vartheta}} & \mathbf{J}_{\tilde{\boldsymbol{\psi}}\boldsymbol{\varphi}} & \mathbf{J}_{\tilde{\boldsymbol{\psi}}\boldsymbol{\beta}_{\Re}} & \mathbf{J}_{\tilde{\boldsymbol{\psi}}\boldsymbol{\beta}_{\Im}} & \mathbf{J}_{\tilde{\boldsymbol{\psi}}\boldsymbol{\tau}} & \mathbf{J}_{\tilde{\boldsymbol{\psi}}\tilde{\boldsymbol{\psi}}}
\end{bmatrix} \tag{5.19}$$

matrix in the sequence of number of paths. For the l-th path, the estimation of phase shift of IS ψ_l and time delay τ_l is independent of other parameters. The complex channel gain of IS-aided paths, $\beta_l, l \in \Lambda_{\mathrm{R}}$ is dependent on the angle parameters $\nu_{\mathrm{bw},p}, \mu_{\mathrm{bw},p}, \nu_{\mathrm{fw},p}, \mu_{\mathrm{fw},p}$ and orientation of the IS $\hat{\mathbf{n}}$, while the phase shifts ψ_p, and channel gain of the cluster reflective channels and the direct link channel, $\beta_l, l \in \Lambda_{\mathrm{s}}$ or $l = 1$ are independent of the other parameters. All the submatrices of $\mathbf{J}_{\boldsymbol{\Omega}}$ are obtained as (D.2) in Appendix D. The CRLB of all interested parameters is calculated as $\mathrm{CRLB}_{\boldsymbol{\Omega}} = \mathbf{J}_{\boldsymbol{\Omega}}^{-1}$.

Based on the relation between channel parameters and location information, the FIM of localisation error can be obtained by applying transformation [11] to that of channel parameters. Denote the set of location and orientation of MS and IS as $\boldsymbol{\omega}_2 \equiv [\mathbf{o}_{\mathrm{MS}}^{\mathrm{T}}, \mathbf{v}^{\mathrm{T}}, \mathbf{Q}_{\mathrm{cl}}, \mathbf{o}_{\mathrm{IS}}^{\mathrm{T}}, \mathbf{P}_{\mathrm{IS}}] \in \mathbb{C}^{1\times N_3}$, where the set $\mathbf{P}_{\mathrm{IS}} = [\mathbf{p}_{\mathrm{I},1}^{\mathrm{T}}, \ldots, \mathbf{p}_{\mathrm{I},N_{\mathrm{IS}}}^{\mathrm{T}}] \in \mathbb{C}^{1\times 3N_{\mathrm{IS}}}, \mathbf{Q}_{\mathrm{cl}} = [\mathbf{q}_1^{\mathrm{T}}, \ldots, \mathbf{q}_C^{\mathrm{T}}]$, $N_3 = 3N_{\mathrm{IS}} + 7 + 3C$, the FIM of localisation is calculated as

$$\mathbf{J}_{\boldsymbol{\omega}_2} = \bigtriangledown_{\boldsymbol{\omega}_2}(\boldsymbol{\Omega}) \mathbf{J}_{\boldsymbol{\Omega}} \bigtriangledown_{\boldsymbol{\omega}_2}^{\mathrm{T}}(\boldsymbol{\Omega}) \tag{5.20}$$

where $\bigtriangledown_{\boldsymbol{\omega}_2}(\boldsymbol{\Omega}) = [\bigtriangledown_{\boldsymbol{\omega}_2}(\boldsymbol{\omega}_1), \mathbf{0}_{N_{\mathrm{IS}}}]$ is the Jacobian matrix of $\boldsymbol{\Omega}$ over $\boldsymbol{\omega}_2$, and $\bigtriangledown_{\boldsymbol{\omega}_2}(\boldsymbol{\omega}_1)$ is expressed as (E.1) in Appendix E. Thus, the CRLB of localisation error is calculated as $\mathrm{CRLB}_{\boldsymbol{\omega}_2} = \mathbf{J}_{\boldsymbol{\omega}_2}^{-1}$.

5.3.2 Effective Fisher Information of Location Parameters

Considering that the phase shift $\tilde{\psi}_p$ is unrelated to location parameters, the EFIM proposed in [11] is used to eliminate the impact of $\tilde{\psi}_p$ on CRLB. According to the definition of EFIM proposed by [11], EFIM of channel parameters $\boldsymbol{\omega}_1$ is obtained as the Schur complement of $\mathbf{J}_{\tilde{\boldsymbol{\psi}}}$ in (5.19), which is

$$F_{\boldsymbol{\omega}_1} = \mathbf{J}_{\boldsymbol{\omega}_1} - \mathbf{J}_{\boldsymbol{\omega}_1\tilde{\boldsymbol{\psi}}} \mathbf{J}_{\tilde{\boldsymbol{\psi}}}^{-1} \mathbf{J}_{\tilde{\boldsymbol{\psi}}\boldsymbol{\omega}_1} \tag{5.21}$$

where $\mathbf{J}_{\boldsymbol{\omega}_1} = [\mathbf{J}_{\boldsymbol{\Omega}}]_{1:N_2,1:N_2}$, $\mathbf{J}_{\boldsymbol{\omega}_1\tilde{\boldsymbol{\psi}}} = [\mathbf{J}_{\boldsymbol{\Omega}}]_{1:N_2,N_2+1:N_1}$, $\mathbf{J}_{\tilde{\boldsymbol{\psi}}} = [\mathbf{J}_{\boldsymbol{\Omega}}]_{N_2+1:N_1,N_2+1:N_1}$, $\mathbf{J}_{\tilde{\boldsymbol{\psi}}\boldsymbol{\omega}_1} = [\mathbf{J}_{\boldsymbol{\Omega}}]_{N_2+1:N_1,1:N_2}$. $\mathbf{J}_{\tilde{\boldsymbol{\psi}}}$ is a $N_{\mathrm{IS}} \times N_{\mathrm{IS}}$ diagonal matrix, due to independent $\tilde{\boldsymbol{\psi}}$. Thus, it is straightforward to obtain that the FIMs of IS angles in $F_{\boldsymbol{\omega}_1}$ are equal to 0, resulting into infinite CRLBs. Therefore, it is necessary to set $\tilde{\boldsymbol{\psi}}$ as given values when calculating FIM and EFIM of other variables, thus

$$F_{\boldsymbol{\omega}_1} = \mathbf{J}_{\boldsymbol{\omega}_1} \tag{5.22}$$

$\boldsymbol{\mathcal{F}}_{\boldsymbol{\omega}_1}$ is converted to the EFIM of location information through multiplying $\boldsymbol{\mathcal{F}}_{\boldsymbol{\omega}_1}$ with the transition matrix $\bigtriangledown_{\boldsymbol{\omega}_2}(\boldsymbol{\omega}_1)$, as shown by the following:

$$\boldsymbol{\mathcal{F}}_{\boldsymbol{\omega}_2} = \bigtriangledown_{\boldsymbol{\omega}_2}(\boldsymbol{\omega}_1)\boldsymbol{\mathcal{F}}_{\boldsymbol{\omega}_1} \bigtriangledown^{\mathrm{T}}_{\boldsymbol{\omega}_2}(\boldsymbol{\omega}_1) \tag{5.23}$$

The EFIM of MS position and orientation is obtained by inverse matrix theorem as

$$\boldsymbol{\mathcal{F}}_{\mathrm{MS}} = [\boldsymbol{\mathcal{F}}_{\boldsymbol{\omega}_2}]_{1:5,1:5} - [\boldsymbol{\mathcal{F}}_{\boldsymbol{\omega}_2}]_{1:5,6:N_3}[\boldsymbol{\mathcal{F}}_{\boldsymbol{\omega}_2}]^{-1}_{6:N_3,6:N_3}[\boldsymbol{\mathcal{F}}_{\boldsymbol{\omega}_2}]_{6:N_3,1:5} \tag{5.24}$$

Therefore, the squared position error bound (SPEB) $\mathcal{P}_{\mathrm{MS,posi}}$ and squared orientation error bound (SOEB) $\mathcal{P}_{\mathrm{MS,orin}}$ of MS are calculated as

$$\mathcal{P}_{\mathrm{MS,posi}} = trace\left\{\left[\boldsymbol{\mathcal{F}}^{-1}_{\mathrm{MS}}\right]_{3:5,3:5}\right\} \tag{5.25a}$$

$$\mathcal{P}_{\mathrm{MS,orin}} = trace\left\{\left[\boldsymbol{\mathcal{F}}^{-1}_{\mathrm{MS}}\right]_{1:2,1:2}\right\} \tag{5.25b}$$

The dimension of $\boldsymbol{\mathcal{F}}^{-1}_{\mathrm{MS}}$ seems generally increases with N_{IS}.

Note that, the aforementioned FIMs $\mathbf{J}_{\boldsymbol{\Omega}}$ and $\mathbf{J}_{\boldsymbol{\omega}_2}$ are obtained with IS of unknown position and orientation, whereas $\mathbf{J}_{\boldsymbol{\Omega}}$ and $\mathbf{J}_{\boldsymbol{\omega}_2}$ with perfectly known IS are free of the forward link parameters, due to known channel between BS and IS.

5.3.3 Approximate Fisher Information Matrix for Intelligent Surface in the Far-Field

When IS is sufficiently small, the difference of parameters at the Ix element $p = p_e$, where $p_e = 1, \ldots, p_c{-}1, p_c{+}1, N_{\mathrm{IS}}$, and those at the centre, $p = p_c$, is negligible, thus the IS parameters approximate to $\boldsymbol{\omega}_{1,l} \approx \boldsymbol{\omega}_{1,\mathrm{ap}}, l = 2{+}C, \ldots, L$, where $\boldsymbol{\omega}_{1,\mathrm{ap}} = [\theta_{p_c}, \phi_{p_c}, \nu_{p_c}, \mu_{p_c}, \nu_{p_c}, \mu_{p_c}, \vartheta_{p_c}, \varphi_{p_c}, \beta_{\Re,p_c}, \beta_{\Im,p_c}, \tau_{p_c}]$, and p_c is the index of the centre element. Substitute $\boldsymbol{\omega}_{1,\mathrm{ap}}$ and (5.15) to (5.16), and follow the same progress as (5.21)-(5.25), the approximated FIM (aFIM)of the l-th path and approximated EFIM (aEFIM) of MS location information are respectively calculated as

$$\boldsymbol{\mathcal{F}}_{\boldsymbol{\omega}_{1,\mathrm{ap}}} = -\mathbb{E}\left\{\frac{\partial^2 \ln f(\mathbf{Y}|\boldsymbol{\omega}_{1,\mathrm{ap}})}{\partial\boldsymbol{\omega}_{1,\mathrm{ap}}\partial\boldsymbol{\omega}^{\mathrm{T}}_{1,\mathrm{ap}}}\right\} \tag{5.26a}$$

$$\boldsymbol{\mathcal{F}}_{\mathrm{ap,MS}} = [\boldsymbol{\mathcal{F}}_{\mathrm{ap},\boldsymbol{\omega}_2}]_{1:5,1:5} - [\boldsymbol{\mathcal{F}}_{\mathrm{ap},\boldsymbol{\omega}_2}]_{1:5,6:10}[\boldsymbol{\mathcal{F}}_{\mathrm{ap},\boldsymbol{\omega}_2}]^{-1}_{6:10,6:10}[\boldsymbol{\mathcal{F}}_{\mathrm{ap},\boldsymbol{\omega}_2}]_{6:10,1:5} \tag{5.26b}$$

where $\boldsymbol{F}_{\text{ap},\boldsymbol{\omega}_2} = \bigtriangledown_{\boldsymbol{\omega}_2}(\boldsymbol{\omega}_{1,\text{ap}})\boldsymbol{F}_{\boldsymbol{\omega}_{1,\text{ap}}}\bigtriangledown^{\text{T}}_{\boldsymbol{\omega}_2}(\boldsymbol{\omega}_{1,\text{ap}})$ is aFIM of location parameters. The approximation error of $\boldsymbol{\omega}_{1,\text{ap}}$ mainly occur to the elements of $\mathbf{k}(\theta_{p_e},\phi_{p_e})$, $\mathbf{k}(\vartheta_{p_e},\varphi_{p_e})$, $\mathbf{k}(\nu_{\text{bw},p_e},\mu_{\text{bw},p_e})$ and $\mathbf{k}(\nu_{\text{fw},p_e},\mu_{\text{fw},p_e})$. The relative approximation error (RAE) of direction vector of Rx $\mathbf{k}(\theta_{p_e},\phi_{p_e})$ is calculated as $\mathbf{K}(\theta_{p_e},\phi_{p_e}) = |\mathbf{1}_3 - (diag\{\mathbf{k}(\theta_l,\phi_l)\})^{-1}\mathbf{k}(\theta_{p_e},\phi_{p_e})|$. If the distance error is sufficiently small, *i.e.*, $r_{\text{fw},p_c} \approx r_{\text{fw},p_e}$, it is realised that $\mathbf{K}(\theta_{p_e},\phi_{p_e}) \approx |\mathbf{1}_3 - (diag\{\boldsymbol{\chi}_{p_e}\})^{-1}\boldsymbol{\chi}_{p_c}|/r_{\text{bw},p_c}$. RAE of direction vectors of Tx and Ix, $\mathbf{K}(\vartheta_{p_e},\varphi_{p_e})$, $\mathbf{K}(\nu_{\text{fw},p_e},\mu_{\text{fw},p_e})$ and $\mathbf{K}(\nu_{\text{bw},p_e},\mu_{\text{bw},p_e})$ are obtained through the same progress. The delay factors α_p could be mitigated by IS phase shifter $\tilde{\psi}_p$, thus, plays minor impact on FIM and EFIM.

The approximate SPEB (aSPEB) $\mathcal{A}_{\text{MS,posi}}$ and approximate SOEB (aSPOB) $\mathcal{A}_{\text{MS,orin}}$ of MS are calculated as

$$\mathcal{A}_{\text{MS,posi}} = trace\left\{\left[\boldsymbol{F}^{-1}_{\text{ap,MS}}\right]_{3:5,3:5}\right\} \approx \mathcal{P}_{\text{MS,posi}} \tag{5.27a}$$

$$\mathcal{A}_{\text{MS,orin}} = trace\left\{\left[\boldsymbol{F}^{-1}_{\text{ap,MS}}\right]_{1:2,1:2}\right\} \approx \mathcal{P}_{\text{MS,orin}} \tag{5.27b}$$

For a large IS array, the entire Ix URA array is separated into $s = 1,\ldots,S_{\text{IS}}$ non-overlapping sub-arrays with number of elements smaller than $N_{\text{sr}} = (2d_i/\lambda)$, which is determined by *Fraunhofer distance* of a near-field zone. Then, far-field approximated parameters can be applied for each individual sub-array.

5.3.4 Analysis on Fisher Information Matrix and Effect of Intelligent Surface Phase Shifter

According to Appendix D, each submatrix of (5.19) consists of the terms related to the Rx and Tx steering vectors, named as 'Rx factors' and 'Tx fractors' respectively [8], and the remaining terms of IS array response, phase shifts and complex channel, are named as 'IS factors' in this research. The Rx factors contains the terms $\mathbf{A}^{\text{H}}_{\text{T},l}\mathbf{F}_{\text{B}}$, $\dot{\mathbf{A}}^{\text{H}}_{\text{T},l}\mathbf{F}_{\text{B}}$, or $\grave{\mathbf{A}}^{\text{H}}_{\text{T},l}\mathbf{F}_{\text{B}}$, while the Tx factor contains the terms $\mathbf{A}_{\text{R},l}$, $\dot{\mathbf{A}}_{\text{R},l}$, or $\grave{\mathbf{A}}_{\text{R},l}$. The explicit expressions of these Rx-related and Tx-related terms are calculated and interpret the properties of the CRLBs.

For the Tx factors, assume the number of elements on each row and column of Tx, $N_x = 0.5\sqrt{N_{\text{T}}} - 0.5$ being an integer value, and $d_{\text{T}} = 0.5\lambda$, the inner product $\left|\mathbf{a}^{\text{H}}_{\text{T},l}\mathbf{f}_{\text{B},b}\right|$ is

obtained as following:

$$\begin{aligned}
\left|\mathbf{a}_{\mathrm{T},l}^{\mathrm{H}}\mathbf{f}_{\mathrm{B},b}\right| &= \frac{1}{N_{\mathrm{T}}\sqrt{N_{\mathrm{B}}}}\left|\sum_{t_1=-N_x}^{N_x}\sum_{t_2=-N_x}^{N_x}\left(e^{-j\pi t_1(x_b-x)}e^{-j\pi t_2(z_b-z)}\right)\right| \\
&\overset{(a)}{=} \frac{1}{N_{\mathrm{T}}\sqrt{N_{\mathrm{B}}}}\left|\left(1+2\sum_{t_1=1}^{N_x}\cos(t_1\pi(x_b-x))\right)\left(1+2\sum_{t_2=1}^{N_x}\cos(t_2\pi(z_b-z))\right)\right| \\
&= \frac{1}{N_{\mathrm{T}}\sqrt{N_{\mathrm{B}}}}\left|\frac{\sin((N_x+0.5)\pi(x_b-x))}{\sin(0.5\pi(x_b-x))}\frac{\sin((N_x+0.5)\pi(z_b-z))}{\sin(0.5\pi(z_b-z))}\right| \\
&\overset{(b)}{=} \frac{1}{N_{\mathrm{T}}\sqrt{N_{\mathrm{B}}}}\left|\frac{\sin((2N_x+1)x_b')}{\sin(x_b')}\right|\left|\frac{\sin((2N_x+1)z_b')}{\sin(z_b')}\right| \\
&= \frac{1}{\sqrt{N_{\mathrm{B}}}}F_{\sqrt{N_{\mathrm{T}}}}(x_b')F_{\sqrt{N_{\mathrm{T}}}}(z_b') \qquad (5.28)
\end{aligned}$$

where $x = \frac{2d_{\mathrm{T}}}{\lambda}[1,0,0]\mathbf{R}(\mathbf{o}_{\mathrm{MS}})^{\mathrm{T}}\mathbf{k}(\vartheta_l,\varphi_l)$, $z = \frac{2d_{\mathrm{T}}}{\lambda}[0,0,1]\mathbf{R}(\mathbf{o}_{\mathrm{MS}})^{\mathrm{T}}\mathbf{k}(\vartheta_l,\varphi_l)$, $x_b = \frac{2d_{\mathrm{T}}}{\lambda}\cos\varphi_b\cos\vartheta_b$, $z_b = \frac{2d_{\mathrm{T}}}{\lambda}\sin\vartheta_b$ are uniformly distributed in the range $[-1,\ 1]$. The progress (a) utilises the trigonometric identity to convert the summation of exponential function to a closed form function. The progress (b) utilises the substitution $x_b' = 0.5\pi(x_b - x)$ and $z_b' = 0.5\pi(z_b - z)$ to convert the closed form function to the product of two *Fejér kernel* $F_{\sqrt{N_{\mathrm{T}}}}(\cdot)$ of order $\sqrt{N_{\mathrm{T}}}$ [41]. Therefore, the value of $\left|\mathbf{a}_{\mathrm{T},l}^{\mathrm{H}}\mathbf{f}_{\mathrm{B},b}\right|$ fluctuates between the range $[0, 1/\sqrt{N_{\mathrm{B}}}]$. If the direction of the b-th beam is sufficiently close to the real direction of the transmitted signal, *i.e.*, $x_b = x + \delta_{x,b}$ and $z_b = z + \delta_{z,b}$, and $\delta_{x,b}$ and $\delta_{z,b}$ are sufficiently small, the absolute value of transmitted beam in (5.18) is approximated to $\left|\mathbf{a}_{\mathrm{T},l}^{\mathrm{H}}\mathbf{f}_{\mathrm{B},b}\right| \approx \left|\frac{\sin\frac{\pi\delta_{x,b}}{2}}{\frac{\pi\delta_{x,b}}{2}}\right|\left|\frac{\sin\frac{\pi\delta_{z,b}}{2}}{\frac{\pi\delta_{z,b}}{2}}\right| \to 1$. Thus,

$$\begin{aligned}
\mathbf{a}_{\mathrm{T},l}^{\mathrm{H}}\mathbf{F}_{\mathrm{B}}\mathbf{F}_{\mathrm{B}}^{\mathrm{H}}\mathbf{a}_{\mathrm{T},l} &= \sum_{b=1}^{N_{\mathrm{B}}}|\mathbf{a}_{\mathrm{T},l}^{\mathrm{H}}\mathbf{f}_{\mathrm{B},b}|^2 \\
&= \frac{1}{N_{\mathrm{T}}^2 N_{\mathrm{B}}}\sum_{b=1}^{N_{\mathrm{B}}}\left(\frac{\sin((N_x+0.5)\pi(x_b-x))}{\sin(0.5\pi(x_b-x))}\right)^2\left(\frac{\sin((N_x+0.5)\pi(z_b-z))}{\sin(0.5\pi(z_b-z))}\right)^2 \\
&\overset{(b)}{=} \frac{1}{N_{\mathrm{B}}}\sum_{b=1}^{N_{\mathrm{B}}}\left(F_{\sqrt{N_{\mathrm{T}}}}^2(x_b')F_{\sqrt{N_{\mathrm{T}}}}^2(z_b')\right) \qquad (5.29)
\end{aligned}$$

According to the property of the *Fejér kernel*, (5.19) decreases with N_{T}, N_{B}, x_b' and z_b' increasing. This is attributed to: 1. the more elements and beams on the Tx of constant

transmit power, the less power assigned to each element and each beam, and 2. the larger difference between the beamforming direction and real direction of transmitted signal, the less power given to the real direction of transmitted signal.

Based on (5.19), $\dot{\mathbf{a}}_{\mathrm{T},l}^{\mathrm{H}}\mathbf{F}_{\mathrm{B}}\mathbf{F}_{\mathrm{B}}^{\mathrm{H}}\mathbf{a}_{\mathrm{T},l}$ and $\grave{\mathbf{a}}_{\mathrm{T},l}^{\mathrm{H}}\mathbf{F}_{\mathrm{B}}\mathbf{F}_{\mathrm{B}}^{\mathrm{H}}\mathbf{a}_{\mathrm{T},l}$ are respectively calculated as

$$\begin{aligned}\dot{\mathbf{a}}_{\mathrm{T},l}^{\mathrm{H}}\mathbf{F}_{\mathrm{B}}\mathbf{F}_{\mathrm{B}}^{\mathrm{H}}\mathbf{a}_{\mathrm{T},l} &= \frac{\partial \mathbf{a}_{\mathrm{T},l}^{\mathrm{H}}}{\partial \vartheta_l}\mathbf{F}_{\mathrm{B}}\mathbf{F}_{\mathrm{B}}^{\mathrm{H}}\mathbf{a}_{\mathrm{T},l} = \frac{1}{N_{\mathrm{T}}^2 N_{\mathrm{B}}}\frac{\partial \sum_{b=1}^{N_{\mathrm{B}}}\frac{1-\cos((2N_x+1)x_b')}{1-\cos(x_b')}\frac{1-\cos((2N_x+1)z_b')}{1-\cos(z_b')}}{\partial \vartheta_l} \\ &= \frac{1}{N_{\mathrm{T}}^2 N_{\mathrm{B}}}\sum_{b=1}^{N_{\mathrm{B}}}\left(\frac{\sin((2N_x+1)x_b')(2N_x+1)}{1-\cos(x_b')} + \frac{(1-\cos((2N_x+1)x_b'))\sin(x_b')}{(1-\cos(x_b'))^2}\right) \\ &\frac{1-\cos((2N_x+1)z_b')}{1-\cos(z_b')}j\pi\dot{x}_b' + \frac{1-\cos((2N_x+1)x_b')}{1-\cos(x_b')}\left(\frac{\sin((2N_x+1)z_b')(2N_x+1)}{1-\cos(z_b')} + \right. \\ &\left.\frac{(1-\cos((2N_x+1)z_b'))\sin(z_b')}{(1-\cos(z_b'))^2}\right)(-j\pi)\dot{z}_b'\end{aligned} \tag{5.30}$$

where $\dot{x}_b' = \frac{\partial x_b'}{\partial \vartheta}, \dot{z}_b' = \frac{\partial z_b'}{\partial \vartheta}$. Therefore, the Tx factors with the terms in $\digamma_{\boldsymbol{\omega}_1}$ generally increase with N_{T} and N_{B}.

For the Rx factors, it is straightforward to obtain the terms $\mathbf{a}_{\mathrm{R},l}^{\mathrm{H}}\mathbf{a}_{\mathrm{R},l} = 1$, and

$$\dot{\mathbf{a}}_{\mathrm{R},l}^{\mathrm{H}}\mathbf{a}_{\mathrm{R},l} = \frac{\partial \mathbf{a}_{\mathrm{R},l}}{\partial \theta_l}^{\mathrm{H}}\mathbf{a}_{\mathrm{R},l} = \mathbf{a}_{\mathrm{R},l}^{\mathrm{H}} diag\left\{j2\pi\mathbf{p}_{\mathrm{R}}^{\mathrm{T}}\underbrace{\mathbf{R}(\mathbf{o}_{\mathrm{MS}})^{\mathrm{T}}\frac{\partial \mathbf{k}(\theta_l,\phi_l)}{\partial \theta_l}}_{\equiv\mathbf{K}_{\theta,l}\in\mathbb{C}^{3\times 1}}\right\}\mathbf{a}_{\mathrm{R},l} = \frac{1}{N_{\mathrm{R}}}\mathbf{1}_{N_{\mathrm{R}}}^{\mathrm{T}}\mathbf{p}_{\mathrm{R}}^{\mathrm{T}}\mathbf{K}_{\theta,l} \tag{5.31}$$

$$\grave{\mathbf{a}}_{\mathrm{R},l}^{\mathrm{H}}\mathbf{a}_{\mathrm{R},l} = \frac{\partial \mathbf{a}_{\mathrm{R},l}}{\partial \phi_l}^{\mathrm{H}}\mathbf{a}_{\mathrm{R},l} = \mathbf{a}_{\mathrm{R},l}^{\mathrm{H}} diag\left\{j2\pi\mathbf{p}_{\mathrm{R}}^{\mathrm{T}}\underbrace{\mathbf{R}(\mathbf{o}_{\mathrm{MS}})^{\mathrm{T}}\frac{\partial \mathbf{k}(\phi_l,\phi_l)}{\partial \phi_l}}_{\equiv\mathbf{K}_{\phi,l}\in\mathbb{C}^{3\times 1}}\right\}\mathbf{a}_{\mathrm{R},l} = \frac{1}{N_{\mathrm{R}}}\mathbf{1}_{N_{\mathrm{R}}}^{\mathrm{T}}\mathbf{p}_{\mathrm{R}}^{\mathrm{T}}\mathbf{K}_{\phi,l} \tag{5.32}$$

where $\mathbf{1}_{N_{\mathrm{R}}}^{\mathrm{T}}\mathbf{p}_{\mathrm{R}}^{\mathrm{T}}$ represents the respective sum coordinates of all Rx elements on each dimension. When Rx elements are distributed symmetrically around the array centre, as the assumption made in the section 5.2, the summation is calculated as $\mathbf{1}_{N_{\mathrm{R}}}^{\mathrm{T}}\mathbf{p}_{\mathrm{R}}^{\mathrm{T}} = [0,0,0]$, and the Rx-related terms $\dot{\mathbf{A}}_{\mathrm{R}}^{\mathrm{H}}\mathbf{A}_{\mathrm{R}}$ and $\grave{\mathbf{A}}_{\mathrm{R}}^{\mathrm{H}}\mathbf{A}_{\mathrm{R}}$ are consequently equal to $\mathbf{0}_{\mathrm{L}}\mathbf{0}_{\mathrm{L}}^{\mathrm{T}}$. $\mathbf{K}_{\theta,l}$ and $\mathbf{K}_{\phi,l}$ are constant matrices with given $\mathbf{o}_{\mathrm{MS}}$, θ_l and ϕ_l.

5.4 Intelligent Surface Phase Shifter Design for Localisation

The performance of localisation can be further improved by allocating localisation-aimed ISpsf, which maximises the value of FIMs of IS related parameters $\boldsymbol{\omega}_{3,p} = [\nu_{\mathrm{fw},p}, \mu_{\mathrm{fw},p}, \nu_{\mathrm{bw},p}, \mu_{\mathrm{bw},p}, \beta_{\Re,p}, \beta_{\Im,p}]$ through allocating proper $\boldsymbol{\Psi}_{\mathrm{R}}$ to minimise the imaginary parts. The problem of deriving the localisation-aimed ISpsf of minimum PEB can be formulated as an SDP programming problem

$$(P5.1) \quad \min_{\boldsymbol{\Psi}_{\mathrm{R}}} \quad trace\{[\mathbf{M}]_{3:5,3:5}\} \tag{5.33}$$

$$s.t.$$

$$\begin{bmatrix} \mathbf{M} & \mathbf{I}_{10} \\ \mathbf{I}_{10} & \digamma_{\mathrm{MS}} \end{bmatrix} \succcurlyeq 0 \tag{5.34}$$

$$\mathbf{M} \succcurlyeq 0 \tag{5.35}$$

where $\mathbf{M}$ is the auxiliary variable, and EFIM of location information $\digamma_{\mathrm{MS}}$ is semi-definite matrix [11],[91]. $(P5.1)$ can be solved by the existing iterative algorithms, *e.g.*, gradient descent method, when a proper initialisation is provided, and N_{IS} is sufficiently small. However, iterative algorithms may consume tremendous computation for large value of N_{IS}. The problem is turned to find the maximal derivatives related to ISpsf.

For the derivatives of IS array response displayed as (D.4) in Appendix D, the terms related to ISpsf are denoted by $\varpi_p = \rho_{\mathrm{bw},p}\rho_{\mathrm{fw},p}e^{j\zeta_p}a^{\mathrm{H}}_{\mathrm{bw},p}e^{j\tilde{\psi}_p}a_{\mathrm{fw},p}$, and $\{C_{\mathrm{fe},p}, C_{\mathrm{fa},p}, C_{\mathrm{be},p}, C_{\mathrm{ba},p}\}$ and $\{E_{\mathrm{fe},p}, E_{\mathrm{fa},p}, E_{\mathrm{be},p}, E_{\mathrm{ba},p}\}$ are respectively the amplitudes and phases of derivatives of ϖ_p to $\boldsymbol{\omega}_{3,p}$, which are rewritten as following :

$$\frac{\partial \varpi_p}{\partial \nu_{\mathrm{fw},p}} = C_{\mathrm{fe},p}E_{\mathrm{fe},p}e^{j\tilde{\psi}_p} \tag{5.36}$$

$$\frac{\partial \varpi_p}{\partial \mu_{\mathrm{fw},p}} = C_{\mathrm{fa},p}E_{\mathrm{fa},p}e^{j\tilde{\psi}_p} \tag{5.37}$$

$$\frac{\partial \varpi_p}{\partial \nu_{\mathrm{bw},p}} = C_{\mathrm{be},p}E_{\mathrm{be},p}e^{j\tilde{\psi}_p} \tag{5.38}$$

$$\frac{\partial \varpi_p}{\partial \mu_{\mathrm{bw},p}} = C_{\mathrm{ba},p}E_{\mathrm{ba},p}e^{j\tilde{\psi}_p} \tag{5.39}$$

$$\frac{\partial \varpi_p}{\partial \beta_{\Re,p}} = a^{\mathrm{H}}_{\mathrm{bw},p}a_{\mathrm{fw},p}e^{j\tilde{\psi}_p} \tag{5.40}$$

$$\frac{\partial \varpi_p}{\partial \beta_{\Im,p}} = j a_{\mathrm{bw},p}^{\mathrm{H}} a_{\mathrm{fw},p} e^{j\tilde{\psi}_p} \tag{5.41}$$

where the expressions of the amplitudes and phases are shown as (D.5) in Appendix D. Each of the maximum values of (5.36)-(5.41) are equal to their individual amplitudes. The optimal ISpsfs for (5.36)-(5.41) are denoted by $\acute{\boldsymbol{\psi}} = [\acute{\psi}_1, \ldots, \acute{\psi}_{N_{\mathrm{IS}}}]$, where $\acute{\psi}_p \in \{\psi_{\nu,\mathrm{bw},p}, \psi_{\mu,\mathrm{bw},p}, \psi_{\nu,\mathrm{fw},p}, \psi_{\mu,\mathrm{fw},p}, \psi_{\beta,\Re,p}, \psi_{\beta,\Im,p}\}$ can be obtained through the following optimisation :

$$\min_{\hat{\psi}_p} |\angle E_p - \hat{\psi}_p| \tag{5.42}$$

where $E_p \in \{E_{\mathrm{fe},p}, E_{\mathrm{fa},p}, E_{\mathrm{be},p}, E_{\mathrm{ba},p}\}$ are designed for optimal ISpsf in (5.36)-(5.41). $E_p = a_{\mathrm{bw},p}^{\mathrm{H}} a_{\mathrm{fw},p}$ is applied for the optimal ISpsf of other parameters $\boldsymbol{\omega}_{4,p} = [\theta_p, \phi_p, \vartheta_p, \varphi_p, \tau_p]$, and $\angle(a_{\mathrm{bw},p}^{\mathrm{H}} a_{\mathrm{fw},p}) = 2\pi \boldsymbol{\chi}_{\mathrm{I},p}(\mathbf{k}(\nu_{\mathrm{bw},p}, \mu_{\mathrm{bw},p}) - \mathbf{k}(\nu_{\mathrm{fw},p}, \mu_{\mathrm{fw},p}))/\lambda$.

Note that, the information of $\boldsymbol{\omega}_{3,p}$ in received signals are eliminated by $\hat{\psi}_p$, even if the corresponding elements of FIMs $\mathbf{J}_{\boldsymbol{\omega}_1}$ are increased. Therefore, the optimal ISpsf of other channel parameters $[\theta_p, \phi_p, \vartheta_p, \varphi_p, \tau_p]$ are not considered, in order to remain sufficient position-related channel parameters to localisation. Therefore, the FIM with optimal ISpsf can be calculated as

$$\acute{\mathbf{J}}_{\boldsymbol{\omega}_1} = \mathbf{J}_{\boldsymbol{\omega}_1} \odot \mathbf{Q}_{\mathrm{or}} \odot \acute{\mathbf{P}} \tag{5.43}$$

where $\mathbf{Q}_{\mathrm{or}}$ is the matrix that all elements are reciprocal of those in $\mathbf{P}$, and $\acute{\mathbf{P}} = \mathbf{p}_{\mathrm{I}}^{\mathrm{H}} \mathbf{p}_{\mathrm{I}}$, where $\mathbf{p}_{\mathrm{I}} = \left[\mathbf{1}_{1+C} \ \acute{\boldsymbol{\Psi}}_{\mathrm{R}}\right]$, $\acute{\boldsymbol{\Psi}}_{\mathrm{R}}$ is the ISpsf matrix of $\acute{\psi}_p$. Substitute $\acute{\mathbf{J}}_{\boldsymbol{\omega}_1}$ to (5.21)-(5.26), it is straightforward to calculate the EFIM of localisation-aimed ISpsf as $\acute{F}_{\boldsymbol{\omega}_2} = \bigtriangledown_{\boldsymbol{\omega}_2}(\boldsymbol{\omega}_1) \acute{\mathbf{J}} \bigtriangledown_{\boldsymbol{\omega}_2}^{\mathrm{T}}(\boldsymbol{\omega}_1)$. Therefore, $(P5.1)$ is converted to

$$(P5.2) \quad \min_{\acute{\boldsymbol{\Psi}}_{\mathrm{R}}} \quad trace\{[\mathbf{M}]_{3:5,3:5}\} \tag{5.44}$$

$$s.t.$$

$$\begin{bmatrix} \mathbf{M} & \bigtriangledown_{\boldsymbol{\omega}_2}(\boldsymbol{\omega}_1) \\ \bigtriangledown_{\boldsymbol{\omega}_2}^{\mathrm{T}}(\boldsymbol{\omega}_1) & \acute{\mathbf{J}}_{\boldsymbol{\omega}_1} \end{bmatrix} \succcurlyeq 0 \tag{5.45}$$

$$\mathbf{M} \succcurlyeq 0 \tag{5.46}$$

The optimal solution to $(P5.2)$ is obtained as that of (5.43) which maximise the values of (5.36)-(5.41).

5.5 Simulation Results

We consider a scenario where single MS is localised by a BS operating at $f_c = 30$ GHz ($\lambda = 0.01$ m), bandwidth of $W = 100$ MHz, observation noise of psd $N_0 = 1e-8$ mw/GHz, transmit power $Pt = 1$ mw, and 32 subcarriers through a LOS link, a single bounced NLOS link and a RIS-aided link. Both BS and MS are equipped with $N_{\mathrm{T}}, N_{\mathrm{R}} = 10 \times 10$ antenna elements, which are distributed as rectangular grids with element spacing $0.5\lambda = 0.005$ m. IS is fixed at the position $\mathbf{r}_{\mathrm{I}} = [24, 21, 15]^{\mathrm{T}}$, and BS is at $\mathbf{w} = [0, 0, 10]^{\mathrm{T}}$. The position of MS is randomly generated in the farther range than BS to IS, and $N_{\mathrm{sr}} = 6456$. Cell radius is 100 m. The performance of localisation is evaluated by PEB and OEB of MS within both cases of known and unknown IS, where known IS is referred to the IS with complete awareness of its position and orientation, and unknown IS is the IS with the awareness absent.

Figs. 5.2 and 5.3 present that the average PEB and OEB of MS are generally decreasing when $N_{\mathrm{IS}} \in [6^2, 128^2]$, and location and orientation of IS are perfectly known. It is observed that the localisation-aimed ISpsf (lo-ISpsf) always outperforms communication-aimed ISpsf (co-ISpsf) [13],[14], since lo-ISpsf adjusts the phase of all derivatives, while co-ISpsf[13],[14] only considers those of parameters at BS and MS. aPEB and aOEB usually approximate ePEB and eOEB with the relative approximation error (RAE) below 5%. Thus, far-field approximation error is effectively reduced by restricting the sub-arrays to N_{sr} elements. The 8-bit quantizer always achieve the highest performance than the other quantizers. However, the prominent effectiveness of lo-ISPsf is reflected on 1-bit quantizer, 100 times improvement on PEB and OEB with co-ISpsf[13],[14], whose performance also approximates to that of an 8-bit quantizer with co-ISpsf[13],[14].

Figs. 5.4 and 5.5 display the average PEB and OEB achieved by unknown ISs of 1, 4, 8-bit quantizers with the same simulation setup. PEB and OEB fluctuates severely and even increases when $N_{\mathrm{IS}} > 841$, since the absence of perfect knowledge of IS disables the location information of IS-aided paths. These results emphases the importance of knowledge of IS location information. The difference between approximated data and exact data is only acceptable with $N_{\mathrm{IS}} \leqslant 64$. The RAE of PEB and OEB is even up to 42% and 117% at $N_{\mathrm{IS}} = 16384$. Notice the minor superiority of 4 and 8-bit quantizers than the 1-bit quantizer, it is down to conclude that the 1-bit quantizer is still the most valuable choice for the scenario with unknown IS.

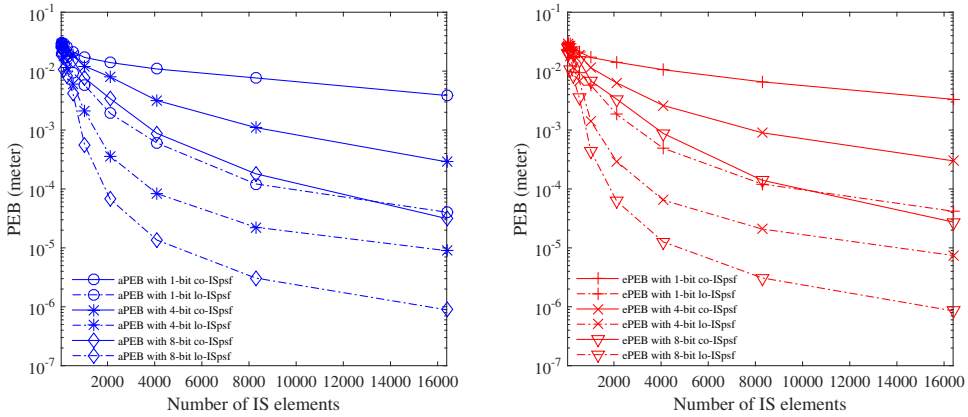

Figure 5.2: Average of approximated PEB and exact PEB with known IS.

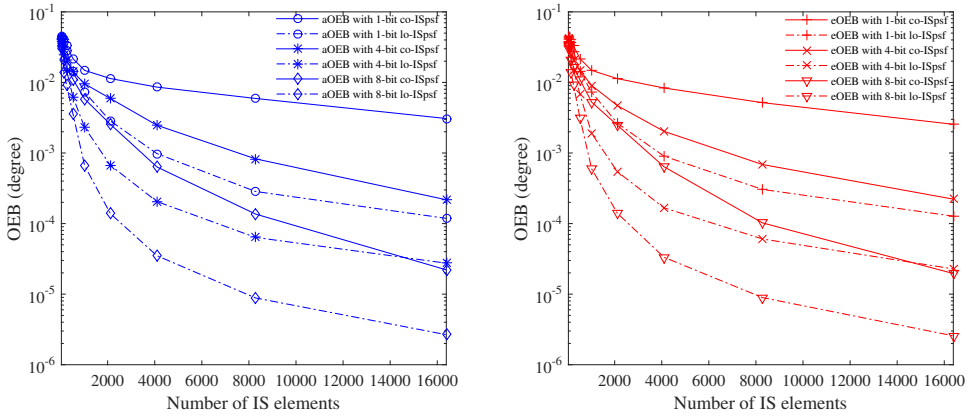

Figure 5.3: Average of approximated OEB and exact OEB with known IS.

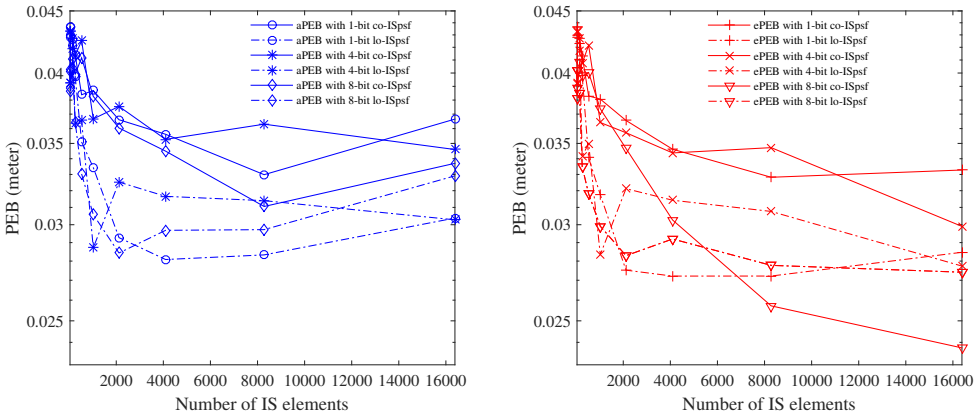

Figure 5.4: Average of approximated PEB and exact PEB with unknown IS.

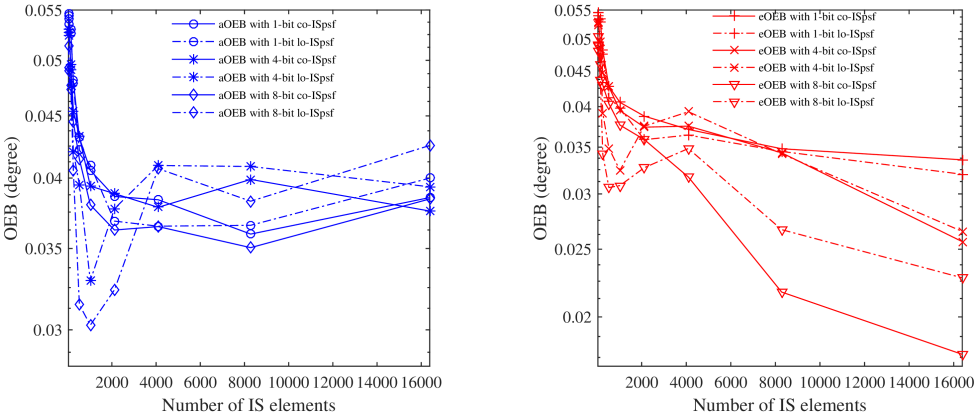

Figure 5.5: Average of approximated OEB and exact OEB with unknown IS.

5.6 Summary

In this chapter, we have studied the fundamental limits of IS assisted and massive MIMO based localisation. The impacts of number of IS elements and number of quantization bits have been investigated with approximated FIM and exact FIM for far-field localisation. Simulation results show minor approximation error derived by the approximated FIM with perfect awareness of IS position and orientation, while huge values of up to 42% and 117% RAE of PEB and OEB are drawn by that without the awareness, which implies the importance of the knowledge of IS position and orientation. A novel localisation-aimed ISpsf is proposed to improve accuracy than the existing communication-aimed ISpsf [13],[14]. However, it brings greater improvement on accuracy of 1-bit quantizer than expensive quantizers. Moreover, localisation-aimed ISpsf could be disabled by the absence of knowledge of IS, where the Ix elements deteriorate into single bounced scatters.

Chapter 6

Conclusion and Future Work

6.1 Conclusion

This thesis investigated the mobile localisation technologies applied for 5G and B5G cellular networks, including centralised cooperative localisation based on hybrid measurements, UAV BS assisted and RSS based localisation, and IS assisted massive MIMO based localisation.

In Chapter 3, the centralised cooperative localisation approach based on TOA, AOA, AOD and RSS has been proposed to localise the MS in single bounced NLOS environment. The proposed approach is enhanced by another proposed weight functions and MS grouping scheme, in order to further improve accuracy of localisation, and reduce the computation cost. It has been shown that the proposed CLTAAR, wCLTAAR and eCLTAAR approaches achieve higher accuracy, and eCLTAAR costs 74% less computation time than the conventional approach in [2].

In Chapter 4, the fixed-wing UAV mounted BS assisted and RSS based localisation with airframe shadowing has been studied. This localisation problem can not be effectively solved by the existing approaches, due to the nonlinear and non-convex expression of PLE. We first propose to partition the EAPL model to a power-like function of two sub-functions through piecewise convex approximation and curve fitting. Based on the approximated model, the problem of UAV assisted localisation with unknown and unequal PLEs is addressed by the proposed PCAL approach. The ambiguous estimates caused by the approximated model are eliminated by a proposed GSAE method, which is more effective than the conventional PLM method in [37]. The localisation problem with un-

known transmit power is solved by the proposed PCAL-gsDRSS approach with estimated transmit power. Furthermore, an anti-common sense finding has proved the higher accuracy of localisation and ranging distance achieved by EPt and EPLEs than that of real transmit power and real PLEs, and suggests to use estimated parameters rather than the real parameters, even in the scenario with perfectly known real parameters. Besides, a PCAL-EPt-gsDRSS localisation scheme has been proposed with estimated EPt. Simulation results shown the much higher accuracy of proposed PCAL and PCAL-GSAE with unknown and unequal PLEs, PCAL-gsDRSS and PCAL-EPt-gsDRSS with unknown transmit power, and unknown and unequal PLEs than the existing approaches [7],[8],[10],[63] with perfectly known PLEs and transmit power, and [9] with unknown transmit power, and unknown and unequal PLEs. PCAL-GSAE and PCAL-EPt-gsDRSS approach the CRLB derived.

In Chapter 5, an IS assisted massive MIMO based localisation has been investigated. Large IS array is partitioned into non-overlapping sub-arrays, in order to mitigate far-field approximation error on channel parameters and aFIM. The derived eFIM and eEFIM prove the necessity on separating the progresses of localisation and ISpsf design. Through analysing eFIM, localisation-aimed ISpsf is designed to decrease the theoretical limits on PEB and OEB of MS. The impacts of number of Ix elements, number of ISpsf quantizer bits and knowledge of IS on the obtained approximated PEB, OEB and exact PEB and OEB of localisation have been investigated by numerical results. The overall results imply the importance of the perfect knowledge of IS, and the effectiveness of proposed localisation-aimed ISpsf. When the IS is perfectly known, aFIM achieves negligible RAE, and ISpsf of 8-bit quantizer has the highest accuracy. However, when the knowledge of IS is absent, RAE of PEB and OEB increases up to 42% and 117%, and ISpsf of 1-bit quantizer achieve comparable accuracy as the other expensive quantizers. The proposed localisation-aimed ISpsf with the perfect knowledge has performed 100 times higher accuracy than the existing communication-aimed ISpsf [13],[14], but also deteriorates dramatically when IS is unknown.

6.2 Future Work

In the research on mobile localisation techniques in this thesis, some assumptions made are far beyond the realistic. For example, in the practical system, the radio resource allocated to localisation is limited and less important than other missions of the networks,

like power control, interference management, channel estimation, etc, which might influence the accuracy and quantity of measurements accessible for localisation. Besides, the upcoming 6G network offers an opportunity for localisation, including the enablers, like THz communication, intelligent surface and artificial intelligent system. Hence, the future research topics are summarised in the following.

1. Joint optimisation of available radio resources for each mission are needed for different purposes of networks. Currently, most network missions are processing independently. The impacts of different missions on localisation have not been adequately investigated, except power control on fundamental limits of localisation. For example, the performance of localisation may not be degraded by giving more resources to channel estimation, which can beneficial for localisation through providing more accurate measurements. Another example is that, inter-user interference may contain eligible location information of users in neighbouring cells, which assists localisation of the interfering users. Therefore, the joint optimisation of multiple missions for improving the entire performance of multi-user localisation is still challenging and will be investigated thoroughly.

2. Some promising technologies envisioned for the future 6G offer new opportunity to localisation. Simultaneous localisation and mapping will be enabled by a unified interface of 6G, which is a challenging problem due to the insufficient accuracy of measurements. The passive IS has been investigated by this thesis, but the active IS, which works as transmitter, and hybrid passive and active IS are different with passive IS, which upper bound of power is limited by the transmit power of BS or MS, thus active IS and hybrid IS could make the smart radio environment more configurable. THz communication is different with the existing mmWave communication, and is distorted by molecular absorption. The proposed methods could benefit from the higher frequency, larger bandwidth and smaller wavelength, which bring more direct and less indirect paths, more accurate estimation on position-related parameters and smaller antennas. The envisioned challenging problems include investigation on new channel model in THz communication environment, non-stationary channel for extremely large array and channel estimation at ISs.

3. The models employed by this thesis could be more realistic, and the environmental and system parameters should be considered, such as transmit power, antenna

gain, amplifier, multipath fading and interference. Polarization influences the directional antenna gain, and contains information of incident and reflection angle [36]. Multipath fading could be significant in 5G low-bands, as the delay spread and angular spread of propagation in a cluster cause extra measurement error on TOA and AOA. TOA measurements could be distorted by synchronisation error (caused by imperfect channel estimation and interference), clock drift and clock skew (caused by hardware). Consideration of the aforementioned more realistic factors could not only enrich the knowledge of location information, but also paves the way for field test in future.

4. The proposed work in Chapters 3-5 can be verified by field test. Chapter 3 can be examined with simplified facilities. For example, BSs can be replaced with RF sensors or spectrum analysers equipped with receivers, and MSs can be replaced with mobile phone or signal generators (such as E82257D PSG) equipped with transmitters (such as Model-TRA-5960W). The measurements of TOA, AOA, AOD and RSS are collected and processed by the connected computer, which works as location server centre in cellular networks. The measurement system set for Chapter 4 includes four aircraft and a ground station. The aircraft could be NASA's S-3B Viking airplane equipped with GPS and synchronised notebook. A four-channel ground station of four monopoles is employed as the transmitter. Parameters of the airplane and collected RSS measurements are sent to the notebook and processed online. However, it is difficult to apply the work proposed in Chapter 5, due to the lack of massive MIMO arrays. The relevant field test can utilise the aforementioned signal generators and analysers to transmit and receive signals, and build an IS made of off-the-shelf antenna elements, such as 'RFocus prototype' designed by researchers of the Massachusetts Institute of Technology.

5. The proposed methods in Chapters 3 and 4 can be applied for Internet of things (IoT) through simply replacing the architecture of 5G system with other IoT based system, such as LoraWAN system. In the LoraWAN system, end-node transmit data to gateways, which pass the received data to The Things Network (TTN) through UDP/IP. Then, TTN processes the data and deliver the message to the third party client, which estimates the position of end-node with the proposed methods. Chapter 5 can be examined with experiment, if the ongoing work on IoT connections envisioned in 5G, massive machine-type communication (mMTC) and ultra-reliable

low-latency communication (URLLC) come true. Then, IoT user equipments (UEs) could be directly connected to 5G massive MIMO BSs. Additionally, Chapter 3 can also be directly applied for emergency services, *e.g.*, E911 emergency call, based on the RSS measurements reported by either MSs or UAV BSs.

Bibliography

[1] F. Gustafsson and F. Gunnarsson, "Mobile positioning using wireless networks: possibilities and fundamental limitations based on available wireless network measurements," *IEEE Sig. Process. Mag.*, vol. 22, no. 1, pp. 41–53, Jan. 2019.

[2] S. Frattasi and F. D. Rosa, *Mobile positioning and tracking: from conventional to cooperative techniques, 2nd ed.* Wiley Press, 2017.

[3] F. Boccardi and R. W. Heath, "Five disruptive technology directions for 5g," *IEEE Commun. Mag.*, vol. 52, no. 3, pp. 74–80, Feb. 2014.

[4] Y. Liu, X. Shi, S. He, and Z. Shi, "Prospective positioning architecture and technologies in 5g networks," *IEEE Netw.*, vol. 31, no. 6, p. 115–121, Nov. 2017.

[5] R. D. Taranto and *et al*, "Location-aware communications for 5g networks: how location information can improve scalability, latency, and robustness of 5g," *IEEE Sig. Process. Mag.*, vol. 31, no. 6, pp. 102–112, Oct. 2014.

[6] M. Agiwal, A. Roy, and N. Saxena, "Next generation 5g wireless networks: a comprehensive survey," *IEEE Commun. Surveys Tuts.*, vol. 18, no. 3, pp. 1617–1655, 3rd Quart., 2016.

[7] Z. Wang, H. Zhang, T. Lu, and T. A. Gulliver, "Cooperative rss-based localization in wireless sensor networks using relative error estimation and semidefinite programming," *IEEE Trans. Veh. Tech.*, vol. 68, no. 1, pp. 483–497, Jan. 2019.

[8] Y. Hu and G. Leus, "Robust differential received signal strength - based localization," *IEEE Trans. Sig. Process.*, vol. 65, no. 12, pp. 3261 – 3276, Jul. 2017.

[9] J. Shi, G. Wang, and L. Jin, "Least squared relative error estimator for rss based localization with unknown transmit power," *IEEE Sig. Process. Lett.*, vol. 27, pp. 1165 – 1169, Jun. 2020.

[10] S. Mazuelas and *et al*, "Robust indoor positioning provided by real-time rssi values in unmodified wlan networks," *IEEE J. Sel. Topics Sig. Process.*, vol. 3, no. 5, pp. 821 – 831, Oct. 2009.

[11] Y. Shen and M. Z. Win, "Fundamental limits of wideband localization - part i: a general framework," *IEEE Trans. Inf. Theory*, vol. 56, no. 10, pp. 4956–4980, Oct. 2010.

[12] A. Guerra, F. Guidi, and D. Dardari, "Single-anchor localization and orientation performance limits using massive arrays: Mimo vs. beamforming," *IEEE Trans. Wireless Commun.*, vol. 17, no. 8, pp. 5241 – 5255, Aug. 2018.

[13] Y. Liang and *et al*, "Large intelligent surface/antennas (lisa): making reflective radios smart," *J. Commun. Inf. Netw.*, vol. 4, no. 2, p. 40 – 50, Jun. 2019.

[14] H. W. J. He, T. Sanguanpuak, O. Silven, and M. Juntti, "Adaptive beamforming design for mmwave ris-aided joint localization and communication," in *Proc. 2020 IEEE Wireless Commun. Netw. Conf. Wkshps. (WCNCW)*. Seoul, Korea (South), Apr. 2020.

[15] J. A. del Peral-Rosado, R. Raulefs, J. A. L. spez Salcedo, and G. SecoGranados, "Survey of cellular mobile radio localization methods: from 1g to 5g," *IEEE Commun. Surveys Tuts.*, vol. 20, no. 2, pp. 1124–1148, Secondquarter 2018.

[16] C. Laoudias, A. Moreira, S. Kim, S. Lee, L. Wirola, and C. Fischione, "A survey of enabling technologies for network localization, tracking, and navigation," *IEEE Commun. Surveys Tuts.*, vol. 20, no. 4, p. 3607–3644, Jul. 2018.

[17] J. J. Caffery, "A new approach to the geometry of toa location," in *Proc. IEEE 52nd Veh. Tech. Conf. Fall 2020 (VTC Fall 2020)*. Boston, MA, U.S.A., Sep. 2000.

[18] Y. T. Chan and *et al*, "Time of arrival based localization under nlos conditions," *IEEE Trans. Veh. Tech.*, vol. 55, no. 1, pp. 17–24, Jan 2006.

[19] D. Dardari, C. C. Chong, and M. Z. Win, "Threshold-based time of arrival estimators in uwb dense multipath channels," *IEEE Trans. Commun.*, vol. 56, no. 8, pp. 1366–1378, Aug. 2008.

[20] L. Xiong, "A aelective model to suppress nlos signals in angle-of-arrival (aoa) location estimation," in *Proc. IEEE 9th Inter. Symposium on Pers. Ind. and Mobile Radio Commun. (PIMRC)*. Boston, MA, U.S.A., Sep. 1998.

[21] A. Pages-Zamora, J. Vidal, and D. H. Brooks, "Closed-form solution for positioning based on angle of arrival measurements," in *Proc. IEEE 13th Inter. Symposium on Pers. Ind. and Mobile Radio Commun. (PIMRC)*. Pavilhao Altantico, Portugal, Sep. 2002.

[22] A. Mallat, J. Louveaux, and L. Vandendorpe, "Uwb based positioning in multipath channels: Crbs for aoa and for hybrid toa-aoa based methods," in *Proc. 2007 IEEE Inter. Conf. Commun.* Glasgow, U.K., Jun. 2007.

[23] A. Kangas and T. Wigren, "Angle of arrival localization in lte using mimo pre-coder index feedback," *IEEE Commun. Lett.*, vol. 17, no. 8, pp. 1584–1587, Aug. 2013.

[24] R. B. Ertel and J. H. Reed, "Angle and time of arrival statistics for circular and elliptical scattering models," *IEEE J. Sel. Areas Commun.*, vol. 17, p. 1829 – 1840, Nov. 1999.

[25] A. Borhani and M. Patzold, "A unified disk scattering model and its angle-of-departure and time-of-arrival statistics," *IEEE Trans. Veh. Technol.*, vol. 62, no. 2, p. 473 – 485, Feb. 2013.

[26] G. Lee, Y. Sung, and J. Seo, "Randomly-directional beamforming in millimeter-wave multi-user miso downlink," *IEEE Trans. Wireless Commun.*, vol. 15, no. 2, p. 1086 – 1100, Feb. 2016.

[27] J. Chung, C. S. Hwang, K. Kim, and Y. K. Kim, "A random beamforming technique in mimo systems exploiting multiuser diversity," *IEEE J. Sel. Areas Commun.*, vol. 21, p. 848 – 855, Jun. 2003.

[28] K. Zarb-Adami, A. Faulkner, J. G. B. de Vaate, G. W. Kant, and P. Picard, "Beamforming techniques for large-n aperture arrays," in *Proc. 4th IEEE Inter. Symposium*

on Phased Array Syst. and Technol. (ARRAY '10). Waltham, MA, U.S.A., Oct. 2010.

[29] E. Basar and *et al*, "Wireless communications through reconfigurable intelligent surface," *IEEE Access*, vol. 7, pp. 116 753 – 116 773, Aug. 2019.

[30] 3rd Generation Partnership Project, "Technical specification group radio access network; user equipment (ue) conformance specification; radio transmission and reception; part 1: Conformance testing," *TS 36.521-1, V14.3.0*, Aug. 2017.

[31] M. D. Renzo and *et al*, "Smart radio environments empowered by reconfigurable intelligent surfaces: How it works, state of research, and road ahead," *arXiv:2004.09352 [cs.IT]*, Apr. 2020.

[32] J. V. Alegría and F. Rusek, "Cramér-rao lower bounds for positioning with large intelligent surfaces using quantized amplitude and phase," in *Proc. 2019 53rd Asilomar Conf. on Sig., Syst., and Computers.* Pacific Grove, CA, U.S.A., Nov. 2019.

[33] S. Hu, F. Rusek, and O. Edfors, "Cramer-rao lower bounds for positioning with large intelligent surfaces," in *Proc. IEEE Veh. Technol. Conf. (VTC).* Toronto, Canada, Sep. 2017.

[34] S. Hu, F.Rusek, and O. Edfors, "Beyond massive mimo: The potential of data transmission with large intelligent surfaces," *IEEE Trans. Signal Process.*, vol. 66, no. 10, p. 2746–2758, May 2018.

[35] E. Bjornson and L. Sanguinetti, "Demystifying the power scaling law of intelligent reflecting surfaces and metasurfaces," in *Proc. IEEE Int. Wkshps. Computat. Adv. Multi-Sensor Adaptive Process. (CAMSAP).* Le gosier, Guadeloupe, Dec. 2019.

[36] E. Bjornson and L.Sanguinetti, "Power scaling laws and near-field behaviors of massive mimo and intelligent reflecting surfaces," *IEEE Open Journal of the Communications Society*, vol. 1, pp. 1306–1324, Sep. 2020.

[37] S. Boyd and L. Vandenberghe, *Convex Optimization.* Cambridge University Press, 2004.

[38] Z. Abu-Shaban, X. Zhou, and T. D. Abhayapala, "A novel toa-based mobile localization technique under mixed los/nlos conditions for cellular networks," *IEEE Trans. Veh. Technol.*, vol. 65, no. 11, p. 8841 – 8853, Nov. 2016.

[39] W. Zhang, Q. Yin, H. Chen, F. Gao, and N. Ansari, "Distributed angle estimation for localization in wireless sensor networks," *IEEE Trans. Wireless Commun.*, vol. 12, no. 2, p. 527 – 537, Feb. 2013.

[40] J. Li, J. Conan, and S. Pierre, "Mobile terminal location for mimo communication systems," *IEEE Trans. Antennas Propag.*, vol. 55, no. 8, p. 2417 – 2420, Aug. 2007.

[41] C. Chen and K. Feng, "Statistical distance estimation algorithms with rss measurements for indoor lte-a networks," *IEEE Trans. Veh. Technol.*, vol. 66, no. 2, p. 1709 – 1722, Feb. 2017.

[42] Y. Xie, Y. Wang, and X. You, "Closed-form location estimator from toa/aoa/aod measurements in mimo communication systems," in *Proc. IEEE Sarnoff Symposium.* Princeton, NJ, U.S.A., Apr. 2009.

[43] B. Y. Shikur and T. Weber, "Tdoa/aod/aoa localization in nlos environments," in *Proc. IEEE Int. Conf. on Acoustics, Speech and Sig. Process. (ICASSP).* Florence, Italy, May 2014.

[44] S. W. Chen, C. K. Seow, and S. Y. Tan, "Elliptical lagrange-based nlos tracking localization scheme," *IEEE Trans. Wireless Commun.*, vol. 15, no. 5, pp. 3212 – 3225, May 2016.

[45] D. Liu, K. Liu, Y. Ma, and J. Yu, "Joint toa and doa localization in indoor environment using virtual stations," *IEEE Commun. Lett.*, vol. 18, no. 8, pp. 1423 – 1426, Aug. 2014.

[46] M. Kyro, V. Kolmonen, and P. Vainikainen, "Experimental propagation channel characterization of mm-wave radio links in urban scenarios," *IEEE Antennas Wireless Propag. Lett.*, vol. 11, p. 865 – 868, Jul. 2012.

[47] A. Shahmansoori, G. E. Garcia, G. Destino, G. Seco-Granados, and H. Wymeersch, "5g position and orientation estimation through millimeter wave mimo," in *Proc. IEEE Globecom Wkshps. (GC Wkshps).* San Diego, CA, U.S.A., Dec. 2015.

[48] S. A. Banani, M. Najibi, and R. G. Vaughan, "Range-based localisation and tracking in non-line-of-sight wireless channels with gaussian scatterer distribution model," *IET Commun.*, vol. 7, no. 18, p. 2034 – 2043, Jul. 2013.

[49] K. Das and H. Wymeersch, "Censoring for bayesian cooperative positioning in dense wireless networks," *IEEE J. Sel. Areas in Commun.*, vol. 30, no. 9, p. 1835 – 1842, Oct. 2012.

[50] J. Cui, Z. Wang, C. Zhang, Y. Zhang, and Z. Zhu, "Message passing localisation algorithm combining bp with vmp for mobile wireless sensor networks," *IET Commun.*, vol. 11, no. 7, pp. 1106–1113, May 2017.

[51] F. D. Rosa, T. Paakki, H. Leppäkoski, , and J. Nurmi, "A cooperative framework for path loss calibration and indoor mobile positioning," in *Proc. IEEE 7th Wkshps. Positioning Navig. and Commun. (WPNC)*. Dresden, Germany, Mar. 2010.

[52] K. McDermott, R. M. Vaghefi, and R. M. Buehrer, "Cooperative utdoa positioning in lte cellular systems," in *Proc. IEEE Globecom Wkshps. (GC Wkshps)*. San Diego, CA, U.S.A., Dec. 2015.

[53] A. Dammann, R. Raulefs, , and S. Zhang, "On prospects of positioning in 5g," in *Proc. IEEE Inter. Conf. Commun. Wkshps. (ICCW)*. London, U.K., Jun. 2015.

[54] C. Gentile, N. Alsindi, R. Raulefs, and C. Teolis, *Geolocation Techniques Principles and Applications*. Springer, 2013.

[55] X. Wei, N. Palleit, and T. Weber, "Aod/aoa/toa-based 3d positioning in nlos multipath environments," in *Proc. IEEE 22nd Inter. Symposium on Pers. Ind. and Mobile Radio Commun. (PIMRC)*. Toronto, Canada, Sep. 2011.

[56] F. Penna, M. A. Caceres, and H. Wymeersch, "Cramér-rao bound for hybrid gnss-terrestrial cooperative positioning," *IEEE Commun. Lett.*, vol. 14, no. 11, p. 1005 – 1007, Nov. 2010.

[57] I.-R. report M.2135, "Guidelines for evaluation of radio interface technologies for imt-advanced," 2008.

[58] M. Alzenad, F. L. A. El-Keyi, and H. Yanikomeroglu, "3-d placement of an unmanned aerial vehicle base station (uav-bs) for energy-efficient maximal coverage," *IEEE Wireless Commun. Lett.*, vol. 6, no. 4, pp. 434 – 437, Aug. 2017.

[59] A. Merwaday and I. Guvenc, "Uav assisted heterogeneous networks for public safety communications," in *Proc. 2015 IEEE Wireless Commun. Netw. Conf. Wkshps.* New Orleans, LA, U.S.A., Mar. 2015.

[60] C. Luo, S. I. McClean, G. Parr, L. Teacy, and R. D. Nardi, "Uav position estimation and collision avoidance using the extended kalman filter," *IEEE Trans. Veh. Tech.*, vol. 62, no. 6, pp. 2749 – 2162, Jul. 2013.

[61] R. M. Vaghefi, M. R. Gholami, R. M. Buehrer, and E. G. Strom, "Cooperative received signal strength-based sensor localization with unknown transmit powers," *IEEE Trans. Sig. Process.*, vol. 61, no. 6, pp. 1389 – 1403, Mar. 2013.

[62] S. Tomic, M. Beko, and R. Dinis, "Rss-based localization in sensor networks using convex relaxation: noncooperative and cooperative schemes," *IEEE Trans. Veh. Tech.*, vol. 64, no. 5, pp. 2037 – 2050, May 2015.

[63] V. Kumar, R. Arablouei, R. Jurdak, B. Kusy, and N. W. Bergmann, "Rssi-based self-localization with perturbed anchor positions," in *Proc. IEEE 28th Int. Symp. Personal, Indoor and Mobile Radio Communications (PIMRC).* Montreal, Canada, Oct. 2017.

[64] S. Mazuelas and *et al*, "Topology assessment provided by weighted barycentric parameters in harsh environment wireless location systems," *IEEE Trans. Sig. Process.*, vol. 58, no. 7, pp. 3842 – 3857, Jul. 2010.

[65] J. Prieto and *et al*, "Adaptive data fusion for wireless localization in harsh environments," *IEEE Trans. Sig. Process.*, vol. 60, no. 4, pp. 1585 – 1596, Apr. 2012.

[66] S. Fang, Y. Hsu, B. Lu, and W. Kuo, "A calibration-free rss-based mobile positioning system," in *Proc. IEEE VTC-Spring 2012.* Yokohama, Japan, May 2012.

[67] L. Cheng, C. Wu, Y. Zhang, and Y. Wang, "An indoor localization strategy for a mini-uav in the presence of obstacles," *Int. J. Advanced Robot. Syst.*, vol. 9, no. 4, pp. 1 – 8, Oct. 2012.

[68] I. Ahmad, N. W. Bergmann, R. Jurdak, and B. Kusy, "Towards probabilistic localization using airborne mobile anchors," in *Proc. 2016 IEEE PerCom. Wkshps.* Sydney, Australia, Mar. 2016.

[69] D. W. Matolak and R. Sun, "Air–ground channel characterization for unmanned aircraft systems—part i- methods, measurements, and models for over-water settings," *IEEE Trans. Veh. Tech.*, vol. 66, no. 1, pp. 26 – 44, Jan. 2017.

[70] K. Wang and *et al*, "Path loss measurement and modeling for low-altitude uav access channels," in *Proc. IEEE VTC-Fall 2017.* Toronto, Canada, Sep. 2017.

[71] A. Al-Hourani and K. Gomez, "Modeling cellular-to-uav path-loss for suburban environments," *IEEE Wireless Commun. Lett.*, vol. 7, no. 1, pp. 82 – 85, Feb. 2018.

[72] D. W. Matolak, R. Sun, and W. Rayess, "Air-ground channel characterization for unmanned aircraft systems—part iv airframe shadowing," *IEEE Trans. Veh. Tech.*, vol. 66, no. 9, pp. 7643 – 7652, Sep. 2017.

[73] H. Sallouha, M. M. Azari, A. Chiumento, and S. Pollin, "Aerial anchors positioning for reliable rss-based outdoor localization in urban environments," *IEEE Wireless Commun. Lett.*, vol. 7, no. 3, pp. 376 – 379, Jun. 2018.

[74] S. Chang, Y. Li, H. Wang, and G. Wang, "Received signal strength–based target localization under spatially correlated shadowing via convex optimization relaxation," *Int. J. of Distrib. Sens. Netw.*, vol. I4, no. 6, pp. 1–9, Jun. 2018.

[75] J. H. Lee and R. M. Buehrer, "Location estimation using differential rss with spatially correlated shadowing," in *Proc. 2009 IEEE Global Telecom. Conf. (GLOBECOM).* Honolulu, HI, U.S.A., Dec. 2009.

[76] J. Huang, P. Liu, W. Lin, and G. Gui, "Rss based method for sensor localization with unknown transmit power and uncertainty in path loss exponent," *Sensors*, vol. 16, no. 1452, pp. 1–20, Sep. 2016.

[77] N. Salman, M. Ghogho, and A. H. Kemp, "On the joint estimation of the rss-based location and path-loss exponent," *IEEE Wireless Commun. Lett.*, vol. 1, no. 1, p. 34–37, Feb. 2012.

[78] M. Hasanzade and *et al*, "Localization and tracking of rf emitting targets with multiple unmanned aerial vehicles in large scale environments with uncertain transmitter power," in *Proc. 2017 Int. Conf. Unmanned Aircraft Syst.* Miami, FL, U.S.A., Jul. 2017.

[79] M. D. Buhmann and A. Iserles, *Approximation theory and optimization.* Cambridge University Press, 1997.

[80] 3GPP, "3gpp specification release 15." [Online]. Available: https://www.3gpp.org/DynaReport/SpecReleaseMatrix.htm.

[81] L. A. Vandenberghe and S. B. Boyd, "Semidefinite programming," *SIAM Rev.*, vol. 38, no. 1, p. 49–95, Mar. 1996.

[82] A. Bourdoux and *et al*, "6g white paper on localization and sensing," *arXiv:2006.01779 [eess.SY]*, Jun. 2020.

[83] M. D. Renzo and *et al*, "Smart radio environments empowered by reconfigurable ai meta-surfaces: an idea whose time has come," *EURASIP J. Wireless Commun. and Netw.*, vol. 129, 2019.

[84] Z. Abu-Shaban, X. Zhou, T. Abhayapala, G. Seco-Granados, and H. Wymeersch, "Error bounds for uplink and downlink 3d localization in 5g millimeter wave systems," *IEEE Trans. Wireless Commun.*, vol. 17, no. 8, pp. 4939 – 4954, Aug. 2018.

[85] R. Mendrzik, H. Wymeersch, G. Bauch, and Z. Abu-Shaban, "Harnessing nlos components for position and orientation estimation in 5g millimeter wave mimo," *IEEE Trans. Wireless Commun.*, vol. 18, no. 1, pp. 93–107, Jan. 2019.

[86] A. Kakkavas, M. H. C. García, R. A. Stirling-Gallacher, and J. A. Nossek, "Performance limits of single-anchor millimeter-wave positioning," *IEEE Trans. Wireless Commun.*, vol. 18, no. 11, pp. 5196 – 5210, Nov. 2019.

[87] A. Shahmansoori, G. E. Garcia, G. Destino, G. Seco-Granados, and H. Wymeersch, "Position and orientation estimation through millimeter-wave mimo in 5g systems," *IEEE Trans. Wireless Commun.*, vol. 17, no. 3, p. 1822–1835, Mar. 2018.

[88] E. Basar, "Reconfigurable intelligent surface-based index modulation: A new beyond mimo paradigm for 6g," *IEEE Transactions on Communications*, vol. 68, no. 5, pp. 3187–3196, 2020.

[89] S. Ellingson, "Path loss in reconfigurable intelligent surface-enabled channels," *arXiv: 1912.06759 [eess.SP]*, Dec. 2019.

[90] H. Wymeersch, "A fisher information analysis of joint localization and synchronization in near-field," in *Proc. IEEE Inter. Conf. Commun. Wkshps. (ICCW)*. Dublin, Ireland, Jun. 2020.

[91] Y. Han, Y. Shen, X. Zhang, M. Z. Win, and H. Meng, "Performance limits and geometric properties of array localization," *IEEE Trans. Inf. Theory*, vol. 62, no. 2, pp. 1054–1075, Feb. 2016.

Appendices

Appendix A

Parameters in Lemma 1

The parameters $t1 \sim t6$ employed by EPt-range of power-like ranging function in (4.24) are calculated as

$$t1 = Pr_i - X_{\mathrm{PL},i} + C_{i,g_i} \tag{A.1}$$

$$t2 = |A_{i,g_i}|(2d_i - \tilde{d}_i)^{B_{i,g_i}} \tag{A.2}$$

$$t3 = |A_{i,g_i}|\tilde{d}_i^{B_{i,g_i}} \tag{A.3}$$

The six events in (4.24) for EPt-range of power-like ranging function are defined as

$$\text{Event D: } \tilde{d}_i \geqslant 2d_i \ \&\ B_{i,g_i} < 0 \tag{A.4}$$

$$\text{Event E: } d_i < \tilde{d}_i < 2d_i \ \&\ B_{i,g_i} < 0 \tag{A.5}$$

$$\text{Event F: } \tilde{d}_i < d_i \ \&\ B_{i,g_i} < 0 \tag{A.6}$$

$$\text{Event G: } \tilde{d}_i < d_i \ \&\ B_{i,g_i} > 0 \tag{A.7}$$

$$\text{Event H: } \tilde{d}_i \geqslant 2d_i \ \&\ B_{i,g_i} > 0 \tag{A.8}$$

$$\text{Event I: } d_i < \tilde{d}_i < 2d_i \ \&\ B_{i,g_i} > 0 \tag{A.9}$$

And the three events in (4.23) for EPt-range of exponential-like ranging function are defined as

$$\text{Event A:}\quad X_{\mathrm{PL},i} \geqslant 10\eta_i \log_{10}(2) + Pt \tag{A.10}$$

$$\text{Event B:}\quad 0 < X_{\mathrm{PL},i} < 10\eta_i \log_{10}(2) + Pt \tag{A.11}$$

$$\text{Event C:}\quad X_{\mathrm{PL},i} < 0 \tag{A.12}$$

Appendix B

Derivation of Lemma 2

Denote the i-th ranging distance using any PLE $\hat{\eta}_i$ in EPLE range and that using real PLE as $\hat{d}_i = 10^{\widetilde{PL}_i/(10\hat{\eta}_i)}$ and $\tilde{d}_i = 10^{\widetilde{PL}_i/(10\eta_i)}$, respectively. If the ranging error of $\hat{d}_i$ is smaller than that of $\tilde{d}_i$, it claims that $\hat{e}_i = |\hat{d}_i - d_i| \leqslant \tilde{e}_i = |\tilde{d}_i - d_i|$, which is equivalent with

$$\begin{aligned} &(\hat{d}_i - d_i)^2 \leqslant (\tilde{d}_i - d_i)^2 \Rightarrow (\hat{d}_i + \tilde{d}_i - 2d_i)(\hat{d}_i - \tilde{d}_i) < 0 \\ &\Rightarrow \begin{cases} \hat{d}_i < \tilde{d}_i \ \& \ \hat{d}_i > 2d_i - \tilde{d}_i \\ \hat{d}_i > \tilde{d}_i \ \& \ \hat{d}_i < 2d_i - \tilde{d}_i \end{cases} \end{aligned} \tag{B.1}$$

Substituting the expressions of $\hat{d}_i$ and $\tilde{d}_i$ to (A.129), it is rewritten as that

$$\begin{cases} 10^{\frac{\widetilde{PL}_i}{10\hat{\eta}_i}} > 10^{\frac{\widetilde{PL}_i}{10\eta_i}} \ \& \ 10^{\frac{\widetilde{PL}_i}{10\hat{\eta}_i}} < 2 \times 10^{\frac{PL_i}{10\eta_i}} - 10^{\frac{\widetilde{PL}_i}{10\eta_i}}, & X_{S,i} > 0 \\ 10^{\frac{\widetilde{PL}_i}{10\hat{\eta}_i}} < 10^{\frac{\widetilde{PL}_i}{10\eta_i}} \ \& \ 10^{\frac{\widetilde{PL}_i}{10\hat{\eta}_i}} > 2 \times 10^{\frac{PL_i}{10\eta_i}} - 10^{\frac{\widetilde{PL}_i}{10\eta_i}}, & X_{S,i} < 0 \end{cases} \tag{B.2}$$

When $2 \times 10^{\frac{PL_i}{10\eta_i}} - 10^{\frac{\widetilde{PL}_i}{10\eta_i}} > 0$, real PLE is bounded by $\eta_i > \epsilon_i = X_{S,i}/(10\log_{10} 2)$, then taking logarithm of equations on both sides of inequality equations in (A.130) implies that

$$\begin{cases} \hat{\eta}_i > \eta_i \ \& \ \hat{\eta}_i < \check{\eta}_i, & \text{Event J} \\ \hat{\eta}_i < \eta_i \ \& \ \hat{\eta}_i > \check{\eta}_i, & \text{Event K} \end{cases} \tag{B.3}$$

where $\check{\eta}_i = \frac{(PL_i+n)\eta_i}{PL_i+10\eta_i \log_{10}\left(2-10^{\frac{X_{S,i}}{10\eta_i}}\right)}$. The events are defined as, Event J : $\eta_i > \epsilon_i \& X_{S,i} > 0$, Event K : $\eta_i > \epsilon_i \& X_{S,i} < 0$.

Another case $2 \times 10^{\frac{PL_i}{10\eta_i}} - 10^{\frac{\widetilde{PL}_i}{10\eta_i}} < 0$, *i.e.*, $\eta_i < \epsilon_i$, is contradictory with the condition $X_{S,i} < 0$ in (A.130), since PLE must be greater than 0. Thus, (A.130) with $\eta_i < \epsilon_i$ is calculated as

$$\hat{\eta}_i > \eta_i \text{ when Event L} \tag{B.4}$$

where Event L : $\eta_i < \epsilon_i \&\ X_{S,i} > 0$. Combining (A.131) and (A.132) leads to (4.33).

Appendix C

Proof of Lemma 3

Lemma 3 can be proved by verifying any values of $\hat{\mathbf{v}}_{\mathrm{g}}$ near the optimal $\mathbf{v}_{\mathrm{e}}$ could reached by unEPLEs or unEPt. This can be done through expanding the expression of $\|\mathbf{E}_{\mathrm{g}}\|$ at the points near optimal $\mathbf{v}_{\mathrm{e}}$. If the expanded expression could achieve either greater or smaller than minimum value of $\|\mathbf{E}_{\mathrm{e}}\|$, the lemma is proved.

In this appendix, "unEdist" is referred to Edist obtained with unEPLEs and unEpt, and "eEdist" is referred to the Edist obtained with eEPLE and eEPt. The localisation error of $(P4.7)$ with eEPLE or eEPt, and that of $(P4.8)$ with unEPLEs or unEPt, are respectively calculated as

$$\mathbf{E}_{\mathrm{g}} \equiv \mathbf{\Phi}\mathbf{B}_{\mathrm{g}} - \mathbf{v} = \sum_{r=1}^{R_{\mathrm{BS}}} \mathbf{g}_r \tag{C.1}$$

$$\mathbf{E}_{\mathrm{e}} \equiv \mathbf{\Phi}\mathbf{B}_{\mathrm{e}} - \mathbf{v} = \sum_{r=1}^{R_{\mathrm{BS}}} \mathbf{e}_r \tag{C.2}$$

where the information matrix is calculated as $\mathbf{\Phi} = (\mathbf{A}^{\mathrm{T}}\mathbf{A})^{-1}\mathbf{A}$ is information matrix expressed in $(P4.7)$, $\boldsymbol{\phi}_i$ is the i-th row of $\mathbf{\Phi}$. $\mathbf{B}_{\mathrm{g}}$ and $\mathbf{B}_{\mathrm{e}}$ are the ranging matrices of unEdist and eEdist. Let $\Upsilon_{R_{\mathrm{BS}}} = [\upsilon_1, \ldots, \upsilon_{R_{\mathrm{BS}}}]$ denotes the set of N BSs in R_{BS} group, and any symbol with the subscript υ_r denotes the corresponding submatrix or elements of the BSs in r-th group. Thus, $\boldsymbol{\phi}_{\upsilon_r}$ and $\mathbf{b}_{\upsilon_r}$ represent the information submatrix and ranging submatrix of r-th group. Therefore, the path loss measures $\widetilde{\mathbf{PL}} = [\widetilde{PL}_1, \ldots, \widetilde{PL}_N]$ and information matrix $\mathbf{\Phi}$, ranging $\mathbf{B}$ of these R_{BS} groups are reordered as $\widetilde{\mathbf{PL}}_{\mathrm{ro}} = [\mathbf{PL}_{\upsilon_1}, \ldots, \mathbf{PL}_{\upsilon_R}]$, $\mathbf{\Phi}_{\mathrm{ro}} = [\boldsymbol{\phi}_{\upsilon_1}, \ldots, \boldsymbol{\phi}_{\upsilon_{R_{\mathrm{BS}}}}]$, respectively.Localisation error of estimated unEPLEs is calculated

as $\|\mathbf{E}_{\mathrm{g}}\| = \|\mathbf{\Phi}_{\mathrm{ro}}\mathbf{B}_{\mathrm{ro,g}} - \mathbf{v}\|$, where the reordered effective ranging matrix with unEPLE or unEPt is $\mathbf{B}_{\mathrm{ro,g}} = [\mathbf{b}_{\mathrm{g},1}, \ldots, \mathbf{b}_{\mathrm{g},R}]^{\mathrm{T}}$, and $\mathbf{b}_{\upsilon_r} = [d^2_{\mathrm{g},r,1} - s_{\mathrm{g},r,1}, \ldots, d^2_{\mathrm{g},r,K_r} - s_{\mathrm{g},r,K_r}]^{\mathrm{T}}$, and $d_{\mathrm{g},r,1}$ is the effective ranging distance obtained with unEPLE or unEPt, as defined in $(P4.8)$. Thus, the partial estimation error of r-th group with unEPLE $\eta_{\mathrm{g},r}$ is expressed as $\mathbf{g}_r = \boldsymbol{\phi}_{\upsilon_r}\mathbf{b}_{\mathrm{g},r} - \mathbf{v}$, and that with eEPLE is η_{e} is $\mathbf{e}_r = \boldsymbol{\phi}_{\upsilon_r}\mathbf{b}_{\mathrm{e},r} - \mathbf{v}$.

The exponential term of r-th unEdist and eEdist are respectively denoted by $\mathbf{t}_{\mathrm{g},r} = 10^{0.1/\eta_{\mathrm{g},r}}$ and $t_{\mathrm{e},r} = 10^{0.1/\eta_{\mathrm{e}}}$, then the ranging matrix employed by LS optimisation with unEPLE (LSO-unEPLE) in $(P4.8)$ and LS optimisation with eEPLE (LSO-eEPLE) in $(P4.7)$ are respectively rewritten as $\mathbf{B}_{\mathbf{t},\mathrm{g}} = \left[t_{\mathrm{g},1}^{\mathbf{PL}_{\upsilon_1}}, \ldots, t_{\mathrm{g},R}^{\mathbf{PL}_{\upsilon_R}}\right] - \mathbf{S}$ and $\mathbf{B}_{t,\mathrm{e}} = \left[t_{\mathrm{e}}^{\mathbf{PL}_{\upsilon_1}}, \ldots, t_{\mathrm{e}}^{\mathbf{PL}_{\upsilon_R}}\right] - \mathbf{S}$.

Assume equal PLE applied for the BS groups $r = 1, \ldots, k1-1, k1+1, \ldots, K_r$, except the $k1$-th group of (K_1) BSs, then the partial estimation error of these $(K_r - 1)$ unEPLEs is equal to that of eEPLE, *i.e.*, $\mathbf{e}_r = \mathbf{g}_r, r = 1, \ldots, k1-1, k1+1, \ldots, K_r$. The problem is converted to prove $\mathbf{g}_{k1}$ could be either greater or smaller than $\mathbf{e}_{k1}$. Assume optimal eEPLE is obtained at $\eta_{\mathrm{e}} = \eta_0$, corresponding to $t_{\mathrm{e},r} = t_0$. Apply Taylor series expansion for $\mathbf{g}_r$ near $t_{g,k1} = t_0 \pm \Delta t$ as

$$\begin{aligned}\mathbf{g}_{\upsilon_{k1}} \approx & \mathbf{e}_{\upsilon_{k1}} + \left.\frac{\partial \mathbf{g}_{\upsilon_{k1}}}{\partial t_{g,k1}}\right|_{t_{g,k1}=t_0\pm\Delta t} \\ = & \mathbf{e}_{\upsilon_{k1}} \pm \boldsymbol{\phi}_{\upsilon_{k1}}\left(\widetilde{\mathbf{PL}}_{\upsilon_{k1}} \odot \left[t_0^{\mathbf{PL}_{\upsilon_{k1},1}-1}, \ldots, t_0^{\mathbf{PL}_{\upsilon_{k1},K_1}-1}\right]\right)^{\mathrm{T}}\Delta t \end{aligned} \tag{C.3}$$

Through modifying the value of Δt, the partial estimation error $\mathbf{g}_{\upsilon_{k1}}$ could be located at any position surround $\mathbf{e}_{\upsilon_{k1}}$. As a result, $\mathbf{E}_{\mathrm{g}}$ could reach any position near $\mathbf{E}_{\mathrm{e}}$, including the points with the shorter distances to real location of MS than $\mathbf{E}_{\mathrm{e}}$.

Lemma 3 is proved.

Appendix D

Derivation of Fisher Information Matrices of Position-Related Channel Parameters

The derivative function of the received signal $\mathbf{Y}(t)$ in (5.14) over the interested parameters, besides $\frac{\partial \mathbf{y}(t)}{\partial \theta_l}$ in (5.14), are calculated as the following equations

$$\frac{\partial \mathbf{y}(t)}{\partial \phi_l} = \begin{cases} \alpha_l \beta_l \grave{\mathbf{a}}_{\mathrm{R},l} \mathbf{a}_{\mathrm{T},l}^{\mathrm{H}} \mathbf{F}_{\mathrm{B}} \mathbf{x}(t-\tau_l), & l \in \Lambda_{\mathrm{s}} \text{ or } l = 1 \\ \alpha_l \beta_l e^{j\psi_l} \mathbf{a}_{\mathrm{bw},l}^{\mathrm{H}} \mathbf{a}_{\mathrm{fw},l} \grave{\mathbf{a}}_{\mathrm{R},l} \mathbf{a}_{\mathrm{T},l}^{\mathrm{H}} \mathbf{F}_{\mathrm{B}} \mathbf{x}(t-\tau_l), & l \in \Lambda_{\mathrm{R}} \end{cases} \tag{D.1a}$$

$$\frac{\partial \mathbf{y}(t)}{\partial \nu_{\mathrm{bw},l}} = \begin{cases} 0, & l \in \Lambda_{\mathrm{s}} \text{ or } l = 1 \\ \alpha_l e^{j\psi_l} (\dot{\beta}_{l,\mathrm{R}} \mathbf{a}_{\mathrm{bw},l}^{\mathrm{H}} \mathbf{a}_{\mathrm{fw},l} + \beta_l \dot{\mathbf{a}}_{\mathrm{bw},l}^{\mathrm{H}} \mathbf{a}_{\mathrm{fw},l}) \mathbf{a}_{\mathrm{R},l} \mathbf{a}_{\mathrm{T},l}^{\mathrm{H}} \mathbf{F}_{\mathrm{B}} \mathbf{x}(t-\tau_l), & l \in \Lambda_{\mathrm{R}} \end{cases} \tag{D.1b}$$

$$\frac{\partial \mathbf{y}(t)}{\partial \mu_{\mathrm{bw},l}} = \begin{cases} 0, & l \in \Lambda_{\mathrm{s}} \text{ or } l = 1 \\ \alpha_l e^{j\psi_l} (\grave{\beta}_{l,\mathrm{R}} \mathbf{a}_{\mathrm{bw},l}^{\mathrm{H}} \mathbf{a}_{\mathrm{fw},l} + \beta_l \grave{\mathbf{a}}_{\mathrm{bw},l}^{\mathrm{H}} \mathbf{a}_{\mathrm{fw},l}) \mathbf{a}_{\mathrm{R},l} \mathbf{a}_{\mathrm{T},l}^{\mathrm{H}} \mathbf{F}_{\mathrm{B}} \mathbf{x}(t-\tau_l), & l \in \Lambda_{\mathrm{R}} \end{cases} \tag{D.1c}$$

$$\frac{\partial \mathbf{y}(t)}{\partial \nu_{\mathrm{fw},l}} = \begin{cases} 0, & l \in \Lambda_{\mathrm{s}} \text{ or } l = 1 \\ \alpha_l e^{j\psi_l} (\dot{\beta}_{l,\mathrm{T}} \mathbf{a}_{\mathrm{bw},l}^{\mathrm{H}} \mathbf{a}_{\mathrm{fw},l} + \beta_l \dot{\mathbf{a}}_{\mathrm{bw},l}^{\mathrm{H}} \mathbf{a}_{\mathrm{fw},l}) \mathbf{a}_{\mathrm{R},l} \mathbf{a}_{\mathrm{T},l}^{\mathrm{H}} \mathbf{F}_{\mathrm{B}} \mathbf{x}(t-\tau_l), & l \in \Lambda_{\mathrm{R}} \end{cases} \tag{D.1d}$$

$$\frac{\partial \mathbf{y}(t)}{\partial \mu_{\mathrm{fw},l}} = \begin{cases} 0, & l \in \Lambda_{\mathrm{s}} \text{ or } l = 1 \\ \alpha_l e^{j\psi_l}(\dot{\beta}_{l,\mathrm{T}} \mathbf{a}_{\mathrm{bw},l}^{\mathrm{H}} \mathbf{a}_{\mathrm{fw},l} + \beta_l \dot{\mathbf{a}}_{\mathrm{bw},l}^{\mathrm{H}} \mathbf{a}_{\mathrm{fw},l}) \mathbf{a}_{\mathrm{R},l} \mathbf{a}_{\mathrm{T},l}^{\mathrm{H}} \mathbf{F}_{\mathrm{B}} \mathbf{x}(t-\tau_l), & l \in \Lambda_{\mathrm{R}} \end{cases} \tag{D.1e}$$

$$\frac{\partial \mathbf{y}(t)}{\partial \vartheta_l} = \begin{cases} \alpha_l \beta_l \mathbf{a}_{\mathrm{R},l} \dot{\mathbf{a}}_{\mathrm{T},l}^{\mathrm{H}} \mathbf{F}_{\mathrm{B}} \mathbf{x}(t-\tau_l), & l \in \Lambda_{\mathrm{s}} \text{ or } l = 1 \\ \alpha_l \beta_l e^{j\psi_l} \mathbf{a}_{\mathrm{bw},l}^{\mathrm{H}} \mathbf{a}_{\mathrm{fw},l} \mathbf{a}_{\mathrm{R},l} \dot{\mathbf{a}}_{\mathrm{T},l}^{\mathrm{H}} \mathbf{F}_{\mathrm{B}} \mathbf{x}(t-\tau_l), & l \in \Lambda_{\mathrm{R}} \end{cases} \tag{D.1f}$$

$$\frac{\partial \mathbf{y}(t)}{\partial \varphi_l} = \begin{cases} \alpha_l \beta_l \mathbf{a}_{\mathrm{R},l} \grave{\mathbf{a}}_{\mathrm{T},l}^{\mathrm{H}} \mathbf{F}_{\mathrm{B}} \mathbf{x}(t-\tau_l), & l \in \Lambda_{\mathrm{s}} \text{ or } l = 1 \\ \alpha_l \beta_l e^{j\psi_l} \mathbf{a}_{\mathrm{bw},l}^{\mathrm{H}} \mathbf{a}_{\mathrm{fw},l} \mathbf{a}_{\mathrm{R},l} \grave{\mathbf{a}}_{\mathrm{T},l}^{\mathrm{H}} \mathbf{F}_{\mathrm{B}} \mathbf{x}(t-\tau_l), & l \in \Lambda_{\mathrm{R}} \end{cases} \tag{D.1g}$$

$$\frac{\partial \mathbf{y}(t)}{\partial \tau_l} = \begin{cases} (-j2\pi f) \alpha_l \beta_l \mathbf{a}_{\mathrm{R},l} \mathbf{a}_{\mathrm{T},l}^{\mathrm{H}} \mathbf{F}_{\mathrm{B}} \mathbf{x}(t-\tau_l), & l \in \Lambda_{\mathrm{s}} \text{ or } l = 1 \\ (-j2\pi f) \alpha_l \beta_l e^{j\psi_l} \mathbf{a}_{\mathrm{bw},l}^{\mathrm{H}} \mathbf{a}_{\mathrm{fw},l} \mathbf{a}_{\mathrm{R},l} \mathbf{a}_{\mathrm{T},l}^{\mathrm{H}} \mathbf{F}_{\mathrm{B}} \mathbf{x}(t-\tau_l), & l \in \Lambda_{\mathrm{R}} \end{cases} \tag{D.1h}$$

$$\frac{\partial \mathbf{y}(t)}{\partial \beta_{\Re,l}} = \begin{cases} \alpha_l \mathbf{a}_{\mathrm{R},l} \mathbf{a}_{\mathrm{T},l}^{\mathrm{H}} \mathbf{F}_{\mathrm{B}} \mathbf{x}(t-\tau_l), & l \in \Lambda_{\mathrm{s}} \text{ or } l = 1 \\ \alpha_l e^{j\psi_l} \mathbf{a}_{\mathrm{bw},l}^{\mathrm{H}} \mathbf{a}_{\mathrm{fw},l} \mathbf{a}_{\mathrm{R},l} \mathbf{a}_{\mathrm{T},l}^{\mathrm{H}} \mathbf{F}_{\mathrm{B}} \mathbf{x}(t-\tau_l), & l \in \Lambda_{\mathrm{R}} \end{cases} \tag{D.1i}$$

$$\frac{\partial \mathbf{y}(t)}{\partial \beta_{\Im,l}} = \begin{cases} \alpha_l j \mathbf{a}_{\mathrm{R},l} \mathbf{a}_{\mathrm{T},l}^{\mathrm{H}} \mathbf{F}_{\mathrm{B}} \mathbf{x}(t-\tau_l), & l \in \Lambda_{\mathrm{s}} \text{ or } l = 1 \\ \alpha_l e^{j\psi_l} j \mathbf{a}_{\mathrm{bw},l}^{\mathrm{H}} \mathbf{a}_{\mathrm{fw},l} \mathbf{a}_{\mathrm{R},l} \mathbf{a}_{\mathrm{T},l}^{\mathrm{H}} \mathbf{F}_{\mathrm{B}} \mathbf{x}(t-\tau_l), & l \in \Lambda_{\mathrm{R}} \end{cases} \tag{D.1j}$$

$$\frac{\partial \mathbf{y}(t)}{\partial \tilde{\psi}_l} = \begin{cases} 0, & l \in \Lambda_{\mathrm{s}} \text{ or } l = 1 \\ \alpha_l j e^{j\tilde{\psi}_l} \beta_l \mathbf{a}_{\mathrm{R},l} \mathbf{a}_{\mathrm{T},l}^{\mathrm{H}} \mathbf{F}_{\mathrm{B}} \mathbf{x}(t-\tau_l), & l \in \Lambda_{\mathrm{R}} \end{cases} \tag{D.1k}$$

where the derivative equations are calculated as $\dot{\mathbf{a}}_{\mathrm{R},l} = \frac{\partial \mathbf{a}_{\mathrm{R},l}}{\partial \theta_l}$, $\grave{\mathbf{a}}_{\mathrm{R},l} = \frac{\mathbf{a}_{\mathrm{R},l}}{\partial \phi_l}$, $\dot{\mathbf{a}}_{\mathrm{T},l} = \frac{\partial \mathbf{a}_{\mathrm{T},l}}{\partial \vartheta_l}$, $\grave{\mathbf{a}}_{\mathrm{T},l} = \frac{\mathbf{a}_{\mathrm{T},l}}{\partial \varphi_l}$, $\dot{\beta}_{l,\mathrm{R}} = \frac{\partial \beta_l}{\partial \nu_{\mathrm{bw},l}}$, $\dot{\beta}_{l,\mathrm{R}} = \frac{\partial \beta_l}{\partial \mu_{\mathrm{bw},l}}$, $\dot{\beta}_{l,\mathrm{T}} = \frac{\partial \beta_l}{\partial \nu_{\mathrm{fw},l}}$, $\dot{\beta}_{l,\mathrm{T}} = \frac{\partial \beta_l}{\partial \mu_{\mathrm{fw},l}}$. All the elements of FIM in (5.19) are calculated as

$$\mathbf{J}_{\boldsymbol{\theta\theta}} = \Re\{(\dot{\mathbf{A}}_{\mathrm{R}}^{\mathrm{H}} \dot{\mathbf{A}}_{\mathrm{R}}) \odot \mathbf{P} \odot (\mathbf{b}_{\beta}^{\mathrm{H}} \mathbf{A}_{\mathrm{I}}^{\mathrm{H}} \mathbf{A}_{\mathrm{I}} \mathbf{b}_{\beta}) \odot (\mathbf{A}_{\mathrm{T}}^{\mathrm{H}} \mathbf{F}_{\mathrm{B}} \mathbf{F}_{\mathrm{B}}^{\mathrm{H}} \mathbf{A}_{\mathrm{T}}) \odot \mathbf{B}_1\} \tag{D.2a}$$

$$\mathbf{J}_{\boldsymbol{\phi\phi}} = \Re\{(\grave{\mathbf{A}}_{\mathrm{R}}^{\mathrm{H}} \grave{\mathbf{A}}_{\mathrm{R}}) \odot \mathbf{P} \odot (\mathbf{b}_{\beta}^{\mathrm{H}} \mathbf{A}_{\mathrm{I}}^{\mathrm{H}} \mathbf{A}_{\mathrm{I}} \mathbf{b}_{\beta}) \odot (\mathbf{A}_{\mathrm{T}}^{\mathrm{H}} \mathbf{F}_{\mathrm{B}} \mathbf{F}_{\mathrm{B}}^{\mathrm{H}} \mathbf{A}_{\mathrm{T}}) \odot \mathbf{B}_1\} \tag{D.2b}$$

$$\mathbf{J}_{\boldsymbol{\nu}_2\boldsymbol{\nu}_2} = \Re\{(\mathbf{A}_{\mathrm{R}}^{\mathrm{H}} \mathbf{A}_{\mathrm{R}}) \odot \mathbf{P} \odot [(\dot{\mathbf{A}}_{\mathrm{I},2} \mathbf{b}_{\beta} + \mathbf{A}_{\mathrm{I}} \dot{\mathbf{b}}_{\beta,2})^{\mathrm{H}} (\dot{\mathbf{A}}_{\mathrm{I},2} \mathbf{b}_{\beta} + \mathbf{A}_{\mathrm{I}} \dot{\mathbf{b}}_{\beta,2})] \odot (\mathbf{A}_{\mathrm{T}}^{\mathrm{H}} \mathbf{F}_{\mathrm{B}} \mathbf{F}_{\mathrm{B}}^{\mathrm{H}} \mathbf{A}_{\mathrm{T}}) \odot \mathbf{B}_1\} \tag{D.2c}$$

$$\mathbf{J}_{\boldsymbol{\mu}_2\boldsymbol{\mu}_2} = \Re\{(\mathbf{A}_{\mathrm{R}}^{\mathrm{H}} \mathbf{A}_{\mathrm{R}}) \odot \mathbf{P} \odot [(\grave{\mathbf{A}}_{\mathrm{I},2} \mathbf{b}_{\beta} + \mathbf{A}_{\mathrm{I}} \grave{\mathbf{b}}_{\beta,2})^{\mathrm{H}} (\grave{\mathbf{A}}_{\mathrm{I},2} \mathbf{b}_{\beta} + \mathbf{A}_{\mathrm{I}} \grave{\mathbf{b}}_{\beta,2})] \odot (\mathbf{A}_{\mathrm{T}}^{\mathrm{H}} \mathbf{F}_{\mathrm{B}} \mathbf{F}_{\mathrm{B}}^{\mathrm{H}} \mathbf{A}_{\mathrm{T}}) \odot \mathbf{B}_1\} \tag{D.2d}$$

$$\mathbf{J}_{\boldsymbol{\nu}_1\boldsymbol{\nu}_1} = \Re\{(\mathbf{A}_{\mathrm{R}}^{\mathrm{H}} \mathbf{A}_{\mathrm{R}}) \odot \mathbf{P} \odot [(\dot{\mathbf{A}}_{\mathrm{I},1} \mathbf{b}_{\beta} + \mathbf{A}_{\mathrm{I}} \dot{\mathbf{b}}_{\beta,1})^{\mathrm{H}} (\dot{\mathbf{A}}_{\mathrm{I},1} \mathbf{b}_{\beta} + \mathbf{A}_{\mathrm{I}} \dot{\mathbf{b}}_{\beta,1})] \odot (\mathbf{A}_{\mathrm{T}} \mathbf{F}_{\mathrm{B}} \mathbf{F}_{\mathrm{B}}^{\mathrm{H}} \mathbf{A}_{\mathrm{T}}) \odot \mathbf{B}_1\} \tag{D.2e}$$

$$\mathbf{J}_{\boldsymbol{\mu}_1\boldsymbol{\mu}_1} = \Re\{(\mathbf{A}_{\mathrm{R}}^{\mathrm{H}}\mathbf{A}_{\mathrm{R}}) \odot \mathbf{P} \odot [(\grave{\mathbf{A}}_{\mathrm{I},1}\mathbf{b}_\beta + \mathbf{A}_{\mathrm{I}}\grave{\mathbf{b}}_{\beta,1})^{\mathrm{H}}(\grave{\mathbf{A}}_{\mathrm{I},1}\mathbf{b}_\beta + \mathbf{A}_{\mathrm{I}}\grave{\mathbf{b}}_{\beta,1})] \odot (\mathbf{A}_{\mathrm{T}}^{\mathrm{H}}\mathbf{F}_{\mathrm{B}}\mathbf{F}_{\mathrm{B}}^{\mathrm{H}}\mathbf{A}_{\mathrm{T}}) \odot \mathbf{B}_1\} \tag{D.2f}$$

$$\mathbf{J}_{\boldsymbol{\vartheta}\boldsymbol{\vartheta}} = \Re\{(\mathbf{A}_{\mathrm{R}}^{\mathrm{H}}\mathbf{A}_{\mathrm{R}}) \odot \mathbf{P} \odot (\mathbf{b}_\beta^{\mathrm{H}}\mathbf{A}_{\mathrm{I}}^{\mathrm{H}}\mathbf{A}_{\mathrm{I}}\mathbf{b}_\beta) \odot (\dot{\mathbf{A}}_{\mathrm{T}}^{\mathrm{H}}\mathbf{F}_{\mathrm{B}}\mathbf{F}_{\mathrm{B}}^{\mathrm{H}}\dot{\mathbf{A}}_{\mathrm{T}}) \odot \mathbf{B}_1\} \tag{D.2g}$$

$$\mathbf{J}_{\boldsymbol{\varphi}\boldsymbol{\varphi}} = \Re\{(\mathbf{A}_{\mathrm{R}}^{\mathrm{H}}\mathbf{A}_{\mathrm{R}}) \odot \mathbf{P} \odot (\mathbf{b}_\beta^{\mathrm{H}}\mathbf{A}_{\mathrm{I}}^{\mathrm{H}}\mathbf{A}_{\mathrm{I}}\mathbf{b}_\beta) \odot (\grave{\mathbf{A}}_{\mathrm{T}}^{\mathrm{H}}\mathbf{F}_{\mathrm{B}}\mathbf{F}_{\mathrm{B}}^{\mathrm{H}}\grave{\mathbf{A}}_{\mathrm{T}}) \odot \mathbf{B}_1\} \tag{D.2h}$$

$$\mathbf{J}_{\boldsymbol{\tau}\boldsymbol{\tau}} = \Re\{(\mathbf{A}_{\mathrm{R}}^{\mathrm{H}}\mathbf{A}_{\mathrm{R}}) \odot \mathbf{P} \odot (\mathbf{b}_\beta^{\mathrm{H}}\mathbf{A}_{\mathrm{I}}^{\mathrm{H}}\mathbf{A}_{\mathrm{I}}\mathbf{b}_\beta) \odot (\mathbf{A}_{\mathrm{T}}^{\mathrm{H}}\mathbf{F}_{\mathrm{B}}\mathbf{F}_{\mathrm{B}}^{\mathrm{H}}\mathbf{A}_{\mathrm{T}}) \odot \mathbf{B}_3\} \tag{D.2i}$$

$$\mathbf{J}_{\boldsymbol{\beta}_{\Re}\boldsymbol{\beta}_{\Re}} = \mathbf{J}_{\boldsymbol{\beta}_{\Im}\boldsymbol{\beta}_{\Im}} = \Re\{(\mathbf{A}_{\mathrm{R}}^{\mathrm{H}}\mathbf{A}_{\mathrm{R}}) \odot \mathbf{P} \odot (\mathbf{A}_{\mathrm{I}}^{\mathrm{H}}\mathbf{A}_{\mathrm{I}}) \odot (\mathbf{A}_{\mathrm{T}}^{\mathrm{H}}\mathbf{F}_{\mathrm{B}}\mathbf{F}_{\mathrm{B}}^{\mathrm{H}}\mathbf{A}_{\mathrm{T}}) \odot \mathbf{B}_1\} \tag{D.2j}$$

$$\mathbf{J}_{\tilde{\boldsymbol{\psi}}\tilde{\boldsymbol{\psi}}} = \Re\{[\mathbf{b}_{\beta,2}^{\mathrm{H}}\mathbf{A}_{\mathrm{R}}^{\mathrm{H}}\mathbf{A}_{\mathrm{R}}\mathbf{b}_{\beta,2}] \odot \ddot{\mathbf{P}} \odot (\mathbf{b}_\beta^{\mathrm{H}}\mathbf{A}_{\mathrm{I}}^{\mathrm{H}}\mathbf{A}_{\mathrm{I}}\mathbf{b}_\beta) \odot (\mathbf{A}_{\mathrm{T}}^{\mathrm{H}}\mathbf{F}_{\mathrm{B}}\mathbf{F}_{\mathrm{B}}^{\mathrm{H}}\mathbf{A}_{\mathrm{T}}) \odot \mathbf{B}_1\} \tag{D.2k}$$

$$\mathbf{J}_{\boldsymbol{\theta}\boldsymbol{\phi}} = \Re\{(\dot{\mathbf{A}}_{\mathrm{R}}^{\mathrm{H}}\grave{\mathbf{A}}_{\mathrm{R}}) \odot \mathbf{P} \odot (\mathbf{b}_\beta^{\mathrm{H}}\mathbf{A}_{\mathrm{I}}^{\mathrm{H}}\mathbf{A}_{\mathrm{I}}\mathbf{b}_\beta) \odot (\mathbf{A}_{\mathrm{T}}^{\mathrm{H}}\mathbf{F}_{\mathrm{B}}\mathbf{F}_{\mathrm{B}}^{\mathrm{H}}\mathbf{A}_{\mathrm{T}}) \odot \mathbf{B}_1\} \tag{D.2l}$$

$$\mathbf{J}_{\boldsymbol{\theta}\boldsymbol{\vartheta}} = \Re\{(\dot{\mathbf{A}}_{\mathrm{R}}^{\mathrm{H}}\mathbf{A}_{\mathrm{R}}) \odot \mathbf{P} \odot (\mathbf{b}_\beta^{\mathrm{H}}\mathbf{A}_{\mathrm{I}}^{\mathrm{H}}\mathbf{A}_{\mathrm{I}}\mathbf{b}_\beta) \odot (\dot{\mathbf{A}}_{\mathrm{T}}^{\mathrm{H}}\mathbf{F}_{\mathrm{B}}\mathbf{F}_{\mathrm{B}}^{\mathrm{H}}\mathbf{A}_{\mathrm{T}}) \odot \mathbf{B}_1\} \tag{D.2m}$$

$$\mathbf{J}_{\boldsymbol{\theta}\boldsymbol{\nu}_2} = \Re\{(\dot{\mathbf{A}}_{\mathrm{R}}^{\mathrm{H}}\mathbf{A}_{\mathrm{R}}) \odot \mathbf{P} \odot [(\mathbf{A}_{\mathrm{I}}\mathbf{b}_\beta)^{\mathrm{H}}(\dot{\mathbf{A}}_{\mathrm{I},2}\mathbf{b}_\beta + \mathbf{A}_{\mathrm{I}}\dot{\mathbf{b}}_{\beta,2})] \odot (\mathbf{A}_{\mathrm{T}}^{\mathrm{H}}\mathbf{F}_{\mathrm{B}}\mathbf{F}_{\mathrm{B}}^{\mathrm{H}}\mathbf{A}_{\mathrm{T}}) \odot \mathbf{B}_1\} \tag{D.2n}$$

$$\mathbf{J}_{\boldsymbol{\theta}\boldsymbol{\mu}_2} = \Re\{(\dot{\mathbf{A}}_{\mathrm{R}}^{\mathrm{H}}\mathbf{A}_{\mathrm{R}}) \odot \mathbf{P} \odot [(\mathbf{A}_{\mathrm{I}}\mathbf{b}_\beta)^{\mathrm{H}}(\grave{\mathbf{A}}_{\mathrm{I},2}\mathbf{b}_\beta + \mathbf{A}_{\mathrm{I}}\grave{\mathbf{b}}_{\beta,2})] \odot (\mathbf{A}_{\mathrm{T}}^{\mathrm{H}}\mathbf{F}_{\mathrm{B}}\mathbf{F}_{\mathrm{B}}^{\mathrm{H}}\mathbf{A}_{\mathrm{T}}) \odot \mathbf{B}_1\} \tag{D.2o}$$

$$\mathbf{J}_{\boldsymbol{\theta}\boldsymbol{\nu}_1} = \Re\{(\dot{\mathbf{A}}_{\mathrm{R}}^{\mathrm{H}}\mathbf{A}_{\mathrm{R}}) \odot \mathbf{P} \odot [(\mathbf{A}_{\mathrm{I}}\mathbf{b}_\beta)^{\mathrm{H}}(\dot{\mathbf{A}}_{\mathrm{I},1}\mathbf{b}_\beta + \mathbf{A}_{\mathrm{I}}\dot{\mathbf{b}}_{\beta,1})] \odot (\mathbf{A}_{\mathrm{T}}^{\mathrm{H}}\mathbf{F}_{\mathrm{B}}\mathbf{F}_{\mathrm{B}}^{\mathrm{H}}\mathbf{A}_{\mathrm{T}}) \odot \mathbf{B}_1\} \tag{D.2p}$$

$$\mathbf{J}_{\boldsymbol{\theta}\boldsymbol{\mu}_1} = \Re\{(\dot{\mathbf{A}}_{\mathrm{R}}^{\mathrm{H}}\mathbf{A}_{\mathrm{R}}) \odot \mathbf{P} \odot [(\mathbf{A}_{\mathrm{I}}\mathbf{b}_\beta)^{\mathrm{H}}(\grave{\mathbf{A}}_{\mathrm{I},1}\mathbf{b}_\beta + \mathbf{A}_{\mathrm{I}}\grave{\mathbf{b}}_{\beta,1})] \odot (\mathbf{A}_{\mathrm{T}}^{\mathrm{H}}\mathbf{F}_{\mathrm{B}}\mathbf{F}_{\mathrm{B}}^{\mathrm{H}}\mathbf{A}_{\mathrm{T}}) \odot \mathbf{B}_1\} \tag{D.2q}$$

$$\mathbf{J}_{\boldsymbol{\theta}\boldsymbol{\varphi}} = \Re\{(\dot{\mathbf{A}}_{\mathrm{R}}^{\mathrm{H}}\mathbf{A}_{\mathrm{R}}) \odot \mathbf{P} \odot (\mathbf{b}_\beta^{\mathrm{H}}\mathbf{A}_{\mathrm{I}}^{\mathrm{H}}\mathbf{A}_{\mathrm{I}}\mathbf{b}_\beta) \odot (\grave{\mathbf{A}}_{\mathrm{T}}^{\mathrm{H}}\mathbf{F}_{\mathrm{B}}\mathbf{F}_{\mathrm{B}}^{\mathrm{H}}\mathbf{A}_{\mathrm{T}}) \odot \mathbf{B}_1\} \tag{D.2r}$$

$$\mathbf{J}_{\boldsymbol{\theta}\boldsymbol{\tau}} = \Re\{(\dot{\mathbf{A}}_{\mathrm{R}}^{\mathrm{H}}\mathbf{A}_{\mathrm{R}}) \odot \mathbf{P} \odot (\mathbf{b}_\beta^{\mathrm{H}}\mathbf{A}_{\mathrm{I}}^{\mathrm{H}}\mathbf{A}_{\mathrm{I}}\mathbf{b}_\beta) \odot (\mathbf{A}_{\mathrm{T}}^{\mathrm{H}}\mathbf{F}_{\mathrm{B}}\mathbf{F}_{\mathrm{B}}^{\mathrm{H}}\mathbf{A}_{\mathrm{T}}) \odot (-\mathbf{B}_2)\} \tag{D.2s}$$

$$\mathbf{J}_{\boldsymbol{\theta}\boldsymbol{\beta}_{\Re}} = \Re\{(\dot{\mathbf{A}}_{\mathrm{R}}^{\mathrm{H}}\mathbf{A}_{\mathrm{R}}) \odot \mathbf{P} \odot (\mathbf{b}_\beta^{\mathrm{H}}\mathbf{A}_{\mathrm{I}}^{\mathrm{H}}\mathbf{A}_{\mathrm{I}}) \odot (\mathbf{A}_{\mathrm{T}}^{\mathrm{H}}\mathbf{F}_{\mathrm{B}}\mathbf{F}_{\mathrm{B}}^{\mathrm{H}}\mathbf{A}_{\mathrm{T}}) \odot \mathbf{B}_1\} \tag{D.2t}$$

$$\mathbf{J}_{\boldsymbol{\theta}\boldsymbol{\beta}_{\Im}} = \Re\{j(\dot{\mathbf{A}}_{\mathrm{R}}^{\mathrm{H}}\mathbf{A}_{\mathrm{R}}) \odot \mathbf{P} \odot (\mathbf{b}_\beta^{\mathrm{H}}\mathbf{A}_{\mathrm{I}}^{\mathrm{H}}\mathbf{A}_{\mathrm{I}}) \odot (\mathbf{A}_{\mathrm{T}}^{\mathrm{H}}\mathbf{F}_{\mathrm{B}}\mathbf{F}_{\mathrm{B}}^{\mathrm{H}}\mathbf{A}_{\mathrm{T}}) \odot \mathbf{B}_1\} \tag{D.2u}$$

$$\mathbf{J}_{\boldsymbol{\theta}\tilde{\boldsymbol{\psi}}} = \Re\{(\dot{\mathbf{A}}_{\mathrm{R}}^{\mathrm{H}}\mathbf{A}_{\mathrm{R}}) \odot \dot{\mathbf{P}} \odot (\mathbf{b}_\beta^{\mathrm{H}}\mathbf{A}_{\mathrm{I}}^{\mathrm{H}}\mathbf{A}_{\mathrm{I}}\mathbf{b}_\beta) \odot (\mathbf{A}_{\mathrm{T}}^{\mathrm{H}}\mathbf{F}_{\mathrm{B}}\mathbf{F}_{\mathrm{B}}^{\mathrm{H}}\mathbf{A}_{\mathrm{T}}) \odot \mathbf{B}_1\} \tag{D.2v}$$

$$\mathbf{J}_{\boldsymbol{\phi}\boldsymbol{\nu}_2} = \Re\{(\grave{\mathbf{A}}_{\mathrm{R}}^{\mathrm{H}}\mathbf{A}_{\mathrm{R}}) \odot \mathbf{P} \odot [(\mathbf{A}_{\mathrm{I}}\mathbf{b}_\beta)^{\mathrm{H}}(\dot{\mathbf{A}}_{\mathrm{I},2}\mathbf{b}_\beta + \mathbf{A}_{\mathrm{I}}\dot{\mathbf{b}}_{\beta,2})] \odot (\mathbf{A}_{\mathrm{T}}^{\mathrm{H}}\mathbf{F}_{\mathrm{B}}\mathbf{F}_{\mathrm{B}}^{\mathrm{H}}\mathbf{A}_{\mathrm{T}}) \odot \mathbf{B}_1\} \tag{D.2w}$$

$$\mathbf{J}_{\boldsymbol{\phi}\boldsymbol{\mu}_2} = \Re\{(\grave{\mathbf{A}}_{\mathrm{R}}^{\mathrm{H}}\mathbf{A}_{\mathrm{R}}) \odot \mathbf{P} \odot [(\mathbf{A}_{\mathrm{I}}\mathbf{b}_\beta)^{\mathrm{H}}(\grave{\mathbf{A}}_{\mathrm{I},2}\mathbf{b}_\beta + \mathbf{A}_{\mathrm{I}}\grave{\mathbf{b}}_{\beta,2})] \odot (\mathbf{A}_{\mathrm{T}}^{\mathrm{H}}\mathbf{F}_{\mathrm{B}}\mathbf{F}_{\mathrm{B}}^{\mathrm{H}}\mathbf{A}_{\mathrm{T}}) \odot \mathbf{B}_1\} \tag{D.2x}$$

$$\mathbf{J}_{\boldsymbol{\phi}\boldsymbol{\nu}_1} = \Re\{(\grave{\mathbf{A}}_{\mathrm{R}}^{\mathrm{H}}\mathbf{A}_{\mathrm{R}}) \odot \mathbf{P} \odot [(\mathbf{A}_{\mathrm{I}}\mathbf{b}_\beta)^{\mathrm{H}}(\dot{\mathbf{A}}_{\mathrm{I},1}\mathbf{b}_\beta + \mathbf{A}_{\mathrm{I}}\dot{\mathbf{b}}_{\beta,1})] \odot (\mathbf{A}_{\mathrm{T}}^{\mathrm{H}}\mathbf{F}_{\mathrm{B}}\mathbf{F}_{\mathrm{B}}^{\mathrm{H}}\mathbf{A}_{\mathrm{T}}) \odot \mathbf{B}_1\} \tag{D.2y}$$

$$\mathbf{J}_{\boldsymbol{\phi}\boldsymbol{\mu}_1} = \Re\{(\grave{\mathbf{A}}_{\mathrm{R}}^{\mathrm{H}}\mathbf{A}_{\mathrm{R}}) \odot \mathbf{P} \odot [(\mathbf{A}_{\mathrm{I}}\mathbf{b}_\beta)^{\mathrm{H}}(\grave{\mathbf{A}}_{\mathrm{I},1}\mathbf{b}_\beta + \mathbf{A}_{\mathrm{I}}\grave{\mathbf{b}}_{\beta,1})] \odot (\mathbf{A}_{\mathrm{T}}^{\mathrm{H}}\mathbf{F}_{\mathrm{B}}\mathbf{F}_{\mathrm{B}}^{\mathrm{H}}\mathbf{A}_{\mathrm{T}}) \odot \mathbf{B}_1\} \tag{D.2z}$$

$$\mathbf{J}_{\boldsymbol{\phi}\boldsymbol{\vartheta}} = \Re\{(\grave{\mathbf{A}}_{\mathrm{R}}^{\mathrm{H}}\mathbf{A}_{\mathrm{R}}) \odot \mathbf{P} \odot (\mathbf{b}_\beta^{\mathrm{H}}\mathbf{A}_{\mathrm{I}}^{\mathrm{H}}\mathbf{A}_{\mathrm{I}}\mathbf{b}_\beta) \odot (\dot{\mathbf{A}}_{\mathrm{T}}^{\mathrm{H}}\mathbf{F}_{\mathrm{B}}\mathbf{F}_{\mathrm{B}}^{\mathrm{H}}\mathbf{A}_{\mathrm{T}}) \odot \mathbf{B}_1\} \tag{D.2aa}$$

$$\mathbf{J}_{\boldsymbol{\phi}\boldsymbol{\varphi}} = \Re\{(\grave{\mathbf{A}}_{\mathrm{R}}^{\mathrm{H}}\mathbf{A}_{\mathrm{R}}) \odot \mathbf{P} \odot (\mathbf{b}_\beta^{\mathrm{H}}\mathbf{A}_{\mathrm{I}}^{\mathrm{H}}\mathbf{A}_{\mathrm{I}}\mathbf{b}_\beta) \odot (\grave{\mathbf{A}}_{\mathrm{T}}^{\mathrm{H}}\mathbf{F}_{\mathrm{B}}\mathbf{F}_{\mathrm{B}}^{\mathrm{H}}\mathbf{A}_{\mathrm{T}}) \odot \mathbf{B}_1\} \tag{D.2ab}$$

$$\mathbf{J}_{\boldsymbol{\phi}\boldsymbol{\tau}} = \Re\{(\grave{\mathbf{A}}_{\mathrm{R}}^{\mathrm{H}}\mathbf{A}_{\mathrm{R}}) \odot \mathbf{P} \odot (\mathbf{b}_\beta^{\mathrm{H}}\mathbf{A}_{\mathrm{I}}^{\mathrm{H}}\mathbf{A}_{\mathrm{I}}\mathbf{b}_\beta) \odot (\mathbf{A}_{\mathrm{T}}^{\mathrm{H}}\mathbf{F}_{\mathrm{B}}\mathbf{F}_{\mathrm{B}}^{\mathrm{H}}\mathbf{A}_{\mathrm{T}}) \odot (-\mathbf{B}_2)\} \tag{D.2ac}$$

$$\mathbf{J}_{\boldsymbol{\phi}\boldsymbol{\beta}_{\Re}} = \Re\{(\grave{\mathbf{A}}_{\mathrm{R}}^{\mathrm{H}}\mathbf{A}_{\mathrm{R}}) \odot \mathbf{P} \odot (\mathbf{b}_\beta^{\mathrm{H}}\mathbf{A}_{\mathrm{I}}^{\mathrm{H}}\mathbf{A}_{\mathrm{I}}) \odot (\mathbf{A}_{\mathrm{T}}^{\mathrm{H}}\mathbf{F}_{\mathrm{B}}\mathbf{F}_{\mathrm{B}}^{\mathrm{H}}\mathbf{A}_{\mathrm{T}}) \odot \mathbf{B}_1\} \tag{D.2ad}$$

$$\mathbf{J}_{\boldsymbol{\phi}\boldsymbol{\beta}_{\Im}} = \Re\{j(\grave{\mathbf{A}}_{\mathrm{R}}^{\mathrm{H}}\mathbf{A}_{\mathrm{R}}) \odot \mathbf{P} \odot (\mathbf{b}_{\beta}^{\mathrm{H}}\mathbf{A}_{\mathrm{I}}^{\mathrm{H}}\mathbf{A}_{\mathrm{I}}) \odot (\mathbf{A}_{\mathrm{T}}^{\mathrm{H}}\mathbf{F}_{\mathrm{B}}\mathbf{F}_{\mathrm{B}}^{\mathrm{H}}\mathbf{A}_{\mathrm{T}}) \odot \mathbf{B}_1\} \tag{D.2ae}$$

$$\mathbf{J}_{\tilde{\boldsymbol{\phi}}\tilde{\boldsymbol{\psi}}} = \Re\{(\grave{\mathbf{A}}_{\mathrm{R}}^{\mathrm{H}}\mathbf{A}_{\mathrm{R}}) \odot \ddot{\mathbf{P}} \odot (\mathbf{b}_{\beta}^{\mathrm{H}}\mathbf{A}_{\mathrm{I}}^{\mathrm{H}}\mathbf{A}_{\mathrm{I}}\mathbf{b}_{\beta}) \odot (\mathbf{A}_{\mathrm{T}}^{\mathrm{H}}\mathbf{F}_{\mathrm{B}}\mathbf{F}_{\mathrm{B}}^{\mathrm{H}}\mathbf{A}_{\mathrm{T}}) \odot \mathbf{B}_1\} \tag{D.2af}$$

$$\mathbf{J}_{\boldsymbol{\nu}_2\boldsymbol{\mu}_2} = \Re\{(\mathbf{A}_{\mathrm{R}}^{\mathrm{H}}\mathbf{A}_{\mathrm{R}}) \odot \mathbf{P} \odot [(\dot{\mathbf{A}}_{\mathrm{I},2}\mathbf{b}_{\beta} + \mathbf{A}_{\mathrm{I}}\dot{\mathbf{b}}_{\beta,2})^{\mathrm{H}}(\grave{\mathbf{A}}_{\mathrm{I},2}\mathbf{b}_{\beta} + \mathbf{A}_{\mathrm{I}}\grave{\mathbf{b}}_{\beta,2})] \odot (\mathbf{A}_{\mathrm{T}}^{\mathrm{H}}\mathbf{F}_{\mathrm{B}}\mathbf{F}_{\mathrm{B}}^{\mathrm{H}}\mathbf{A}_{\mathrm{T}}) \odot \mathbf{B}_1\} \tag{D.2ag}$$

$$\mathbf{J}_{\boldsymbol{\nu}_2\boldsymbol{\nu}_1} = \Re\{(\mathbf{A}_{\mathrm{R}}^{\mathrm{H}}\mathbf{A}_{\mathrm{R}}) \odot \mathbf{P} \odot [(\dot{\mathbf{A}}_{\mathrm{I},2}\mathbf{b}_{\beta} + \mathbf{A}_{\mathrm{I}}\dot{\mathbf{b}}_{\beta,2})^{\mathrm{H}}(\dot{\mathbf{A}}_{\mathrm{I},1}\mathbf{b}_{\beta} + \mathbf{A}_{\mathrm{I}}\dot{\mathbf{b}}_{\beta,1})] \odot (\mathbf{A}_{\mathrm{T}}^{\mathrm{H}}\mathbf{F}_{\mathrm{B}}\mathbf{F}_{\mathrm{B}}^{\mathrm{H}}\mathbf{A}_{\mathrm{T}}) \odot \mathbf{B}_1\} \tag{D.2ah}$$

$$\mathbf{J}_{\boldsymbol{\nu}_2\boldsymbol{\mu}_1} = \Re\{(\mathbf{A}_{\mathrm{R}}^{\mathrm{H}}\mathbf{A}_{\mathrm{R}}) \odot \mathbf{P} \odot [(\dot{\mathbf{A}}_{\mathrm{I},2}\mathbf{b}_{\beta} + \mathbf{A}_{\mathrm{I}}\dot{\mathbf{b}}_{\beta,2})^{\mathrm{H}}(\grave{\mathbf{A}}_{\mathrm{I},1}\mathbf{b}_{\beta} + \mathbf{A}_{\mathrm{I}}\grave{\mathbf{b}}_{\beta,1})] \odot (\mathbf{A}_{\mathrm{T}}^{\mathrm{H}}\mathbf{F}_{\mathrm{B}}\mathbf{F}_{\mathrm{B}}^{\mathrm{H}}\mathbf{A}_{\mathrm{T}}) \odot \mathbf{B}_1\} \tag{D.2ai}$$

$$\mathbf{J}_{\boldsymbol{\vartheta}\boldsymbol{\varphi}} = \Re\{(\mathbf{A}_{\mathrm{R}}^{\mathrm{H}}\mathbf{A}_{\mathrm{R}}) \odot \mathbf{P} \odot (\mathbf{b}_{\beta}^{\mathrm{H}}\mathbf{A}_{\mathrm{I}}^{\mathrm{H}}\mathbf{A}_{\mathrm{I}}\mathbf{b}_{\beta}) \odot (\grave{\mathbf{A}}_{\mathrm{T}}^{\mathrm{H}}\mathbf{F}_{\mathrm{B}}\mathbf{F}_{\mathrm{B}}^{\mathrm{H}}\dot{\mathbf{A}}_{\mathrm{T}}) \odot \mathbf{B}_1\} \tag{D.2aj}$$

$$\mathbf{J}_{\boldsymbol{\vartheta}\boldsymbol{\tau}} = \Re\{(\mathbf{A}_{\mathrm{R}}^{\mathrm{H}}\mathbf{A}_{\mathrm{R}}) \odot \mathbf{P} \odot (\mathbf{b}_{\beta}^{\mathrm{H}}\mathbf{A}_{\mathrm{I}}^{\mathrm{H}}\mathbf{A}_{\mathrm{I}}\mathbf{b}_{\beta}) \odot (\mathbf{A}_{\mathrm{T}}^{\mathrm{H}}\mathbf{F}_{\mathrm{B}}\mathbf{F}_{\mathrm{B}}^{\mathrm{H}}\dot{\mathbf{A}}_{\mathrm{T}}) \odot (-\mathbf{B}_2)\} \tag{D.2ak}$$

$$\mathbf{J}_{\boldsymbol{\vartheta}\boldsymbol{\beta}_{\Re}} = \Re\{(\mathbf{A}_{\mathrm{R}}^{\mathrm{H}}\mathbf{A}_{\mathrm{R}}) \odot \mathbf{P} \odot (\mathbf{b}_{\beta}^{\mathrm{H}}\mathbf{A}_{\mathrm{I}}^{\mathrm{H}}\mathbf{A}_{\mathrm{I}}) \odot (\mathbf{A}_{\mathrm{T}}^{\mathrm{H}}\mathbf{F}_{\mathrm{B}}\mathbf{F}_{\mathrm{B}}^{\mathrm{H}}\dot{\mathbf{A}}_{\mathrm{T}}) \odot \mathbf{B}_1\} \tag{D.2al}$$

$$\mathbf{J}_{\boldsymbol{\vartheta}\boldsymbol{\beta}_{\Im}} = \Re\{j(\mathbf{A}_{\mathrm{R}}^{\mathrm{H}}\mathbf{A}_{\mathrm{R}}) \odot \mathbf{P} \odot (\mathbf{b}_{\beta}^{\mathrm{H}}\mathbf{A}_{\mathrm{I}}^{\mathrm{H}}\mathbf{A}_{\mathrm{I}}) \odot (\mathbf{A}_{\mathrm{T}}^{\mathrm{H}}\mathbf{F}_{\mathrm{B}}\mathbf{F}_{\mathrm{B}}^{\mathrm{H}}\dot{\mathbf{A}}_{\mathrm{T}}) \odot \mathbf{B}_1\} \tag{D.2am}$$

$$\mathbf{J}_{\boldsymbol{\vartheta}\tilde{\boldsymbol{\psi}}} = \Re\{(\mathbf{A}_{\mathrm{R}}^{\mathrm{H}}\mathbf{A}_{\mathrm{R}}) \odot \dot{\mathbf{P}} \odot (\mathbf{b}_{\beta}^{\mathrm{H}}\mathbf{A}_{\mathrm{I}}^{\mathrm{H}}\mathbf{A}_{\mathrm{I}}\mathbf{b}_{\beta}) \odot (\mathbf{A}_{\mathrm{T}}^{\mathrm{H}}\mathbf{F}_{\mathrm{B}}\mathbf{F}_{\mathrm{B}}^{\mathrm{H}}\dot{\mathbf{A}}_{\mathrm{T}}) \odot \mathbf{B}_1\} \tag{D.2an}$$

$$\mathbf{J}_{\boldsymbol{\varphi}\boldsymbol{\tau}} = \Re\{(\mathbf{A}_{\mathrm{R}}^{\mathrm{H}}\mathbf{A}_{\mathrm{R}}) \odot \mathbf{P} \odot (\mathbf{b}_{\beta}^{\mathrm{H}}\mathbf{A}_{\mathrm{I}}^{\mathrm{H}}\mathbf{A}_{\mathrm{I}}\mathbf{b}_{\beta}) \odot (\mathbf{A}_{\mathrm{T}}^{\mathrm{H}}\mathbf{F}_{\mathrm{B}}\mathbf{F}_{\mathrm{B}}^{\mathrm{H}}\grave{\mathbf{A}}_{\mathrm{T}}) \odot (-\mathbf{B}_2)\} \tag{D.2ao}$$

$$\mathbf{J}_{\boldsymbol{\varphi}\boldsymbol{\beta}_{\Re}} = \Re\{(\mathbf{A}_{\mathrm{R}}^{\mathrm{H}}\mathbf{A}_{\mathrm{R}}) \odot \mathbf{P} \odot (\mathbf{b}_{\beta}^{\mathrm{H}}\mathbf{A}_{\mathrm{I}}^{\mathrm{H}}\mathbf{A}_{\mathrm{I}}) \odot (\mathbf{A}_{\mathrm{T}}^{\mathrm{H}}\mathbf{F}_{\mathrm{B}}\mathbf{F}_{\mathrm{B}}^{\mathrm{H}}\grave{\mathbf{A}}_{\mathrm{T}}) \odot \mathbf{B}_1\} \tag{D.2ap}$$

$$\mathbf{J}_{\boldsymbol{\varphi}\boldsymbol{\beta}_{\Im}} = \Re\{j(\mathbf{A}_{\mathrm{R}}^{\mathrm{H}}\mathbf{A}_{\mathrm{R}}) \odot \mathbf{P} \odot (\mathbf{b}_{\beta}^{\mathrm{H}}\mathbf{A}_{\mathrm{I}}^{\mathrm{H}}\mathbf{A}_{\mathrm{I}}) \odot (\mathbf{A}_{\mathrm{T}}^{\mathrm{H}}\mathbf{F}_{\mathrm{B}}\mathbf{F}_{\mathrm{B}}^{\mathrm{H}}\grave{\mathbf{A}}_{\mathrm{T}}) \odot \mathbf{B}_1\} \tag{D.2aq}$$

$$\mathbf{J}_{\boldsymbol{\tau}\boldsymbol{\beta}_{\Re}} = \Re\{(\mathbf{A}_{\mathrm{R}}^{\mathrm{H}}\mathbf{A}_{\mathrm{R}}) \odot \mathbf{P} \odot (\mathbf{b}_{\beta}^{\mathrm{H}}\mathbf{A}_{\mathrm{I}}^{\mathrm{H}}\mathbf{A}_{\mathrm{I}}) \odot (\mathbf{A}_{\mathrm{T}}^{\mathrm{H}}\mathbf{F}_{\mathrm{B}}\mathbf{F}_{\mathrm{B}}^{\mathrm{H}}\mathbf{A}_{\mathrm{T}}) \odot (-\mathbf{B}_2)\} \tag{D.2ar}$$

$$\mathbf{J}_{\boldsymbol{\tau}\boldsymbol{\beta}_{\Im}} = \Re\{j(\mathbf{A}_{\mathrm{R}}^{\mathrm{H}}\mathbf{A}_{\mathrm{R}}) \odot \mathbf{P} \odot (\mathbf{b}_{\beta}^{\mathrm{H}}\mathbf{A}_{\mathrm{I}}^{\mathrm{H}}\mathbf{A}_{\mathrm{I}}) \odot (\mathbf{A}_{\mathrm{T}}^{\mathrm{H}}\mathbf{F}_{\mathrm{B}}\mathbf{F}_{\mathrm{B}}^{\mathrm{H}}\mathbf{A}_{\mathrm{T}}) \odot (-\mathbf{B}_2)\} \tag{D.2as}$$

$$\mathbf{J}_{\boldsymbol{\tau}\boldsymbol{\psi}} = \Re\{(\mathbf{A}_{\mathrm{R}}^{\mathrm{H}}\mathbf{A}_{\mathrm{R}}) \odot \dot{\mathbf{P}} \odot (\mathbf{b}_{\beta}^{\mathrm{H}}\mathbf{A}_{\mathrm{I}}^{\mathrm{H}}\mathbf{A}_{\mathrm{I}}\mathbf{b}_{\beta}) \odot (\mathbf{A}_{\mathrm{T}}^{\mathrm{H}}\mathbf{F}_{\mathrm{B}}\mathbf{F}_{\mathrm{B}}^{\mathrm{H}}\mathbf{A}_{\mathrm{T}}) \odot (-\mathbf{B}_2)\} \tag{D.2at}$$

$$\mathbf{J}_{\boldsymbol{\beta}_{\Re}\boldsymbol{\beta}_{\Im}} = \Re\{j(\mathbf{A}_{\mathrm{R}}^{\mathrm{H}}\mathbf{A}_{\mathrm{R}}) \odot \mathbf{P} \odot (\mathbf{A}_{\mathrm{I}}^{\mathrm{H}}\mathbf{A}_{\mathrm{I}}) \odot (\mathbf{A}_{\mathrm{T}}^{\mathrm{H}}\mathbf{F}_{\mathrm{B}}\mathbf{F}_{\mathrm{B}}^{\mathrm{H}}\mathbf{A}_{\mathrm{T}}) \odot \mathbf{B}_1\} \tag{D.2au}$$

$$\mathbf{J}_{\boldsymbol{\beta}_{\Re}\tilde{\boldsymbol{\psi}}} = \Re\{(\mathbf{A}_{\mathrm{R}}^{\mathrm{H}}\mathbf{A}_{\mathrm{R}}) \odot \dot{\mathbf{P}} \odot (\mathbf{A}_{\mathrm{I}}^{\mathrm{H}}\mathbf{A}_{\mathrm{I}}\mathbf{b}_{\beta}) \odot (\mathbf{A}_{\mathrm{T}}^{\mathrm{H}}\mathbf{F}_{\mathrm{B}}\mathbf{F}_{\mathrm{B}}^{\mathrm{H}}\mathbf{A}_{\mathrm{T}}) \odot \mathbf{B}_1\} \tag{D.2av}$$

$$\mathbf{J}_{\boldsymbol{\beta}_{\Im}\tilde{\boldsymbol{\psi}}} = \Re\{-j(\mathbf{A}_{\mathrm{R}}^{\mathrm{H}}\mathbf{A}_{\mathrm{R}}) \odot \dot{\mathbf{P}} \odot (\mathbf{A}_{\mathrm{I}}^{\mathrm{H}}\mathbf{A}_{\mathrm{I}}\mathbf{b}_{\beta}) \odot (\mathbf{A}_{\mathrm{T}}^{\mathrm{H}}\mathbf{F}_{\mathrm{B}}\mathbf{F}_{\mathrm{B}}^{\mathrm{H}}\mathbf{A}_{\mathrm{T}}) \odot \mathbf{B}_1\} \tag{D.2aw}$$

where $\mathbf{P}$ is the matrix of phase shift of all paths, and

$$\mathbf{P} = \begin{bmatrix} \mathbf{1}_{1+C}\mathbf{1}_{1+C}^{\mathrm{T}} & \mathbf{1}_{1+C}\boldsymbol{\Psi}_{\mathrm{R}} \\ \boldsymbol{\Psi}_{\mathrm{R}}^{\mathrm{H}}\mathbf{1}_{1+C}^{\mathrm{T}} & {}^{2}\boldsymbol{\Psi}_{\mathrm{R}}^{\mathrm{H}}\boldsymbol{\Psi}_{\mathrm{R}} \end{bmatrix} \tag{D.3}$$

The derivative functions $\dot{\mathbf{A}}_{\mathrm{R}}$, $\grave{\mathbf{A}}_{\mathrm{R}}$, $\dot{\mathbf{A}}_{\mathrm{T}}$, $\grave{\mathbf{A}}_{\mathrm{T}}$, $\dot{\mathbf{b}}_{\beta,1}$,$\grave{\mathbf{b}}_{\beta,1}$,$\dot{\mathbf{b}}_{\beta,2}$,$\grave{\mathbf{b}}_{\beta,2}$, $\dot{\mathbf{P}}$, $\ddot{\mathbf{P}}$ in (5.17) are calculated as

$$\dot{\mathbf{A}}_{\mathrm{R}} = \frac{\partial \mathbf{A}_{\mathrm{R}}}{\partial \boldsymbol{\theta}} = \left[\dot{\mathbf{a}}_{\mathrm{R},1}, \ldots, \dot{\mathbf{a}}_{\mathrm{R},L}\right], \dot{\mathbf{a}}_{\mathrm{R},l} = \frac{\partial(\boldsymbol{\chi}_{\mathrm{R}}\mathbf{k}(\theta_l, \phi_l))}{\partial \theta_l} \odot \mathbf{a}_{\mathrm{R},l} \tag{D.4a}$$

$$\grave{\mathbf{A}}_{\mathrm{R}} = \frac{\partial \mathbf{A}_{\mathrm{R}}}{\partial \boldsymbol{\phi}} = \left[\grave{\mathbf{a}}_{\mathrm{R},1}, \ldots, \grave{\mathbf{a}}_{\mathrm{R},L}\right], \grave{\mathbf{a}}_{\mathrm{R},l} = \frac{\partial(\boldsymbol{\chi}_{\mathrm{R}}\mathbf{k}(\theta_l, \phi_l))}{\partial \phi_l} \odot \mathbf{a}_{\mathrm{R},l} \tag{D.4b}$$

$$\dot{\mathbf{A}}_{\mathrm{T}} = \frac{\partial \mathbf{A}_{\mathrm{T}}}{\partial \boldsymbol{\vartheta}} = \left[\dot{\mathbf{a}}_{\mathrm{T},1}, \ldots, \dot{\mathbf{a}}_{\mathrm{T},L}\right], \dot{\mathbf{a}}_{\mathrm{T},l} = \frac{\partial(\boldsymbol{\chi}_{\mathrm{T}}\mathbf{k}(\vartheta_l, \varphi_l))}{\partial \vartheta_l} \odot \mathbf{a}_{\mathrm{T},l} \tag{D.4c}$$

$$\grave{\mathbf{A}}_{\mathrm{T}} = \frac{\partial \mathbf{A}_{\mathrm{T}}}{\partial \boldsymbol{\varphi}} = \left[\grave{\mathbf{a}}_{\mathrm{T},1}, \ldots, \grave{\mathbf{a}}_{\mathrm{T},L}\right], \grave{\mathbf{a}}_{\mathrm{T},l} = \frac{\partial(\boldsymbol{\chi}_{\mathrm{T}}\mathbf{k}(\vartheta_l, \varphi_l))}{\partial \varphi_l} \odot \mathbf{a}_{\mathrm{T},l} \tag{D.4d}$$

$$\begin{aligned}\dot{\mathbf{b}}_{\beta,1} = \frac{\partial \mathbf{b}_\beta}{\partial \boldsymbol{\nu}_1} = diag\left\{\mathbf{0}_{1+C}^{\mathrm{T}}, \dot{b}_{\beta,\mathrm{T},1}, \ldots, \dot{b}_{\beta,\mathrm{T},N_{\mathrm{IS}}}\right\}, \dot{b}_{\beta,\mathrm{T},p} = \tilde{\rho}_{\mathrm{bw},p}\frac{\partial \rho_{\mathrm{fw},p}}{\partial \nu_{\mathrm{fw},p}},\\ \frac{\partial \rho_{\mathrm{fw},p}}{\partial \nu_{\mathrm{fw},p}} = \frac{q_0\sqrt{a_{\mathrm{eff}}}(\mathbf{k}^{\mathrm{T}}(\nu_{\mathrm{fw},p}, \mu_{\mathrm{fw},p})\hat{\mathbf{n}}_{\mathrm{I}})^{q_0-1}}{\sqrt{4\pi}r_{\mathrm{fw},p}}(\mathbf{k}^{\mathrm{T}}(\nu_{\mathrm{fw},p} + \pi/2, \mu_{\mathrm{fw},p})\hat{\mathbf{n}}_{\mathrm{I}})\end{aligned} \tag{D.4e}$$

$$\begin{aligned}\grave{\mathbf{b}}_{\beta,1} = \frac{\partial \mathbf{b}_\beta}{\partial \boldsymbol{\mu}_1} = diag\left\{\mathbf{0}_{1+C}^{\mathrm{T}}, \grave{b}_{\beta,\mathrm{T},1}, \ldots, \grave{b}_{\beta,\mathrm{T},N_{\mathrm{IS}}}\right\}, \grave{b}_{\beta,\mathrm{T},p} = \tilde{\rho}_{\mathrm{bw},p}\frac{\partial \rho_{\mathrm{fw},p}}{\partial \mu_{\mathrm{fw},p}},\\ \frac{\partial \rho_{\mathrm{fw},p}}{\partial \mu_{\mathrm{fw},p}} = \frac{q_0\sqrt{a_{\mathrm{eff}}}(\mathbf{k}^{\mathrm{T}}(\nu_{\mathrm{fw},p}, \mu_{\mathrm{fw},p})\hat{\mathbf{n}}_{\mathrm{I}})^{q_0-1}}{\sqrt{4\pi}r_{\mathrm{fw},p}}(\mathbf{k}^{\mathrm{T}}(\nu_{\mathrm{fw},p}, \mu_{\mathrm{fw},p} + \pi/2)\hat{\mathbf{n}}_{\mathrm{I}})\end{aligned} \tag{D.4f}$$

$$\begin{aligned}\dot{\mathbf{b}}_{\beta,2} = \frac{\partial \mathbf{b}_\beta}{\partial \boldsymbol{\nu}_2} = diag\left\{\mathbf{0}_{1+C}^{\mathrm{T}}, \dot{b}_{\beta,\mathrm{R},1}, \ldots, \dot{b}_{\beta,\mathrm{R},N_{\mathrm{IS}}}\right\}, \dot{b}_{\beta,\mathrm{R},p} = \frac{\partial \tilde{\rho}_{\mathrm{bw},p}}{\partial \nu_{\mathrm{bw},p}}\rho_{\mathrm{fw},p}\\ \frac{\partial \tilde{\rho}_{\mathrm{bw},p}}{\partial \nu_{\mathrm{bw},p}} = \frac{q_0\sqrt{a_{\mathrm{eff}}}(\mathbf{k}^{\mathrm{T}}(\nu_{\mathrm{bw},p}, \mu_{\mathrm{bw},p})\hat{\mathbf{n}}_{\mathrm{I}})^{q_0-1}}{\sqrt{4\pi}r_{\mathrm{bw},p}}(\mathbf{k}^{\mathrm{T}}(\nu_{\mathrm{bw},p} + \pi/2, \mu_{\mathrm{bw},p})\hat{\mathbf{n}}_{\mathrm{I}})e^{j\zeta_p}\end{aligned} \tag{D.4g}$$

$$\begin{aligned}\grave{\mathbf{b}}_{\beta,2} = \frac{\partial \mathbf{b}_\beta}{\partial \boldsymbol{\mu}_2} = diag\left\{\mathbf{0}_{1+C}^{\mathrm{T}}, \grave{b}_{\beta,\mathrm{R},1}, \ldots, \grave{b}_{\beta,\mathrm{R},N_{\mathrm{IS}}}\right\}, \grave{b}_{\beta,\mathrm{R},p} = \frac{\partial \tilde{\rho}_{\mathrm{bw},p}}{\partial \mu_{\mathrm{bw},p}}\rho_{\mathrm{fw},p}\\ \frac{\partial \tilde{\rho}_{\mathrm{bw},p}}{\partial \mu_{\mathrm{bw},p}} = \frac{q_0\sqrt{a_{\mathrm{eff}}}(\mathbf{k}^{\mathrm{T}}(\nu_{\mathrm{bw},p}, \mu_{\mathrm{bw},p})\hat{\mathbf{n}}_{\mathrm{I}})^{q_0-1}}{\sqrt{4\pi}r_{\mathrm{bw},p}}(\mathbf{k}^{\mathrm{T}}(\nu_{\mathrm{bw},p}, \mu_{\mathrm{bw},p} + \pi/2)\hat{\mathbf{n}}_{\mathrm{I}})e^{j\zeta_p}\end{aligned} \tag{D.4h}$$

$$\dot{\mathbf{P}} = \begin{bmatrix}\mathbf{1}_{1+C}\mathbf{1}_{1+C}^{\mathrm{T}} & \mathbf{1}_{1+C}\mathbf{1}_{N_{\mathrm{IS}}}^{\mathrm{T}}\\ \mathbf{1}_{N_{\mathrm{IS}}}\mathbf{1}_{1+C}^{\mathrm{T}} & \boldsymbol{\Psi}_{\mathrm{R}}^{\mathrm{H}}\dot{\boldsymbol{\Psi}}_{\mathrm{R}}\end{bmatrix}, \dot{\boldsymbol{\Psi}}_{\mathrm{R}} = [je^{j\tilde{\psi}_1}, \ldots, je^{j\tilde{\psi}_{N_{\mathrm{IS}}}}] \tag{D.4i}$$

$$\ddot{\mathbf{P}} = \begin{bmatrix}\mathbf{1}_{1+C}\mathbf{1}_{1+C}^{\mathrm{T}} & \mathbf{1}_{1+C}\mathbf{1}_{N_{\mathrm{IS}}}^{\mathrm{T}}\\ \mathbf{1}_{N_{\mathrm{IS}}}\mathbf{1}_{1+C}^{\mathrm{T}} & \dot{\boldsymbol{\Psi}}_{\mathrm{R}}^{\mathrm{H}}\dot{\boldsymbol{\Psi}}_{\mathrm{R}}\end{bmatrix} \tag{D.4j}$$

$$\dot{\mathbf{A}}_{\mathrm{I},1} = \frac{\partial \mathbf{A}_{\mathrm{I}}}{\partial \boldsymbol{\nu}_{\mathrm{fw}}} = \left[\mathbf{0}_{1+C}^{\mathrm{T}}, a_{\mathrm{bw},1}^{\mathrm{H}} \frac{\partial a_{\mathrm{fw},1}}{\partial \nu_{\mathrm{fw},1}}, \ldots, a_{\mathrm{bw},N_{\mathrm{IS}}}^{\mathrm{H}} \frac{\partial a_{\mathrm{fw},N_{\mathrm{IS}}}}{\partial \nu_{\mathrm{fw},N_{\mathrm{IS}}}}\right], \tag{D.4k}$$
$$a_{\mathrm{bw},p}^{\mathrm{H}} \frac{\partial a_{\mathrm{fw},p}}{\partial \nu_{\mathrm{fw},p}} = e^{j2\pi \boldsymbol{\chi}_{\mathrm{I},p}(\mathbf{k}(\nu_{\mathrm{bw},p},\mu_{\mathrm{bw},p}) - \mathbf{k}(\nu_{\mathrm{fw},p},\mu_{\mathrm{fw},p}))}(-j2\pi \boldsymbol{\chi}_{\mathrm{I},p} \mathbf{k}(\nu_{\mathrm{fw},p}, \mu_{\mathrm{fw},p} + \pi/2))$$

$$\grave{\mathbf{A}}_{\mathrm{I},1} = \frac{\partial \mathbf{A}_{\mathrm{I}}}{\partial \boldsymbol{\mu}_{\mathrm{fw}}} = \left[\mathbf{0}_{1+C}^{\mathrm{T}}, a_{\mathrm{bw},1}^{\mathrm{H}} \frac{\partial a_{\mathrm{fw},1}}{\partial \mu_{\mathrm{fw},1}}, \ldots, a_{\mathrm{bw},N_{\mathrm{IS}}}^{\mathrm{H}} \frac{\partial a_{\mathrm{fw},N_{\mathrm{IS}}}}{\partial \mu_{\mathrm{fw},N_{\mathrm{IS}}}}\right], \tag{D.4l}$$
$$a_{\mathrm{bw},p}^{\mathrm{H}} \frac{\partial a_{\mathrm{fw},p}}{\partial \mu_{\mathrm{fw},p}} = e^{j2\pi \boldsymbol{\chi}_{\mathrm{I},p}(\mathbf{k}(\nu_{\mathrm{bw},p},\mu_{\mathrm{bw},p}) - \mathbf{k}(\nu_{\mathrm{fw},p},\mu_{\mathrm{fw},p}))}(-j2\pi \boldsymbol{\chi}_{\mathrm{I},p} \mathbf{k}(\nu_{\mathrm{fw},p} + \pi/2, \mu_{\mathrm{fw},p}))$$

$$\dot{\mathbf{A}}_{\mathrm{I},2} = \frac{\partial \mathbf{A}_{\mathrm{I}}}{\partial \boldsymbol{\nu}_{\mathrm{bw}}} = \left[\mathbf{0}_{1+C}^{\mathrm{T}}, \frac{\partial a_{\mathrm{bw},1}^{\mathrm{H}}}{\partial \nu_{\mathrm{bw},1}} a_{\mathrm{fw},1}, \ldots, \frac{\partial a_{\mathrm{bw},N_{\mathrm{IS}}}^{\mathrm{H}}}{\partial \nu_{\mathrm{bw},N_{\mathrm{IS}}}} a_{\mathrm{fw},N_{\mathrm{IS}}}\right], \tag{D.4m}$$
$$\frac{\partial a_{\mathrm{bw},p}^{\mathrm{H}}}{\partial \nu_{\mathrm{bw},p}} a_{\mathrm{fw},p} = e^{j2\pi \boldsymbol{\chi}_{\mathrm{I},p}(\mathbf{k}(\nu_{\mathrm{bw},p},\mu_{\mathrm{bw},p}) - \mathbf{k}(\nu_{\mathrm{fw},p},\mu_{\mathrm{fw},p}))}(j2\pi \boldsymbol{\chi}_{\mathrm{I},p} \mathbf{k}(\nu_{\mathrm{bw},p}, \mu_{\mathrm{bw},p} + \pi/2))$$

$$\grave{\mathbf{A}}_{\mathrm{I},2} = \frac{\partial \mathbf{A}_{\mathrm{I}}}{\partial \boldsymbol{\mu}_{\mathrm{bw}}} = \left[\mathbf{0}_{1+C}^{\mathrm{T}}, \frac{\partial a_{\mathrm{bw},1}^{\mathrm{H}}}{\partial \mu_{\mathrm{bw},1}} a_{\mathrm{fw},1}, \ldots, \frac{\partial a_{\mathrm{bw},N_{\mathrm{IS}}}^{\mathrm{H}}}{\partial \mu_{\mathrm{bw},N_{\mathrm{IS}}}} a_{\mathrm{fw},N_{\mathrm{IS}}}\right], \tag{D.4n}$$
$$\frac{\partial a_{\mathrm{bw},p}^{\mathrm{H}}}{\partial \mu_{\mathrm{bw},p}} a_{\mathrm{fw},p} = e^{j2\pi \boldsymbol{\chi}_{\mathrm{I},p}(\mathbf{k}(\nu_{\mathrm{bw},p},\mu_{\mathrm{bw},p}) - \mathbf{k}(\nu_{\mathrm{fw},p},\mu_{\mathrm{fw},p}))}(j2\pi \boldsymbol{\chi}_{\mathrm{I},p} \mathbf{k}(\nu_{\mathrm{bw},p} + \pi/2, \mu_{\mathrm{bw},p}))$$

The amplitudes and phase of derivative functions in (5.26)-(5.29) are defined as $C_{\mathrm{fe},p} = c_{\mathrm{fe},p}\rho_{\mathrm{bw},p}\rho_{\mathrm{fw},p}, C_{\mathrm{fa},p} = c_{\mathrm{fa},p}\rho_{\mathrm{bw},p}\rho_{\mathrm{fw},p}, C_{\mathrm{be},p} = c_{\mathrm{be},p}\rho_{\mathrm{bw},p}\rho_{\mathrm{fw},p}, C_{\mathrm{ba},P} = c_{\mathrm{ba},p}\rho_{\mathrm{bw},p}\rho_{\mathrm{fw},p}$ and $E_{\mathrm{fe},p} = e^{j\theta_{\mathrm{fw},p}} e^{j\zeta_p} a_{\mathrm{bw},p}^{\mathrm{H}} a_{\mathrm{fw},p}, E_{\mathrm{fa},p} = e^{j\phi_{\mathrm{fw},p}} e^{j\zeta_p} a_{\mathrm{bw},p}^{\mathrm{H}} a_{\mathrm{fw},p}, E_{\mathrm{be},p} = e^{j\theta_{\mathrm{bw},p}} e^{j\zeta_p} a_{\mathrm{bw},p}^{\mathrm{H}} a_{\mathrm{fw},p}, E_{\mathrm{ba},p} =$

$e^{j\phi_{\mathrm{bw},p}}e^{j\zeta_p}a_{\mathrm{bw},p}^{\mathrm{H}}a_{\mathrm{fw},p}$, where

$$c_{\mathrm{fe},p} = \sqrt{\cot^2(\nu_{\mathrm{fw},p}) + \left(\frac{2\pi}{\lambda}\boldsymbol{\chi}_{\mathrm{I},p}\dot{\mathbf{k}}(\nu_{\mathrm{fw},p},\mu_{\mathrm{fw},p})\right)^2} \tag{D.5a}$$

$$c_{\mathrm{fa},p} = \sqrt{\cot^2(\mu_{\mathrm{fw},p}) + \left(\frac{2\pi}{\lambda}\boldsymbol{\chi}_{\mathrm{I},p}\grave{\mathbf{k}}(\nu_{\mathrm{fw},p},\mu_{\mathrm{fw},p})\right)^2} \tag{D.5b}$$

$$c_{\mathrm{be},p} = \sqrt{\cot^2(\nu_{\mathrm{bw},p}) + \left(\frac{2\pi}{\lambda}\boldsymbol{\chi}_{\mathrm{I},p}\dot{\mathbf{k}}(\nu_{\mathrm{bw},p},\mu_{\mathrm{bw},p})\right)^2} \tag{D.5c}$$

$$c_{\mathrm{ba},p} = \sqrt{\cot^2(\mu_{\mathrm{bw},p}) + \left(\frac{2\pi}{\lambda}\boldsymbol{\chi}_{\mathrm{I},p}\grave{\mathbf{k}}(\nu_{\mathrm{bw},p},\mu_{\mathrm{bw},p})\right)^2} \tag{D.5d}$$

$$\theta_{\mathrm{fw},p} = \arcsin(\frac{2\pi}{\lambda c_{\mathrm{fe},p}}\boldsymbol{\chi}_{\mathrm{I},p}\dot{\mathbf{k}}(\nu_{\mathrm{fw},p},\mu_{\mathrm{fw},p})) \tag{D.5e}$$

$$\phi_{\mathrm{fw},p} = \arcsin(\frac{2\pi}{\lambda c_{\mathrm{fa},p}}\boldsymbol{\chi}_{\mathrm{I},p}\grave{\mathbf{k}}(\nu_{\mathrm{fw},p},\mu_{\mathrm{fw},p})) \tag{D.5f}$$

$$\theta_{\mathrm{bw},p} = \arcsin(\frac{2\pi}{\lambda c_{\mathrm{be},p}}\boldsymbol{\chi}_{\mathrm{I},p}\dot{\mathbf{k}}(\nu_{\mathrm{bw},p},\mu_{\mathrm{bw},p})) \tag{D.5g}$$

$$\phi_{\mathrm{bw},p} = \arcsin(\frac{2\pi}{\lambda c_{\mathrm{ba},p}}\boldsymbol{\chi}_{\mathrm{I},p}\grave{\mathbf{k}}(\nu_{\mathrm{bw},p},\mu_{\mathrm{bw},p})) \tag{D.5h}$$

The convolution between the beamspace signals is calculated as $\mathbf{x}(t-\tau_l)\mathbf{x}^{\mathrm{H}}(t-\tau_l) = N_{\mathrm{B}}P_{\mathbf{s}}\mathbf{I}_{N_{\mathrm{B}}}$, where $P_{\mathrm{s}}(f)$ is the power spectral density of baseband signal $\mathbf{s}(f)$. Therefore, according to Parsevar's theorm, the discrete convolution of $\mathbf{x}(t-\tau_l)$ and $\mathbf{x}^{\mathrm{H}}(t-\tau_l)$, the 1st derivative function and 2nd derivatives are respectively calculated as

$$\mathbf{B}_1 = \sum_{l=1}^{L}\mathbf{x}(t-\tau_l)\mathbf{x}^{\mathrm{H}}(t-\tau_l) = \sum_{\iota=1}^{U}|P_{\mathrm{s}}(f_\iota)|^2\boldsymbol{\alpha}_\tau^{\mathrm{T}}\boldsymbol{\alpha}_\tau \mathrm{d}f_\iota \tag{D.6}$$

$$\mathbf{B}_2 = \sum_{l=1}^{L}\frac{\partial\mathbf{x}(t-\tau_l)}{\partial\tau_l}\mathbf{x}^{\mathrm{H}}(t-\tau_l) = \sum_{\iota=1}^{U}2j\pi f_\iota|P_{\mathrm{s}}(f_\iota)|^2\boldsymbol{\alpha}_\tau^{\mathrm{T}}\boldsymbol{\alpha}_\tau \mathrm{d}f_\iota \tag{D.7}$$

$$\mathbf{B}_3 = \sum_{l=1}^{L}\frac{\partial\mathbf{x}(t-\tau_l)}{\partial\tau_l}\frac{\partial\mathbf{x}^{\mathrm{H}}(t-\tau_l)}{\partial\tau_l} = \sum_{\iota=1}^{U}(2\pi f_\iota)^2|P_{\mathrm{s}}(f_\iota)|^2\boldsymbol{\alpha}_\tau^{\mathrm{T}}\boldsymbol{\alpha}_\tau \mathrm{d}f_\iota \tag{D.8}$$

Appendix E

Derivation of the Transition Matrix from Channel Parameters to Mobile Station Location Information

The transition matrix $\bigtriangledown_{\boldsymbol{\omega}_2}(\boldsymbol{\omega}_1)$ in (5.21) and (5.24) is expressed as (E.1). The basic rotation matrix employed by this research is in the format of the following equation

$$\mathbf{R}(\mathbf{o}_{\mathrm{MS}}) = \begin{bmatrix} \mathbf{R}_{1,\mathrm{MS}} \\ \hdashline \mathbf{R}_{2,\mathrm{MS}} \\ \hdashline \mathbf{R}_{3,\mathrm{MS}} \end{bmatrix} = \begin{bmatrix} \cos(\phi_{\mathrm{MS}}) & -\sin(\phi_{\mathrm{MS}})\cos(\theta_{\mathrm{MS}}) & -\sin(\phi_{\mathrm{MS}})\sin(\theta_{\mathrm{MS}}) \\ \hdashline \sin(\phi_{\mathrm{MS}}) & \cos(\phi_{\mathrm{MS}})\cos(\theta_{\mathrm{MS}}) & \cos(\phi_{\mathrm{MS}})\sin(\theta_{\mathrm{MS}}) \\ \hdashline 0 & -\sin(\theta_{\mathrm{MS}}) & \cos(\theta_{\mathrm{MS}}) \end{bmatrix}$$

$$(\bigtriangledown_{\boldsymbol{\omega}_2}(\boldsymbol{\omega}_1))^{\mathrm{T}} = \left(\frac{\partial \boldsymbol{\omega}_1}{\partial \boldsymbol{\omega}_2^{\mathrm{T}}}\right) =$$

$$\begin{bmatrix} \left(\frac{\partial \boldsymbol{\theta}^{\mathrm{T}}}{\partial \mathbf{o}_{\mathrm{MS}}}\right) & \left(\frac{\partial \boldsymbol{\phi}^{\mathrm{T}}}{\partial \mathbf{o}_{\mathrm{MS}}}\right) & \left(\frac{\partial \boldsymbol{\nu}_2^{\mathrm{T}}}{\partial \mathbf{o}_{\mathrm{MS}}}\right) & \left(\frac{\partial \boldsymbol{\mu}_2^{\mathrm{T}}}{\partial \mathbf{o}_{\mathrm{MS}}}\right) & \left(\frac{\partial \boldsymbol{\nu}_1^{\mathrm{T}}}{\partial \mathbf{o}_{\mathrm{MS}}}\right) & \left(\frac{\partial \boldsymbol{\mu}_1^{\mathrm{T}}}{\partial \mathbf{o}_{\mathrm{MS}}}\right) & \left(\frac{\partial \boldsymbol{\vartheta}^{\mathrm{T}}}{\partial \mathbf{o}_{\mathrm{MS}}}\right) & \left(\frac{\partial \boldsymbol{\varphi}^{\mathrm{T}}}{\partial \mathbf{o}_{\mathrm{MS}}}\right) & \left(\frac{\partial \boldsymbol{\tau}^{\mathrm{T}}}{\partial \mathbf{o}_{\mathrm{MS}}}\right) \\ \left(\frac{\partial \boldsymbol{\theta}^{\mathrm{T}}}{\partial \mathbf{v}}\right) & \left(\frac{\partial \boldsymbol{\phi}^{\mathrm{T}}}{\partial \mathbf{v}}\right) & \left(\frac{\partial \boldsymbol{\nu}_2^{\mathrm{T}}}{\partial \mathbf{v}}\right) & \left(\frac{\partial \boldsymbol{\mu}_2^{\mathrm{T}}}{\partial \mathbf{v}}\right) & \left(\frac{\partial \boldsymbol{\nu}_1^{\mathrm{T}}}{\partial \mathbf{v}}\right) & \left(\frac{\partial \boldsymbol{\mu}_1^{\mathrm{T}}}{\partial \mathbf{v}}\right) & \left(\frac{\partial \boldsymbol{\vartheta}^{\mathrm{T}}}{\partial \mathbf{v}}\right) & \left(\frac{\partial \boldsymbol{\varphi}^{\mathrm{T}}}{\partial \mathbf{v}}\right) & \left(\frac{\partial \boldsymbol{\tau}^{\mathrm{T}}}{\partial \mathbf{v}}\right) \\ \left(\frac{\partial \boldsymbol{\theta}^{\mathrm{T}}}{\partial \mathbf{Q}_{\mathrm{cl}}^{\mathrm{T}}}\right) & \left(\frac{\partial \boldsymbol{\phi}^{\mathrm{T}}}{\partial \mathbf{Q}_{\mathrm{cl}}^{\mathrm{T}}}\right) & \left(\frac{\partial \boldsymbol{\nu}_2^{\mathrm{T}}}{\partial \mathbf{Q}_{\mathrm{cl}}^{\mathrm{T}}}\right) & \left(\frac{\partial \boldsymbol{\mu}_2^{\mathrm{T}}}{\partial \mathbf{Q}_{\mathrm{cl}}^{\mathrm{T}}}\right) & \left(\frac{\partial \boldsymbol{\nu}_1^{\mathrm{T}}}{\partial \mathbf{Q}_{\mathrm{cl}}^{\mathrm{T}}}\right) & \left(\frac{\partial \boldsymbol{\mu}_1^{\mathrm{T}}}{\partial \mathbf{Q}_{\mathrm{cl}}^{\mathrm{T}}}\right) & \left(\frac{\partial \boldsymbol{\vartheta}^{\mathrm{T}}}{\partial \mathbf{Q}_{\mathrm{cl}}^{\mathrm{T}}}\right) & \left(\frac{\partial \boldsymbol{\varphi}^{\mathrm{T}}}{\partial \mathbf{Q}_{\mathrm{cl}}^{\mathrm{T}}}\right) & \left(\frac{\partial \boldsymbol{\tau}^{\mathrm{T}}}{\partial \mathbf{Q}_{\mathrm{cl}}^{\mathrm{T}}}\right) \\ \left(\frac{\partial \boldsymbol{\theta}^{\mathrm{T}}}{\partial \mathbf{o}_{\mathrm{RIS}}}\right) & \left(\frac{\partial \boldsymbol{\phi}^{\mathrm{T}}}{\partial \mathbf{o}_{\mathrm{RIS}}}\right) & \left(\frac{\partial \boldsymbol{\nu}_2^{\mathrm{T}}}{\partial \mathbf{o}_{\mathrm{RIS}}}\right) & \left(\frac{\partial \boldsymbol{\mu}_2^{\mathrm{T}}}{\partial \mathbf{o}_{\mathrm{RIS}}}\right) & \left(\frac{\partial \boldsymbol{\nu}_1^{\mathrm{T}}}{\partial \mathbf{o}_{\mathrm{RIS}}}\right) & \left(\frac{\partial \boldsymbol{\mu}_1^{\mathrm{T}}}{\partial \mathbf{o}_{\mathrm{RIS}}}\right) & \left(\frac{\partial \boldsymbol{\vartheta}^{\mathrm{T}}}{\partial \mathbf{o}_{\mathrm{RIS}}}\right) & \left(\frac{\partial \boldsymbol{\varphi}^{\mathrm{T}}}{\partial \mathbf{o}_{\mathrm{RIS}}}\right) & \left(\frac{\partial \boldsymbol{\tau}^{\mathrm{T}}}{\partial \mathbf{o}_{\mathrm{RIS}}}\right) \\ \left(\frac{\partial \boldsymbol{\theta}^{\mathrm{T}}}{\partial \mathbf{P}_{\mathrm{RIS}}^{\mathrm{T}}}\right) & \left(\frac{\partial \boldsymbol{\phi}^{\mathrm{T}}}{\partial \mathbf{P}_{\mathrm{RIS}}^{\mathrm{T}}}\right) & \left(\frac{\partial \boldsymbol{\nu}_2^{\mathrm{T}}}{\partial \mathbf{P}_{\mathrm{RIS}}^{\mathrm{T}}}\right) & \left(\frac{\partial \boldsymbol{\mu}_2^{\mathrm{T}}}{\partial \mathbf{P}_{\mathrm{RIS}}^{\mathrm{T}}}\right) & \left(\frac{\partial \boldsymbol{\nu}_1^{\mathrm{T}}}{\partial \mathbf{P}_{\mathrm{RIS}}^{\mathrm{T}}}\right) & \left(\frac{\partial \boldsymbol{\mu}_1^{\mathrm{T}}}{\partial \mathbf{P}_{\mathrm{RIS}}^{\mathrm{T}}}\right) & \left(\frac{\partial \boldsymbol{\vartheta}^{\mathrm{T}}}{\partial \mathbf{P}_{\mathrm{RIS}}^{\mathrm{T}}}\right) & \left(\frac{\partial \boldsymbol{\varphi}^{\mathrm{T}}}{\partial \mathbf{P}_{\mathrm{RIS}}^{\mathrm{T}}}\right) & \left(\frac{\partial \boldsymbol{\tau}^{\mathrm{T}}}{\partial \mathbf{P}_{\mathrm{RIS}}^{\mathrm{T}}}\right) \end{bmatrix} \tag{E.1}$$

which is an orthogonal matrix. The rotation matrix of IS is of the same formula as the function above, but replace the angles observed at MS $(\theta_{\mathrm{MS}}, \phi_{\mathrm{MS}})$ with those of IS $(\nu_{\mathrm{IS}}, \mu_{\mathrm{IS}})$. Thus, these rotation matrices satisfy that $\mathbf{R}(\mathbf{o}_{\mathrm{MS}})^{-1} = \mathbf{R}(\mathbf{o}_{\mathrm{MS}})^{\mathrm{T}}, \mathbf{R}(\mathbf{o}_{\mathrm{IS}})^{-1} = \mathbf{R}(\mathbf{o}_{\mathrm{IS}})^{\mathrm{T}}$. For the direct path and cluster reflective paths,

$$\mathbf{R}(\mathbf{o}_{\mathrm{MS}})^{-1} = \begin{bmatrix} \mathbf{R}_{1,\mathrm{MS}} \\ \hdashline \mathbf{R}_{2,\mathrm{MS}} \\ \hdashline \mathbf{R}_{3,\mathrm{MS}} \end{bmatrix} = \begin{bmatrix} \cos(\phi_{\mathrm{MS}}) & \sin(\phi_{\mathrm{MS}}) & 0 \\ \hdashline -\sin(\phi_{\mathrm{MS}})\cos(\theta_{\mathrm{MS}}) & \cos(\phi_{\mathrm{MS}})\cos(\theta_{\mathrm{MS}}) & -\sin(\theta_{\mathrm{MS}}) \\ \hdashline -\sin(\phi_{\mathrm{MS}})\sin(\theta_{\mathrm{MS}}) & \cos(\phi_{\mathrm{MS}})\sin(\theta_{\mathrm{MS}}) & \cos(\theta_{\mathrm{MS}}) \end{bmatrix} \tag{E.2}$$

The derivative functions of $\mathbf{R}(\mathbf{o}_{\mathrm{MS}})^{-1}$ over $(\theta_{\mathrm{MS}}, \phi_{\mathrm{MS}})$ are

$$\dot{\mathbf{R}}_{\mathrm{MS}} = \frac{\partial \mathbf{R}(\mathbf{o}_{\mathrm{MS}})^{-1}}{\partial \theta_{\mathrm{MS}}} = \begin{bmatrix} \dot{\mathbf{R}}_{1,\mathrm{MS}} \\ \hdashline \dot{\mathbf{R}}_{2,\mathrm{MS}} \\ \hdashline \dot{\mathbf{R}}_{3,\mathrm{MS}} \end{bmatrix} = \begin{bmatrix} 0 & 0 & 0 \\ \hdashline \sin(\phi_{\mathrm{MS}})\sin(\theta_{\mathrm{MS}}) & -\cos(\phi_{\mathrm{MS}})\sin(\theta_{\mathrm{MS}}) & -\cos(\theta_{\mathrm{MS}}) \\ \hdashline -\sin(\phi_{\mathrm{MS}})\cos(\theta_{\mathrm{MS}}) & \cos(\phi_{\mathrm{MS}})\cos(\theta_{\mathrm{MS}}) & -\sin(\theta_{\mathrm{MS}}) \end{bmatrix} \tag{E.3a}$$

$$\grave{\mathbf{R}}_{\mathrm{MS}} = \frac{\partial \mathbf{R}(\mathbf{o}_{\mathrm{MS}})^{-1}}{\partial \phi_{\mathrm{MS}}} = \begin{bmatrix} \grave{\mathbf{R}}_{1,\mathrm{MS}} \\ \hdashline \grave{\mathbf{R}}_{2,\mathrm{MS}} \\ \hdashline \grave{\mathbf{R}}_{3,\mathrm{MS}} \end{bmatrix} = \begin{bmatrix} -\sin(\phi_{\mathrm{MS}}) & \cos(\phi_{\mathrm{MS}}) & 0 \\ \hdashline -\cos(\phi_{\mathrm{MS}})\cos(\theta_{\mathrm{MS}}) & -\sin(\phi_{\mathrm{MS}})\cos(\theta_{\mathrm{MS}}) & 0 \\ \hdashline -\cos(\phi_{\mathrm{MS}})\sin(\theta_{\mathrm{MS}}) & -\sin(\phi_{\mathrm{MS}})\sin(\theta_{\mathrm{MS}}) & 0 \end{bmatrix} \tag{E.3b}$$

The derivative functions of rotated Tx and Rx elements over the rotation angles are omitted, since we consider the near-field case for Tx and Rx. For the cluster reflective paths $l \in \Lambda_{\mathrm{s}}$, the derivative functions of channel parameters over the location information can be calculated as

$$\frac{\partial \theta_l}{\partial \mathbf{v}} = -\frac{1}{\sqrt{v_{\mathrm{R},x,l}^2 + v_{\mathrm{R},y,l}^2}} \left(\frac{v_{\mathrm{R},z,l} \mathbf{v}_{\mathrm{R},l}^{\mathrm{T}} \mathbf{R}(\mathbf{o}_{\mathrm{MS}})^{-1}}{\|\mathbf{v}_{\mathrm{R,l}}\|^2} - \mathbf{R}_{3,\mathrm{MS}} \right) \tag{E.4a}$$

$$\frac{\partial \phi_l}{\partial \mathbf{v}} = -\frac{1}{v_{\mathrm{R},x,l}^2 + v_{\mathrm{R},y,l}^2} \left(v_{\mathrm{R},x,l} \mathbf{R}_{2,\mathrm{MS}} - v_{\mathrm{R},y,l} \mathbf{R}_{1,\mathrm{MS}} \right) \tag{E.4b}$$

$$\frac{\partial \vartheta_l}{\partial \mathbf{v}} = [0, 0, 0] \tag{E.4c}$$

$$\frac{\partial \varphi_l}{\partial \mathbf{v}} = [0, 0, 0] \tag{E.4d}$$

$$\frac{\partial \theta_l}{\partial \theta_{\mathrm{MS}}} = \frac{1}{\sqrt{v_{\mathrm{R},x,l}^2 + v_{\mathrm{R},y,l}^2}} \left(\frac{v_{\mathrm{R},z,l} \mathbf{v}_{\mathrm{R},l}^{\mathrm{T}} \dot{\mathbf{R}}_{\mathrm{MS}} (\mathbf{v}_l - \mathbf{v})}{\|\mathbf{v}_{\mathrm{R},l}\|^2} - \dot{\mathbf{R}}_{3,\mathrm{MS}} (\mathbf{v}_l - \mathbf{v}) \right) \tag{E.4e}$$

$$\frac{\partial \theta_l}{\partial \phi_{\mathrm{MS}}} = \frac{1}{\sqrt{v_{\mathrm{R},x,l}^2 + v_{\mathrm{R},y,l}^2}} \left(\frac{v_{\mathrm{R},z,l} \mathbf{v}_{\mathrm{R},l}^{\mathrm{T}} \grave{\mathbf{R}}_{\mathrm{MS}} (\mathbf{v}_l - \mathbf{v})}{\|\mathbf{v}_{\mathrm{R},l}\|^2} - \grave{\mathbf{R}}_{3,\mathrm{MS}} (\mathbf{v}_l - \mathbf{v}) \right) \tag{E.4f}$$

$$\frac{\partial \phi_l}{\partial \theta_{\mathrm{MS}}} = \frac{v_{\mathrm{R},x,l} \dot{\mathbf{R}}_{2,\mathrm{MS}} (\mathbf{v}_l - \mathbf{v}) - v_{\mathrm{R},y,l} \dot{\mathbf{R}}_{1,\mathrm{MS}} (\mathbf{v}_l - \mathbf{v})}{v_{\mathrm{R},x,l}^2 + v_{\mathrm{R},y,l}^2} \tag{E.4g}$$

$$\frac{\partial \phi_l}{\partial \phi_{\mathrm{MS}}} = \frac{v_{\mathrm{R},x,l} \grave{\mathbf{R}}_{2,\mathrm{MS}} (\mathbf{v}_l - \mathbf{v}) - v_{\mathrm{R},y,l} \grave{\mathbf{R}}_{1,\mathrm{MS}} (\mathbf{v}_l - \mathbf{v})}{v_{\mathrm{R},x,l}^2 + v_{\mathrm{R},y,l}^2} \tag{E.4h}$$

$$\frac{\partial \vartheta_l}{\partial \theta_{\mathrm{MS}}} = 0 \tag{E.4i}$$

$$\frac{\partial \varphi_l}{\partial \phi_{\mathrm{MS}}} = 0 \tag{E.4j}$$

$$\frac{\partial \theta_l}{\partial \mathbf{v}_l} = -\frac{\partial \theta_l}{\partial \mathbf{v}} = \frac{1}{\sqrt{v_{\mathrm{R},x,l}^2 + v_{\mathrm{R},y,l}^2}} \left(\frac{v_{\mathrm{R},z,l} \mathbf{v}_{\mathrm{R},l}^{\mathrm{T}} \mathbf{R} (\mathbf{o}_{\mathrm{MS}})^{-1}}{\|\mathbf{v}_{\mathrm{R,l}}\|^2} - \mathbf{R}_{3,\mathrm{MS}} \right) \tag{E.4k}$$

$$\frac{\partial \phi_l}{\partial \mathbf{v}_l} = -\frac{\partial \phi_l}{\partial \mathbf{v}} = \frac{1}{v_{\mathrm{R},x,l}^2 + v_{\mathrm{R},y,l}^2} \left(v_{\mathrm{R},x,l} \mathbf{R}_{2,\mathrm{MS}} - v_{\mathrm{R},y,l} \mathbf{R}_{1,\mathrm{MS}} \right) \tag{E.4l}$$

$$\frac{\partial \vartheta_l}{\partial \mathbf{v}_l} = \frac{1}{\sqrt{w_{\mathrm{T},x,l}^2 + w_{\mathrm{T},y,l}^2}} \left(\frac{w_{\mathrm{T},z,l} \mathbf{w}_{\mathrm{T},l}^{\mathrm{T}}}{\|\mathbf{w}_{\mathrm{T},l}\|^2} - [0, 0, 1] \right) \tag{E.4m}$$

$$\frac{\partial \varphi_l}{\partial \mathbf{v}_l} = \frac{1}{w_{\mathrm{T},x,l}^2 + w_{\mathrm{T},y,l}^2} [-w_{\mathrm{T},y,l}, w_{\mathrm{T},x,l}, 0] \tag{E.4n}$$

Additionally, for the direct path $l = 1$, the derivative function of parameters of the direct path over the location information is calculated as

$$\frac{\partial \vartheta_1}{\partial \mathbf{v}} = \frac{1}{\sqrt{x_{\mathrm{MS}}^2 + y_{\mathrm{MS}}^2}} \left([0, 0, 1] - \frac{w_{\mathrm{T},z,1} \mathbf{w}_1^{\mathrm{T}}}{\|\mathbf{v}\|^2} \right) \tag{E.5a}$$

$$\frac{\partial \varphi_1}{\partial \mathbf{v}} = \frac{1}{x_{\mathrm{MS}}^2 + y_{\mathrm{MS}}^2} [-y_{\mathrm{MS}}, x_{\mathrm{MS}}, 0] \tag{E.5b}$$

For the IS-aided paths $l \in \Lambda_{\mathrm{R}}$, when the rotation matrix of IS is

$$\mathbf{R}(\mathbf{o}_{\mathrm{IS}})^{-1} = \begin{bmatrix} \mathbf{R}_{1,\mathrm{IS}} \\ \hdashline \mathbf{R}_{2,\mathrm{IS}} \\ \hdashline \mathbf{R}_{3,\mathrm{IS}} \end{bmatrix} = \begin{bmatrix} \cos(\mu_{\mathrm{IS}}) & \sin(\mu_{\mathrm{IS}}) & 0 \\ \hdashline -\sin(\mu_{\mathrm{IS}})\cos(\nu_{\mathrm{IS}}) & \cos(\mu_{\mathrm{IS}})\cos(\nu_{\mathrm{IS}}) & -\sin(\nu_{\mathrm{IS}}) \\ \hdashline -\sin(\mu_{\mathrm{IS}})\sin(\nu_{\mathrm{IS}}) & \cos(\mu_{\mathrm{IS}})\sin(\nu_{\mathrm{IS}}) & \cos(\nu_{\mathrm{IS}}) \end{bmatrix}$$

$$\mathbf{R}(\mathbf{o}_{\mathrm{BS}})^{-1} = \begin{bmatrix} \mathbf{R}_{1,\mathrm{BS}} \\ \hdashline \mathbf{R}_{2,\mathrm{BS}} \\ \hdashline \mathbf{R}_{3,\mathrm{BS}} \end{bmatrix} = \begin{bmatrix} 1 & 0 & 0 \\ \hdashline 0 & 1 & 0 \\ \hdashline 0 & 0 & 1 \end{bmatrix}$$

And the derivative functions of $\mathbf{R}(\mathbf{o}_{\mathrm{MS}})^{-1}$ over $(\theta_{\mathrm{MS}}, \phi_{\mathrm{MS}})$ are

$$\dot{\mathbf{R}}_{\mathrm{IS}} = \frac{\partial \mathbf{R}(\mathbf{o}_{\mathrm{IS}})^{-1}}{\partial \nu_{\mathrm{IS}}} = \begin{bmatrix} \dot{\mathbf{R}}_{1,\mathrm{IS}} \\ \hdashline \dot{\mathbf{R}}_{2,\mathrm{IS}} \\ \hdashline \dot{\mathbf{R}}_{3,\mathrm{IS}} \end{bmatrix}$$

$$= \begin{bmatrix} 0 & 0 & 0 \\ \hdashline \sin(\mu_{\mathrm{IS}})\sin(\nu_{\mathrm{IS}}) & -\cos(\mu_{\mathrm{IS}})\sin(\nu_{\mathrm{IS}}) & -\cos(\nu_{\mathrm{IS}}) \\ \hdashline -\sin(\mu_{\mathrm{IS}})\cos(\nu_{\mathrm{IS}}) & \cos(\mu_{\mathrm{IS}})\cos(\nu_{\mathrm{IS}}) & -\sin(\nu_{\mathrm{IS}}) \end{bmatrix} \tag{E.6a}$$

$$\grave{\mathbf{R}}_{\mathrm{IS}} = \frac{\partial \mathbf{R}(\mathbf{o}_{\mathrm{IS}})^{-1}}{\partial \mu_{\mathrm{IS}}} = \begin{bmatrix} \grave{\mathbf{R}}_{1,\mathrm{IS}} \\ \hdashline \grave{\mathbf{R}}_{2,\mathrm{IS}} \\ \hdashline \grave{\mathbf{R}}_{3,\mathrm{IS}} \end{bmatrix} = \begin{bmatrix} -\sin(\mu_{\mathrm{IS}}) & \cos(\mu_{\mathrm{IS}}) & 0 \\ \hdashline -\cos(\mu_{\mathrm{IS}})\cos(\nu_{\mathrm{IS}}) & -\sin(\mu_{\mathrm{IS}})\cos(\nu_{\mathrm{IS}}) & 0 \\ \hdashline -\cos(\mu_{\mathrm{IS}})\sin(\nu_{\mathrm{IS}}) & -\sin(\mu_{\mathrm{IS}})\sin(\nu_{\mathrm{IS}}) & 0 \end{bmatrix} \tag{E.6b}$$

As aforementioned in the section 5.2, we consider general case for IS, thus, the derivative functions of rotated Ix elements over the rotation angles $(\nu_{\mathrm{IS}}, \mu_{\mathrm{IS}})$ is calculated as $\dot{\boldsymbol{\chi}}_{\mathrm{I},p}^{\mathrm{T}} = \frac{\partial \boldsymbol{\chi}_{\mathrm{I},p}}{\partial \nu_{\mathrm{IS}}} = \dot{\mathbf{R}}_{\mathrm{IS}} \mathbf{p}_{\mathrm{I},p}$ and $\grave{\boldsymbol{\chi}}_{\mathrm{I},p}^{\mathrm{T}} = \frac{\partial \boldsymbol{\chi}_{\mathrm{I},p}}{\partial \mu_{\mathrm{IS}}} = \grave{\mathbf{R}}_{\mathrm{IS}} \mathbf{p}_{\mathrm{I},p}$. The derivative functions of channel parameters over location information can be calculated as

$$\frac{\partial \theta_p}{\partial \mathbf{r}_{\mathrm{I}}} = \frac{\partial \theta_p}{\partial \boldsymbol{\chi}_{\mathrm{I},p}^{\mathrm{T}}} = -\frac{\partial \theta_p}{\partial \mathbf{v}} = \frac{1}{\sqrt{v_{\mathrm{R},x,p}^2 + v_{\mathrm{R},y,p}^2}} \left(\frac{v_{\mathrm{R},z,p} \mathbf{v}_{\mathrm{R},p}^{\mathrm{T}} \mathbf{R}(\mathbf{o}_{\mathrm{MS}})^{-1}}{\|\mathbf{v}_{\mathrm{R,p}}\|^2} - \mathbf{R}_{3,\mathrm{MS}} \right) \tag{E.7a}$$

$$\frac{\partial \phi_p}{\partial \mathbf{r}_{\mathrm{I}}} = \frac{\partial \phi_p}{\partial \boldsymbol{\chi}_{\mathrm{I},p}^{\mathrm{T}}} = -\frac{\partial \phi_p}{\partial \mathbf{v}} = \frac{1}{v_{\mathrm{R},x,p}^2 + v_{\mathrm{R},y,p}^2} \left(v_{\mathrm{R},x,p} \mathbf{R}_{2,\mathrm{MS}} - v_{\mathrm{R},y,p} \mathbf{R}_{1,\mathrm{MS}} \right) \tag{E.7b}$$

$$\frac{\partial \theta_p}{\partial \mu_{\mathrm{IS}}} = \frac{1}{\sqrt{v_{\mathrm{R},x,p}^2 + v_{\mathrm{R},y,p}^2}} \left(\frac{v_{\mathrm{R},z,p} \mathbf{v}_{\mathrm{R},p}^{\mathrm{T}} \mathbf{R}(\mathbf{o}_{\mathrm{MS}})^{-1} \grave{\boldsymbol{\chi}}_{\mathrm{I},p}^{\mathrm{T}}}{\|\mathbf{v}_{\mathrm{R,p}}\|^2} - \mathbf{R}_{3,\mathrm{MS}} \grave{\boldsymbol{\chi}}_{\mathrm{I},p}^{\mathrm{T}} \right) \tag{E.7c}$$

$$\frac{\partial \phi_p}{\partial \mu_{\mathrm{IS}}} = \frac{1}{v_{\mathrm{R},x,p}^2 + v_{\mathrm{R},y,p}^2} \left(v_{\mathrm{R},x,p} \mathbf{R}_{2,\mathrm{MS}} \grave{\boldsymbol{\chi}}_{\mathrm{I},p}^{\mathrm{T}} - v_{\mathrm{R},y,p} \mathbf{R}_{1,\mathrm{MS}} \grave{\boldsymbol{\chi}}_{\mathrm{I},p}^{\mathrm{T}} \right) \tag{E.7d}$$

$$\frac{\partial \theta_p}{\partial \nu_{\mathrm{IS}}} = \frac{1}{\sqrt{v_{\mathrm{R},x,p}^2 + v_{\mathrm{R},y,p}^2}} \left(\frac{v_{\mathrm{R},z,p} \mathbf{v}_{\mathrm{R},p}^{\mathrm{T}} \mathbf{R}(\mathbf{o}_{\mathrm{MS}})^{-1} \dot{\boldsymbol{\chi}}_{\mathrm{I},p}^{\mathrm{T}}}{\|\mathbf{v}_{\mathrm{R},p}\|^2} - \mathbf{R}_{3,\mathrm{MS}} \dot{\boldsymbol{\chi}}_{\mathrm{I},p}^{\mathrm{T}} \right) \tag{E.7e}$$

$$\frac{\partial \phi_p}{\partial \nu_{\mathrm{IS}}} = \frac{1}{v_{\mathrm{R},x,p}^2 + v_{\mathrm{R},y,p}^2} \left(v_{\mathrm{R},x,p} \mathbf{R}_{2,\mathrm{MS}} \dot{\boldsymbol{\chi}}_{\mathrm{I},p}^{\mathrm{T}} - v_{\mathrm{R},y,p} \mathbf{R}_{1,\mathrm{MS}} \dot{\boldsymbol{\chi}}_{\mathrm{I},p}^{\mathrm{T}} \right) \tag{E.7f}$$

$$\frac{\partial \vartheta_p}{\partial \mu_{\mathrm{IS}}} = \frac{1}{\sqrt{w_{\mathrm{T},x,p}^2 + w_{\mathrm{T},y,p}^2}} \left(\frac{w_{\mathrm{T},z,p} \mathbf{w}_{\mathrm{T},p}^{\mathrm{T}} \mathbf{R}(\mathbf{o}_{\mathrm{BS}})^{-1} \grave{\boldsymbol{\chi}}_{\mathrm{I},p}^{\mathrm{T}}}{\|\mathbf{w}_{\mathrm{T},p}\|^2} - \mathbf{R}_{3,\mathrm{BS}} \grave{\boldsymbol{\chi}}_{\mathrm{I},p}^{\mathrm{T}} \right) \tag{E.7g}$$

$$\frac{\partial \varphi_p}{\partial \mu_{\mathrm{IS}}} = \frac{1}{w_{\mathrm{T},x,p}^2 + w_{\mathrm{T},y,p}^2} \left(w_{\mathrm{T},x,p} \mathbf{R}_{2,\mathrm{BS}} \grave{\boldsymbol{\chi}}_{\mathrm{I},p}^{\mathrm{T}} - w_{\mathrm{T},y,p} \mathbf{R}_{1,\mathrm{BS}} \grave{\boldsymbol{\chi}}_{\mathrm{I},p}^{\mathrm{T}} \right) \tag{E.7h}$$

$$\frac{\partial \vartheta_p}{\partial \nu_{\mathrm{IS}}} = \frac{1}{\sqrt{w_{\mathrm{T},x,p}^2 + w_{\mathrm{T},y,p}^2}} \left(\frac{w_{\mathrm{T},z,p} \mathbf{w}_{\mathrm{T},p}^{\mathrm{T}} \mathbf{R}(\mathbf{o}_{\mathrm{BS}})^{-1} \dot{\boldsymbol{\chi}}_{\mathrm{I},p}^{\mathrm{T}}}{\|\mathbf{w}_{\mathrm{T},p}\|^2} - \mathbf{R}_{3,\mathrm{BS}} \dot{\boldsymbol{\chi}}_{\mathrm{I},p}^{\mathrm{T}} \right) \tag{E.7i}$$

$$\frac{\partial \varphi_p}{\partial \nu_{\mathrm{IS}}} = \frac{1}{w_{\mathrm{T},x,p}^2 + w_{\mathrm{T},y,p}^2} \left(w_{\mathrm{T},x,p} \mathbf{R}_{2,\mathrm{BS}} \dot{\boldsymbol{\chi}}_{\mathrm{I},p}^{\mathrm{T}} - w_{\mathrm{T},y,p} \mathbf{R}_{1,\mathrm{BS}} \dot{\boldsymbol{\chi}}_{\mathrm{I},p}^{\mathrm{T}} \right) \tag{E.7j}$$

$$\frac{\partial \mu_{\mathrm{fw},p}}{\partial \mathbf{v}} = [0,0,0]^{\mathrm{T}} \tag{E.7k}$$

$$\frac{\partial \nu_{\mathrm{fw},p}}{\partial \mathbf{v}} = [0,0,0]^{\mathrm{T}} \tag{E.7l}$$

$$\frac{\partial \mu_{\mathrm{bw},p}}{\partial \mathbf{v}} = \frac{1}{x_{p,\mathrm{MS}}^2 + y_{p,\mathrm{MS}}^2} \left(\mathbf{R}_{2,\mathrm{IS}} x_{p,\mathrm{MS}} - \mathbf{R}_{1,\mathrm{IS}} y_{p,\mathrm{MS}} \right) \tag{E.7m}$$

$$\frac{\partial \nu_{\mathrm{bw},p}}{\partial \mathbf{v}} = \frac{-1}{\sqrt{x_{p,\mathrm{MS}}^2 + y_{p,\mathrm{MS}}^2}} \left(\mathbf{R}_{3,\mathrm{IS}} - \frac{z_{p,\mathrm{MS}} \mathbf{r}_{p,\mathrm{MS}}^{\mathrm{T}} \mathbf{R}(\mathbf{o}_{\mathrm{IS}})^{-1}}{\|\mathbf{r}_{p,\mathrm{MS}}\|^2} \right) \tag{E.7n}$$

$$\frac{\partial \mu_{\mathrm{bw},p}}{\partial \mathbf{r}_{\mathrm{I}}} = \frac{\partial \mu_{\mathrm{bw},p}}{\partial \boldsymbol{\chi}_{\mathrm{I}}, p} = -\frac{\partial \mu_{\mathrm{bw},p}}{\partial \mathbf{v}} = \frac{1}{x_{p,\mathrm{MS}}^2 + y_{p,\mathrm{MS}}^2} \left(\mathbf{R}_{1,\mathrm{IS}} y_{p,\mathrm{MS}} - \mathbf{R}_{2,\mathrm{IS}} x_{p,\mathrm{MS}} \right) \tag{E.7o}$$

$$\frac{\partial \nu_{\mathrm{fw},p}}{\partial \mathbf{r}_{\mathrm{I}}} = \frac{\partial \nu_{\mathrm{fw},p}}{\partial \boldsymbol{\chi}_{\mathrm{I}}, p} = \frac{1}{\sqrt{x_{p,\mathrm{BS}}^2 + y_{p,\mathrm{BS}}^2}} \left(\mathbf{R}_{3,\mathrm{IS}} - \frac{z_{p,\mathrm{BS}} \mathbf{r}_{p,\mathrm{BS}}^{\mathrm{T}} \mathbf{R}(\mathbf{o}_{\mathrm{IS}})^{-1}}{\|\mathbf{r}_{p,\mathrm{BS}}\|^2} \right) \tag{E.7p}$$

$$\frac{\partial \mu_{\mathrm{fw},p}}{\partial \mathbf{r}_{\mathrm{I}}} = \frac{\partial \mu_{\mathrm{fw},p}}{\partial \boldsymbol{\chi}_{\mathrm{I}}, p} = \frac{1}{x_{p,\mathrm{BS}}^2 + y_{p,\mathrm{BS}}^2} \left(\mathbf{R}_{1,\mathrm{IS}} y_{p,\mathrm{BS}} - \mathbf{R}_{2,\mathrm{IS}} x_{p,\mathrm{BS}} \right) \tag{E.7q}$$

$$\frac{\partial \nu_{\mathrm{bw},p}}{\partial \mathbf{r}_{\mathrm{I}}} = \frac{\partial \nu_{\mathrm{bw},p}}{\partial \boldsymbol{\chi}_{\mathrm{I}}, p} = -\frac{\partial \nu_{\mathrm{bw},p}}{\partial \mathbf{v}} = \frac{1}{\sqrt{x_{p,\mathrm{MS}}^2 + y_{p,\mathrm{MS}}^2}} \left(\mathbf{R}_{3,\mathrm{IS}} - \frac{z_{p,\mathrm{MS}} \mathbf{r}_{p,\mathrm{MS}}^{\mathrm{T}} \mathbf{R}(\mathbf{o}_{\mathrm{IS}})^{-1}}{\|\mathbf{r}_{p,\mathrm{MS}}\|^2} \right) \tag{E.7r}$$

$$\frac{\partial \mu_{\mathrm{bw},p}}{\partial \mu_{\mathrm{IS}}} = \frac{(x_{p,\mathrm{MS}} \grave{\mathbf{R}}_{2,\mathrm{IS}} - y_{p,\mathrm{MS}} \grave{\mathbf{R}}_{1,\mathrm{IS}})(\mathbf{v} - \mathbf{r}_{\mathrm{I}})}{x_{p,\mathrm{MS}}^2 + y_{p,\mathrm{MS}}^2} \tag{E.7s}$$

$$\frac{\partial \mu_{\mathrm{fw},p}}{\partial \mu_{\mathrm{IS}}} = \frac{(x_{p,\mathrm{BS}}\grave{\mathbf{R}}_{2,\mathrm{IS}} - y_{p,\mathrm{BS}}\grave{\mathbf{R}}_{1,\mathrm{IS}})(\mathbf{w}-\mathbf{r}_{\mathrm{I}})}{x_{p,\mathrm{BS}}^2 + y_{p,\mathrm{BS}}^2} \tag{E.7t}$$

$$\frac{\partial \mu_{\mathrm{bw},p}}{\partial \nu_{\mathrm{IS}}} = \frac{(x_{p,\mathrm{MS}}\dot{\mathbf{R}}_{2,\mathrm{IS}} - y_{p,\mathrm{MS}}\dot{\mathbf{R}}_{1,\mathrm{IS}})(\mathbf{v}-\mathbf{r}_{\mathrm{I}})}{x_{p,\mathrm{MS}}^2 + y_{p,\mathrm{MS}}^2} \tag{E.7u}$$

$$\frac{\partial \mu_{\mathrm{fw},p}}{\partial \nu_{\mathrm{IS}}} = \frac{(x_{p,\mathrm{BS}}\dot{\mathbf{R}}_{2,\mathrm{IS}} - y_{p,\mathrm{BS}}\dot{\mathbf{R}}_{1,\mathrm{IS}})(\mathbf{w}-\mathbf{r}_{\mathrm{I}})}{x_{p,\mathrm{BS}}^2 + y_{p,\mathrm{BS}}^2} \tag{E.7v}$$

$$\frac{\partial \nu_{\mathrm{bw},p}}{\partial \mu_{\mathrm{IS}}} = \frac{-1}{\sqrt{x_{p,\mathrm{MS}}^2 + y_{p,\mathrm{MS}}^2}}\left(\grave{\mathbf{R}}_{3,\mathrm{IS}} - \frac{z_{p,\mathrm{MS}}\mathbf{r}_{p,\mathrm{MS}}^{\mathrm{T}}\grave{\mathbf{R}}_{\mathrm{IS}}}{\|\mathbf{r}_{p,\mathrm{MS}}\|^2}\right)(\mathbf{v}-\mathbf{r}_{\mathrm{I}}) \tag{E.7w}$$

$$\frac{\partial \nu_{\mathrm{fw},p}}{\partial \mu_{\mathrm{IS}}} = \frac{-1}{\sqrt{x_{p,\mathrm{BS}}^2 + y_{p,\mathrm{BS}}^2}}\left(\grave{\mathbf{R}}_{3,\mathrm{IS}} - \frac{z_{p,\mathrm{BS}}\mathbf{r}_{p,\mathrm{BS}}^{\mathrm{T}}\grave{\mathbf{R}}_{\mathrm{IS}}}{\|\mathbf{r}_{p,\mathrm{BS}}\|^2}\right)(\mathbf{v}-\mathbf{r}_{\mathrm{I}}) \tag{E.7x}$$

$$\frac{\partial \nu_{\mathrm{bw},p}}{\partial \nu_{\mathrm{IS}}} = \frac{-1}{\sqrt{x_{p,\mathrm{MS}}^2 + y_{p,\mathrm{MS}}^2}}\left(\dot{\mathbf{R}}_{3,\mathrm{IS}} - \frac{z_{p,\mathrm{MS}}\mathbf{r}_{p,\mathrm{MS}}^{\mathrm{T}}\dot{\mathbf{R}}_{\mathrm{IS}}}{\|\mathbf{r}_{p,\mathrm{MS}}\|^2}\right)(\mathbf{v}-\mathbf{r}_{\mathrm{I}}) \tag{E.7y}$$

$$\frac{\partial \nu_{\mathrm{fw},p}}{\partial \nu_{\mathrm{IS}}} = \frac{-1}{\sqrt{x_{p,\mathrm{BS}}^2 + y_{p,\mathrm{BS}}^2}}\left(\dot{\mathbf{R}}_{3,\mathrm{IS}} - \frac{z_{p,\mathrm{BS}}\mathbf{r}_{p,\mathrm{BS}}^{\mathrm{T}}\dot{\mathbf{R}}_{\mathrm{IS}}}{\|\mathbf{r}_{p,\mathrm{BS}}\|^2}\right)(\mathbf{v}-\mathbf{r}_{\mathrm{I}}) \tag{E.7z}$$